Wear Characterisation and Usage Level Estimation of Small DC Motors

Ulrich Wienrich

A thesis submitted in partial fulfilment of the requirements
of the University of Glamorgan for the degree of
Doctor of Philosophy

School of Electronics
University of Glamorgan
Pontypridd
CF37 1DL

7th April 1999

Certificate of Research

This is to certify that, except where specific reference is made, the work described in this thesis is the result of the candidate. Neither this thesis, nor any part of it, has been presented, or is currently submitted, in candidature for any degree at any other University.

Signed .....
Candidate

Signed .....
Director of Studies

Date 7th April 1999

Acknowledgements

I am most grateful for the outstanding supervision of my Director of Studies, Dr. M. A. Wahab. He combined careful guidance and continuous help throughout the project with genuine warmth and humour, and created the motivating atmosphere which helped me to quickly overcome the rare phases of doubts and frustration. Working with him was a pleasure and I can hardly ask for a better supervisor.

I am thankful to my supervisors Mr. E. J. C. Thomas for establishing an maintaining the collaboration with Xerox, and Mr. R. J. Williams for his valuable suggestions. They were of great help for the completion of this work.

I am also greatly indebted to Mr. C. R. M. Bartholomew, Mr. K. Jones, Mr. P. Turner and Mr. D. A. Emm from the collaborating establishment, Xerox. It was their initiative that induced the project and the fruitful discussions with them were of essential value, assuring that the project resulted in a test system which is tailored for test purposes. I am also grateful to the Xerox Corporation for funding this research project throughout all its phases.

My gratitude to Dr. N. A. J. Gough and Dr. P. Plassmann. Their contribution, constructive criticism and their valuable suggestions were of great help for the completion of this work.

I thankfully acknowledge the assistance from all my friends, colleagues and the University's employees whose expertise helped me to overcome a lot of obstacles.

Thanks to my wife Sahar for her listening, understanding and sharing of my problems, for her support and for being there when she was needed.

Finally in these acknowledgements but at a prominent place in my heart I wish to thank my family. Especially my parents Manfred and Edeltraud. I dedicate this thesis to my parents in gratitude for their reassuring support and encouragement throughout the project.

Abstract

This study was concerned with investigating the wear characteristics of small direct current electric motors which are widely used in commercial and consumer machinery. This was aimed at developing the enabling techniques and methodologies to allow the establishment of effective and economical asset recovery processes for small electro-mechanical assemblies by manufacturers of commercial machinery. The wear process in small dc motors that are used in photocopying machines was investigated and physical wear parameters that can be used to estimate the usage level of these motors were identified. Accelerated life test laboratory experiments were conducted to investigate the changes in the characteristics of the wear indicating parameters with motor usage level. The experimental results have identified the reverse current waveforms as the single most reliable wear indicating parameter for the investigated motors. Detailed investigations were conducted into signal processing methods and data analysis techniques to interpret the experimental data. A novel transform for feature extraction (TFE) has been investigated and enhancements in its application were proposed. It was demonstrated that the TFE has data reduction and feature extraction capabilities which are superior to other existing techniques. Artificial neural networks (ANNs) were investigated to determine their suitability in estimating the motor usage level from experimental data of the wear indicating parameters. Optimum ANN architectures were developed and utilised to classify the motor usage level in discrete bands. Finally, a production motor test system for asset recovery screening was developed using the findings of the experimental results. This study has demonstrated the significance of reliable asset recovery screening for small electro-mechanical assemblies and developed the test and analysis techniques to achieve it.

Contents

List of Figures

Glossary of Symbols

Symbol	Description	Unit
a	Proportional constant	-
ANN	Artificial neural network	-
A_{min}	Minimum stop-band attenuation	dB
B	Magnetic flux density	T
B_m	Motor damping factor	$\frac{\text{Nm s}}{\text{rad}}$
B_{AD}	ADC converter resolution	Bit
BP	Back-propagation	-
C	Coefficient of variation	%
$D(r)$	Time domain transform vector	-
DFT	Discrete Fourier transform	-
e_a	Induced armature voltage	V
$\overline{E_{less}}$	Misclassification error in lesser class(es)	-
f_c	Cut-off frequency	Hz
FIR	Finite impulse response	-
f_0	Frequency resolution	Hz
f_s	Sampling frequency	Hz
$g(n)$	FIR filter output	-
i_a	Armature current	A
J	Current density	$\frac{\text{A}}{\text{m}^2}$
J_r	Rotor inertia	kg m^2
k	Armature winding constant	-
K	Linear current density	$\frac{\text{A}}{\text{m}}$
l_m	Length	m
l	Signal length	-
L_a	Armature inductance	H
LSB	Least significant bit	-
LVQ	Learning vector quantization	-
$MTTF$	Mean-time-to-failure	h
μ	Confidence interval	-
n	Number of discrete samples	-

Symbol	Description	Unit
N	Sample length	-
N_a	Number of armature turns	-
N_f	No. of FIR filter coefficients	-
ω	Angular frequency	$\frac{\text{rad}}{\text{s}}$
Ω	Rotor rotation frequency	$\frac{\text{rad}}{\text{s}}$
ϕ	Phase angle of current	rad, deg
Φ	Magnetic flux	Wb
P	Power	W
r	Ruler length	-
r_m	Radius	m
r_{max}	Maximum ruler length	-
R_a	Armature resistance	Ω
R_L	Motor terminal load resistor	Ω
$S(n)$	Windowed and corrected signal	-
SPL	Sound pressure level	dB
$STFT$	Short-time Fourier transform	-
t	Time	s
THD	Total harmonic distortion	-
TFE	Transform for feature extraction	-
V_t	Motor terminal voltage	V
V_{tR_L}	Terminal voltage with R_L connected	V
w	Window length	-
w_m	Pole width	m
w_{brush}	Brush wear	-
w_n	Window function	-
$WD(r, w)$	Windowed time domain transform	-
WT	Wavelet transform	-
$WTFE$	Windowed transform for feature extraction	-
WVD	Wigner-Ville distribution	-
x_i	Discrete input data	-
$\overline{x}$	Mean value	-

Chapter 1

Introduction

In today's highly competitive global market, it is becoming increasingly difficult for industries to maintain their profitability. Amongst the means of maintaining profitability are reducing costs and market expansion. Cost reduction covers both manufacturing and maintenance. Market expansion, on the other hand, is highly dependent on the product quality and customer satisfaction. As a result, machinery manufacturers face several challenges including:

1. Reduction of manufacturing costs by reducing the cost of the machinery components.

2. Cost reduction by minimising unnecessary maintenance.

3. Minimising the probability of catastrophic failure in the field by ensuring the delivery of high quality machinery. This has the effect of customer satisfaction and increased confidence in the company's products.

Of course, there are other challenges that have a direct effect on profitability such as utilising emerging technologies in the product and its manufacturing process. However, the above challenges were not listed because they are not directly

related to the subject of this study.

Unplanned maintenance, also known as the run-to-failure approach, where a machine is repaired when it has broken down otherwise no action is taken, is not acceptable for modern industrial and commercial environments. Planned maintenance is the first step towards a machine management technique which is aimed at preventing unscheduled machine failures. Scheduled maintenance tasks, as part of planned maintenance, are based on elapsed time or hours of operation, and assumes that a machine will degrade within a time frame typical of its particular mean-time-to-failure (MTTF) statistics. The problem with this approach is that the specific mode of operation may result in a different MTTF to the predicted one. A MTTF of a motor driving a dynamic load may be different to that of a motor driving a static load. The results of this are either unnecessary repairs or catastrophic failure.

An improved approach of planned maintenance is preventive maintenance. The goal of preventive maintenance is the elimination of machine breakdown by applying technology to assess the condition of the machine, identify any present or impending problems and predict when corrective action should be taken. Knowing when a machine requires maintenance allows users to perform the necessary maintenance at their convenience instead of costly unscheduled shutdowns [1–4].

The first stage in preventive maintenance is condition monitoring. Condition monitoring is the continuous health evaluation of equipment throughout its serviceable life. Condition monitoring should be designed to pre-empt fault conditions. It can in many cases be extended to provide primary protection, but its real function is to recognise the development of fault conditions at an early stage. The second

stage is fault identification and diagnosis. Having identified a fault condition the next stage is to identify the causes and location of the fault [5,6].

An enhanced approach in preventive maintenance is usage level estimation. Usage level estimation is distinct from condition monitoring in two aspects. First, the monitoring process does not have to take place continuously. Second, the usage level of a machine can be estimated without a fault condition. The technique is based on monitoring the natural wear of a machine. Since most machine faults introduce extensive wear, these faults may be detected well in advance of failure. To be able to estimate the usage level of a machine, knowledge of wear patterns of the monitored machine should be available.

The main emphasis of previous and current research is in fault detection and condition monitoring of large electromechanical assemblies, such as large induction and direct current (dc) motors. This is due to the particulary high costs of unscheduled repair and maintenance procedures, which may be reduced with appropriate condition monitoring. Condition monitoring and fault detection processes for small electromechanical assemblies, such as small dc motors, have received little attention from researchers to date. Very few studies have been reported in the literature [7,8].

However, if small electromechanical assemblies recovered from one product, can be reused in another product, the cost of manufacturing this product can be reduced. This is particulary significant if the product includes a large number of small electromechanical assemblies. The process of recovering and reusing electronic components and electromechanical assemblies is known as asset recovery. Asset recovery is operated by several large equipment and machinery manufacturers such as Sony,

IBM and Xerox, and consists of the following stages [9]:

1. Return or reclaim: Recovering products from the customer at end-of-use and returning them to the plant for asset recovery.

2. Disassembly: Dismantling of the product including cleaning and visual inspection.

3. Component reprocessing: Assemblies are tested to assess their residual life cycle and useability in other products.

Every reused component or assembly will save costs on both, waste disposal and in purchasing new parts. Asset recovery has also gained importance because environmental issues, such as recycling and recovering of electronic and electromechanical assemblies, have become part of high profile environmental management systems and strategies. Several international standards have covered these issues including ISO14001, BS7750 and EMAS [10]. However, as only few companies have implemented asset recovery processes, objective methods of assessing the reusability of small electromechanical assemblies, have not yet been sufficiently investigated.

Condition monitoring techniques are not normally applied to small electromechanical assemblies, such as small dc motors. The low cost of such assemblies makes the use of condition monitoring methods uneconomical. In addition, such small assemblies are difficult to access for condition monitoring purposes during their normal operation. Therefore, the decision to reuse a small electromechanical assembly that has been recovered from a product cannot be based on a prior knowledge of the assembly's condition. Another complicating factor is that most manufacturers of machinery do not implement a tracing system for electromechanical assemblies.

The products are disassembled in one plant and the recovered assemblies are shipped to another plant for reuse without any historical data. It is therefore, essential to establish test and decision making methodologies to enable a successful asset recovery operation. The important decision whether a reclaimed component will be reused is dependent on the implemented screening procedure. This can have major economic implications. On the one hand, if large numbers of reused assemblies fail in the field, customers will be dissatisfied and markets may be lost. On the other hand, rejecting a large number of usable recovered assemblies during asset recovery screening will reduce the impact of this process on manufacturing and waste disposal costs. An accurate and reliable test system is therefore, essential to integrate the asset recovery operation into the manufacturing process, thus decreasing production costs and maintaining customer satisfaction.

This study is concerned with investigating the methodologies and enabling technologies for reliable asset recovery of small electromechanical assemblies that are used in commercial machinery. It is aimed at addressing a significant research gap in the field of wear characterisation and assessment of this type of assemblies and the challenges posed by the requirements of a modern asset recovery process.

This research work is part of a joint project between the School of Electronics at the University of Glamorgan[1] and the Asset Recovery Department at Xerox[2] on asset recovery of photocopying machine parts. The study was fully funded by the Xerox Corporation. The object of the study was selected by the University and the company as a small dc motor of the type used in the paper trays of most of the company's copying machines. This type of electromechanical assembly is used in

[1]University of Glamorgan, Pontypridd, CF37 1DL.
[2]Xerox Corporation, Mitcheldean Plant, Mitcheldean.

large numbers in each copying machine and is therefore, a typical target of an asset recovery process.

Xerox, which is a major manufacturer of copying machines has operated an asset recovery process for several years. The screening method used by the company is carried out manually by an operator who subjectively decides to pass or fail the used motors. The decision to reuse a motor is only based on the operators judgment of the acoustic noise emitted from the motor. This is an industry wide method of screening motors [8, 11]. This method suffers from serious limitations including:

1. Influence of the ambient noise, the distance and angle of the operator in relation to the motor.

2. Results are dependent on the psychological condition, the experience and hearing capabilities of the operator.

3. Low repeatability of the test results.

The reliability of this screening process is highly dependent upon replacing the subjective operator based approach with an objective and automated method.

1.1 Statement of the Problem

Asset recovery of small electromechanical assemblies in commercial machinery, such as copying machines, has a significant impact on reducing the product's manufacturing costs and improving profitability. A successful asset recovery operation should not result in compromising the reliability of the product, otherwise markets may be lost due to customer dissatisfaction. Therefore, it is essential that only those recovered parts which will survive for the life time of the product are reused. Current

asset recovery processes for small electromechanical assemblies rely on the subjective judgement of an operator and normally result in discarding many parts which are perfectly reusable or reusing parts that will fail before the end of the product's life.

Establishing objective and automated screening methods for the asset recovery of small electromechanical assemblies, especially motors, face the following obstacles:

1. Condition monitoring of small dc motors throughout their lives is not possible due to cost and accessibility constraints.
2. Asset recovery departments do not have access to the usage history of recovered small dc motors.
3. Condition monitoring and fault detection processes of small dc motors have rarely been considered in past and current research work.

The development of a reliable asset recovery process for small dc motors requires:

1. Studying the wear characteristics of dc motors and identifying physical parameters that can serve as wear indicators.
2. Establishing relationships between the wear indicating physical parameters and the level of usage of the motor.
3. Establishing reliable motor test methodologies and acquisition techniques for the wear indicating parameters.
4. Developing processing and analysis techniques to enable the accurate interpretation of the information conveyed by the wear indicating physical parameters.

5. Developing a reliable asset recovery test and screening system that is suitable for use in a manufacturing environment.

1.2 Aim and Objectives

This study is aimed at investigating the mechanical wear characteristics of small dc motors and the enabling technologies that are necessary to establish a reliable asset recovery process for copying machines. Small dc motors are used as a typical example of recyclable small electromechanical assemblies. The objectives of the research work are as follows:

- To conduct a literature survey into wear characterisation, condition monitoring and fault detection in electromechanical assemblies to determine the relevance of previous research work to the asset recovery of small electromechanical assemblies.

- To investigate and establish physical parameters that can serve as wear indicators for small dc motors.

- To conduct an investigation into motor test methodologies to demonstrate the relationship between the wear indicating parameters and the motor usage level. This will include developing motor test equipment and conducting controlled laboratory tests on motors supplied by Xerox.

- To conduct a survey of signal processing techniques and analysis methods and to investigate their suitability for use in this study to analyse and interpret the results of the experimental investigations.

- To investigate the processing and analysis methodologies for relating the motor usage level to the characteristics of the signals of the wear indicating parameters. This will include identifying the optimum wear indicating parameters and the most suitable analysis techniques.

- To develop an automated asset recovery test system for the screening of small dc motors in a manufacturing environment.

1.3 The Present Work

This thesis describes the work conducted during the study and its results. Chapter two describes the results of the literature survey and relates this study to research work and applications that were conducted in areas such as condition monitoring and signal processing. Chapter three introduces the operation and wear parameters of the test object that was investigated in the experimental part of the study. Details of the methodology for acquiring motor usage related wear information in an accelerated life test, including the design of the test equipment are covered in chapter four. In chapter five, the utilised processing techniques are described and the processing results are presented. The analysis of the processed signals is described in chapter six, which includes details of the use of artificial neural networks classifiers for motor usage level estimation. The outcomes of this study are discussed in chapter seven. The conclusions of this study and recommendations for future work are presented in chapter eight.

Chapter 2

Literature Survey

The aim of this literature survey is to study previous research work into wear characterisation, condition monitoring and fault detection in electromechanical machines. This will enable the selection of suitable approaches in the present study for wear characterisation and usage level estimation of small dc motors. The survey is also aimed at establishing the position of the study in relation to the work of other researchers. As most of the reported research work did not cover small electromechanical assemblies, the bulk of the literature survey presents work related to large motors.

Existing theoretical and practical methods of predicting the reliability of electric motors and common motor faults were investigated (section 2.1). This included the results of reliability surveys of motors in different industrial applications.

Different approaches and methods of machine and motor condition monitoring and fault identification were studied (section 2.2). This included their historical development, advantages and limitations.

Section 2.3 presents a survey of signal processing, feature extraction and data processing techniques that may be suitable for use in identifying the level of motor usage and relating it to the wear indicating parameters. The surveyed signal processing techniques included both common and novel transforms. The data analysis methods covered statistical and artificial neural network (ANN) approaches.

A summary of the findings of the literature survey is presented in section 2.4.

2.1 Faults in Electrical Motors

Ever since electric motors have been used, their reliability has been investigated. Continuous operation of electric motors is essential to the function of modern society. They are used in all branches of daily life. They are used today in the automotive field as starter motors for cars, most domestic machines, in buildings as air conditioning fans, in office equipment and in many more fields.

Research has clearly shown that motor downtime is independent of motor size [12]. Reliability prediction is a widely used theoretical concept. However, it has two limitations. First, the difficulty to accumulate data of known validity for new applications. Second, the complexity of the prediction techniques, which when using very simple techniques can suffer from inaccuracy. More detailed techniques are costly, mainly due to the additional transducers, data acquisition equipment and computation requirements [7].

A source of reliability data of large motors are surveys. Very detailed surveys, including their analyses, were carried out by the IEEE Industry Applications Soci-

ety [13–15]. The surveys focused mainly on induction motors larger than 200 hp[1] and not older than fifteen years. A survey of the reliability of power generator motors was conducted by Albrecht *et al*, [16]. Thorsen and Dalva [17], conducted a survey on cage and squirrel cage motors which are used in the offshore industry. Table 2.1 compares the results of the surveys from O'Donnel [13] and Thorsen and Dalva [17]. Both surveys showed that most of the faults in large induction motors were caused by bearing failures.

Failed component	*Thorsen and Dalva [17] (%)*	*O'Donnel [13] (%)*
Bearing related	51.07	41
Stator winding related	15.76	37
Rotor related	4.7	10
External related	15.58	-
Others	12.89	12

Table 2.1: Distribution of failures in faulty motors.

The surveys were carried out with emphasis on very large induction motors which are mainly used in industrial applications. In the case of dc motors, it is possible to relate some of the induction motor survey results. Despite the difference in the operational principle of induction and dc motors, the materials used, such as winding insulation, are similar. Both motor types have a rotating shaft supported by bearings. If a bearing fault is the most important failure factor in induction motors (table 2.1), it may be considered as an important failure factor for dc motors as well. The link between the failure factors of ac and dc motors is supported by Tavner and Penman [5], who considered commutator and brushgear defects as factors that may lead to faults in ac commutator and dc machines. They also considered carbon dust as an additional fault factor in dc machines.

[1] 1 horsepower(hp) = 746W.

The failure mechanisms of small dc motors of the type used in office equipment have rarely been investigated, probably due to their low cost. One source for calculating an average motor failure rate with power ratings below one horsepower is the U.S. Military Handbook [7]. The handbook is used to develop high reliability electronic military equipment. However, the failure rate model did not cover all types of electric motors and was dedicated to bearing and winding failures only.

The theoretical reliability approach can only provide a rough estimate of a motor's life. Surveys can help to overcome the lack of theoretical models for some applications. However, if the functionality of electric machines is vital, a rough estimate is not precise enough. Therefore, the condition of motors and machines need to be monitored during their usage.

2.2 Condition Monitoring and Fault Detection

Diagnosis of machines and mechanical installations were first developed and applied in air and sea transport, and in power engineering [18]. Condition monitoring and early fault detection of electrical machines have been widely investigated. Some of the reported techniques require expensive diagnostic equipment and off-line fault analysis to determine the machine condition. Techniques, such as particle or oil debris analysis which require laboratory analysis of motor oil samples to determine the motor condition, are more suitable for overhaul or routine check up rather than on-line monitoring and fault detection [5]. Even when the result indicates a fault it is difficult to determine the cause of the fault since metal abrasion can be due to a number of faults such as a gear misalignment or extensive bearing wear. Many faults such as a cracked gear cannot be detected since they do not produce

any debris [19]. There are three factors which have prompted the development of automated diagnosis. These are the complexity of the system, the great number of machines operating without any supervision and the high level of reliability required.

Three different kind of parameters are accessible for diagnostic observation [18]:

1. Functional parameters, such as current or maximum speed.
2. Direct symptoms of wear in the form of dimension changes of mechanical components, such as the brush lengths of motors.
3. Dynamic residual parameters which are undesired but accompany the function of the motor such as vibration or acoustic noise.

For the motor in this study, the direct symptoms of wear, such as the brush lengths are difficult to access and measure due to the motor construction. Therefore, only functional or dynamic residual parameters, used in non-invasive fault detection schemes, can be implemented. Non-invasive fault detection schemes are based on easily accessible and inexpensive measurements to predict the motor's condition without dismantling the motor. These schemes are suitable for on-line monitoring and fault detection purposes [20]. They include acoustic noise, vibration and electrical parameter measurements.

2.2.1 Acoustic noise

Acoustic signals carry information about exciting forces and their propagation paths. A motor generates a certain acoustic pattern when it is in a healthy operational state. Wear of a component within the motor may result in a change in its acoustic pattern. These changes may differ when different components wear or fail [5, 18].

Acoustic noise as an indicator of a fault condition is routinely used in different applications. For example, a faulty car exhaust will be detected by the change of its acoustic sound pressure level.

The acoustic noise of motors with attached gearboxes have two major sources. These are the motor noise itself which includes the noise due to its rotation, and the noise generated by an attached gearbox that may consist of straight cut or helical gear meshing, or a combination of both [21].

Motor noise

Acoustic information from rotating machinery has long been used for fault detection [22]. Some of the noise sources are different for dc and induction motors due to their construction. Niwa [11] differentiated two typical noises for small induction motors with sintered porous bearings. One is electromagnetic noise due to the magnetic strain of the stator core. The second source is bearing noise due to the structure of the bearing parts. Instead of a microphone, an accelerometer was attached to the motor frame by means of a magnet, to measure the acoustic noise level. This had the advantage that the ambient noise did not influence the evaluation. Niwa also included an investigation into human perception of motor noise.

Gear noise

Most motors drive a load using a gearbox in order to produce a speed and torque which varies from that of the driving motor. If a motor uses an attached gearbox it has to be considered as a potential source of noise. Blankenship and Singh [23], divided gear noise into two main categories. These are gear rattle and gear whine. Gear rattle is a highly nonlinear, impulsive phenomenon which generally occurs

under light loaded conditions. It consists of repeated gear tooth impacts through backlash due to torsional vibrations of the geared system. Gear whine is a continuous steady state sound which is primarily attributed to transmission error and elastic deformations of the gear teeth under load.

Dynamic gear mesh force, which is the primary exciter of gear noise, is known to be highly dependent on the mean transmitted torque and system gear pair dynamics [23]. The noise depends not only on the gear material but also on the gear geometry. The two main geometries used for motor gearboxes are spur and helical gears. Disadvantages of spur gears arise mainly from their vibration and therefore, noise generation. Their profile gives rise to a regular once-per-tooth excitation, similar to a Dirac impulse, which is very powerful. This results in high vibration levels. Helical gears overcome this disadvantage since their profiles have the effect of averaging the force distribution [21].

The most commonly used gear materials are brass, steel and polymers such as nylon. From the noise aspect, nylon gears have a big advantage over metal gears. The reduction in once-per-tooth excitation forces attenuates the noise in the order of 30 dB [21].

An investigation conducted by Murphy and Sayegh [8] showed that an acoustic screening method for small dc motors could differentiate between good and worn motors based on the auditory judgement of an experienced operator. However, an analysis of the causes of the faults was not reported. Trmal and Johnson [24], have investigated the noise signature of reconditioned gearboxes, driven by a 4 kW motor, for the automotive industry to evaluate their condition. They developed the CROS

(Correlated RMS values in overlapping sections) parameter, which is based on the RMS value in overlapping signal sections, and power deviation as methods to measure the non-uniformity of noise signals. They compared the subjective assessment of the acoustic signal with the calculated CROS parameter value. The authors observed that the recorded signals differed, depending on the consistency of the gearbox to generate repeatable acoustic patterns. As a result, the CROS parameter proved to be a "reasonably reliable" indicator compared to subjective noise assessment. Gaylard *et al*, [25] applied acoustic measurements to identify loose stator coils in 4 MW induction motors. They compared the acoustic measurement results with an electrical off-line winding test method. The acoustic signals were measured by means of a microphone for different motor operational modes such as steady state and start-up. The normalised frequency domain spectrum of the acoustic signal was used as a neural network training vector. They found a close correlation between the electrical and the acoustic method using the start-up noise signals. However, Gaylard *et al*, reported that the majority of the different neural networks that were tested performed "very poorly" due to the use of acoustic data.

2.2.2 Machine vibration

Machine vibration can be measured and analysed to provide a cost-effective and non-destructive method of diagnosing the development of wear or fault conditions. Vibration analysis has been used satisfactorily to assess the condition of electromechanical machines [5]. The vibration signal is usually measured with accelerometers attached to the motor casing. In practice, all machines have associated characteristic vibration patterns. A deterioration in the machine running condition normally produces a corresponding change in vibration signature due to misalignment and increased clearances [26]. Using vibration measurements, it is possible to obtain

information about the machine condition. Mechanical vibration has proved to be one of the most reliable parameters that were used in condition monitoring of large machines [27–29]. However, Emm [30] reported that vibration monitoring of small ac and dc motors resulted in "poor discrimination" between good and faulty motors. This was mainly due to low level repeatability of the results.

Further comprehensive coverage of possible vibration sources in electric motors is given by Cempel [18] and Knights [31]. Dalpiaz and Rivola [32], pointed out that common techniques used to analyse vibration are effective for health assessment, but may not be able to give information about faults in early stages.

Even though vibration monitoring has been utilised for decades, most of the recent research was concerned with electrical monitoring techniques of a motor's condition [33]. One of the reasons for this is that the cost of accelerometers, which are usually used to measure vibration, is prohibitive.

2.2.3 Radio frequency monitoring

One of the first direct electrical methods of testing the condition of an electric motor was based on radio frequency monitoring. This method involves the injection of radio frequency signals into the stator winding of a machine and measuring the changes of the signal waveform to determine whether the winding insulation contains faults [34]. This technique requires expensive equipment and is justified only for use with large and expensive machines. Another technique used to detect winding insulation faults is the surge comparison method reported by Schump [12]. This test generates a high turn-to-turn voltage by discharging a capacitor into the armature windings. The rapid discharge generates a damped sine wave due to oscillation

resulting from the capacitor and the inductance of the motor winding. By comparing the waveforms of the three motor windings of an induction motor, insulation faults were detected. However, a problem is that the surge test gives little warning before winding conduction occurs. Therefore, this method is not suitable to measure wear of the motor.

2.2.4 Motor current signature analysis

An alternative approach to fault detection utilises motor current signature analysis. The basic idea of monitoring the current of a motor is that variations in the load's torque or speed will cause corresponding changes in the motor current. The energy to sustain the mechanical oscillation or vibration must come from the electric motor supply and therefore, it must be detectable in the motor current. The motor could then be used as a sensor akin to an accelerometer. Unlike an accelerometer, the primary purpose of a motor is to convert electrical energy into mechanical energy. Therefore, it may be difficult to detect small fault components in the current signal in the presence of the large energy conversion component and transients from the commutation [35, 36].

Extensive academic and commercial research has been conducted to detect problems in induction motors using the supply currents. These problems are related to rotor asymmetries and are caused by faulty bearings or misalignment of the shaft [36]. It was shown that, when rotor asymmetry is present, the physical air gap of the machine will vary, thus causing the air gap flux density to be perturbed. This perturbation will rotate at shaft speed. The frequencies of the rotating shaft components in the air gap flux are present in the supply current. An approach to distinguish broken rotor bars from asymmetries relies on an examination of sidebands

in the supply current at the rotor bars rotation frequency of the motor [35]. However, this technique requires a large steady state supply current, which is not achievable if the motor has been taken off line [37]. Burnett and Watson [37], enhanced the method of detecting broken rotor bars by monitoring the supply current of an induction motor during the motor's acceleration period. Schoen *et al*, [33] developed a fully automated motor system for induction motors using the supply current's frequency spectrum for fault characterisation by means of artificial neural networks. Changes in the supply current due to rolling-element bearing faults, broken rotor bars or mechanically unbalance were successfully detected by using this method. It has to be noted that this test method worked without the need for the user's interpretation of the motor's current signature. The artificial neural network was trained using the current frequency spectra characteristics while the non-faulty machine ran under normal load conditions.

Few investigations into the condition monitoring of small dc motors have been conducted to date. Motor current waveform analysis has been used in the medical field to control the brushless dc motor of an artificial heart directly, replacing unreliable pressure transducers [38].

The research work reviewed in this section indicated that current signature analysis was a reliable method of early fault detection in induction motors. Research has shown that changes in the condition of the induction motor components, such as rolling element bearings, can be detected in the motor current. The monitoring of the current can be conducted non-invasively during the motor's normal operation. Another advantage is that in order to monitor the current, no additional transducers are required and therefore, problems with transducer attachment do

not occur. Consequently, this leads to the conclusion that the application of current signature analysis for small dc motors may have excellent potential for non-invasive fault detection and usage level estimation of this type of motor. This is despite the fact that estimation of wear and usage of small dc motors using the motor current has not been investigated by other researchers.

2.3 Processing and Analysis Methods

2.3.1 Signal processing and transformation

Observed signals, as acquired from measurement systems, are collected in the time domain. The intention is to process the time domain signal so that it can be used to discriminate between changes in the signal itself over time or as a result of changes in a physical parameter. The discrimination takes place at the analysis stage. Figure 2.1 shows a block diagram of this basic detection strategy consisting of two fundamental function blocks, processing and analysis. This form of signal flow is commonly used in signal processing tasks.

Figure 2.1: Basic detection strategy.

Some of the extracted features depend on the type of the selected processing technique. They usually describe some specific local waveform property in the time or frequency domain. Examples of such features are the magnitudes of specific spectral components. Other features describe signal properties of more global character, such as the crest factor which can be used as a measure of signal peakness [22].

Time domain processing

Time domain signal processing methods are normally used to describe certain aspects of the signal and reduce the amount of recorded data. These may be certain local properties such as the peak value reached by the signal or statistical information such as the average value of the signal [39]. Traditional time domain signal analysis methods include the mean value,

$$\overline{x} = \frac{1}{N}\sum_{i=1}^{N} x_i \tag{2.1}$$

or the root mean square (RMS) value [40],

$$x_{RMS} = \sqrt{\frac{1}{N}\sum_{i=1}^{N} x_i^2} \tag{2.2}$$

where, x_i is the discrete sample of the signal and N is the number of samples. The RMS value on its own has been used as a feature extraction method by researchers such as Badi *et al*, [41]. Other researchers used a moving average window in order to reduce the noise in a noisy input signal,

$$y_t = \frac{1}{N}\sum_{i=t-(N-1)/2}^{t+(N-1)/2} x_i \tag{2.3}$$

where, x_i is the discrete input data, N is the window length, and y_t represents the data after smoothing [42].

It was reported by Menendez *et al*, [43], that even basic statistical processing can improve the analysis result such as calculating the second statistical moment or variance, σ_n^2, of the input signal:

$$\sigma_n^2 = \frac{1}{N-1}\sum_{i=1}^{N}(x_i - \overline{x})^2 \tag{2.4}$$

Statistical moments describe the characteristics of the probability density of the signal. The second moment indicates the variance of the signal. The third moment, the skew, indicates the symmetry of the signal. An often applied method in vibration analysis is the fourth moment, the kurtosis [22,41]. It is given by,

$$\mu_n^4 = \frac{1}{N-1}\sum_{i=1}^{N}(x_i - \overline{x})^4 \tag{2.5}$$

and describes the tails of the amplitude density function and therefore, the non-uniformity of the signal [24,44].

Some of these methods have the advantage of indicating the machine condition by a single figure. This is useful because a simple threshold function may be used as an indicator if, a machine part has to be maintained or changed. However, complex fault and wear processes cannot be easily identified using a single number combined with a static threshold value [22]. This is especially the case for inexpensive or small machines with high production tolerances and therefore, a high variability of the observed parameters.

Cattarius and Inman [45], investigated the use of a time domain processing method for the analysis of vibration signals. The difference in the time response of vibration signals to a harmonic input signal was used for discriminating between healthy and damaged helicopter blades. The signals were measured using fixed, surface-bonded, piezoceramic patches attached to the blade. This technique enabled the investigators to identify small mass decreases (holes) and increases (bullets).

A different approach in time domain processing is digital demodulation. A fault in rotating machines causes variations that are superimposed on the normal rotation. This can be identified intuitively as a type of modulation process [46, 47]. McFadden [48] used simple demodulation techniques, such as amplitude and phase modulation functions, to detect gear faults. The researcher showed that it is possible to detect and discriminate between fatigue cracks in early and advanced stages. However, this technique is not suitable for analysing the vibration signals of gears that do not have any cracks yet. It should be noted that the definition of an early crack in McFadden's investigation was a crack that is already 20 mm long and 1.2 mm deep.

Another time domain feature extraction method was developed and patented by Wahab and Gough [49]. This technique combined data reduction and extraction of features from time domain signal's shape. It was originally developed for processing of biological signals and used as a signal processing method to generate features for neural network classifiers. No studies on the application of this technique have been reported. However, this technique appears to have some favourable characteristics and will be investigated further in section 5.1.2.

Frequency domain processing

It is possible to characterise signals in other domains by applying specific mathematical operations to them. Some of these operations may be viewed as transformations, with a new variable defining the domain of the signal, such as the Fourier transform [22]. The Fourier transform has been used in the processing and feature extraction of signals recorded during the monitoring of electrical machines. It provides the frequency spectra of signals [50].

The spectra of discrete signals are computed using the discrete Fourier transform (DFT) given by equation 2.6, where $X\left(\frac{n}{NT}\right)$ denotes the discrete Fourier transform of $x(kT)$. In this equation, N is the number of consecutive samples of the signal, T is the sampling interval, and k represents the harmonic number of the transform component [51],

$$X\left(\frac{n}{NT}\right) = \sum_{k=0}^{N-1} x(kT)e^{-j2\pi nk/N} \quad n = 0, 1, ..., N-1 \tag{2.6}$$

It can be assumed that rotating machinery produces a repeating pattern depending upon the speed of the machine. Therefore, speed fluctuations due to fault conditions may change the spectrum of a measured machine parameter. Several approaches in detecting specific faults using spectral analysis have been reported [52, 53]. Kliman and Kögle [54], proposed to examine the relative behaviour of the fundamental and higher harmonic sidebands in the current of induction motors, so as to detect broken rotor bars.

Altawil and Rodd [55], used the first six harmonics in the current spectrum of a shunt-wound dc motor driving a conveyor belt system to detect several faults under various operational conditions. Alguíndigue and Uhrig [56], also used the frequency spectrum of the vibration signal from a steel sheet manufacturing mill combined with a back-propagation artificial neural network for classification.

Cattarius and Inman [45], questioned the reliability of frequency domain analysis of the experimental results for damage detection when the damage is relatively small.

Time-frequency domain processing

The Fourier transform cannot take the temporal variation of the spectral characteristics of a non-periodic signal into account, such as spikes due to defective rolling element bearings [57]. Time-frequency analysis methods apply to signals where the spectral contents or the statistical properties vary with time. In other words the signal is quasi-stationary or non-stationary [58]. Time-frequency analysis methods offer another possible solution for detecting early faults in a machine. By estimating the energy distribution of the signal in the time-frequency plane, changes in the amplitude and phase of the monitored signal can be identified in the time and frequency domain. The three main time-frequency analysis methods currently used are the short-time Fourier transform (STFT), bilinear transforms and the wavelet transform (WT).

The most popular of the time-frequency distributions is the STFT whose square modulus is called the spectrogram. The solution for the analysis of time varying-signals is to turn to local estimations. The STFT analyses the signal using a moving window $w(m)$, with the window length L, in the interval $0 \leq m \leq L-1$ and is given by [59],

$$X(n,k) = \sum_{m=0}^{L-1} x(n+m)w(m)e^{-j2\pi mk/N} \quad 0 \leq k \leq N-1 \tag{2.7}$$

where, x is the input signal, k represents the harmonic number of the transform component and N is the number of consecutive samples of the signal. This approach suffers from limitations due to the fixed time-frequency resolution once a window is chosen. Good time resolution is achieved by a short window, whereas good frequency resolution is achieved by a long window. The fact that the time

and frequency resolutions cannot be made better simultaneously is known as the Heisenberg uncertainty principle [60].

The application of bilinear transforms makes it possible to overcome the limitations of the STFT, since these transforms are not based on signal resolution. Bilinear transforms like the Wigner-Ville distribution (WVD) are characterised by an invariance to time and frequency shifts [61]. The discrete Wigner-Ville distribution is given by [62],

$$W_f(n,\theta) = 2 \sum_{k=-N+1}^{N-1} e^{j2k\theta} f(n+k) f^*(n-k) \quad , \tag{2.8}$$

where, $f(n)$ is the discrete input signal, $f(n)^*$ is its complex conjugate, θ the frequency variable, N the number of samples and k the time delay.

Unfortunately, the bilinear structure of the transform causes interference due to cross-products between the different signal components and this increases with the number of components in the signal [61]. The WVD cannot discriminate between high and low frequencies because of aliasing components that are present in the general case [62]. Further information on WVD can be found in references [62–64].

The WVD is an effective method to obtain time dependent information from supervised machines [65]. Forrester [66] compared the WVD with other existing vibration analysis methods such as the narrow band enhancement technique developed by McFadden [67]. He has shown that the WVD is capable of detecting the type and the extent of gear faults. Compared to the WVD, other methods could not distinguish between different degrees of tooth cracking and therefore, cannot

provide reliable information on the extent of the gear damage.

Chiollaz and Favre [58], investigated the use of the WVD for the noise analysis of a vehicle combustion engine. Noise was measured using nine accelerometers attached to different locations at the cylinder head. The authors concluded that conventional time and frequency domain processing techniques were not sufficiently accurate to identify the vibro-acoustic excitation and transfer mechanisms. In comparison, the WVD has shown precise diagnosis and identification capabilities, in both the time and frequency domains.

Wang and McFadden [68], compared the WVD with the spectrogram for the early detection of gear failures using vibration signals. The signals were obtained from one of a series of large reduction gearboxes, each containing three double-helical gears. They concluded that the spectrogram has advantages over the WVD in the analysis of vibration signals. Since machine or gear vibration signals are usually multi-component or noisy signals, the WVD cross-components make it very difficult to interpret the results obtained. Contrary to Forrester [66] and Chiollaz and Favre [58] they discovered that, due to the spectrogram windowing function short duration signals resulting from local gear tooth damage could not be easily detected.

The Wavelet transform (WT) is the latest time-frequency analysis method used for condition monitoring and fault analysis [69, 70]. The wavelet transform of a signal, $x(t)$, is defined by,

$$(W_\Psi x)(b,a) = \frac{a}{2\pi\sqrt{a^n}} \int_{-\infty}^{\infty} x(t)\Psi^*_{(b,a)}(t)dt \tag{2.9}$$

with the analysing or mother wavelet Ψ defined as,

$$\Psi_{(b,a)}(t) = \frac{1}{\sqrt{a^n}}\Psi\left(\frac{t-b}{a}\right) \tag{2.10}$$

In the above equations n is a constant, b is the translation parameter and scale parameter a can dilate and compress and has no units. The term translation corresponds to time and scale is defined as reciprocal of the frequency. Only a few applications of the WT exist in the field of machine fault diagnosis [32]. One example was reported by Staszewski and Tomlinson [71]. The investigators used the WT to compress the feature elements of the vibration signals which were used to detect broken teeth in a spur gear. Lin and McFadden [72], applied a b-spline linear WT to the vibration signal of a helicopter gearbox to visually detect cracked gears by comparing the plotted transform output. However, like the STFT, the wavelet transform has the disadvantage of signal resolution [61].

2.3.2 Analysis methods

The term, analysis, may cover any context in which some decision or forecast is made on the basis of available information. Various methods such as statistical analysis or artificial neural networks were applied to analyse acquired and processed signals.

One of the simplest analysis methods is to display a raw or processed signal for subjective analysis by an operator. This may be achieved by displaying the signal on an oscilloscope [12] or a computer screen [72]. An operator can then decide what action should be taken based on this visual interpretation. A number of different methods were applied to simplify the analysis and decision making process. A commonly used method is thresholding. As an example, threshold analysis was applied

to the frequency spectrum of an acoustic signal to test cracks in fan blades and aerosol cans [73]. Discrimination between unbeaded, uncleared and dented cans was made possible using this method. However, it was reported that production line noise might influence the test results. This shows that the application of thresholds may not be satisfactory if the test environment changes.

The frequency spectrum as a processing method for later analysis was used in the medical field such as doppler ultrasound applications. The pulsatility index (PI) was a factor calculated by the peak-to-peak excursion divided by the mean height of the frequency spectrum of the blood velocity/time waveform over one cardiac cycle. This technique was reported as achieving a 89% correct classification rate in the diagnosis of diseased lower limbs [74].

Analysis may also involve data classification by learning from experimental data. This is also known as clustering. In order to automate the decision process, the feature vectors generated by processing have to be analysed or classified by a computer. Different methods have been used in the analysis of feature vectors. These include statistical and artificial neural network (ANN) approaches.

Statistical techniques

Statistical approaches can be traced back to the 1930's in the work on linear discriminant analysis [75]. Simple statistical methods such as the nearest neighbourhood technique have shown good results in cases where a distinction between a good and bad condition has to be made [46]. Sigler *et al*, [46] compared a nearest neighbourhood classifier with a perceptron, an artificial neuron with a threshold activation function. The comparison showed that the perceptron could give a more reliable

classification result using the same input vector for both classifiers. Another statistical classification approach was that of Spoerre and Ben Wang [2], who used the exponentially weighted moving average (EWMA), equation 2.11. The EWMA is a statistical process with a characteristic that gives less weight to data as it becomes older. This is given by,

$$EWMA = y_{t+1} = \sum_{i=0}^{t} w_i y_i \tag{2.11}$$

where, the weights are,

$$w_i = \lambda(1-\lambda)^{t-1} \tag{2.12}$$

and, λ is a chosen constant that determines the rate of decay of the weights and in turn the amount of information recollected from past data. It was reported that the EWMA is capable of estimating between four different fault classes of a machine. However, the technique was not able to determine the correct fault class in all cases [2].

Staszewski and Tomlinson [71], used statistical similarity analysis of vibration signals to discriminate between normal and faulty conditions of spur gears after wavelet processing. However, visual inspection of the classifier input signals was still necessary to localise the fault.

A different statistical analysis method is the Kullback-Leibler dissimilarity measure between a time series. The Kullback-Leibler number has a basic role in the information theory approach to statistics and in statistical physics [22].

Artificial neural networks (ANNs)

Artificial neurons are equivalents of the neurons found in the human brain. The concept is based on how biologists believe the brain learns to recognize patterns. Neural networks offer a promising methodology for an improved understanding of problems which are difficult to solve by traditional approaches. They have been successfully used in various pattern recognition and classification tasks [76–78].

ANNs have been widely used in medical signal processing. In areas such as ECG analysis, back-propagation (BP) ANNs were able to classify the ST-T segments of an ECG signal with an accuracy of 90%-95% [79]. Learning vector quantization (LVQ) networks were used for classification purposes in speech recognition applications. McDermott and Katagiri, [80] achieved recognition rates of over 98% for several Japanese phonemic classes.

The previous examples of ANN applications indicate that fault diagnosis of machinery may also benefit from the application of this approach. In general the main problem with analysis methods for fault diagnosis can be summarised briefly by the following statements [77] :

- The relationship between the faults and measurements are unknown.
- Each fault situation affects many measurements.
- The dynamics of the wear process are not taken into account.

Neural networks are particulary useful for the problems of condition monitoring and diagnostics [81]. An ANN can automatically store knowledge about the faults or malfunctions in the machine being monitored by learning to associate faults with

historically collected data. These associative diagnostic capabilities make ANNs superior to conventional methods of machinery fault diagnostics [82].

Brotherton *et al*, [83] and Rock *et al*, [84] showed that ANNs are well suited to classify different faults in gearboxes. Altawil *et al*, [85] used a BP network to discriminate between scoring and scuffing wear modes of gears using the harmonics of the vibration spectra as ANN inputs. A successful analysis of induction motor gear vibration with a four layer BP ANN was reported by Ho and Lau [26].

Paya *et al*, [86] have used the wavelet transform to discriminate between a range of rolling element bearing conditions on a modelled drive-line. The WT has been applied on vibration signals taken from the bearing housing. The ten most dominant features, selected visually, were combined as an ANN input vector. The trained two layer BP network was able to achieve an average correct classification of 96%.

Figure 2.2 shows a simple artificial neuron. The first use of artificial neural networks can be dated back to the 1940's [87]. The key parameters that determine the behaviour of a neuron are its activation function and the pattern of weighted connections over which it sends and receives signals [88].

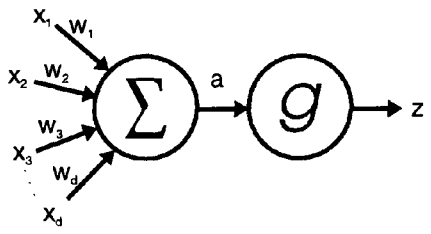

Figure 2.2: Artificial neuron.

The input signal, x_i, at input i is first multiplied by a parameter, w_i, known as

weight, and is then summed with all the other weighted input signals to give,

$$a = \sum_{i=0}^{d} w_i x_i \tag{2.13}$$

The output, z, of the neuron is the result of applying the activation function, g, as shown below,

$$z = g(a) \tag{2.14}$$

A number of activation functions for neurons such as a linear, threshold, threshold linear and sigmoidal were investigated. The sigmoid function is the most frequently used activation function because of its non-linearity and is given by,

$$g(a) = \frac{1 - e^{-\sigma a}}{1 + e^{-\sigma a}} \tag{2.15}$$

where, σ is the steepness factor [88].

When using a multilayer network non-linear activation functions have to be used instead of linear functions. Feeding a signal through two or more layers of linear processing elements are no different from what can be obtained using a single layer network.

This simple model of a neuron is the basic element in many artificial neural network models [89]. It is the highly complex interconnectivity of these artificial neurons which enables them to solve complex recognition, classification and association problems. A set of artificial neurons connected together and arranged in layers is called an artificial neuronal network (ANN). An ANN can be simulated in a computer. Figure 2.3 shows a three layer neural network with an input layer, a

single hidden layer and an output layer. As in the brain, ANN learn by repetitive exposure of problem examples until the measured errors are below a specified minimum. Learning can be either supervised or unsupervised. A comprehensive review of neural network principles and history can be found in Fausett [88] and Harvey [90].

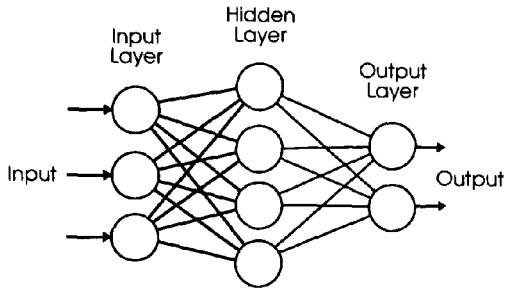

Figure 2.3: Multilayer neural network.

Neural network architectures

Several different neural network paradigms have been developed over the past few decades. Current neural network structures can be divided into three main groups [55]:

- The feedforward error back-propagation networks.
- The self-organising, feature-mapping Kohonen network.
- The massively interconnected networks such as Hopfield nets.

Chow *et al*, [20] estimate that over 80% of the current ANN applications consists of feedforward networks. The term feedforward implies that the input signal flows from the input units to the output units in a forward direction. This section will cover two commonly used feedforward networks which have been used in this study. The ANNs described here are the back-propagation (BP) and the learning vector quantization (LVQ) architectures.

BP ANNs A BP ANN can have multiple layers between the input and output layers. Each layer is fully interconnected to the succeeding layer. A single layer BP ANN is limited in the mapping it can learn, whilst a multilayer network with more than one hidden layer can learn any continuous mapping to an arbitrary accuracy [88]. However, in many applications, neural networks consist of only one hidden layer. This is because multiple layers tend to loose their ability to generalise with increasing complexity [76].

The back-propagation paradigm is the most frequently used algorithm for adjusting the weights of a multilayer neural network during training [85]. A BP network is trained in three steps. These are:

- Feedforward of the input training vector.
- Calculation and back-propagation of the associated error.
- Adjustment of the network weights.

The aim of the training process is to minimise the global error, E, of the network by modifying the weights. A given set of weights, w_{ij}, are adjusted by Δw_{ij} in order to decrease the global error by the gradient descent rule as follows:

$$\Delta w_{ij} = -\eta \frac{\partial E}{\partial w_{ij}} \tag{2.16}$$

where, η is the learning rate [91]. A frequently used error function is the delta-rule which is defined by,

$$\Delta w_{ij} = -\eta x_i (t_j - y_j) \tag{2.17}$$

where, x_i is the training input vector, t_j the target output for input vector, x_i, and y_j is the computed output for input vector, x_i [88].

A problem of the gradient algorithm is the setting of an appropriate learning rate. A fast learning rate causes difficulties in finding the global minima of the error function, whereas a slow learning rate leads to slow or imperfect learning. Two possible consequences are visualised in figures 2.4 and 2.5.

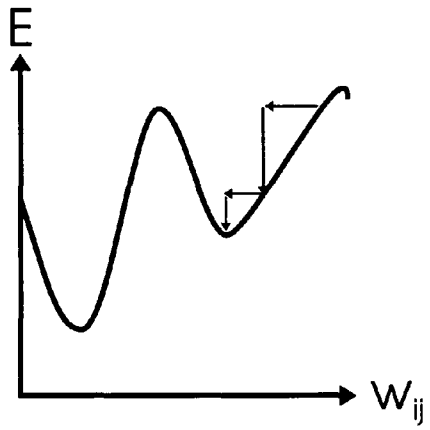

Figure 2.4: The problem of local minima for BP ANNs.

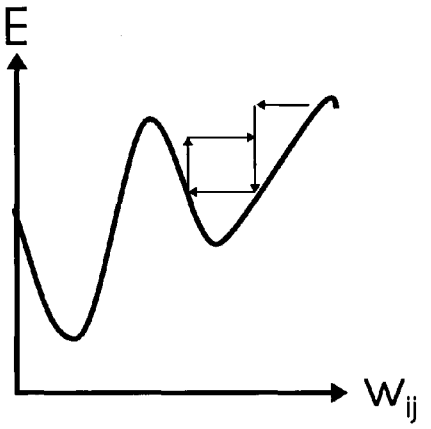

Figure 2.5: The problems of oscillation in steep troughs for BP ANNs.

The effect in figure 2.4 occurs when the neural network cannot be trained to minimise the global minimum because it is trapped in a local minimum. The graph in figure 2.5 shows that the network starts to oscillate in a steep trough. This happens if the gradient at one slope of the trough is steep enough to point to the other slope of the same trough. If the gradient on the other side is as steep as the previous gradient it will point back to the other side and so forth. To overcome this problem, the momentum parameter is introduced with the consequence that at each step, weight adjustments are based on a combination of the current weight adjustment and the weight change from the previous step. This behaves as a low-

pass filter on the weights since general trends are reinforced whereas, oscillatory behaviour is cancelled out [92].

LVQ ANNs LVQ networks are classification networks that assign vectors to one of several classes. An LVQ contains one Kohonen layer which both learns and performs the networks classification. Self-organizing maps (SOM) and LVQ ANNs consist of Kohonen neurons [91]. However, the output of the LVQ training set must be known since it is a supervised learning ANN, unlike the unsupervised learning SOM. If supervised learning is possible, the LVQ is usually two to three times more accurate than SOM networks [93]. The weights of the neurons in a LVQ network are determined by supervised learning as in BP ANNs. The advantage of an LVQ, is that it allows a high variability in a single class unlike the BP ANNs.

LVQ consists of a cluster of unsorted code book or reference vectors distributed in such a way that a good coverage of the input space is achieved. More than one code book vector exists for each class of input vectors. In the training process, a new input vector is compared with all reference vectors. The closest reference vector identifies the class of the new vector. For LVQ networks the input vector is compared with the code book vector and the neuron whose weight vector is closest to the input vector is the winner. The values for the weights which minimise the classification error are defined by,

$$w_c(t+1) = \begin{cases} w_c(t) + \alpha(t)[x(t) - w_c(t)] & if\, class(w_c) = class(x) \\ w_c(t) - \alpha(t)[x(t) - w_c(t)] & if\, class(w_c) \neq class(x) \end{cases} \tag{2.18}$$

where t is the discrete time index and $\alpha(t)$ is a monotonically decreasing function

of time. Figure 2.6 shows a graphical interpretation of equation 2.18. The weight vector of the winner neuron will move closer to the input vector if it is in the same class. Otherwise it will move away from the input vector [91,94].

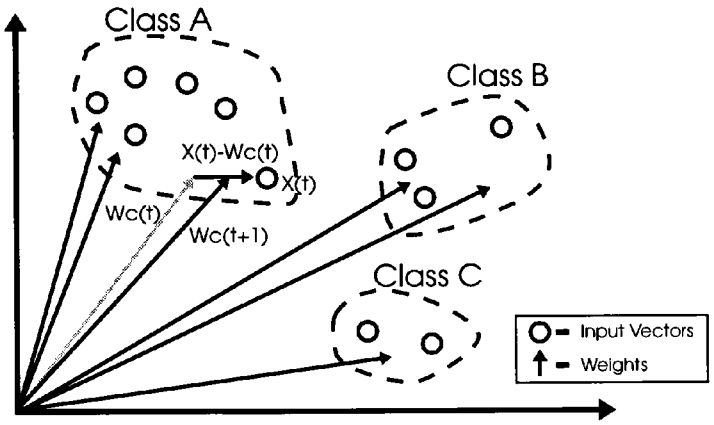

Figure 2.6: Adaption of the next weight, w_c, to the input vector, $x(t)$.

2.4 Summary

This chapter has presented the literature survey that was conducted during this study on faults and wear in electrical motors. It included fault detection and diagnosis, wear parameters and patterns, and usage level estimation. In addition, the chapter has covered signal processing and data analysis methods that are suitable for interpreting the information contained in the physical fault and wear indication parameters of the motors.

The main finding of this literature review is that small dc motors have rarely been investigated for fault detection and usage level estimation. The vast majority of the research work that was conducted on condition monitoring and fault diagnosis covered very large motors, especially induction motors. Therefore, this study covers

new territory and fills a clearly defined research gap in the field of wear characterisation and usage level estimation of small dc motors.

Although most previous research studies have covered large induction motors, their results have significant relevance to this study. Many faults in large induction motors are common to those in smaller dc motors due to the similarities in their mechanical constructions. Therefore, the fault symptoms and wear indication parameters of induction motors may have similarities with those of small dc motors. More important, the test, monitoring, signal processing and data analysis methodologies are significant for this study.

The literature survey has shown that previous researchers used many physical parameters to assess the condition of a motor and for fault detection. The main motor fault and wear indicating parameters were acoustic noise, vibration and current signals. As all these parameters can be measured non-invasively, they were investigated further during this study.

A wide range of processing methods were used by previous researchers to reduce the complexity, enhance the features and reduce the data volume of the wear indicating parameters. These methods were applied to prepare the recorded signals for subsequent analysis.

Time domain processing included signal smoothing and the calculation of statistical parameters, such as the mean, RMS value and several types of statistical moments. Although individual statistical parameters were shown to be insufficient to characterise the signals of the fault and wear indicating parameters, they may

add significant benefits when combined with other signal processing parameters and representations. The technique of Wahab and Gough [49] was identified for further consideration due to its potential in characterising a signal shape.

The Fourier transform and its discrete version was used by many researchers to investigate the spectral contents of the fault and wear related signals. The limitations of the Fourier transform have led many researchers to explore various complex time-frequency transforms. Various degrees of success were reported by researchers in using these transforms, with the STFT being the most popular. In general, most of these transforms have a high computational complexity.

Many researchers used visual inspection of the fault and wear raw signals or their processed versions, others utilised techniques for data analysis. ANNs were reported by many researchers as ideal analysis tools for motor fault detection and classification. Their strength stems from their ability to solve problems where the relationships between the symptoms and outcomes being monitored is not clearly identified and cannot be expressed in clear mathematical terms. The BP and LVQ ANNs were identified as the most suitable for the analysis of the fault and wear indicating parameters.

Chapter 3

DC Motor Operation and Wear Characteristics

This chapter is aimed at describing the operation of dc motors and analysing the wear mechanisms of the selected experimental test object. This analysis is essential to identify potential motor wear indicators, and to enable the planning of the experimental part of this study.

Section 3.1 analyses the operation of dc motors and relates their mechanical and electrical parameters. This analysis describes the relationship between the parameters in an ideal situation and outlines the deviations from it due to imperfections.

The rationale for selecting the dc motor that was used as an experimental test object in this study is presented in section 3.3. The specifications of the motor are described in section 3.4 including the design changes that were introduced by the motor manufacturer throughout its production history. The operation and loading of the test motor in its real life application are described in section 3.5.

A detailed analysis of the wear process in the test motor is presented in section 3.6. This section covers wear in both the electrical and mechanical parts of the motor. It also considers the wear indicators that would enable the assessment of the motor usage level in an application. A summary of this chapter appears in section 3.7 and lists the main causes of wear and their associated indicators.

3.1 Commutator Machines

Commutator machines normally operate with direct voltage supplies and are usually referred to as direct current (dc) machines. They are widely used in battery powered electric vehicles, as vehicle starter motors and as motors for commercial and industrial equipment. Major advantages of dc motors include their high starting torque and the ability to control their speed by varying the supply voltage. This section provides a brief description of dc machines. More comprehensive information about dc motors can be found in Slemon [95] and Meisel [96].

3.1.1 Magnetic system

The magnetic field in a commutator machine is produced by permanent magnets or field coils on the stator. The current-carrying coils that interact with this magnetic field are placed on the rotor. These coils are switched by a copper commutator mounted onto the rotor as it passes stationary carbon brushes that lead to the motor terminals.

3.1.2 Rotor windings and commutator

In order to make efficient use of the available rotor or armature surface area, conductors are distributed in slots over the circumference. To obtain continuous relatively

ripple free torque, it is desirable to have the patterns of the conductor current directions as shown in the winding of figure 3.1.

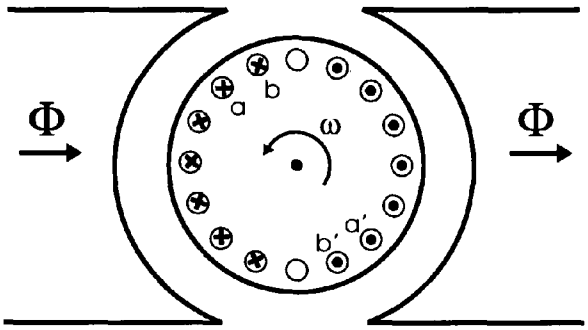

Figure 3.1: Desired pattern of armature conductor current flow.

In order to maintain this pattern, each of the sequential coils is connected to an insulated commutator segment. The stationary brushes are placed onto the commutator surface in such a way that they can feed the current from the external electric system into two parallel paths through the closed loop of the serially connected rotor coils. Each conductor carries half the terminal or armature current, i_a. The width of the brush is such that it causes a short circuit between the two adjacent commutator bars a and b when the coil is ideally located in an area of the rotor between the poles and thus, does not have an induced voltage (figure 3.1). If the commutation is not ideal sparking occurs when the current in the short-circuited coil is forced to change rapidly. This commutation sparking will cause deterioration of both the commutator segments and the brushes, and greatly shorten the operating life of the machine [95].

3.1.3 Torque and generated voltage

The armature winding of a two pole machine has a total of N_a turns in its series-connected coils. Each of the $2N_a$ conductors carries half the armature terminal

current, i_a, with the exception of the turns in the coil being commutated from one path to the other. The linear current density, K, per unit of the rotor periphery is then given by [95],

$$K = \frac{2N_a}{2\pi r_m}\frac{i_a}{2} \tag{3.1}$$

Where, r_m, is the rotor radius. Since the flux density, B, is radially directed, the force per unit area of armature surface under the poles is BK. Thus, the torque exerted on the rotor is

$$\begin{aligned} T &= 2w_m l_m r B K \\ &= \frac{N_a}{\pi}(B w_m l_m) i_a \qquad (3.2) \\ &= k\Phi i_a \qquad (3.3) \end{aligned}$$

where, w_m is the pole width, l_m is the axial length of both pole and rotor, and Φ is the magnetic flux per pole. In a two-pole machine, the constant, k, depends only on the number of armature winding turns.

Ignoring losses, the electrical power input, p_{elec}, to the armature winding equals the mechanical power output.

$$\begin{aligned} p_{elec} &= e_a i_a \\ &= T\omega_0 \qquad (3.4) \\ &= k\Phi i_a \omega_0 \end{aligned}$$

where, e_a is the induced or generated voltage in each parallel path of the winding and is defined by [95–97]

$$e_a = k\Phi\omega_0 \tag{3.5}$$

3.1.4 Equivalent circuit

The ideal motor is described by equations 3.3 to 3.5. For a more realistic model, imperfections have to be considered. There is always a power loss in the armature coils due to their resistance, R_a. The armature circuit also has an inductance, L_a, representing the flux linkage of the armature windings. Including these parameters and the induced voltages, e_a, the armature circuit may be represented as shown in figure 3.2 [95].

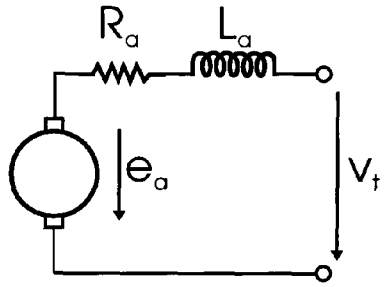

Figure 3.2: Equivalent circuit of an armature controlled dc motor.

3.2 Selection of the Experimental Test Object

This study is aimed at investigating the wear characterisation and usage level estimation of small dc motors which are widely used in commercial and consumer products. As a result, it was essential to select a suitable dc motor as the test object for the experimental work. It should be a typical representation of dc motors

used in modern equipment, both in its application area and operational modes.

Following extensive discussion with the collaborating organisation, Xerox, it was decided that the company's photocopying machine type 5047 represented a typical system which utilises a large number of dc motors. For such equipment, asset recovery related to dc motors can have significant economic and environmental benefits.

The 5047 is a mid-range office photocopying machine. It represents a large electromechanical assembly with multiple functional sub-assemblies such as the paper tray, variable optical zoom, and paper transport sections. The copying machine includes 12 motors of various sizes ranging from 12 V, 1.2 W dc to 220 V, 60 W ac motors. The number of motors used in large copying machines can be as high as 80 [9].

The paper tray sub-assembly and its four motors represents a typical electromechanical section within the machine. As a result it was decided to select the paper tray dc motor for the experimental investigations of this study. The 127K01800, is a middle of the range motor and its operation is typical of all motors within the 5047 and many similar commercial equipment [9]. The specification and operation of this motor are described in the following section.

3.3 Motor Specifications

The test objects of this research project are small dc motors with brushes, that are used in photocopying machines. A typical representative of these motors, which was used during the experimental investigations, has the following specifications [98]:

Description:	Brushed permanent magnet direct current motor with inline gearbox.
Torque Output:	0.65 Nm at 340 rpm nominal.
Supply Voltage:	17 V $\pm$ 1 V (smoothed and regulated).
Number of Commutator Segments:	7
Minimum Expected Usage:	$\geq$1.5 million motor starts.
Typical Operation:	Duty Cycle: 0.5 s on 0.5 s off continuously under maximum load for 15 minutes followed by 3 minutes rest period.
Motor Reference No. :	127K01800
Manufacturer:	Gebrüder Bühler Nachfolger GmbH, Germany.

Motor operating requirements:

Start Torque:	1.2 Nm
Run Torque:	0.65 Nm $\pm$ 0.1 Nm.
Time-to-Speed (section 3.6.2):	0.12 s maximum at 0.75 Nm.
Maximum Running Current:	0.45 A at 16 V.

The motor is used in different photocopying machines. One of its major applications is its use as a paper feed motor in the Xerox photocopying machine of type 5047. Figure A.1 in appendix A shows a mechanical drawing of the motor.

In order to determine the wear factors of this motor the principle of its operation and possible wear indicators were analysed. It should be noted that the motor cannot be disassembled due to its encapsulated, non serviceable construction. Maintenance

of the internal parts of the motor is therefore, not possible. It is also not possible to re-assemble the motor without special equipment. However, the gearbox of the motor can be opened by loosening its M3 screws. Consequently, only non-invasive analysis techniques can be applied to determine the wear and usage of the motor.

3.4 Motor Design Differences

The design of the test motor was modified five times over its manufacturing period. The different designs can be identified by the type number on the motor's label and are listed in table 3.1.

Motor type	*Made in*	*Manufacturing period*
61.46.16	Germany	1987 - 1990
61.46.20	Germany	1990 - 1994
1.61.046.020	Germany	1994 - present
61.46.025	U.S.A.	unknown - 1988
61.46.020	U.S.A.	1988 - present

Table 3.1: Manufacturing periods of the different motor designs.

According to the manufacturer, the main reasons for the changes in the motor design were to reduce the production costs and the emission of acoustic noise. Steel and nylon compound gears were used in the 61.46.16 and 61.46.025 gearbox designs. According to the motor manufacturer, changing to gears made entirely of nylon reduced both the production cost and the acoustic emission [99].

3.4.1 Gear design

Figure 3.3 and Table 3.2 show the different motor design types and gearbox configurations.

Motor type	*G1*	*G2*	*G3*	*G4*
61.46.16	steel, helical	nylon, helical	steel, spur	steel, spur
61.46.020	steel, helical	nylon, helical	nylon, helical	brass, helical
61.46.20	steel, helical	nylon, helical	nylon, helical	brass, helical
61.46.025	steel, helical	nylon, helical	steel, spur	steel, spur
1.61.046.020	steel, helical	nylon, helical	nylon, helical	brass, helical

Table 3.2: Gearbox configurations in different designs.

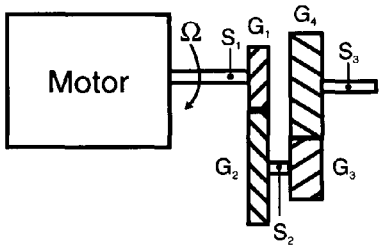

Figure 3.3: Gear arrangement in the gearbox.

Two different gearbox designs were in use with the five motor types. They differed only in gears G3 and G4. Motor designs 61.46.16 and 61.46.025 were configured with steel spur gears and types 61.46.020, 61.46.20 and 1.61.046.020 were configured with nylon helical gears. The three shafts are labelled S1, S2 and S3 in figure 3.3. S1 is the motor shaft, S2 is the shaft coupling gears G2 and G3, and S3 is the output shaft of the motor gearbox, which is used to couple the motor to a load.

3.4.2 Hardness of the graphite brushes

The hardness details of the carbon brushes are unknown [99]. Therefore, an investigation into the brush hardness in the different motor designs was conducted. A constraint on this investigation was the limited number of disassembled motors supplied by Xerox. Therefore, only three motors of three different designs were used to

conduct the experiments. However, the sample size was sufficient to indicate if the brush material has changed significantly. The experiments were carried out using the facilities of the Department of Mechanical and Manufacturing Engineering at the University of Glamorgan.

Most brush materials have a composite structure and their physical properties cannot be held within absolute limits [97]. This is illustrated in figure 3.4 which shows the granular structure of a graphite brush used in commutator machines.

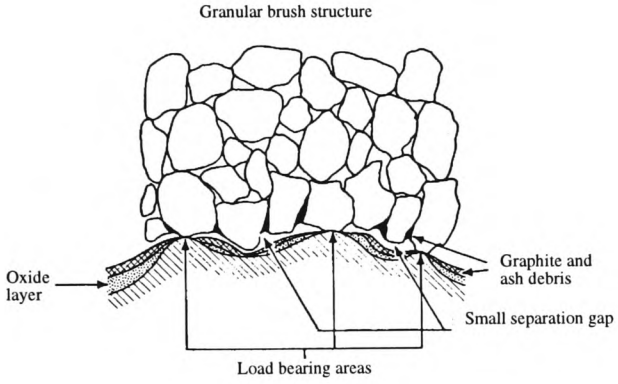

Figure 3.4: Graphite brush structure - Courtesy of Morganite Electrical Carbon Ltd.

The hardness of graphite is measured by instruments such as the scleroscope, the Rockwell ball indenter, and other indentation devices. The Shore scleroscope is a dynamic hardness measuring device used in the carbon industry. Scleroscope hardness is measured by the height of rebound of a diamond-tipped hammer falling freely in a glass scale from a given height. The scleroscope readings are high for a brittle, weak material, and low for a soft, strong material. The Rockwell type machines in contrast, shows low readings for a brittle material that breaks away under load, but high for a soft, strong material that supports the load [100].

A measure of hardness can be used to compare the materials of different brushes. Tests in this investigation were carried out using indenters of the Vickers type. The Vickers test uses a diamond indenter which is pressed onto the surface of the test material. The result is a square-shaped impression. The length of the impression diagonals are a measure of the material hardness which is expressed as the diamond pyramid number (DPN) [101]. Three measurements were made for each brush. The second brush (B) of the 61.46.16 design broke under the applied load of the test machine. Table 3.3 shows the results of these measurements.

Motor type	*Hardness brush A*	*Hardness brush B*	*Hardness mean value*	*95% Confidence interval*
61.46.16	20.65 DPN	-	20.65 DPN	±1.29 DPN
61.46.20	19.69 DPN	17.62 DPN	18.7 DPN	±2.92 DPN
1.61.046.020	22.73 DPN	24.5 DPN	23.6 DPN	±1.73 DPN

Table 3.3: Graphite brush hardness in different motor designs. Experimental test results.

It can be seen that the hardness of the brushes did not vary by more than 7.5% in the same type of motor. This variation can be attributed to manufacturing tolerances and the composite structure of the brushes. The variations of hardness between different designs were not considerably greater than the variations within one motor. Therefore, it is safe to conclude that the brush materials used in different motor designs were similar.

3.5 Operation in the Paper Tray Application

The wear of a motor is determined by its use and operation in its application. Therefore, a typical application of the test motor was chosen to investigate its wear

parameters. This application is the paper trays of the 5047 copying machine. Four separate paper trays are used in a 5047 copying machine. Paper tray 1 to 3 holds A4 paper and paper tray 2 is used to hold A3 paper as described in table 3.4.

3.5.1 Operational modes of the motor

The motor is used in two different mounting directions in the paper trays of the 5047 copying machine, vertically, and tilted horizontally with respect to the vertical axis. Figure 3.5 shows the side view of an A4 paper tray. The load is applied in the same way in all mounting positions. A spring behind the paper feed axis bevel gear drives the paper feeding roller, feeding the paper into the copying machine (figures 3.5 and 3.6).

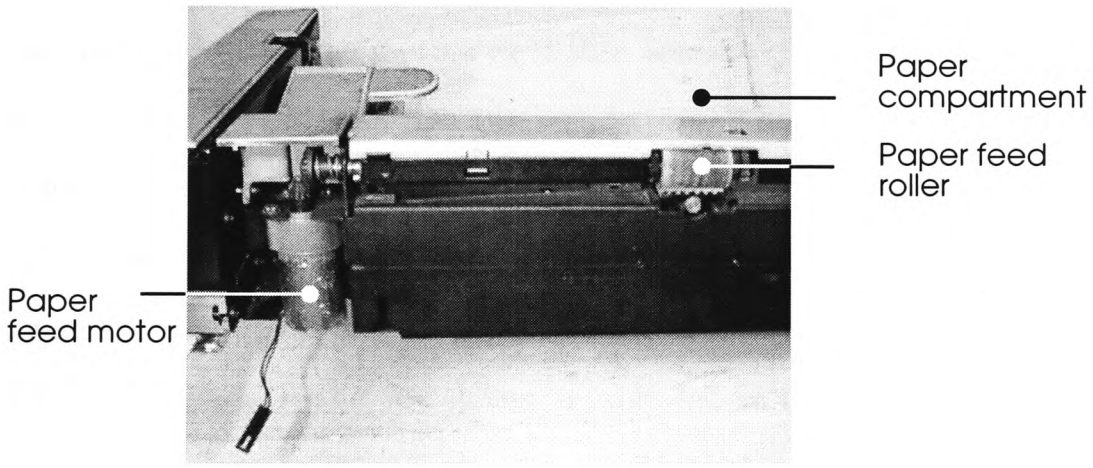

Figure 3.5: The 5047 A4 paper tray.

3.5.2 Motor's load

Experimental measurements were carried out to determine the applied torques on the output shaft of the test motor in a typical application. Due to the nature of the paper tray application it was not possible to measure the loads directly. An indirect measurement approach was used instead. The mean current flowing through

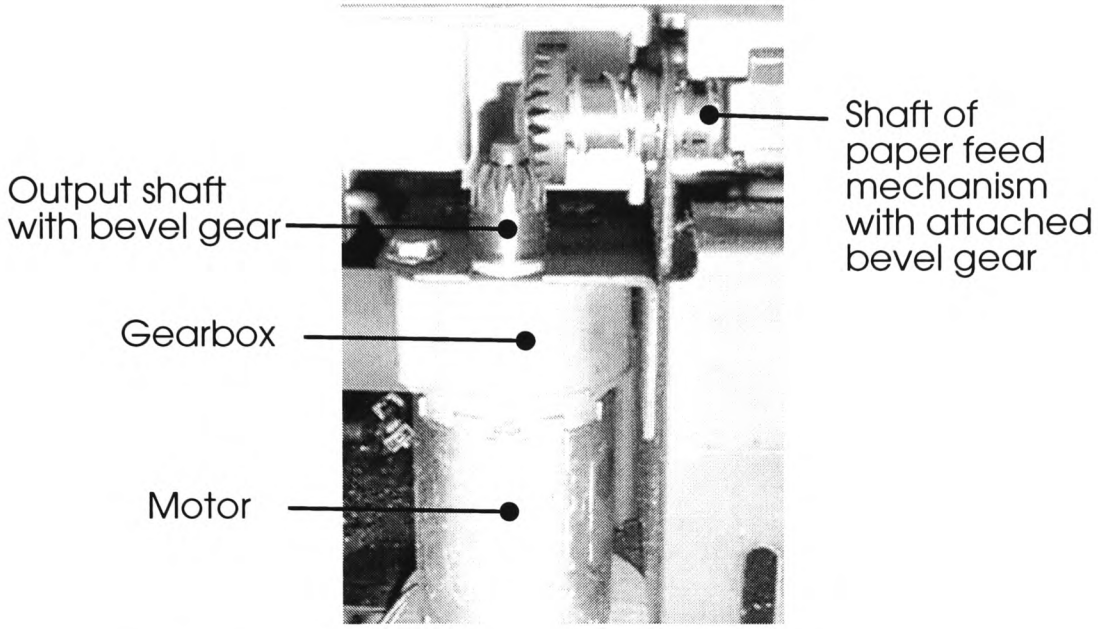

Figure 3.6: Motor mounting position in the 5047 paper tray.

each of the motors, which were still in the machine, during a paper feed operation was measured first. The motors were then removed from the copying machine and attached to a test fixture. On the test fixture, a load was applied by means of a magnetic brake. The load was increased until the mean motor current was identical to the current in the paper tray application. Using the characteristic of the magnetic brake, it was possible to determine the applied torque in the application. The experimental results are shown in table 3.4. In this application range, the torque varied significantly depending on the machine's paper tray in which it is used. Changes of more than 150%, with respect to the load in paper tray 4, were observed.

As a result it can be seen that the motor is used to drive loads which are only 60% of its maximum specified load of 0.75 Nm (section 3.3) in the 5047 paper trays.

Motor location	*Operation mode*	*Load*
Paper tray 1	A4 long edge feed	0.427 Nm
Paper tray 2	A3 short edge feed	0.378 Nm
Paper tray 3	A4 long edge feed	0.287 Nm
Paper tray 4	A4 short edge feed	0.168 Nm

Table 3.4: Motor torque values in different positions in the 5047 copying machine.

3.6 Wear Indicators

In order to estimate the usage level of the motor, it is essential to investigate the physical wear indicators. These indicators may be divided into two groups. The first group relates to the electrical parts of the motor, whilst the second group relates to its mechanical parts.

3.6.1 Wear in the electrical parts

The electrical system of the motor consists mainly of the brushes, commutator and rotor windings. These parts are subject to wear since they are not only exposed to electrical currents and electromagnetic fields, but also to mechanical stresses.

Rotor windings

Rotor winding faults are mainly due to mechanical wear which is caused by looseness and motion. Magnetic forces which turn the motor cause movement of the windings, particularly at start-up when the current is very high. Another factor is the temperature of the motor which increases with higher currents. High temperatures usually increase the temperature of the windings insulation material. In case of a fault the insulation temperature can exceed its maximum limit [12]. A defect in the insulation material will then short-circuit one or more windings of the rotor. This

can be detected by measuring the motor current, since short circuit windings result in a higher input current.

The experience of the photocopying machine manufacturer indicated that short circuited windings were never reported as a cause of failure in the field [9]. The maximum specified temperature of the motor windings is not exceeded in the copying machines operating in a cyclic mode within an office environment. The degradation of the motor winding insulation cannot be monitored before a failure has actually occurred. Even when the winding insulation is deteriorating, it still insulates. A fault is hence, only detectable when windings are short circuited. Therefore, the condition of the winding insulation cannot serve as a useful indicator of the motor wear or its usage level.

Brushes and commutator

Although the brushes are small and relatively inexpensive parts of the motor, they have a major function. They carry high currents without overheating or excessively wearing the parts over which they glide [100]. Since commutators are not perfect cylinders, it is difficult for brushes to maintain continuous contact with their surfaces. Figure 3.7 shows the cross section of the test motor. The ratio of the brush holder, brushes and commutator are true to scale.

The inside radius of a new brush is 4.8 mm and the radius of the commutator is 3.8 mm. As the wear process progresses the inside radius of the brush changes to that of the commutator. The conducting surface area of the brush increases slightly with motor usage due to the bedding-in process. During this process, brush material is transferred onto the commutator. After the brushes have been fully bedded-in,

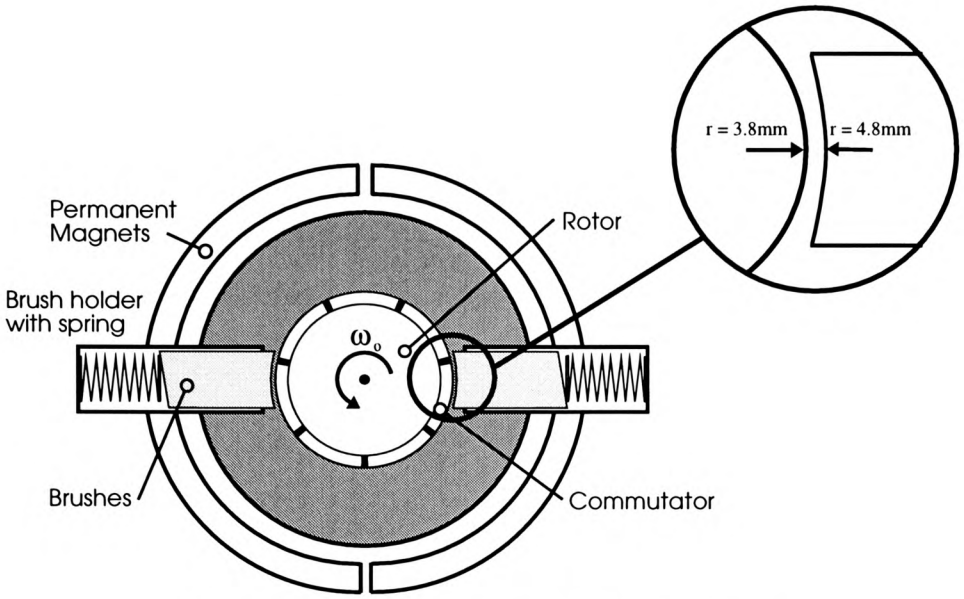

Figure 3.7: Cross section of the test motor.

electrical wear by burning from sparking, surpasses mechanical wear as the most important factor in the brush wear process [102]. Brush wear depends on a number of factors:

- Nature and composition of the carbon material.
- Condition of brush and commutator surfaces.
- Pressure between the brush and commutator surfaces.
- Intervening medium, such as oil.
- Movement type, which includes sliding, rotating and speed.
- Temperature and humidity.
- Current density.
- Factors influencing the intimacy of contact, such as mechanical alignment.

Apart from the current, most of these factors do not change for the same type of motor, making it the most important wear factor. Since the dc motor investigated in this study is a brushed permanent magnet system, the current passing through, i_a, is directly proportional to the applied torque, T, as defined by equation 3.3. This equation is repeated below (equation 3.6) for convenience.

$$T = k\Phi i_a \tag{3.6}$$

where, Φ and k are constants. Therefore,

$$i_a \propto T \tag{3.7}$$

furthermore, the rate of brush wear, dw_{brush}, with time, $\frac{dw_{brush}}{dt}$, increases at least proportionally to the current density of the brush [97].

$$\frac{dw_{brush}}{dt} \propto J \tag{3.8}$$

Where, J is the current density. The brush contact area with the commutator, A_{brush}, can be considered to be constant for a bedded-in brush. It follows that,

$$J = \frac{i_a}{A_{brush}} \tag{3.9}$$

and therefore,

$$w_{brush} \propto T \tag{3.10}$$

Equation 3.10 shows that the brush wear is directly proportional to the load of the motor.

In order to estimate the wear of the motor, the brush length and the condition of the commutator, films of six dismantled used motors were compared with those of four dismantled new motors. The measured difference in the brush length of the new and used motors was 50 μm maximum.

The visual inspection of the commutators showed that the brushes were not worn significantly. Figure 3.8, shows a commutator film similar to the film of the dismantled motors. A picture of the film of the investigated motors cannot be shown due to the small commutator radius. The streaky film indicates that the motors were underloaded, according to the handbook from Morganite Electrical Carbon Limited [97].

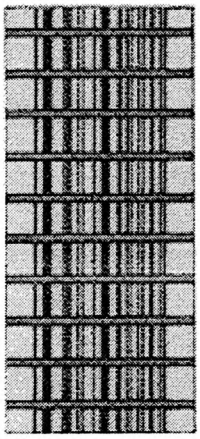

Figure 3.8: Streaky film on commutator - courtesy of Morganite Electrical Carbon Ltd.

It is unlikely that mechanical wear on the commutator surface will occur before that of the brushes because brushes are softer than the commutator. Brushes are made of graphite and commutator segments are made of copper which is harder than graphite [97]. Electrical wear of the commutator is mainly due to sparking caused by unsatisfactory commutation. This results in burning of commutator bars.

3.6.2 Wear in the mechanical parts

The mechanical parts that are subject to wear in the test motor include the bearings and the gears in the gearbox.

Bearings

Faults of the rolling element bearings are a major source of electric motor failures in larger machines as mentioned in section 2.1. Wear in bearings is caused by lack of lubrication, imbalance and vibrations, all leading to abrasion. A failure of the lubrication film results more generally in scoring of the bearing surface. In such a case the very hard particles torn from the bearing surface by initial contact prompts scoring and scratching of the surfaces [103]. Due to their cost effectiveness, plain brass bearings are preferred in the production of small dc motors.

The plain bearings of the test motor used in this study are also made of brass. The bearing condition effects the start characteristic of the motor. This can be monitored using the time-to-speed characteristics of the motor. Figure 3.9 illustrates the time-to-speed parameter. It is a measure of the rise time of the speed of the motor. The time-to-speed index, Δt, is defined as the time between 10% and 90% of the stable motor speed during the start period.

It can be seen in figure 3.9 that the motor's response is identical to a first order system. In general, the transfer function of the motor is of second order. However, the time constant of the electrical system ($\frac{L_a}{R_a}$) is much smaller than the time constant of the mechanical system ($\frac{J_r}{B_m}$) and can therefore be neglected. As the bearing wears out, the motors mechanical damping factor, B_m, increases due to increased friction, which is reflected by a decreased time-to-speed value [20]. The experience of the

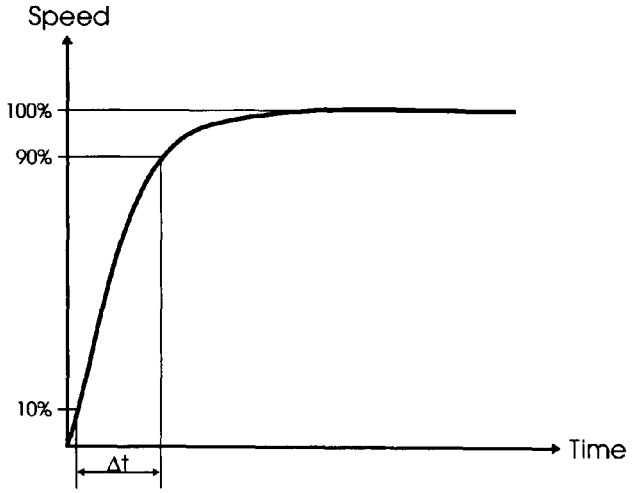

Figure 3.9: Time-to-speed measurement.

copying machine manufacturer has however, shown that problems with faulty plain bearings of copying machine motors have never occurred [9]. The contribution of worn plain brass bearings to motor wear can therefore, be neglected.

Gearbox

Wear in gears involves the steady removal of material from the gear flanks. This effect increases with poor lubrication. Due to averaging effects, helical gears have a tendency of wearing consistently across the whole surface. Gears can lose a large amount of material and still run quietly. Spur gears show a different behaviour since flank loads are much higher. The backlash of gears usually increases with their use. In a copying machine faults in the gearbox due to lack of lubrication are likely to be caused by paper or toner particles. Increased backlash is likely to cause a higher level of acoustic noise and vibration during operation [21].

Acoustic gear noise may be a measurable and repeatable wear indicator if the design of the motor never changes. Changes, especially in the material and the cut of the gears, lead to different noise characteristics for each design. However, it

is important to investigate if the vibration or acoustic noise increases considerably with motor life. The experience of Xerox showed that the majority of motors were rejected by asset recovery operators due to their perceived acoustic noise. However, a systematic study to clarify which motor design resulted in the highest rejection rate due to noise, was never conducted [9].

Dynamic gear meshing forces are the main source of gear noise. They are highly dependant on the transmitted torque and the gearbox characteristics. Amplitude and frequency modulation effects in gearboxes containing multiple gears may also exist and add to the complex signal of the gear noise [23]. Figure 3.3 shows the gear arrangement in the gearbox. Table 3.5 lists the gearbox characteristics where, Ω is the rotation frequency of the rotor. Referring to figure 3.3 the rotating frequencies of the three shafts S1, S2 and S3 are related to the rotor frequency.

Motor gearbox	*Input side*	*System*	*Output side*
Number of Teeth Shaft Frequency, Hz Gear Mesh Frequency, Hz	$G_1 = 10$ $f_{S_1} = \frac{\Omega}{60}$	$f_{G_{12}} = 10 \cdot \frac{\Omega}{60}$	$G_2 = 31$ $f_{S_2} = \frac{10}{31} \cdot \frac{\Omega}{60}$
Number of Teeth Shaft Frequency, Hz Gear Mesh Frequency, Hz	$G_3 = 9$ $f_{S_2} = \frac{10}{31} \cdot \frac{\Omega}{60}$	$f_{G_{34}} = \frac{90}{31} \cdot \frac{\Omega}{60}$	$G_4 = 26$ $f_{S_3} = \frac{22}{197} \cdot \frac{\Omega}{60}$

Table 3.5: Gearbox characteristics dependance on gear shaft frequency.

3.7 Summary

This chapter has presented the construction of dc motors and provided an analysis of the relationships between their electrical and mechanical parameters. This analysis was required to facilitate the investigation of the wear process in the motor and the means of assessing its progress.

This chapter has identified the dc motor that was used as the experimental test object of this study and explained the rationale for selecting it. This motor was shown to be a typical representation of small dc motors that are used in large quantities in commercial applications such as the Xerox 5047 photocopying machine. This makes it a suitable target for asset recovery.

The construction and application environment was thoroughly investigated. It was shown that the construction of the motor did not allow for invasive investigation of the wear characteristics and therefore, it is not a suitable approach for routine assessment of the motor usage level in an asset recovery operation.

Investigating wear in the electrical and mechanical parts of the motor and the associated wear indicators has shown that the brushes and gears are the components that have the potential of providing consistent wear pattern and therefore, suitable indicators of the motor usage level in its application. In addition, wear in these components lends itself for non-invasive monitoring using physical parameters such as voltage, current and vibration. Therefore, the experimental investigation of this study has concentrated on wear in the brushes and gears as the means of assessing the usage level of the motors provided by Xerox. These motors were obtained from

the Asset Recovery Department of the company and did not have any historical data associated with them.

The lack of historical data on the motors' usage levels meant that the only approach that was open for investigating the wear versus usage level in this study was to conduct accelerated life tests experimentally. This experimental methodology is the subject of the next chapter.

Chapter 4

Experimental and Testing Methodologies

This chapter describes the experimental and testing methodologies developed during this study to investigate the wear patterns in the dc motor under test and the corresponding wear indicating parameters.

The use of accelerated life testing is described in section 4.1. Three different test strategies are presented in this section and a selection was made of the approach that was found the most suitable for the purposes of this study. The main parameters of the experimental life test experiments, including the test scheduling and duration, are described.

Details of accelerated life test system design and characteristics are presented in section 4.2. This included the design and construction of the mechanical test fixtures for current and vibration measurements. The electronic control circuitry and data acquisition hardware of the test system is described in detail. The developed

software for experimental control, data recording and user interface is also presented in this section.

Section 4.3 presents the design details of the integrated asset recovery motor screening test system for use in a production environment. This includes the mechanical and electronic sections, and the associated test software.

Section 4.4 describes the experimental methodology and test organisation for measuring the acoustic noise emission of dc motors. The section describes the test environment and the rationale for the selected measurement approach.

A summary of this chapter is provided in section 4.5.

4.1 Accelerated Life Testing

Accelerated life testing is a technique through which the wear of components is accelerated by subjecting them to stresses in excess of their reference conditions. This results in a shorter life time for the components than would be expected under normal conditions of operation. Its main purpose is to establish relationships between a component's wear behaviour, stresses and usage level or time. Once these relationships are known, the behaviour of the component under various test or operating conditions can be estimated by extrapolation from the test results. Accelerated life testing methods are also used to obtain information on the wear of components over a range of conditions that they may encounter in use. Such information can be obtained by testing over the range of conditions of interest, or under more severe conditions in order to extrapolate the results to the range of interest.

4.1.1 Marginal testing

Marginal testing is a method of estimating the probability of an imminent failure due to wear. This involves periodic testing in a fixed schedule. In the case of electronic equipment, it may be achieved by operating at the voltage limits for certain elements and observing the resulting symptoms. This helps to isolate worn components or parts and to replace them before a failure occurs. Figure 4.1 shows the concept of marginal testing. Components are tested continuously in the operating rectangle. This accelerates the wear by continuous operation rather than increased stresses. This test method is suitable for components which are not used continuously in an application [104–106].

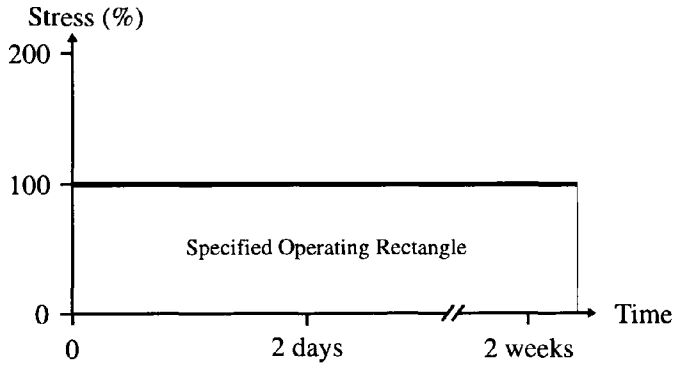

Figure 4.1: Marginal testing.

4.1.2 Enhanced Stresses

The enhanced stresses method is usually used for the purpose of achieving a more rugged design and manufacturing process. It is therefore, mainly used in the design process of a new product.

A batch of resistors for example has to be tested. An approximation of the life expectancy shows that under normal conditions the test would take years to com-

plete. It is therefore, necessary to increase the failure rate artificially by increasing both the test voltage and the ambient temperature. In this way it can be argued that a failure can be detected in a few weeks instead of years. This type of test must be approached with considerable caution. A stress increase above certain limits may lead to false assumptions regarding the expected usage. For example, if in the above mentioned resistor test, the test temperature is increased to 300°C the resistor may fail in a few seconds. This result may not be related to normal ageing at ambient temperature. Figure 4.2 shows the principle of enhanced stress testing. It can be seen that the test time is continuous and that selected stresses are above the operating rectangle [104, 107].

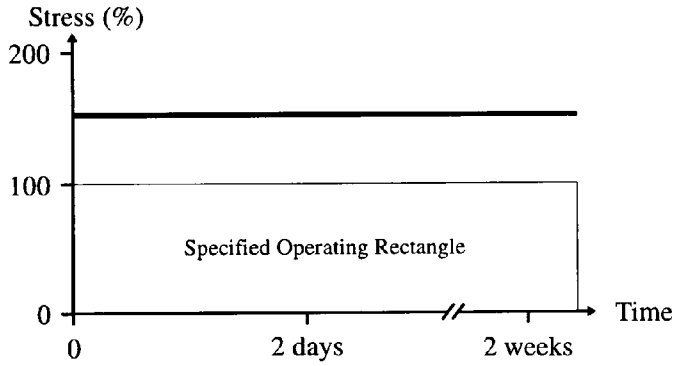

Figure 4.2: Enhanced stress testing.

4.1.3 Stress and life testing

Another method of enhancing stresses is the STRIFE[1]-test also known as step-stress testing [104, 106]. During the STRIFE-Test the component is exercised with random stresses in the operating rectangle. After this period all possible stresses are increased simultaneously by increasing the stress margins of all variables involved in the wear process (figure 4.3). The advantage of the STRIFE-test is that it is an efficient test to confirm that a component is correctly designed.

[1]STRIFE = Stress + Life.

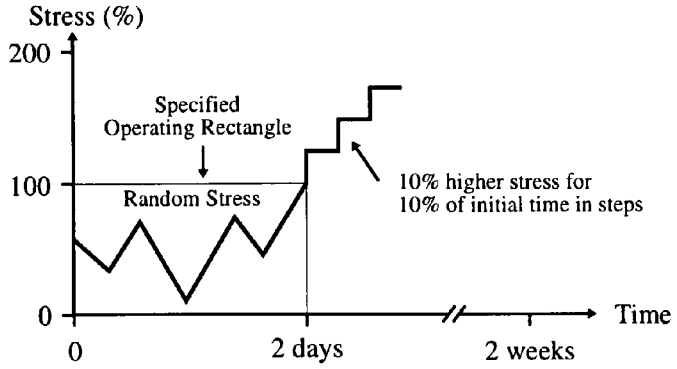

Figure 4.3: STRIFE testing.

4.1.4 Implementation of an accelerated life test

The following considerations must be taken into account when planning an accelerated life test in order to produce valid data that contain the desired information:

- Considerable engineering know-how and effort should be introduced in designing tests that are comparable to actual real life use.
- The operational conditions should be held constant during the experiment, according to a clear test plan, so that the data reflects only the effects of the variables that are of interest.

The life test in this study should reflect the motor's wear in normal usage in the copying machine. A test with enhanced stresses or the STRIFE test is therefore not suitable. The only method to relate the motor's wear to usage in an application is marginal testing.

Duration of the test

The guidelines used for designing the accelerated life test experiments of this study are determined by the motor specification (section 3.3). The maximum usage level of the motor is specified as 1.5 million motor cycles (0.5 s on, 0.5 s off), which consist of 15 minutes under maximum load followed by a rest period of 3 minutes.

It follows that with a continuous 24 hour test, including specified rest periods, 1.5 million cycles can be tested in 20.8 days.

4.1.5 Operational modes

To age the motor without exceeding the specification limits, it has to be loaded up to its maximum torque of 0.75 Nm. The wear of the motor should be monitored with a reasonably high resolution. A resolution of 1% of the 1.5 million test cycles was considered as a good compromise between data storage requirements and resolution. Therefore, the desired motor parameters were sampled after a complete set of 15,000 cycles (figure 4.4).

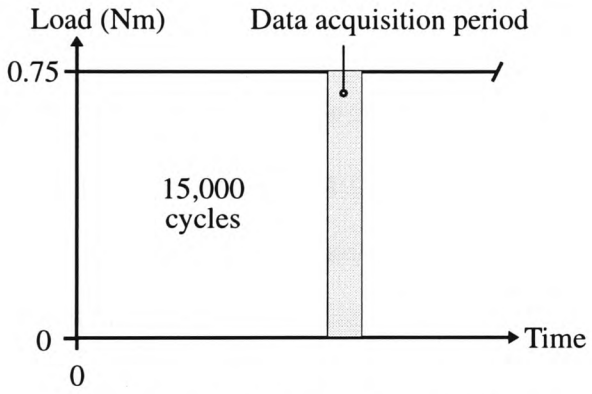

Figure 4.4: Test cycle frequency and duration.

During the data acquisition period the motor was operated in the following modes:

- Forward with 0.75 Nm load.
- Forward without load.
- Time-to-speed (section 3.6.2) without load.
- Time-to-speed (section 3.6.2) with 0.75 Nm load.
- Reverse without load.

- Motor used as a generator.
- Motor used as a generator with a connected load resistor.

The different operational modes were chosen to derive a broad range of information about the motors wear behaviour over its life time. Even though the motor is not operating in all of theses modes in its original application, they can give additional wear information. The time-to-speed operational mode is a measure of the rise time of the motor's speed when it starts. This parameter was used to detect changes in friction and internal motor resistance (section 3.6.2).

The literature review has shown that an accelerometer can be used to monitor the vibration and therefore, indirectly the acoustic noise emission of the test motor. This is aimed at acquiring information on the acoustic noise emission as an indication of wear in the mechanical components of the motor. However, the survey conducted by Emm [30] has shown that vibration monitoring of small motors did not provide satisfactory results due to the inability to obtain repeatable results for the purpose of classifying good and faulty motors. Therefore, the investigation into the use of the motor's vibration as a wear indicator was limited to the monitoring of one motor only. Then intention was to increase the number of motors used for vibration monitoring if the results of the vibration analysis show significant potential for using this parameter in wear characterisation.

4.2 Accelerated Life Test System

Information regarding motor usage history was not available (section 3.5.2). As a result, the only approach to introduce wear that can be related to the motor's usage level is to conduct an accelerated life test according to the marginal test method.

4.2.1 Direction of the motor load

The amplitude and direction of the applied load in the experimental tests should be specified to simulate the wear in the real life of application, including wear in components such as bearings. A high radial load causes faster deterioration of the bearing than an axial load. Since the motor is used in different applications and mounting positions, the radial load on the output shaft may also change. Consequently, a reference direction of the application load cannot be given. The radial load on the output shaft during the accelerated life test should be minimal to avoid excessive bearing wear.

4.2.2 Mechanical construction of the test system

The test fixtures required to meet the following mechanical design constraints:

- The mounting used for vibration measurements should be mechanically isolated from the other test motors.
- Four motors were required to be tested to obtain a significant amount of wear data.
- The coupling of the test and brake motors must be aligned straight to avoid radial loads.
- The test fixture should be made of non-corrosive material to avoid mounting problems due to corrosion.

In order to measure the vibration signal of a single motor it was essential to decouple its fixture mechanically from the other test motors. The motor under vibration test, was attached to a test fixture that was separate from the other motors as shown in figure 4.5.

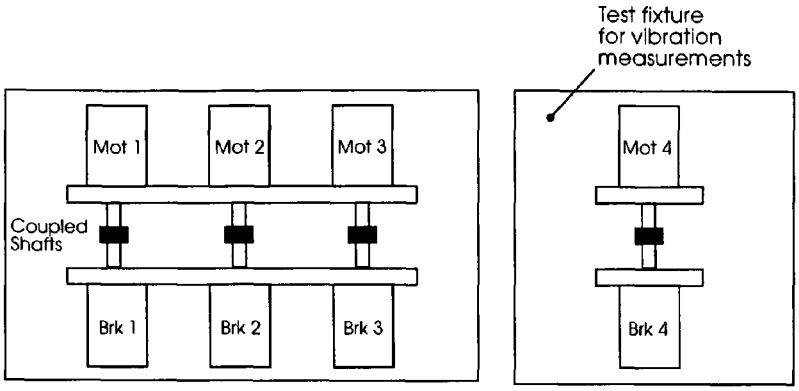

Figure 4.5: Motor test fixtures.

This arrangement resulted in a combined fixture for three motors and a separate fixture for vibration measurements. The mechanical drawings of the single motor fixture can be seen in figures A.2 to A.4. Figure A.5 shows the fixture for the three remaining test motors. For the coupling of the test and brake motors, flexible Oldham couplings[2] were used.

Brake Motor

A mechanical solution to brake the test motor is not possible since the load has to be changed electronically and in a controlled fashion. A magnetic brake is also unsuitable due to the inability to drive the test motor in a generator mode. The most suitable solution is to use a separate motor as a brake. A brake motor was used to apply a load on the test motor. The test system braking mechanism and its control were required to meet the following specifications:

- The applied torque must be controlled over the test time to ensure a time linear wear process.
- The starting friction should be less then 20% of the maximum applied torque to keep the influence on the time-to-speed measurement small.

[2]Huco Engineering Components, Hertford, UK.

- The brake torque load must be switched on and off electronically to be able to run the test automatically.
- The brake motor must be able to drive the test motor when tested as a generator since the brake and test motor shafts are coupled together.
- The wear of the braking mechanism must be less than that of the test motor to avoid influencing the test results due to aging of the brake motor.

Torque is directly proportional to the motor current for permanent magnet dc motors (equation 3.3). As a consequence, the torque of the motor is constant if the motor current is constant. Based on this principle the brake motor control circuit was designed to conform to the stated design constraints. In order to ensure a low starting friction the brake motor did not have a gearbox. A gearbox would also interfere with the vibration measurement of the test motor by introducing an additional source of vibration. A robust permanent magnet dc servo motor with the following specifications was chosen for the experimental test:

Description:	Bidirectional permanent magnet dc motor.
Torque Constant:	0.75 $\frac{Nm}{A}$
Supply Voltage:	0-36 V dc
Continuous Current Rating:	2.2 A
Stall Current at 36 V:	16.2 A
Frictional Torque:	$\leq$ 0.15 Nm
Motor Reference :	127E04611
Manufacturer:	Dunker Motorenwerk, Germany.

4.2.3 Motor control system

An electronic system was designed to control the test and brake motors using digital signals from the PC. The schematics of the control circuits can be seen in figures B.1 to B.4 of appendix B.

Test motor circuits

Section 4.1.5 specified that the test motor should operate in forward and reverse direction. In order to change the rotating direction, the polarity of the motor supply voltage should be reversed. This was accomplished by an h-bridge circuit. A schematic of this circuit is shown in figure B.2 of appendix B.

In order to measure the internal resistance, R_a, of the motor a load resistor, R_L, was connected to the terminal pins of the test motor (figure 4.6). The value of the internal resistance can then be calculated using the value of the load resistor and the motor's terminal voltages:

$$R_a = R_L \frac{V_t - V_{tR_L}}{V_{tR_L}} \tag{4.1}$$

Where, V_t is the open circuit terminal voltage and V_{tR_L} is the terminal voltage with load resistor, R_L, connected.

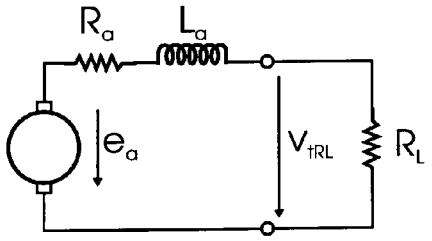

Figure 4.6: Motor internal resistance measurement circuit.

Brake motor circuits

The brake motor was used to apply the specified torque of 0.75 Nm to the test motor. In the generator mode, the brake motor was switched from the brake mode into the motor mode by the circuits of figure 4.7 which are shown as block diagrams. The design is based on an h-bridge circuit similar to the one used for the rotation direction change of the test motor. In the motor mode, transistors T_1 and T_4 are conducting and enable the current, I, to flow through the motor.

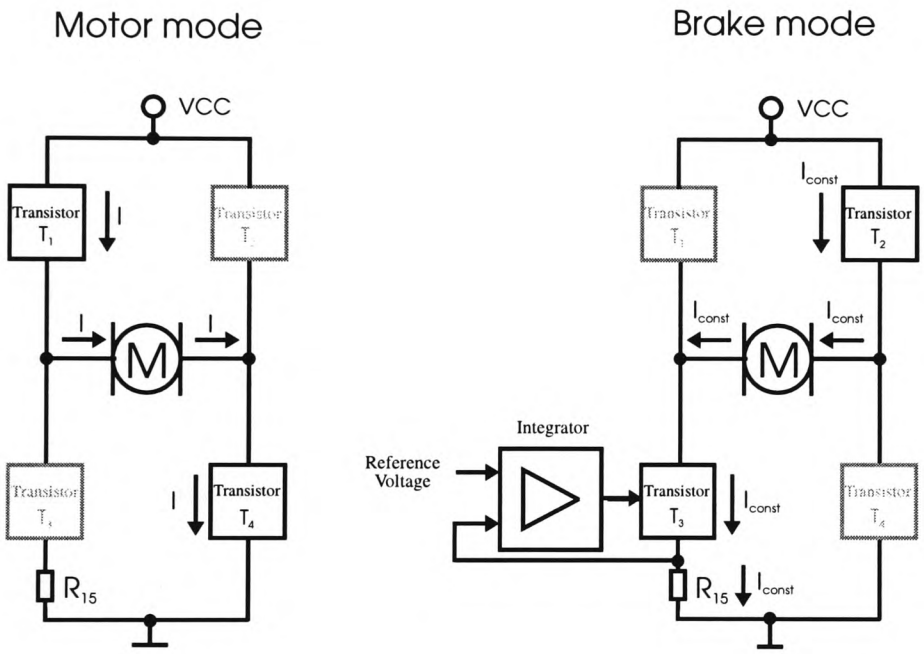

Figure 4.7: Brake motor in motor and brake modes.

The current, I, was held constant in the brake mode by keeping the voltage across resistor R_{15} constant by the control loop, which includes transistor T_3 and an integrator as shown in figure 4.7. The integrator compares a reference voltage with voltage across R_{15} (V_{15}) and adjusts the base current of T_3 in such a way to keep V_{15} constant. A potentiometer was used to adjust the motor torque. The torque was switched on and off by a control voltage on a single pin. A logical high voltage switches the constant current off and therefore, the motor load off. A detailed

schematic diagram of brake and motor circuit is shown in figure B.1 of appendix B.

Speed measurement

The speed of the test motor was measured using an optical shaft encoder on the output shaft of the brake motor. The encoder disc[3] used had a resolution of 10^o, which is equivalent to 36 impulses per revolution. The optical encoder[4] had two optoelectronic channels with open collector outputs.

Digital port extension of the data acquisition card

A digital port extension circuit was designed to generate the 1 Hz frequency for the test cycle (0.5 s on, 0.5 s off) since such a low frequency could not be generated by the data acquisition card itself. It was also used to control the motor circuits with TTL compatible logic voltage levels by buffering and protecting the data acquisition card ports. The schematic diagram of this circuit can be seen in figure B.4 of appendix B.

4.2.4 Data acquisition

The measured motor parameters were digitised and stored for later analysis. A block diagram of the overall test system is shown in figure 4.8. Standard data acquisition boards offer the possibility of fast data acquisition and storage on personal computers (PCs). Therefore, a suitable PC based data aquisition board was selected for the recording of the experimental data.

A suitable data acquisition board must meet the following specifications:

[3]Xerox Ref. No. 146E00671.
[4]Xerox Ref. No. 146E0033.

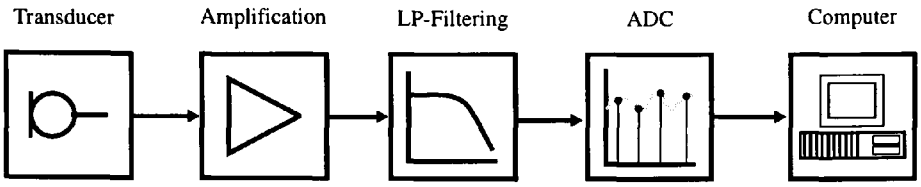

Figure 4.8: Test system block diagram.

- Sampling frequency sufficient to measure the signals without loosing significant information due to bandwidth limitations.
- Differential input channels to reject ground loop-induced errors and noise.
- At least 13 Digital I/O ports (4 motor forward/reverse, 4 brake on/off, 4 brake/motor mode, 1 general stop).
- Software libraries with functions to control the acquisition process. These libraries should be compatible with standard programming languages.

An important feature of a data acquisition board is its sampling frequency which should satisfy the sampling theorem given by [59],

$$f_s \geq 2f_{max} \tag{4.2}$$

The sampling frequency, f_s, should be at least twice as high as the highest frequency component, f_{max}, in the sampled signal. Therefore, the highest frequency component in the signal of interest must be known. If this is not the case, the bandwidth of the signal should be limited using low-pass filters to prevent aliasing [108].

Bandwidth of motor current and vibration signals

To establish the requirements for the measurement system, an experiment was conducted to estimate the highest frequency components in the parameters of interest.

A simple motor holding fixture was used to test five new motors and five used motors which were rejected by the operator during screening for asset recovery. The current was measured using a 1Ω shunt resistor. The motor case vibration was measured using an accelerometer[5] and conditioned by a signal conditioning unit[6]. The accelerometer used had the following features:

- Wide bandwidth (5 to 20 kHz ± 1 dB).
- High sensitivity (25 $\frac{mV}{g}$).
- Light weight (4.8 g).
- Low output impedance ($\leq 200\ \Omega$).
- Low transverse sensitivity ($\leq 5\%$).

The bandwidth was then analysed using an analogue spectrum analyser[7] which can cover the frequency range of 20 Hz to 40 MHz. The experiment showed that the bandwidth of the vibration signal did not exceed 18 kHz and the bandwidth of the motor current waveform did not exceed 30 kHz.

Based on the results of this investigation a suitable data acquisition card[8] was selected. The main features of this data acquisition card are:

- 16 true differential analogue input channels.
- 24 digital I/O ports.

[5]ISOTRON 7259A-25, Endevco U.K. Ltd., Herts., UK.
[6]ISOTRON signal conditioner 4416B, Endevco U.K. Ltd., Herts., UK.
[7]Model 3585A, Hewlett-Packard Ltd., Bracknell, Berkshire, UK.
[8]PC226, Amplicon, Brighton, UK.

- 12 bit analogue to digital converter (ADC) with a signal-to-noise ratio of 60.2 dB.
- Continuous data acquisition in multi-channel mode up to 400 kHz.
- MS DOS and MS Windows[9] programming tools.
- Input analogue voltage range of ± 5 V.

Anti-aliasing filter

To satisfy the sampling theorem (equation 4.2) a bandwidth limiting low-pass filter was used. The minimum stop-band attenuation of the low-pass or anti-aliasing filter, A_{min}, depends on the resolution of the analogue to digital conversion process. It is typically [108]

$$A_{min} = 20 \log \left(\sqrt{1.5}\, 2^{B_{AD}+1}\right) \tag{4.3}$$

where, B_{AD} is the resolution of analogue to digital converter (ADC), which is 12 bits for the selected ADC. From equation 4.3 it follows that

$$A_{min}\Big|_{f=\frac{f_s}{2}} \geq 80\ dB \tag{4.4}$$

When two channels were used, the maximum sampling frequency was 200 kHz due to limitations of the software provided with the data acquisition board. Therefore, the resulting sampling frequency, f_s, for each channel was 100 kHz. Since the maximum frequency components observed in the current may exceed 30 kHz during the accelerated life test due to commutation sparking, an anti-aliasing filter was used. The same filter design was used for the vibration transducer to attenuate

[9]Microsoft Corporation, U.S.A.

signals that are above its linear frequency range of 20 kHz. The filter was used as a precaution since the bandwidth of the signals in the accelerated life test were unknown and could be higher than those observed previously. In order to ensure a high signal bandwidth an active 12th order low-pass filter with a cut-off frequency of 23 kHz and Butterworth characteristic was designed. It provided an attenuation of 78 dB at 50 kHz which is sufficiently close to the 80 dB requirement of equation 4.4. The selected filter characteristic avoided amplitude ripple in the pass-band.

The filter was implemented using a continuous-time active filter circuit (figure B.5 of appendix B). Using a continuous-time filter rather then a switched capacitor filter has the advantage of avoiding problems with digital noise at the clock frequency of the switched capacitor filter. The filter devices that were used had a very low harmonic distortion (THD), which was better than -86 dB and was due to internal capacitors.

In addition to the filter, a pre-amplifier circuit was designed to amplify the input signals to match the input voltage range of the data acquisition board (± 5 V). This enabled the signals to be sampled at the maximum possible resolution. It consisted mainly of a non-inverting low noise operational amplifier circuit. Gains of 1, 10 and 100 could be selected using switches. The schematic diagram of the filter circuit is shown in figure B.5 and B.6 of appendix B.

Current and voltage measurements

The motor current was measured by measuring the voltage drop across a 1 Ω serial resistor. An indirect non-contact method of current measurement includes hall effect devices but tests conducted with such a device produced a poor signal to noise ratio.

The motor voltage is measured using a differential amplifier with an attenuation of 9:1 to ensure that the input voltage did not exceed the limits of the data acquisition board. The schematic of the designed circuit can be seen in figure B.3 of appendix B.

Vibration measurement

The piezoelectric accelerometer described in section 4.2.4 was utilised for vibration measurements. It has a frequency range of 5 to 20 kHz with a linearity of ± 1 dB. The mounting of the accelerometer is critical for the accuracy of the results. In most cases, vibration is a result of the forces transmitted through a machine. Machine elements which constrain these forces, such as gearbox housings, are usually accessible externally so that the vibration resulting from the excitation forces can be measured non-invasively [26].

The vibration signals of the test motor were measured on the gearbox housing. The accelerometer was positioned radially to the gearbox, using cyanoacrylate adhesive to maintain a direct path for the gear vibration (figure 4.9). A magnetic stud could not be used because of the non-magnetic gearbox material. It is also not possible to use a screw mounted stud to attach the accelerometer since the motor does not have additional mounting holes.

4.2.5 Control program

The accelerated life test required continuous operation. This was achieved by controlling the data acquisition board using a PC. The PC software was designed to provide the following features and functions:

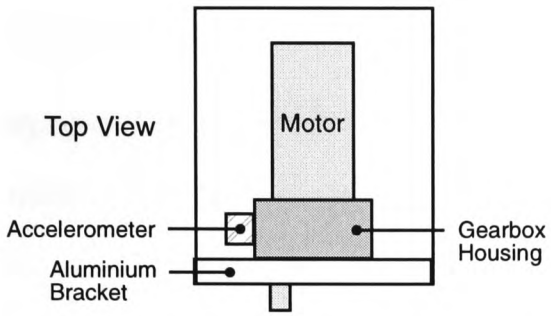

Figure 4.9: Position of the accelerometer on the test motor.

- A graphical user interface to display and control the life test status.
- Control of the on/off cycles of each motor.
- Controlling the 3 minute breaks during the test (section 3.3).
- Monitoring of operational failures during the test and ensuring safe test termination.
- Switching the motor load.
- Acquisition and recording of the physical parameters with specified sampling frequencies.
- Starting of data recording after a predefined number of test cycles.
- Compression and storage of recorded data.
- Protection of data against loss due to power-cuts.

The graphical user interface (GUI) was developed using Microsoft Visual Basic (MSVB) for Windows 3.1. Execution speed was not considered in the choice of the programming language since the accelerated life test is not a time critical application. The control and data acquisition functions were implemented using the software libraries provided by the manufacturer of the data acquisition card.

User interface

The GUI was used to display the status of the running test in a structured way with only one full screen window. The GUI of the accelerated life test can be seen in figure D.1 of appendix D.

Square boxes with an easy to distinguish colour scheme were designed to monitor the status of the accelerated life test. A red square indicated high or active, whilst a green square indicated low or inactive for the digital output ports. In addition, the status of the current-torque motor characteristics were displayed using a x-y plot. It was updated every time new motor current data in the forward mode, with and without load, was acquired.

Each motor can be enabled or disabled manually and individually using the GUI command buttons. Command buttons were programmed to reset the cycle counter individually for each motor and to run the motors manually in different operational modes.

Data acquisition

As outlined in section 4.1.4 the accelerated life test was interrupted every 15,000 cycles to record the parameters of interest. Figure 4.10 shows the program schedule during the sampling period.

The measured parameters were recorded after a five second run-in period to allow a steady operation.

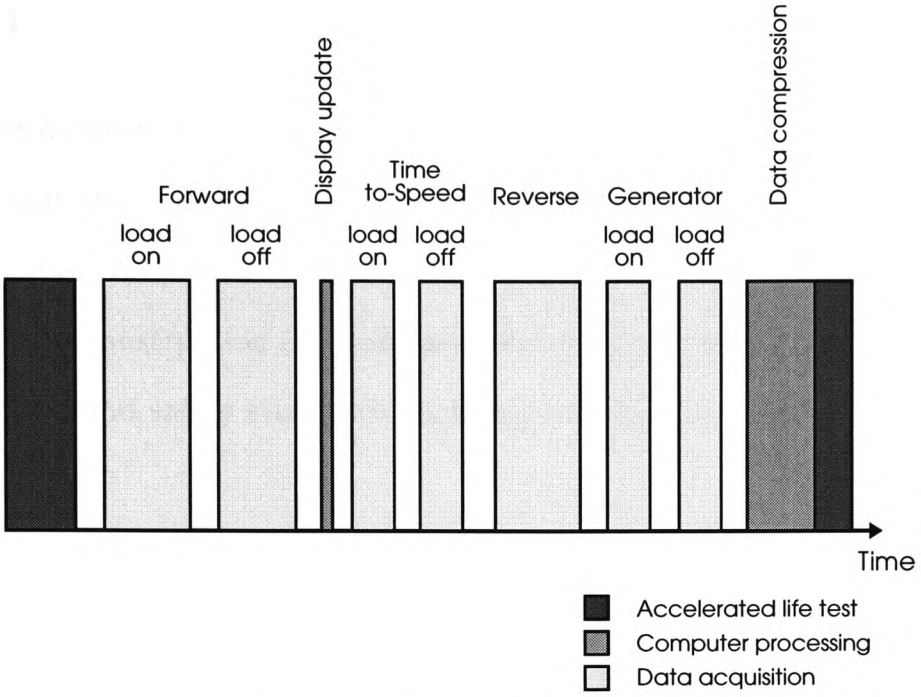

Figure 4.10: Data acquisition schedule

Data compression

The value of the recorded data from a single motor for one sampling interval was approximately 8 MByte, whilst the volume of the complete data set of four motors for the 1.5 million cycles of testing was 3.2 GByte. A number of lossless data compression tools are available on the market. The compression software chosen was the Microsoft Windows version of the compression tool PKZIP[10] [109]. The main MSVB accelerated life test control program made use of the WinZip 6.1[11] command line options enable it to start the compression in the background while running the control program. An overall data compression ratio of approximately 1:4 was achieved.

[10]PKWARE, Inc., Glendale, U.S.A.
[11]Nico Mak Computing, Inc., U.S.A.

4.3 Production Test System for Asset Recovery

The production test system for asset recovery motor screening at Xerox's manufacturing plant incorporated the techniques developed in this study. These were modified to allow their use for practical test purposes in a production environment. The mechanical construction and software were required to be easy to use and comply with health and safety standards such as cover for rotating parts.

Two major points were considered in the design of a test tool for production. The test components must be changed quickly and the testing time is limited. It differed in these two aspects from the laboratory based accelerated life test system. In the accelerated life test system, data processing and analysis took place after the test was finished. In the production test system the computer has to process and analyse the sampled data in order to display the results immediately.

The production test system was also used to measure the influence of torque on the acoustic noise emission of the test motor. This was accomplished by using an electronically adjustable magnetic brake. The laboratory accelerated life test system was not designed to change the torque in steps. It just switched the motor load on and off.

4.3.1 Mechanical construction of the production test system

Due to the differences described above, the mechanical design of the production test system differed from that of the accelerated life test system. A diagram of the system can be seen in figure 4.11.

Specific parameters are measured under different load conditions and therefore,

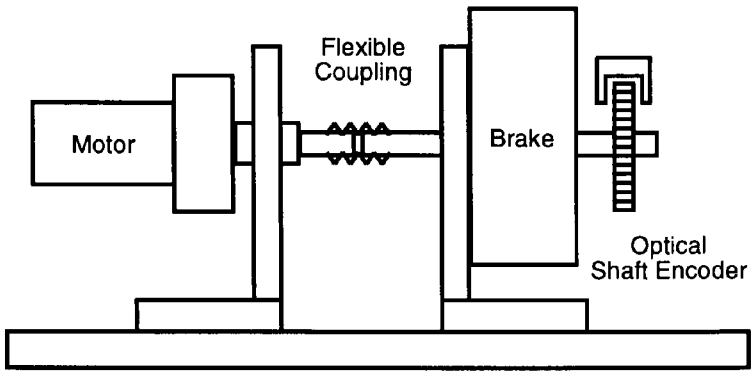

Figure 4.11: Block diagram of the test system.

a magnetic particle brake[12] was used to control the load. The brake was controlled by the data acquisition board.

Flexible coupling

In order to allow for an easy exchange of the test motor a flexible shaft adaptor was utilised to compensate for possible misalignment. Tests with two different types of flexible couplings were conducted in order to select a coupling which offered the best compromise between torque transmission, misalignment compensation and moment of inertia. Torque transmission should be very efficient for measuring the time-to-speed characteristic of the motor. The coupling should also be able to allow for high misalignment compensation. However, torque transmission is normally inversely proportional to the misalignment compensation of flexible couplings. The selected coupling [13] offered the best compromise between those conflicting parameters of the test system.

[12]MP.B.0030, Huco Engineering Components, Hertford, UK, maximum torque 2.8 Nm.
[13]Huco-Flex M, Huco Engineering Components, Hertford, UK.

4.3.2 Motor control circuit

The h-bridge principle used for the accelerated life test was also utilised for the production test motor control circuit (section 4.2.3). The four discrete h-bridge transistors were replaced by an integrated circuit[14] which had a built-in CMOS control circuitry and additional features such as automatic thermal shutdown. A series resistor configuration to measure the motor current as described in section 4.2.4 was also used.

4.3.3 Data acquisition

The hardware for data acquisition is identical to the one used in the accelerated life test system. It included the anti-aliasing filter for current measurement and the current measurement by means of a series resistor (section 4.2.4).

Speed measurement

Due to the use of a magnetic brake instead of a dc servo motor the shaft encoder had to be changed. A high resolution optical shaft encoder[15] with a resolution of 500 impulses per revolution was used instead. The digital signal from the shaft encoder was used as an input to a frequency-to-voltage converter (FVC)[16]. The output of the FVC is a dc voltage that is directly proportional to the input frequency.

4.3.4 Control program

The Xerox Corporation has an international internal software and hardware standard for test tools. Hence, this production test system had to conform to the com-

[14]LMD18200T by National Semiconductors, Swindon, UK.
[15]HEDM-5600-A06, Hewlett-Packard Ltd., Bracknell, Berkshire, UK.
[16]Tachometer Board Ver.2/1, Microgenic Systems, UK.

pany's standard. A National Instruments data acquisition board[17] and its associated software package LabView was used. LabView is a visual programming language and software package to program the data acquisition process including GUI design. LabView differs from programming languages like C or Basic which are text-based. LabView uses a graphical programming language, G, to create programs in block diagram form [110]. An example of the block diagram programming language format can be seen in figure 4.12.

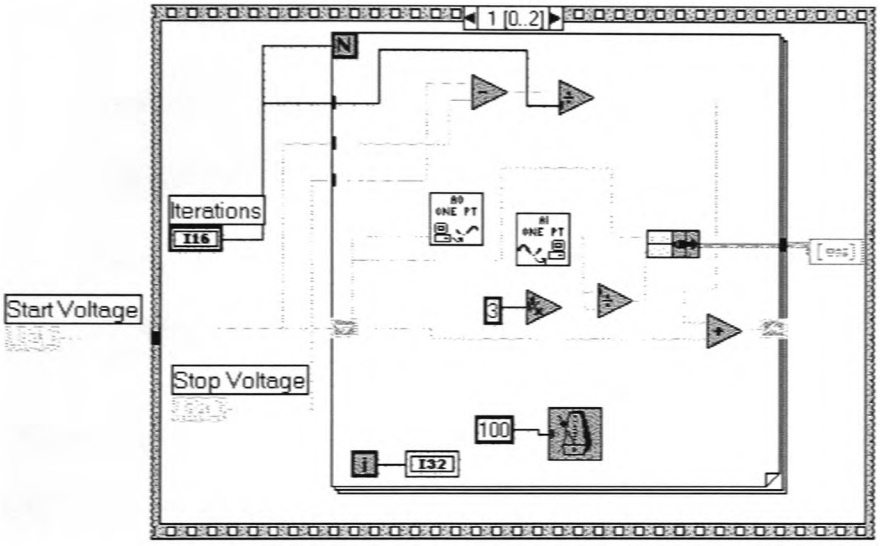

Figure 4.12: Example of the LabView programming language *G*.

User interface

The test system user's interface was kept as simple as possible since it will be used by an operator with little computer experience. The main task for the operator is to change the test motor and to start the test. The GUI can be seen in figure D.2. appendix D.

[17]AT-MIO-16D, National Instruments, Austin Texas, U.S.A.

Implementation of the processing and analysis algorithms

The signal analysis and feature extraction algorithms were originally developed using the programming language of the mathematical software package Matlab for Windows, Version 4.2[18]. These algorithms were then re-programmed and compiled in the form of dynamic link libraries (DLLs) for use in LabView. The DLL usage can be seen in figure 4.13.

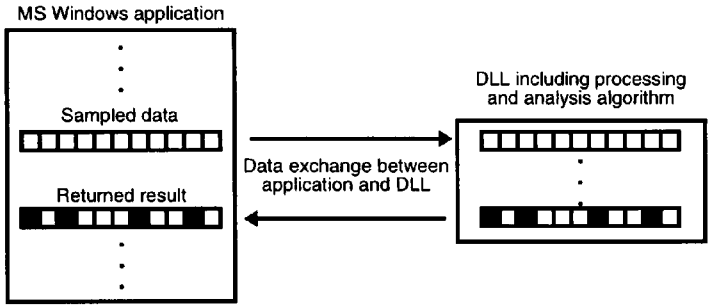

Figure 4.13: Call of a DLL as a function.

The DLL file is executed with a speed dependent on the used DLL file compiler. Microsoft Visual C++ was used to generate the DLL files. Since C is a programming language that works close to native machine code, its execution is fast. A function in a DLL file can be used in LabView with the Call Library Function option. After its declaration it can be used as any other existing Virtual Instrument (VI) block in the program (figure 4.14).

The advantage of a DLL file in the form of a VI is that it is easy to use, fast in execution and of manageable size. Important parameters can still be varied in order to make usage of the processing routine as flexible as possible. Further information about the programming of DLL functions and its use in LabView can be found in application notes from National Instruments [111–113].

[18]The MathWorks, Natick, U.S.A.

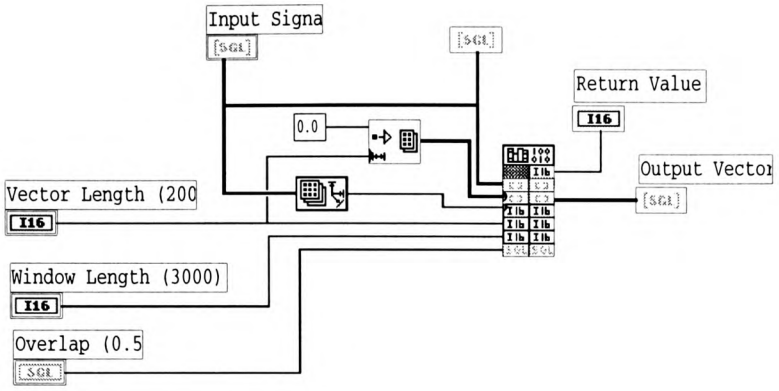

Figure 4.14: Processing and analysis virtual instrument.

4.4 Acoustic Noise Measurements

To measure the torque versus acoustic noise characteristic of the test motor, several experiments were conducted. Acoustic measurements should ideally be carried out in an environment free of any echo or reverberant fields. Spacious acoustic anechoic chambers come close to the ideal free field environment. The acoustic measurements in this study were carried out in an anechoic chamber designed for microwave measurements. The chamber was used because the absorptive materials on its walls and ceiling are similar to those used in an acoustic anechoic chamber. The reverberant field attenuation is not as good as in an acoustic anechoic chamber but it is significantly better than an office or laboratory. The test environment provided an approximation of a free field over a non-reflecting plane. The contribution of the reverberant field to the sound pressure levels at the measurement surface was small compared with those of the direct field of the motor. The motor including the holding fixture was placed on a tripod in the middle of the chamber (figure 4.15). The motor itself was attached to the test system fixture. The system block diagram is the same as that of figure 4.8 except that the transducer in this case is a microphone.

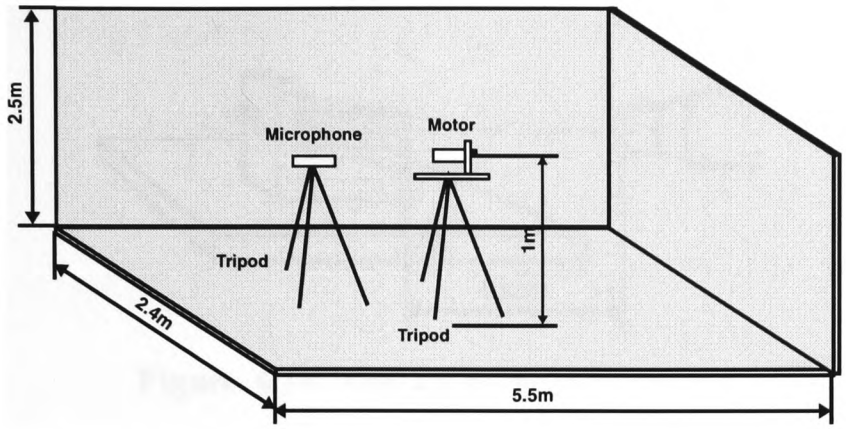

Figure 4.15: Acoustic measurement arrangement in the anechoic chamber.

Acoustic measurements were conducted using a microphone and pre-amplifier[19]. A pre-amplifier buffered the small acoustic signal from the microphone and was integrated in the handle of the microphone. The microphone had a sensitivity of 7.26 $\frac{mV}{P}$ and a flat frequency response from 0 to 12.5 kHz which did not vary by more than ± 0.5 dB. The microphone was calibrated using a pistonphone especially designed for the microphone. The pistonphone produced sinusoidal calibration sounds of 1 kHz at 104 db and 94 db.

The sound pressure levels around the motor varied with the location of the measuring point. The most appropriate microphone position was determined experimentally. Since the investigation should measure the maximum emitted noise, positioning of the microphone at the back of the motor was found to be the most suitable. All measurements were carried out with the microphone facing the back of the test motor and at a distance of 0.15 m (figure 4.16). Doubling the distance attenuates the signal by 6 dB [114]. Measurements conducted with a microphone distance of 0.3 m showed a poor signal-to-noise ratio since, the acoustic signal amplitude was close to the microphones noise level.

[19]Microphone MK202 and pre-amplifier MV181A, Cirrus Research Ltd.

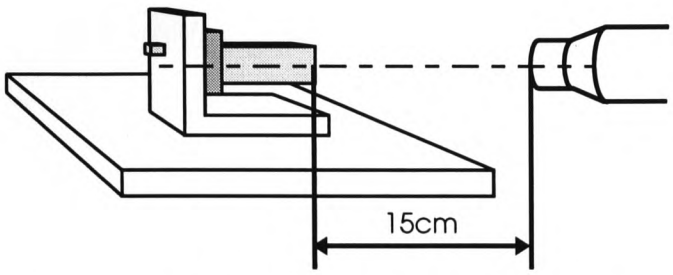

Figure 4.16: Position of the microphone.

Due to the low microphone pre-amplifier output signal amplitude, an amplifier with a gain of 100 was designed to amplify the output signal further. To avoid aliasing (section 4.2.4) an 8th order low-pass filter with a cut-off frequency, f_c, of 15 kHz was designed to provide an attenuation of 42 dB at 25 kHz which represented half of the sampling frequency, $\frac{f_s}{2}$. According to equation 4.4 the attenuation for the system should be 80dB at $\frac{f_s}{2}$. The overall attenuation was 80 dB due to the bandwidth of the microphone which had a cut-off frequency of 12 kHz. Therefore, the selected attenuation value was sufficient. In addition, an active 2nd order high-pass filter was used to eliminate the dc offset and to attenuate any very low frequency components resulting from building movements and walking noises. A cut-off frequency of 10 Hz was used. The schematics of the circuits that were designed for acoustic measurements can be seen in figures B.7 and B.8 of appendix B.

The results of the SPL measurements were required to be comparable with the Xerox Environmental Health and Safety Manual[20]. According to the manual a horizontal distance of 1 m of the test object was required. Since the tests have been conducted with a distance of 0.15 m, all noise level measurements were converted to measurements equivalent to SPLs at one meter. The SPL at distances r_1 and r_2 can be converted using equation 4.5 [115].

[20]CEHS STD No. 8.7.2., X.F.1.

$$SPL_{r2} = SPL_{r1} + 20 \log \frac{r_1}{r_2} \tag{4.5}$$

4.5 Summary

This chapter has presented the experimental and test methodologies that were utilised during this study to investigate the wear patterns in the dc test motors and the corresponding wear indicating parameters. These methodologies were developed after a thorough consideration of the appropriate test techniques for investigating the main wear indicating parameters that were identified in chapter 2. Furthermore the developed test and analysis methodologies were incorporated in the design of a versatile production test system that will enable motor screening for asset recovery purposes.

Accelerated life testing was identified as the only possible approach to investigate the development of wear in the test motors and the changes in the wear indicating parameters as these motors were not monitored in the application and they did not have historical data associated with them when they were recovered from the copying machines. Marginal testing was identified as the most appropriate test approach as it enables the test results to be related to the motor wear in its real life application.

This chapter has also presented the rationale for the best methodology of the experimental investigations of this study. This included the test schedule, duration and test operational modes. These operational modes were selected to provide the maximum amount of information on wear in the tested motors. The design of the accelerated life test system was described in detail. This included the mechanical

construction of the test fixtures for the current and vibration measurements. The rationale for using a brake servo motor was presented and shown to provide a good solution for the maximum control of the test parameters. The electronic control and data acquisition hardware was described alongside the software for the test control and data recording. The GUI display of the experimental test system provided the means of conveying detailed information on the progress of the tests. On screen command buttons were provided to enable manual override of the operation of the motors being tested.

The chapter has also described the design and development of the asset recovery motor screening test system for use in a production environment. This system includes most of the features of the accelerated life test system but was optimised for use in a manufacturing environment. The system allows the operator to mount the motor under test and remove it with ease. In addition, it analyses the acquired motor parameters in a short period of time and displays the analysis result on an easily understandable GUI. This is essential as the test time in a production environment is very limited and the operator is not expected to be experienced in using a computer system.

Finally, the chapter has presented the details of the motor acoustic measurement system and its organisation. This system was used to test the acoustic noise emissions from the tested motors to discover if they provided reliable and consistent indication of the motor usage level.

Chapter 5

Processing Methods and Test Results

This chapter describes the processing techniques that were used for data reduction and feature extraction of signals acquired during the accelerated life test experiments. All experimental results are also presented in this chapter.

Section 5.1 describes the processing methods utilised during this study including both, time domain and frequency domain techniques. Special emphasis is placed on the time domain transform for feature extraction (TFE) due to its novelty, superior data reduction and feature extraction capabilities. The TFE was investigated thoroughly and its windowed version is introduced in this section.

The results of the accelerated life test experiments are presented in section 5.2. The various recorded parameters and the results of processing these parameters using the techniques of section 5.1 are also included. These parameters covered the motor voltage, motor resistance, time-to-speed parameter, emf/speed, motor speed,

motor current and vibration of the motor.

Section 5.3 presents the results of the investigation into the acoustic noise levels of the motors. This includes the differences in the noise levels of different motor designs.

A summary of the main findings of this chapter is provided in section 5.4.

5.1 Processing Methods

This section section presents the details of the methods used to process the signals of the wear indicating parameters that were captured during the accelerated life test experiments. There are three main aims for processing these signals. The first is to remove unwanted components that are known to be caused by factors external to experiments. The second aim is to reduce the volume of collected data which makes these signals difficult to examine and interpret. Finally, these methods were applied to enhance and extract the most significant features in the signals to improve the accuracy of the subsequent analysis process.

5.1.1 Digital Filters

In this study, digital filters were used to remove very low frequency components which fall below 5 Hz. These components were present in the vibration and current signal. In the vibration signal they were mainly due to the building movements and walking noises. The current signal contained low frequency components which were related to misalignment of the motor and the brake shafts. These components could not be completely eliminated even when a flexible coupling was used. The low

frequency signals would add an offset to the signal if they were not attenuated by a filter.

A zero phase shift finite impulse response (FIR) filter was used to filter the signals in order to minimise the influence of phase shift distortions. In comparison with linear phase filters which simply delay the filter output by a fixed number of samples, the delay using the zero shift FIR filter is zero and it reduces also the filter startup transients. A general FIR filter is characterised by the following equation [59]:

$$g(n) = \sum_{k=0}^{N_f-1} h(k)x(n-k), \quad k = 0, 1, ..., N_f - 1 \tag{5.1}$$

where, x is the input signal, $g(n)$ is the filtered signal, $h(k)$ are the impulse response coefficients of the filter and N_f is the filter length. The processing scheme of a zero phase filter is shown in figure 5.1. The sampled input signal, $x(n)$, is time reversed after filtering, which results in $g(-n)$. This is followed by another stage of filtering and time reversal. As a result, the output signal, $s(n)$, has zero phase distortion [59]. The length of the 50-stage filter used in this study was determined experimentally.

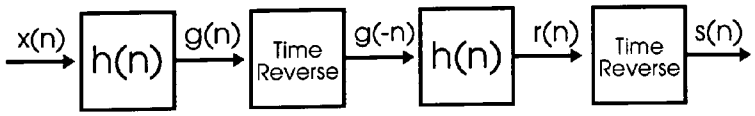

Figure 5.1: Zero phase FIR filtering.

5.1.2 Time domain processing

Statistical methods

Basic statistical methods were used to process the signals. These included the mean value (equation 2.1), RMS value (equation 2.2), kurtosis (equation 2.5) and the variance (equation 2.4) of the signal as described in section 2.3.1.

The coefficient of variation, C, was used to measure the variation of different parameters over a specific motor usage level . The standard deviation, σ_n, is a measure of absolute variability in a set of data. However, of more interest is the relative variability, which is most commonly expressed using the coefficient of variation [116]. It is given by,

$$C = \frac{\sigma_n}{\overline{x}} \, 100\% \tag{5.2}$$

Transform for feature extraction

The literature review has referred to the technique developed and patented by Wahab and Gough [49] for data reduction and waveform feature extraction. This technique appeared to be superior to other time domain analysis methods and therefore, it was selected for detailed investigation in this study. The patent description has reported this technique as a signal processing method for neural network classifiers. It was originally developed for processing biological signals, but no studies on the application of this technique have been reported. It has two main functions:

- To transform the data from an N-sampled vector to an r-sampled vector, where r is smaller than N. This is a data reduction function.

- It enhances the significant features contained in the original data, thus enabling an artificial neural network (ANN) to perform its classification more accurately. This is the feature extraction aspect of the technique.

Therefore, this technique can be thought of as a Transform for Feature Extraction (TFE). The TFE abbreviation will be used for the remainder of this thesis to denote the original Wahab and Gough technique and its derivatives. However, it is important to note that this transform is not reversible.

TFE utilises the shape of the signal as the main feature rather than relying purely on the statistical and spectral information of the signal. The shape of the signal is a combination of a number of factors that also include its spectral and statistical contents. The rationale behind this is that it is possible to have two waveforms with different shapes but with almost identical spectral and statistical contents which makes it difficult to distinguish between them. However, the shape difference may carry information regarding the parameters being monitored.

The TFE was derived from the technique for calculating the fractal dimension of a signal [117]. Therefore, it is important to understand the method of calculating the fractal dimension before presenting the mathematical representation of the TFE. The fractal dimension of a signal is calculated by estimating its geometrical length, l, using rulers of different lengths, r (figure 5.2).

Each ruler provides a different estimate of the signal's geometrical length, with the smallest ruler providing the best estimate. All the signal length estimates, l, are plotted against the different ruler lengths, r. The slope of the resulting log-log graph is the fractal dimension of the signal [118, 119]. The graph itself provides a new representation of the signal.

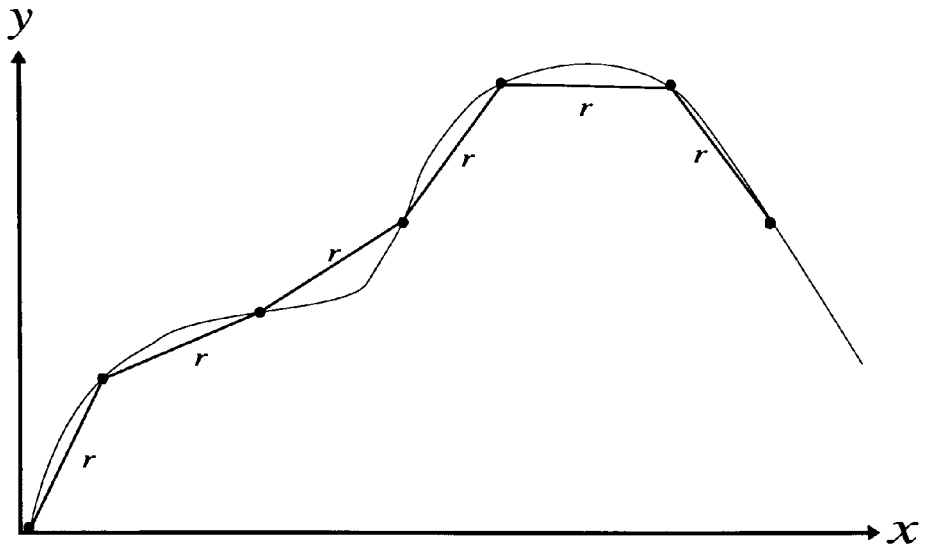

Figure 5.2: Calculation of the fractal dimension suggested by Mandelbrot.

An alternative approach to estimate the signal length versus ruler length graph was proposed by Gough [120] as part of a study on fetal heart rate analysis. In this approach the ruler is kept in a horizontal position and shifted a ruler length, r, at a time as illustrated in figure 5.3. For each ruler position, the amplitude difference of the signal displaced by one ruler gives the vertical difference, h. Using the sample amplitude difference, h, and the ruler length, r, the geometrical length of the signal l, can be approximated by [120],

$$\begin{aligned} l &= \sqrt{(N - rk - 1)^2 + (x_{rk} - x_{N-1})^2} + \sum_{i=0}^{k-1} \sqrt{r^2 + (x_{ir} - x_{(i+1)r})^2} \qquad (5.3) \\ r &= 1, 2, 3 ... r_{max} \end{aligned}$$

where, x_i is the number of the ith signal sample, N is the number of samples of the signal, r_{max} is the maximum ruler length and k gives the number of whole ruler lengths that may be layed end to end along the signal,

$$k = TRUNC\left(\frac{N-1}{r}\right) \tag{5.4}$$

The first square rooted term estimates the length of the last segment of the signal if its number of samples is smaller than the ruler length, or when N-1 is not a factor of r. The *TRUNC* function gives the integer part of $\frac{N-1}{r}$. A graphical illustration of this method is shown in figure 5.3. The error of the approximated length decreases as the ruler length is decreased.

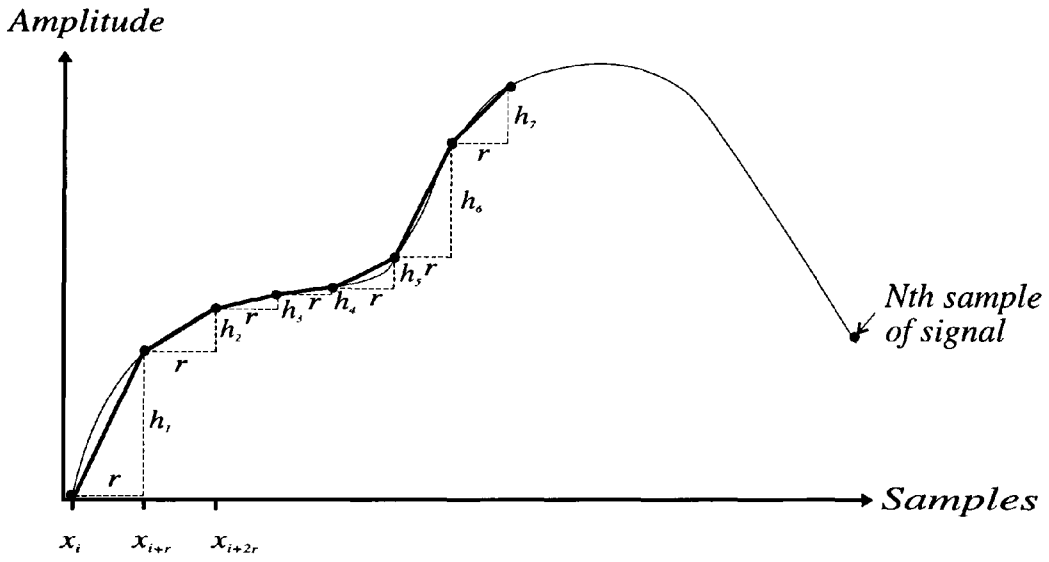

Figure 5.3: Calculation of the fractal dimension suggested by Gough.

For each value of r a new value of l can be calculated and plotted in a log-log graph to calculate the fractal dimension as described earlier. Both methods [118,120] of producing the signal length versus ruler length graph do not characterise the signal in sufficient detail and thus are not useful in extracting its shape features.

The TFE is an evolution of the method of generating the fractal plot of a signal. It provides a better representation of the signal and emphasises its characteristic features. The TFE is calculated by keeping the ruler horizontal as in the previous

method. However, the main difference is that the ruler is shifted by one sample at a time. At each ruler position the amplitude difference, h, is calculated as shown in figure 5.4. The summation of the heights calculated for each ruler position represents a single value, $D(r)$, of the TFE vector. $D(r)$ is calculated for all integer values of r from 1 up to the maximum desired ruler length r_{max}. The resulting feature vector has the same length as the maximum ruler length used. The mathematical representation of the TFE is given by,

$$\begin{aligned} D(r) &= \sum_{i=0}^{n-1} |x_{ir} - x_{(i+1)r}| \ , \\ n &= N - 1 - r \ , \\ \text{and } r &= 1, 2, 3, ..., r_{max} \ , \end{aligned} \tag{5.5}$$

where, $|x_{ir} - x_{(i+1)r}|$ is the amplitude difference of samples i and $i+1$ of the signal, r is the ruler length and N is the number of samples of the input signal. Therefore, the TFE has transformed a signal of length N to a feature vector of length r_{max}.

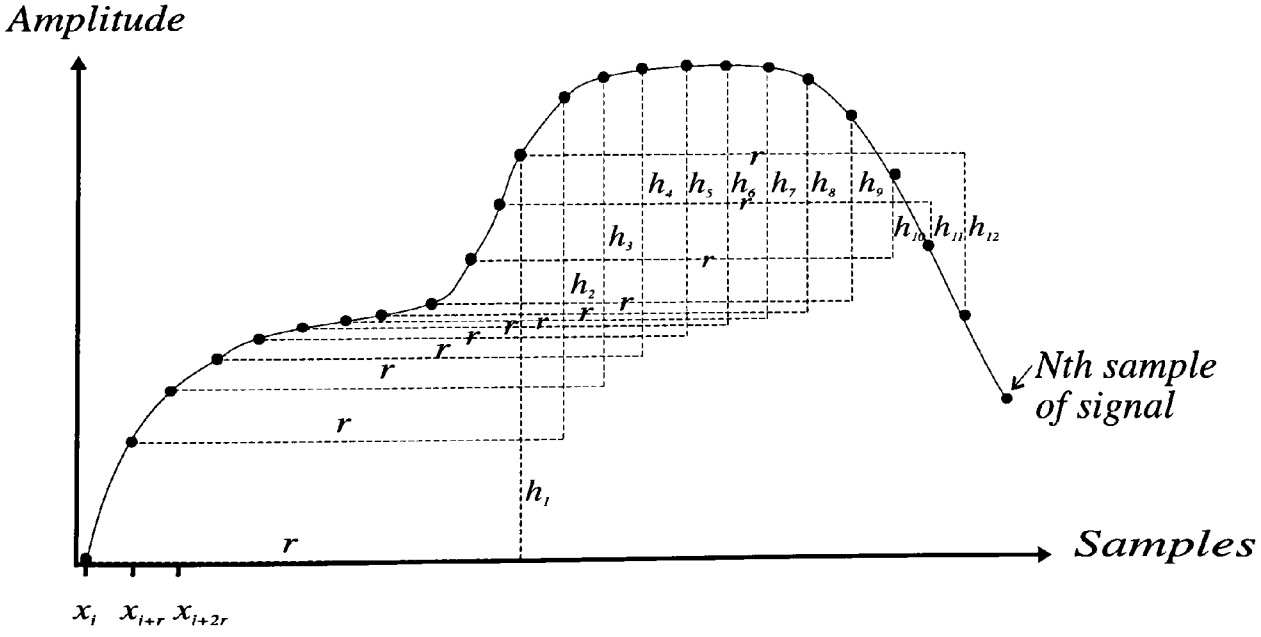

Figure 5.4: Amplitude difference calculation in the TFE.

Since the shape of the signal also depends on its frequency, it is possible to determine the frequency of periodic signals from the TFE vector. A property of the TFE vector is that it has a minimum at the period of the analysed signal. This minimum occurs also at multiples of the analysed signal period. If the signal is periodic as shown in figure 5.5, the TFE vector will show minima at ruler lengths of

$$r = \frac{f_s}{f} n \ , \quad n = 1, 2, 3... \tag{5.6}$$

In equation 5.6, f_s is the sampling frequency and f is the frequency of the periodic signal.

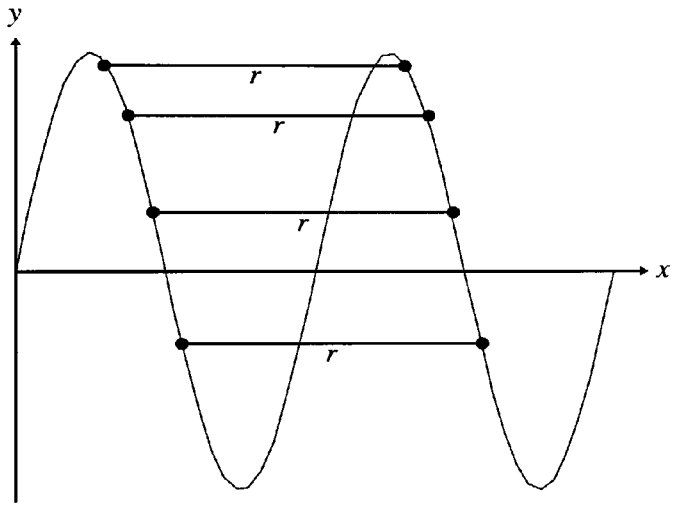

Figure 5.5: Periodic signal.

Figure 5.7 shows the TFE vector for the sinusoidal signal of figure 5.6. The signal frequency is 1 kHz and it was sampled at 200 kHz. Figure 5.7 shows the TFE vector with a maximum length, r, of 600. The feature vector clearly illustrates the local minima at ruler lengths of,

$$r = \frac{f_s}{f} = \frac{200 \text{ kHz}}{1 \text{ kHz}} = 200n \quad n = 1, 2, 3, ... \tag{5.7}$$

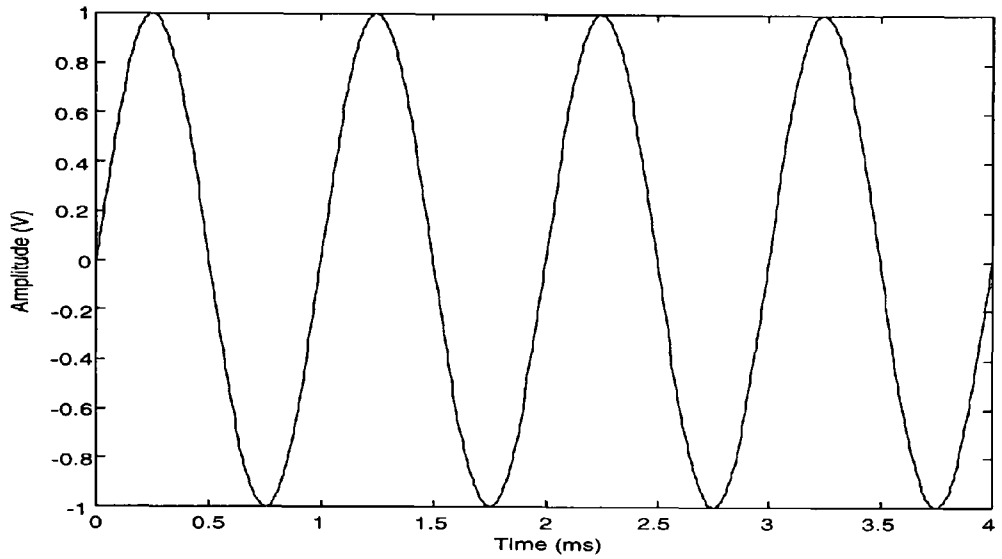

Figure 5.6: Sinusoidal waveform with a frequency of 1 kHz.

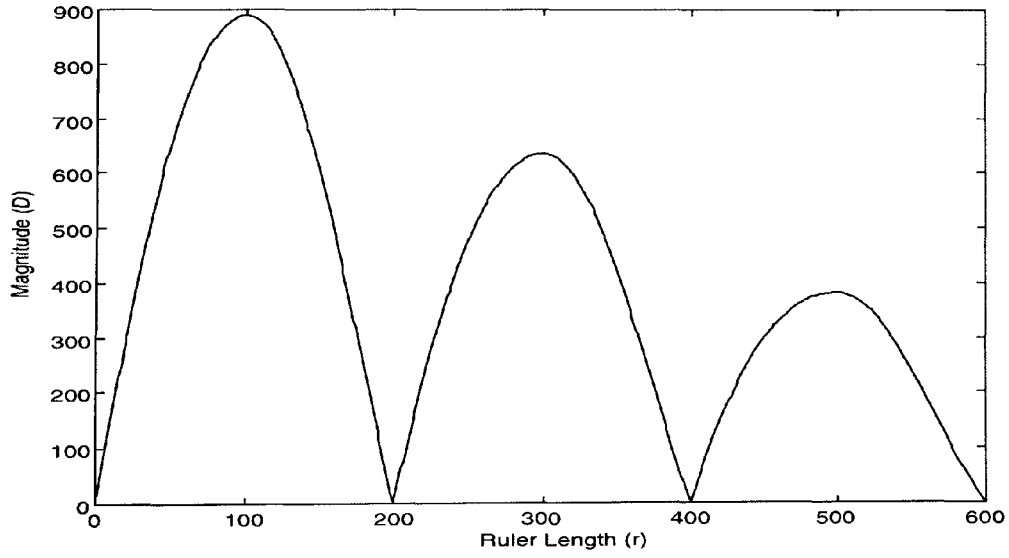

Figure 5.7: TFE vector of the signal of figure 5.6.

The feature extraction and data reduction capability of the TFE was investigated in detail in this study for the first time. Its performance was compared with spectral and statistical methods. Standard signals were utilised in this investigation. Examples of the results obtained are included in this section.

Figure 5.8(a) and (b) show two signals with clearly different shapes. The signal of figure 5.8(a) is a sinusoidal waveform with a frequency sweep of 10%, whilst that of figure 5.8(b) has a sinusoidal waveform superimposed on it. The two signals were sampled at 1 kHz and the number of samples used in the analysis was 1024. Figures 5.8(c) and (d) illustrate the frequency spectra of the signals of figures 5.8(a) and (b) respectively. The two spectra are very similar. This makes the spectra very difficult to use as the means of discriminating between the two signals. In figure 5.8(c) and (d) only 98 points of the spectrum were included for clarity. The remainder of the spectrum does not have any components.

Figures 5.8(e) and (f) show the TFE vectors of the signals of figures 5.8(a) and (b) respectively. These vectors are clearly different and allow a full discrimination between the two signals, even by visual inspection. This illustrates the feature extraction and enhancement capabilities of the TFE. The feature vectors of figures 5.8(e) and (f) were generated using ruler length from 1 to 400. Thus the 1024 points of the original signal were reduced to feature vectors of 400. This provides a data reduction of 2.56:1. To illustrate the data reduction capability of the TFE, every eighth point of the feature vectors in figures 5.8(e) and (f) were plotted to produce the 50 point feature vectors of figures 5.8(g) and (h). The resulting vectors are clearly different and enable a full discrimination between the two signals. The new data reduction ratio is 20.48:1. Plotting every eighth point of the feature vec-

tor is the same as incrementing the ruler length by 8 in calculating the TFE using equation 5.5. This significantly reduces the computation which is already very much simpler than calculating the fast Fourier transform (FFT).

The TFE also has a significant advantage over using statistical parameters to discriminate between signals. To illustrate this consider the two signals of figures 5.9(a) and (b). The two signals are clearly different. Figures 5.9(c) and (d) show the TFE vectors of the signals in figures 5.9(a) and (b) respectively. The two vectors were generated by using ruler lengths of 1 to 400 and they are clearly different.

The statistical parameters for the two signals were calculated and presented in table 5.1. Clearly the two signals have identical statistical parameters and therefore, these parameters cannot be used to discriminate between them. This example demonstrates that the TFE can produce better results than simple signal statistics.

Statistical parameter	*Input signal figure 5.9(a)*	*Input signal figure 5.9(b)*
RMS value	0.7038	0.7038
Variance	0.4957	0.4957
Kurtosis	-1.4962	-1.4962

Table 5.1: Statistical parameters of the signals of figures 5.9(a) and (b).

The two examples comparing the TFE against spectral and statistical analyses illustrate the advantages of this method in extracting the shape features of a signal and discriminating between different signals. In addition, it provides a significant data reduction capability.

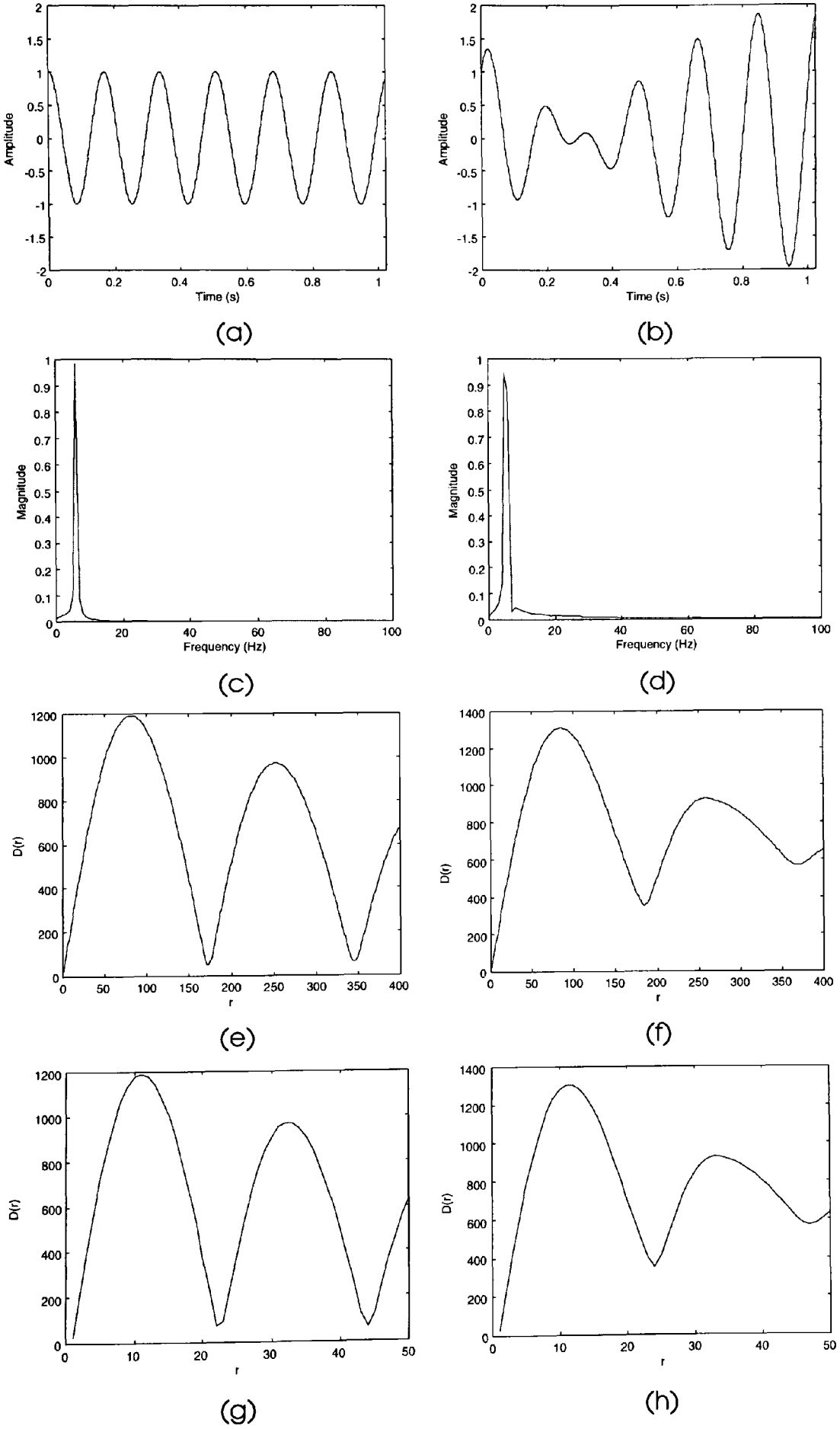

Figure 5.8: Comparison of frequency spectra and TFE processing results.

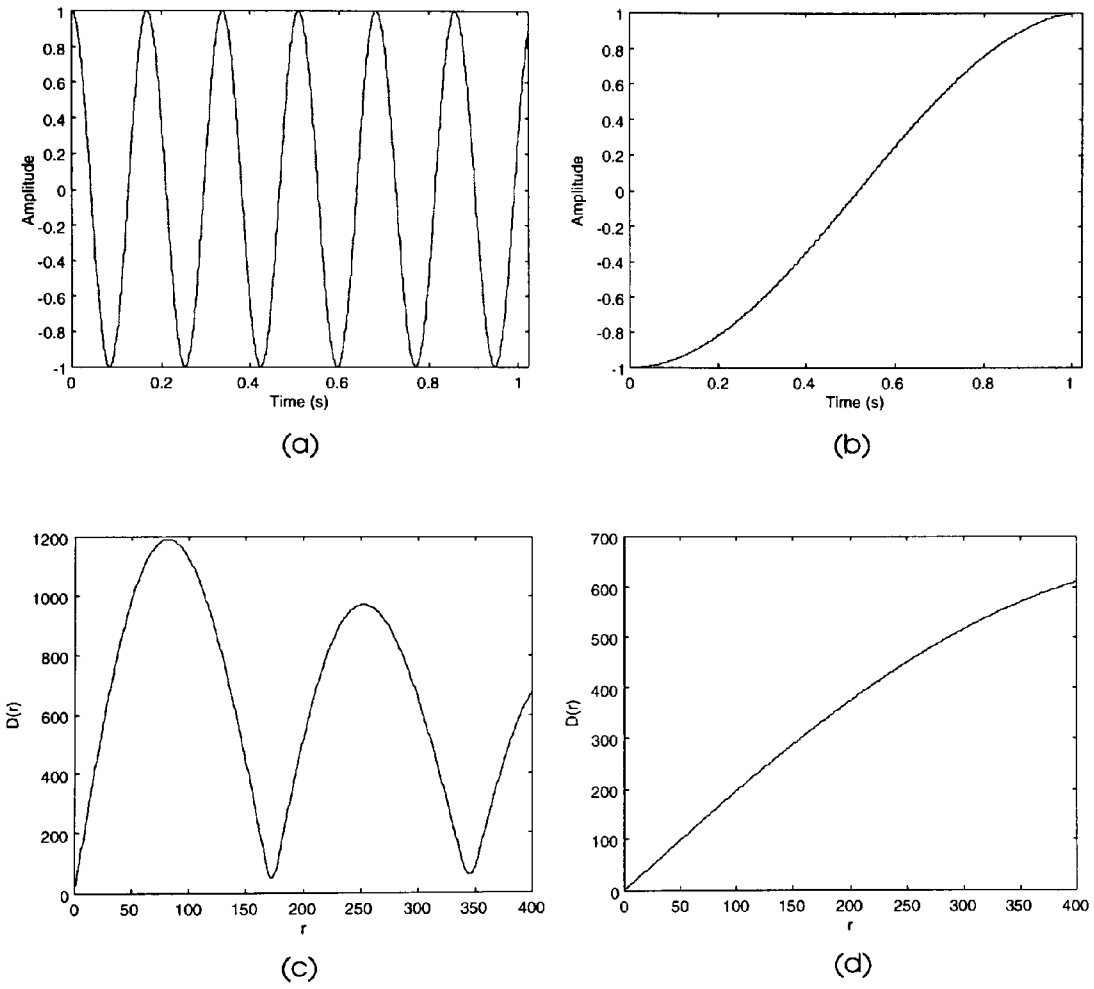

Figure 5.9: Comparison of statistical parameters and TFE processing results.

The windowed TFE (WTFE)

The TFE does not take local variation of the signal shape into account and due to its cumulative summation it has an averaging effect. Therefore, the TFE when applied to a long signal with time varying characteristics may supress important features of the signal. This is similar to applying the Fourier transform (FT) to non-stationary signals. The short time Fourier transform (STFT) is used to overcome the limitations of the FT as described in section 2.3.1. Using a similar approach to the STFT, the windowed TFE (WTFE) was introduced in this study to improve the feature extraction capabilities of the TFE for time varying signals.

The WTFE is calculated, using a sliding window of width w, by,

$$WD(r, nw) = \sum_{i=n}^{n+w-1} |x_{ir} - x_{(i+1)r}| \tag{5.8}$$

where, nw is the window number and,

$$n = 0, w - m, 2(w - m) \ldots N - (w - m) \tag{5.9}$$

The overlap parameter, m specifies the overlapping level between successive windows and is in the interval,

$$0 \leq m \leq w - 1 \tag{5.10}$$

The WTFE results in a three dimensional plot. Two of the axes are the same as those of the TFE and the third axis is the window number, nw. Figure 5.11 shows the WTFE of the signal of figure 5.10. Figure 5.10 shows 2000 samples of a sinusoidal signal with linearly increasing frequency. The WTFE of figure 5.11 was produced with a 400 point wide window, w, an overlap parameter, m of 200

points or 50%, and a maximum ruler length, r_{max}, of 200 points. The plot clearly shows that the feature vectors are changing with time or window number nw. This example shows that the WTFE enables the processing of time varying signals and is more effective in extracting local features of the signal's shape.

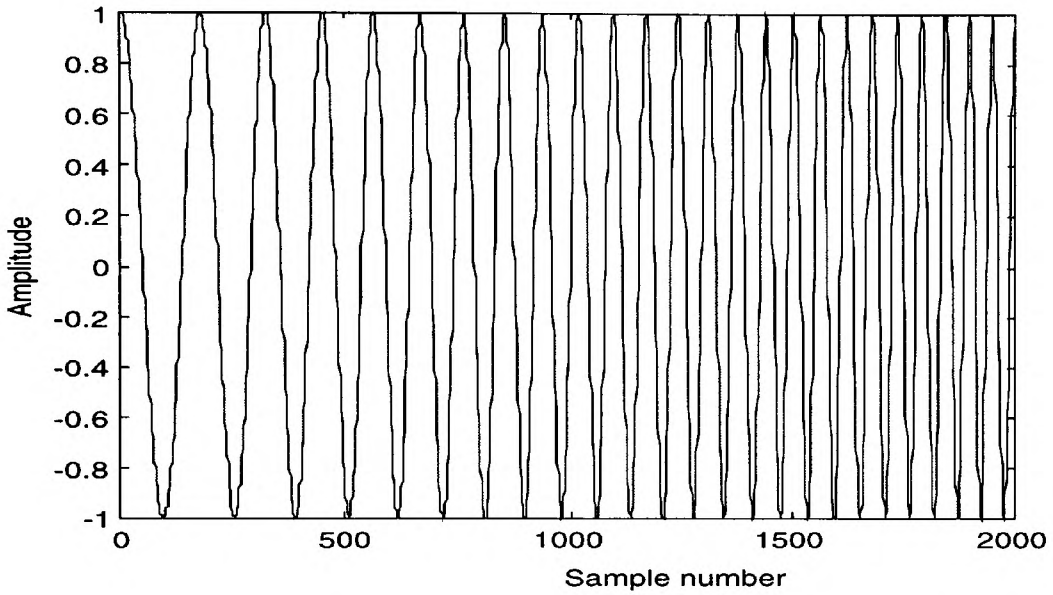

Figure 5.10: Sinusoidal signal with linear swept frequency.

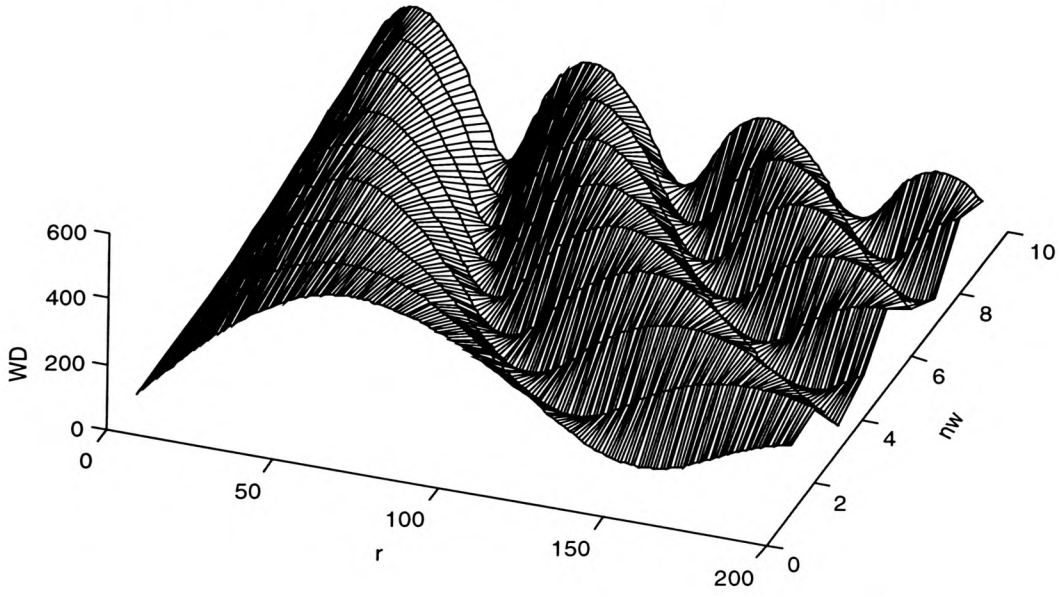

Figure 5.11: The WTFE plot of the signal of figure 5.10.

The overlap parameter m, of the WTFE influences its resolution. Considering an input signal of fixed length the WTFE produces more vectors with a higher overlap ratio than without any overlap. A compromise has to be found between processing speed and resolution. The window length, w, determines the maximum vector length and therefore, also the degree of averaging. More averaging results from wider windows. A compromise between the averaging effect and the ruler length should also be found.

Different maximum ruler lengths, r_{max}, window lengths, w and overlap parameters, m, were investigated in this study. It was found that a window length of 3,000 points, a ruler length of at the most 200 points and an overlap of 50% or 1,500 points produced the best results. Each of the monitored motor parameter from the accelerated life test experiments had a sample length of 30,000 points. Using the 50% overlap and a 3,000 points window resulted in 19 feature vectors with a length of 200 points for each parameter.

5.1.3 Frequency domain processing

The spectra of the signals in this study were computed using the discrete Fourier transform (DFT) described in section 2.3.1 (equation 2.6). Prior to computation of the DFT the input signal was windowed using a Blackman window [121] which is described by

$$w(n) = \begin{cases} 0.42 + 0.50\cos\left(\frac{2\pi n}{N}\right) + 0.08\cos\left(\frac{4\pi n}{N}\right), & n = 0, 1, 2, ..., N-1, \\ 0, & \text{otherwise} \end{cases} \tag{5.11}$$

The windowing process enhances the DFT result by reducing the leakage in the frequency domain. Leakage occurs because the recorded signal is of finite length [51]. The Blackman window has been chosen because its highest sidelobe level has a magnitude of -58 dB and thus shows an advantage over other window types such as Hamming (-43 dB) or Hanning (-31 dB) [121]. Since windowing reduces the signal energy and introduces low frequency components into the spectrum, a linear function of the signal is windowed in order to overcome these disadvantages. This is accomplished using the following function [108]:

$$S(n) = w(n)\left[s(n) - \frac{\sum_{n=0}^{N-1} w(n)s(n)}{\sum_{n=0}^{N-1} w(n)}\right]\left[\frac{N}{\sum_{n=0}^{N-1} w^2(n)}\right]^2 \tag{5.12}$$

where, $s(n)$ is the original sampled signal and $S(n)$ the windowed and corrected signal.

The resolution, f_0, of the DFT depends on the sampling frequency, f_s, the total number of analysed samples, n, and the characteristic window bandwidth. According to Harris [121] it can be calculated for a Blackman window by,

$$f_0 = \frac{f_s}{n}\, 2.13 \tag{5.13}$$

The signals in this study consisted of 30,000 samples which were segmented into three parts with a length of 10,000 samples. The DFT was then been applied to the three segments of 10,000 sample points which resulted in three frequency spectra with a resolution of 21.3 Hz. The spectra were then averaged in order to enhance the significant frequency components and to attenuate noise. This method has been used by other researchers [22].

5.1.4 Confidence interval

In order to determine the confidence interval of the test motor data it was assumed that the data were normally distributed. For small sample sizes and with the assumption that the measured data were normally distributed and the expectation value μ is unknown, the t-distribution can then be used. The t-value is given by,

$$t = \frac{\overline{x} - \mu}{\sigma_{\overline{x}}} \tag{5.14}$$

with, the standard deviation of the mean value $\sigma_{\overline{x}}$,

$$\sigma_{\overline{x}} = \sqrt{\frac{1}{N(N-1)} \sum_{i=1}^{N} (x_i - \overline{x})^2} \tag{5.15}$$

The confidence interval is given by

$$\mu = \overline{x} \pm t\sigma_{\overline{x}} \tag{5.16}$$

where, the t values depend on the chosen confidence interval and the number of samples [40, 122]. In this study the 95% confidence interval has been used to show the spread in the data of the tested set of motors.

5.2 Accelerated Life Test Results

This section presents the results of the accelerated life test experiments of the dc motor sample. The recorded signal of the monitored parameters were processed using the methods described in section 5.1. Table 5.2 lists the number of tested motors and the number of cycles carried out during these tests. The number of motor cycles is commonly referred to as the test time. It is more accurate to consider the number

of cycles as the usage level of the motor.

The 95% confidence intervals were calculated and plotted with the resulting graphs.

Accelerated test time (million cycles)	*Number of motors tested*
0-1.5	8
1.5-4.5	4

Table 5.2: Number of tested motors.

5.2.1 Motor voltage

The recorded motor voltages were almost constant. Figures 5.12 and 5.13 show the voltages in the forward mode without load. Figures 5.14 and 5.15 show the voltages in the reverse mode. The forward voltage with maximum load showed similar steadiness and was therefore, not displayed. Table 5.3 lists the mean voltages and the range for the tested motors.

Table 5.3 and figures 5.12 to 5.15 clearly show that the voltage of the motors did not change significantly during 4.5 million motor cycles. This observation is important since it indicates that the tests were conducted correctly. A high variation in the supply voltage of the motors would have influenced the test results due to the voltage dependency of the motor's speed. A long term range of the mean motor voltages of less then $\pm 0.4\%$ of the mean value is very satisfactory.

Cycles (million)	*Operation mode*	*Mean voltage (V)*	*Range (%)*
0-1.5	Forward, without Load	17.04	+0.308% −0.378%
1.5-4.5	Forward, without Load	17.01	+0.367% −0.28%
0-1.5	Reverse	-17.16	+0.059% −0.1%
1.5-4.5	Reverse	-17.16	+0.072% −0.053%

Table 5.3: Test results of the motor voltages. Results were obtained from 8 tested motors during the first 1.5 million cycles and 4 motors for the remaining 3 million cycles.

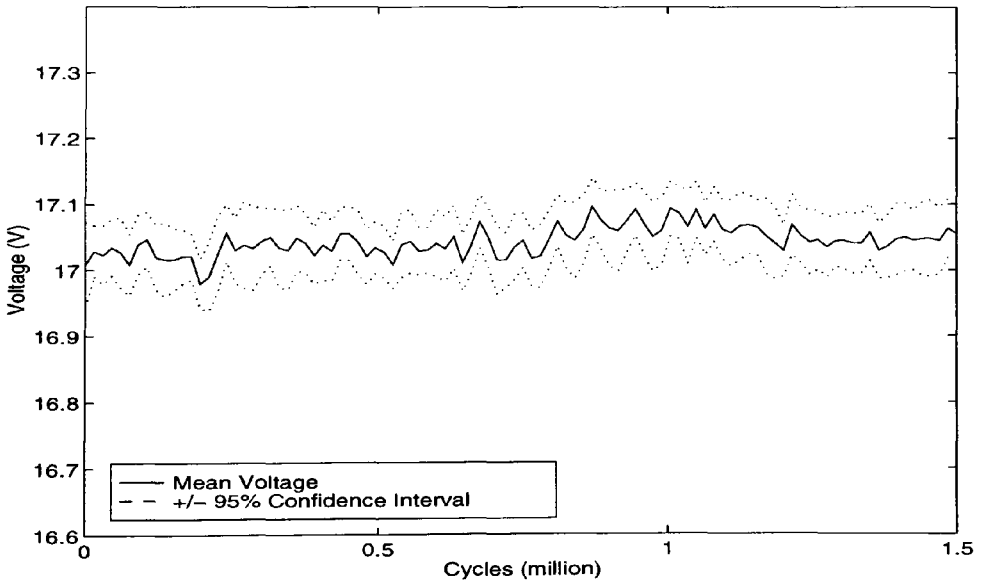

Figure 5.12: Motor voltages in the forward mode without load, during 1.5 million cycles. Results were obtained from 8 tested motors and averaged.

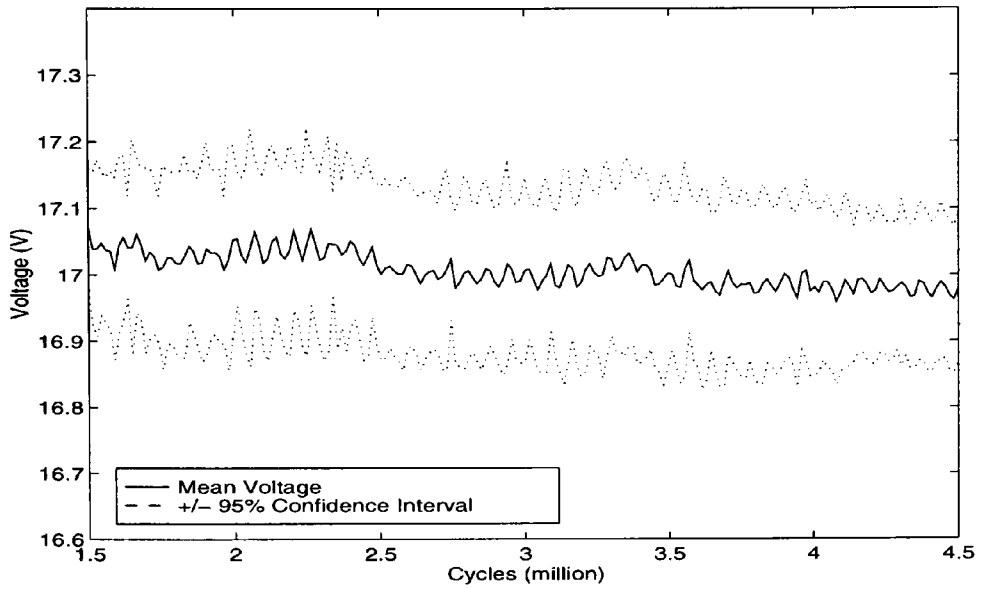

Figure 5.13: Motor voltages in the forward mode without load, during 1.5-4.5 million cycles. Results were obtained from 4 tested motors and averaged.

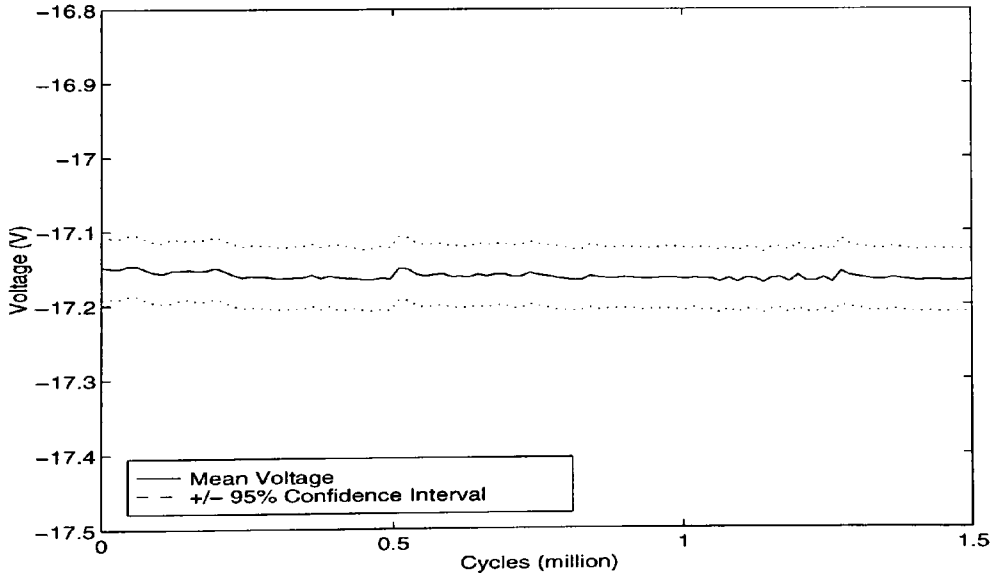

Figure 5.14: Motor voltages in the reverse mode, during 1.5 million cycles. Results were obtained from 8 tested motors and averaged.

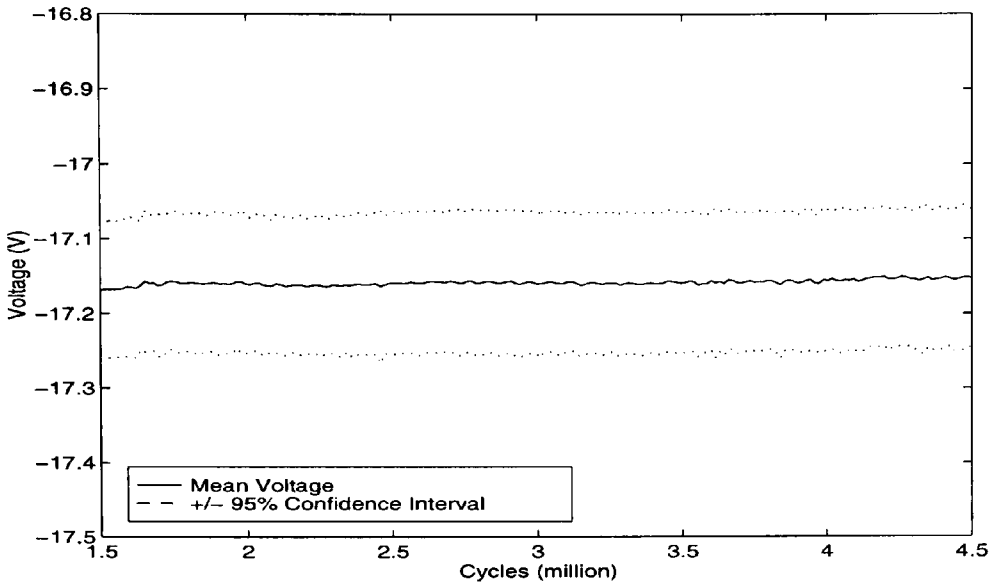

Figure 5.15: Motor voltages in the reverse mode, during 1.5-4.5 million cycles. Results were obtained from 4 tested motors and averaged.

5.2.2 Internal motor resistance

The internal motor resistance, R_a, was derived from the motor current and voltage in the two generator modes. The first mode operated the test motor as a generator in open circuit, whilst the second mode operated the test motor as a generator with a load resistor connected to the motor terminal pins (figure 5.16). The internal resistance consists mainly of the contact resistance of the brushes and the armature winding resistance. A value of 11 Ω for the armature winding resistance was measured on disassembled motors and was considered constant as long as no short circuit occurs in the winding.

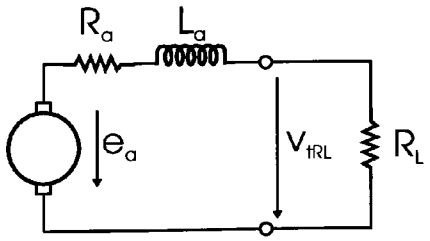

Figure 5.16: Equivalent circuit of a dc motor with the load resistor connected.

Using the measurements in these two operational modes the resistance was cal-

culated using equation 4.1. The used load resistor value of 150 Ω was determined experimentally so that the speed of the test motor in generator mode does not exceed a minimum speed limit of 100 rpm.

Figure 5.17 illustrates the results over 1.5 million cycles and figure 5.18 shows the changes of the internal resistance during the following 3 million motor cycles. It can be seen that the resistance did not change significantly for the 4.5 million cycles after an initial decline in the first 300,000 cycles. The fact that the internal resistance of the motor cannot give a reliable indication of the condition of the carbon brushes was also reported by industry sources [97]. This is mainly due to its composite structure and physical properties (section 3.6.1). An overview of the internal motor resistance range over motor usage level can be seen in table 5.4.

Cycles (million)	*Mean resistance (Ω)*	*Range (%)*
0-1.5	12.4	+11.4% −4.8%
1.5-4.5	12.6	+7.6% −5.71%

Table 5.4: Mean resistance and its range.

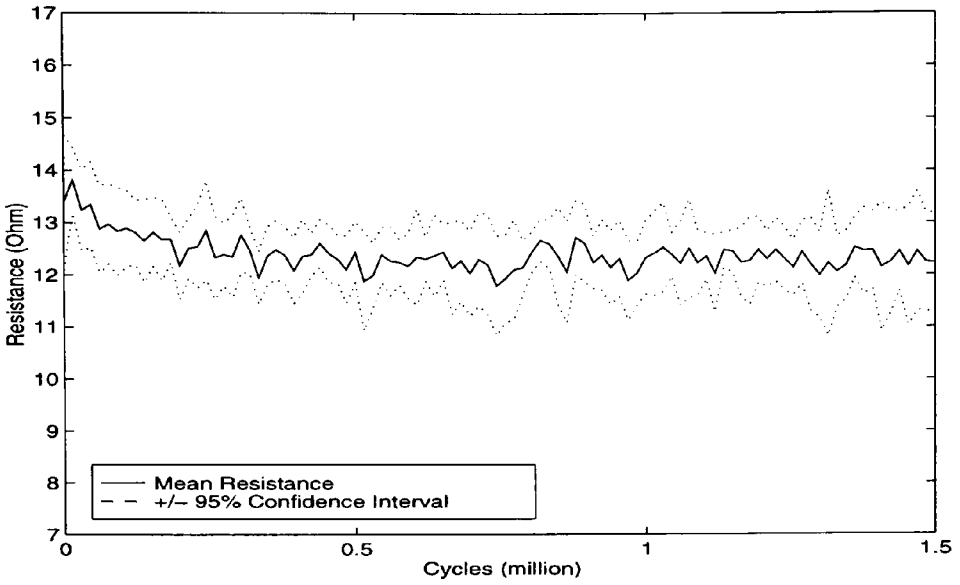

Figure 5.17: Internal motor resistance during 1.5 million cycles. Results were obtained from 8 tested motors and averaged.

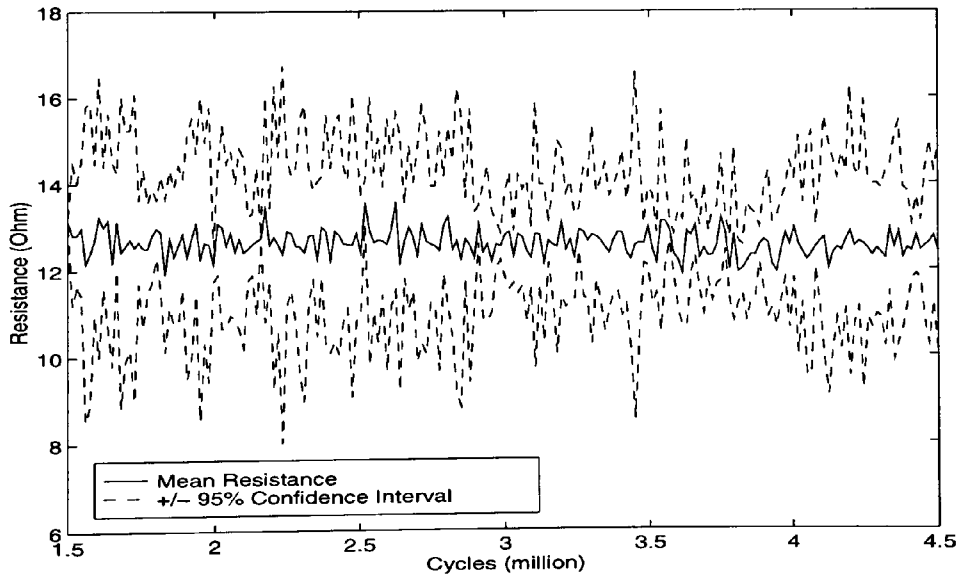

Figure 5.18: Internal motor resistance during 1.5-4.5 million cycles. Results were obtained from 4 tested motors and averaged.

5.2.3 Time-to-Speed

The time-to-speed is an important parameter of the motor performance in the copying machine if used as a paper feed motor due to its cyclic operation (section 3.3). The results of the time-to-speed tests are shown in figures 5.19 to 5.22. Figures 5.19 and 5.20 illustrate the variation of the time-to-speed value during 4.5 million cycles of the unloaded motor. Figures 5.21 and 5.22 show the same parameter, but with maximum motor load. The tests were conducted on eight motors in the first 1.5 million cycles and four motors for the following 3 million cycles, and then averaged to produce the results in figures 5.19 to 5.22. The results presented in the four figures clearly show that the time-to-speed parameter is relatively constant during motor usage. Furthermore, the parameter did not vary significantly with loading of the motor as can be concluded by comparing figures 5.19 and 5.20 with figures 5.21 and 5.22. The variation of the time-to-speed value during the motor's usage are summarised in table 5.5. Finally, it is clear that the motors did not exceed the design specifications of 120 ms for the time-to-speed at maximum load (section 3.3).

Cycles (million)	*Operation mode*	*Mean time-to-speed (ms)*	*Range (%)*
0-1.5	Forward, with Load	73.1	$^{+5.9\%}_{-4.5\%}$
1.5-4.5	Forward, with Load	74.74	$^{+15.1\%}_{-12.1\%}$
0-1.5	Forward, without Load	73.1	$^{+5.9\%}_{-4.5\%}$
1.5-4.5	Forward, without Load	73.59	$^{+8.31\%}_{-9.2\%}$

Table 5.5: Mean time-to-speed values and their ranges.

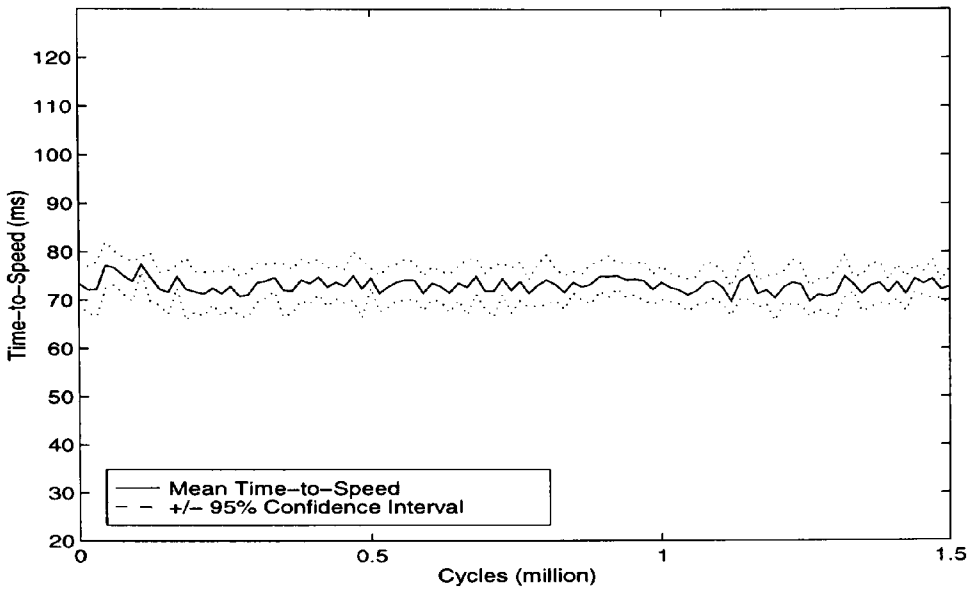

Figure 5.19: Time-to-speed value without load during 1.5 million cycles. Results were obtained from 8 tested motors and averaged.

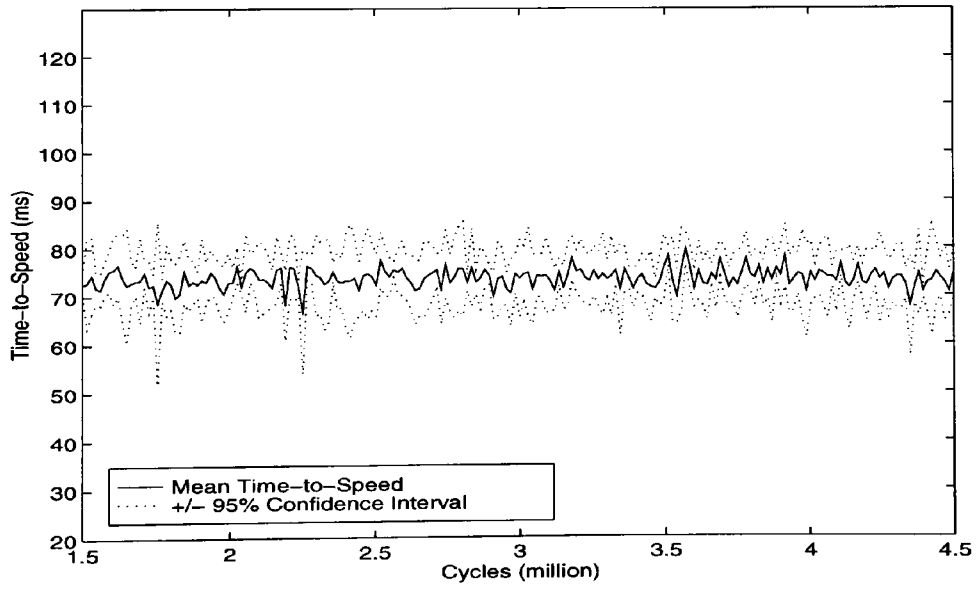

Figure 5.20: Time-to-speed value without load during 1.5-4.5 million cycles. Results were obtained from 4 tested motors and averaged.

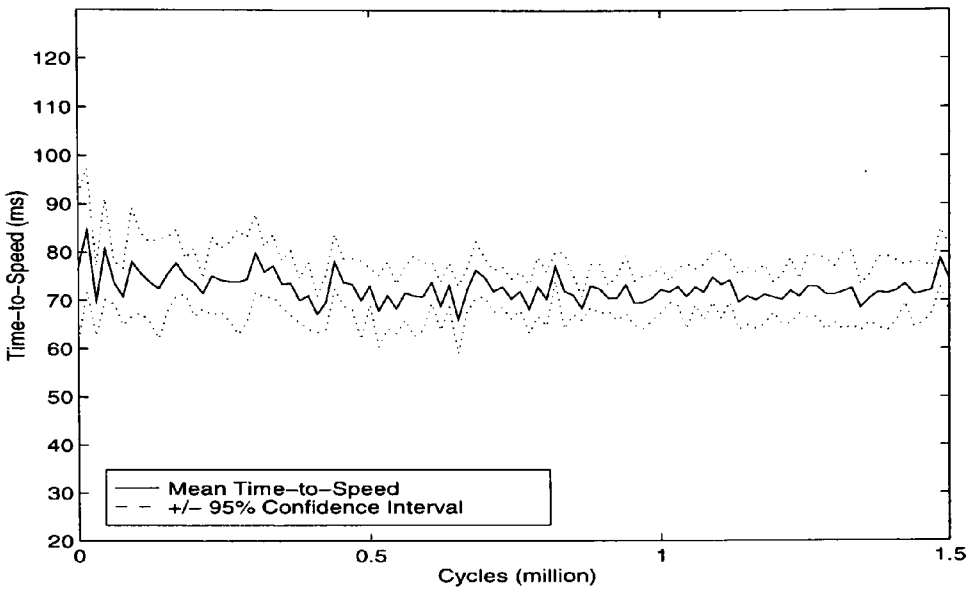

Figure 5.21: Time-to-speed value with maximum load during 1.5 million cycles. Results were obtained from 8 tested motors and averaged.

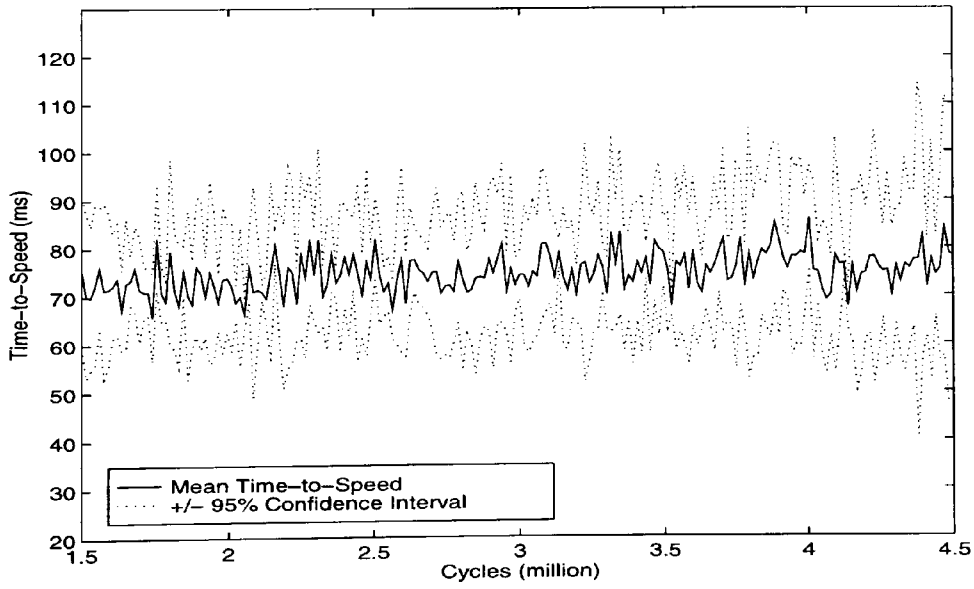

Figure 5.22: Time-to-speed value with maximum load during 1.5-4.5 million cycles. Results were obtained from 4 tested motors and averaged.

5.2.4 EMF/Speed

For permanent magnet dc motors the factor, $k\ \Phi$, where Φ is the magnetic flux and k is the armature winding constant, is constant. It is clear from equation 3.5 that the generated motor voltage, E_a, is proportional to the speed, ω_0, of the motor. Considering a constant magnetic flux, Φ, due to the permanent magnets, this parameter should not change. However, a slight negative trend was observed during the first 1 million cycles. Figures 5.23 and 5.24 show the ratio, $\frac{E_a}{\omega_0}$, during 4.5 million cycles of the motor's usage. It is very likely that this effect was due to a decrease in the magnetic flux, Φ. This means that the permanent magnets might have been subjected to an effect that had changed their magnetic properties. The effect of the decrease in Φ is discussed further in section 5.2.5.

Cycles (million)	*Mean* $\frac{E_a}{\omega_0}$ $(Vmin)$	*Range (%)*
0-1.5	0.033	$^{+2\%}_{-1.27\%}$
1.5-4.5	0.033	$^{+1.35\%}_{-1.37\%}$

Table 5.6: Mean $\frac{E_a}{\omega_0}$ and its range.

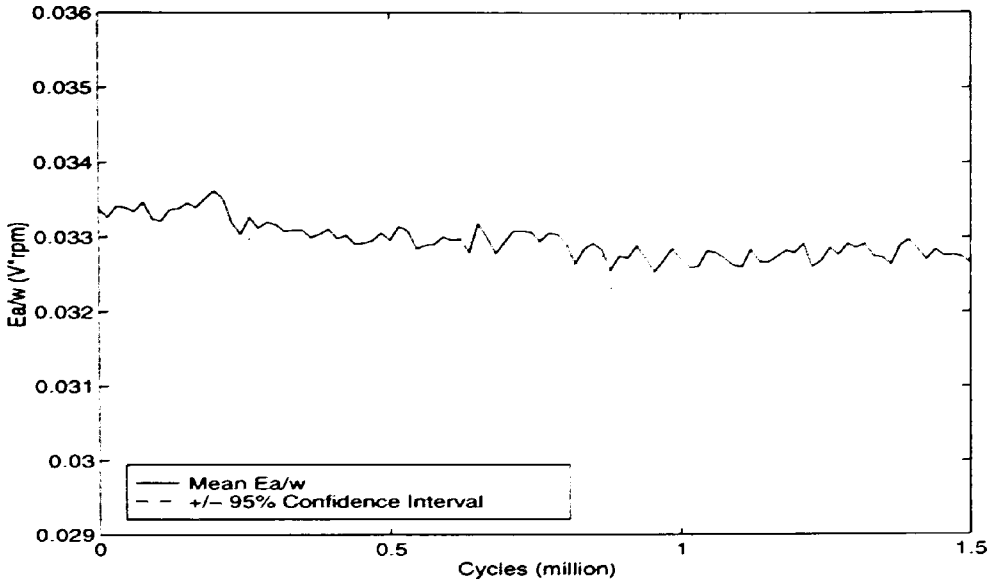

Figure 5.23: $\frac{E_a}{\omega_r}$ during 1.5 million cycles. Results were obtained from 8 tested motors and averaged.

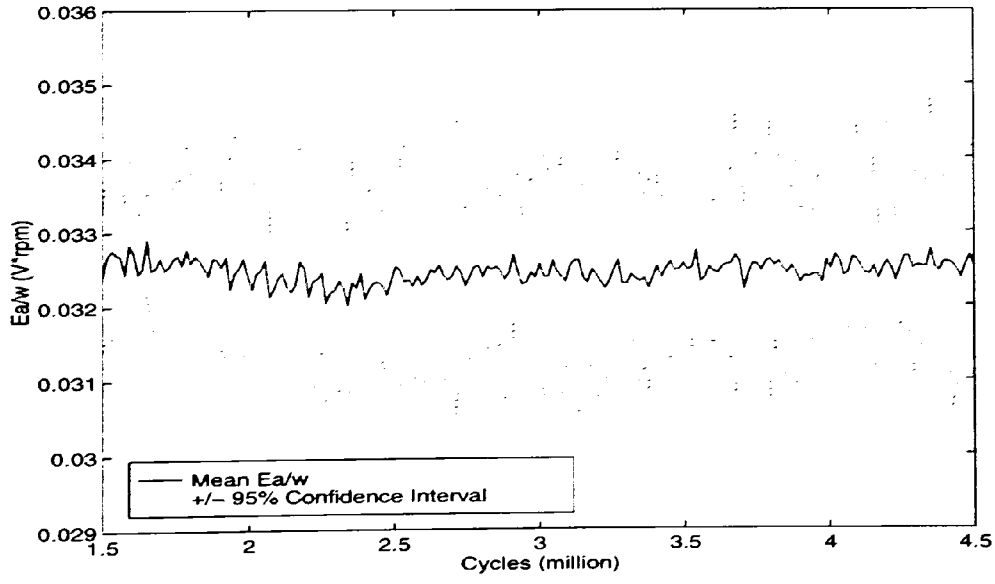

Figure 5.24: $\frac{E_a}{\omega_r}$ during 1.5-4.5 million cycles. Results were obtained from 4 tested motors and averaged.

5.2.5 Speed

The motor speed was measured in the steady state to ensure that the test results were not influenced by the motor's starting behaviour. The results of the speed measurements are shown in figures 5.25 to 5.27.

Figures 5.25 and 5.27 show that the motor's forward speed had increased during the first 1.5 million cycles. The reverse speed showed the same behaviour and was therefore, not presented here. The speed showed an overall range of 4.86% in the forward mode without load (table 5.7). This correlates with an overall range of 3.27% in the $\frac{E_a}{\omega_0}$ parameter (table 5.6). From equation 3.5, it follows that

$$\omega_0 \propto \frac{1}{\Phi} \tag{5.17}$$

the speed of the motor therefore, inversely increases with flux. Figure 5.29 shows the speed and $\frac{E_a}{\omega_0}$ changes with reference to their initial values during 1.5 million cycles of the motor testing. The graph was plotted using a fifth order best fit polynomial to the mean value of the two parameters against the number of cycles of motor usage with reference to the initial value. It can be seen that the changes of $\frac{E_a}{\omega_0}$ and speed are inversely proportional for approximately 70% of the first 1.0 million test cycles, which is in agreement with equation 5.17. After 1.0 million test cycles, the speed shows very little variation as can be seen in figure 5.25 and 5.27.

Cycles (million)	*Operation mode*	*Mean speed (rpm)*	*Range (%)*
0-1.5	Forward, without Load	483.4	+1.86% −3%
1.5-4.5	Forward, without Load	482	+2.15% −1.67%
0-1.5	Forward, with Load	309	+3.43% −5.91%
1.5-4.5	Forward, with Load	296.4	+3.15% −2.99%

Table 5.7: Mean speed and their ranges.

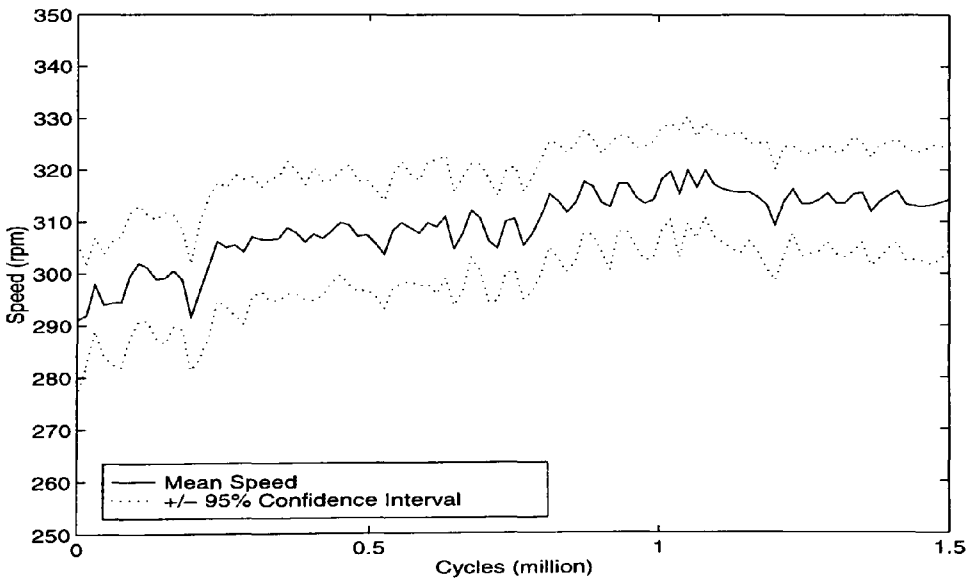

Figure 5.25: Speed in forward mode with maximum load during 1.5 million cycles. Results were obtained from 8 tested motors and averaged.

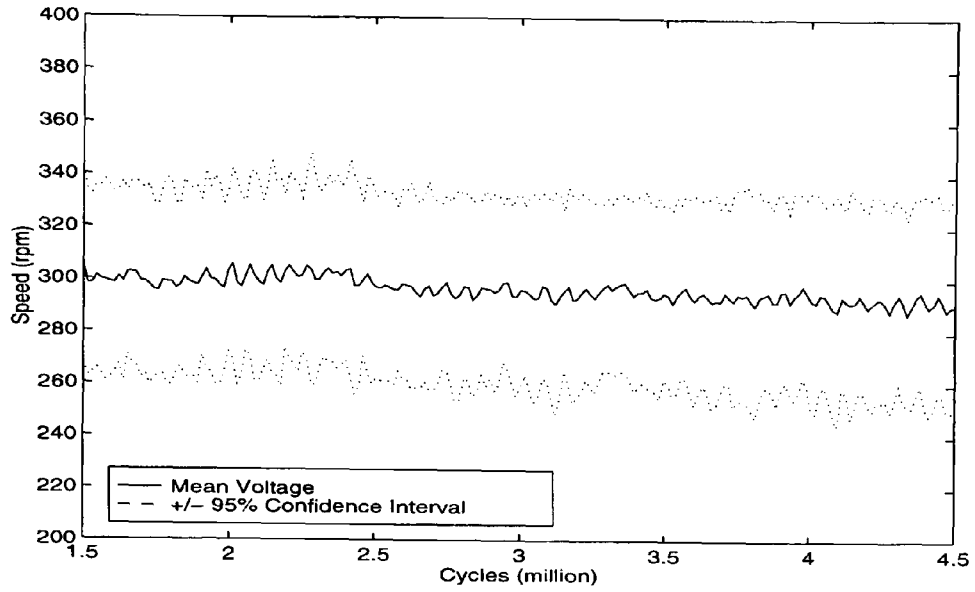

Figure 5.26: Speed in forward mode with maximum load during 1.5-4.5 million cycles. Results were obtained from 4 tested motors and averaged.

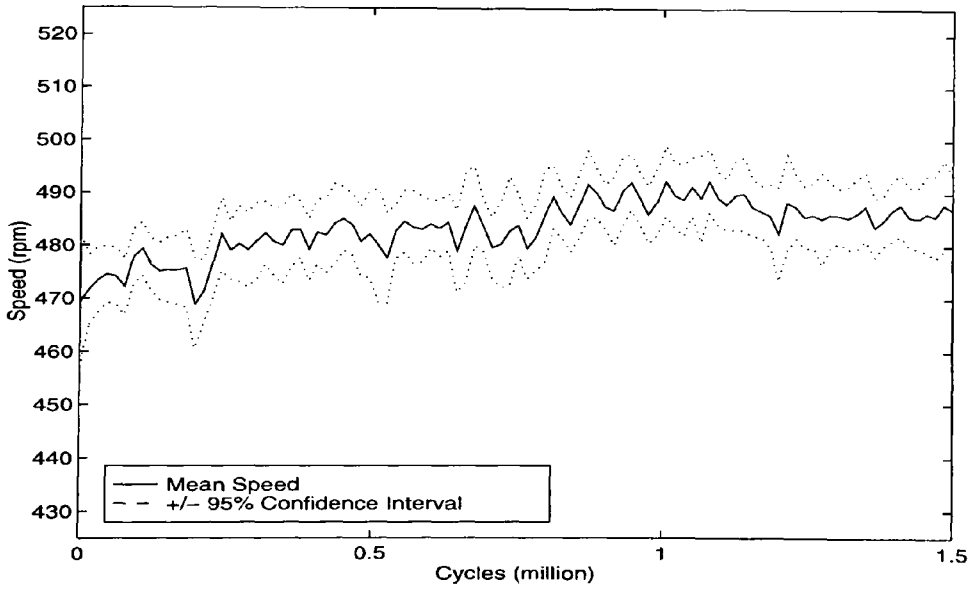

Figure 5.27: Speed in forward mode without load during 1.5 million cycles. Results were obtained from 8 tested motors and averaged.

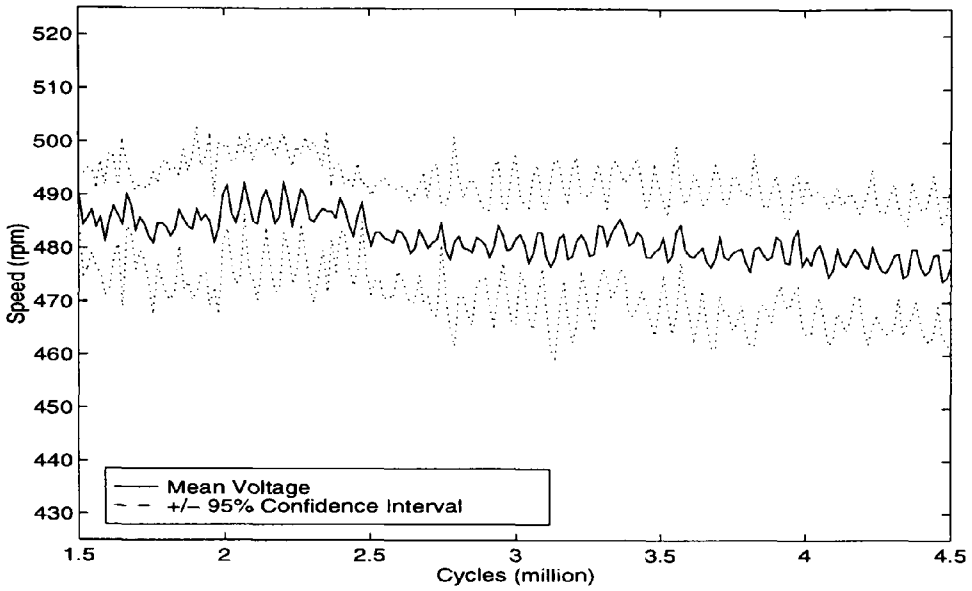

Figure 5.28: Speed in forward mode without load during 1.5-4.5 million cycles. Results were obtained from 4 tested motors and averaged.

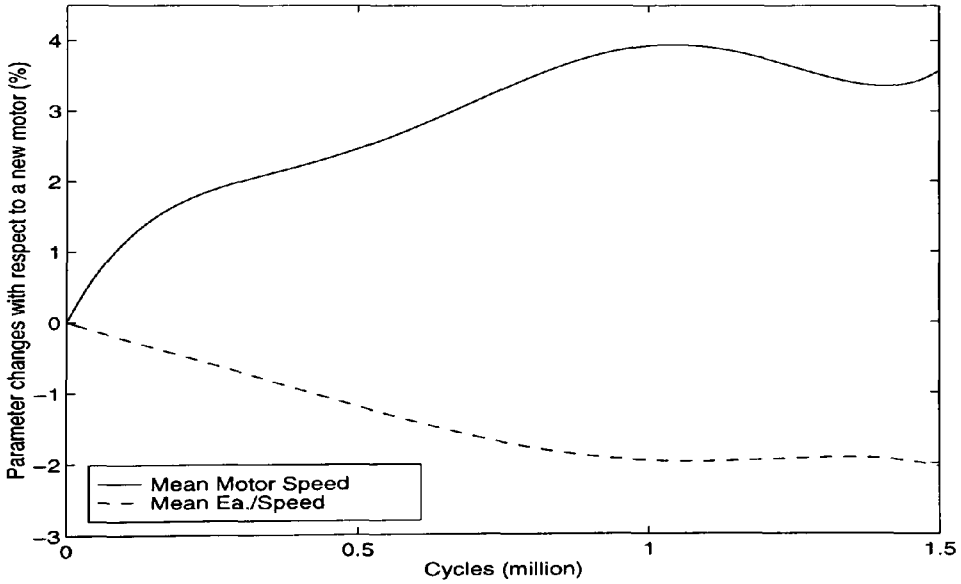

Figure 5.29: Speed and $\frac{E_a}{\omega_0}$ changes with respect to a new motor during 1.5 million cycles. Results were obtained from 8 tested motors, averaged and plotted using a best fit polynomial.

5.2.6 Current

The current of the motors was monitored using a shunt resistor. Due to the location of the shunt resistor in the h-bridge circuit of the life test equipment, the current was recorded as a positive value independent of its operational mode (figure B.2). Figure 5.30 shows a sample segment of the current waveform for a motor that was tested for 150,000 cycles. Figure 5.31 shows a sample segment of the current waveform of the same motor after 450,000 cycles of the test. It can be seen that the current waveforms are similar in appearance, but the current waveform of figure 5.31 exhibits slightly more current spikes than that of figure 5.30.

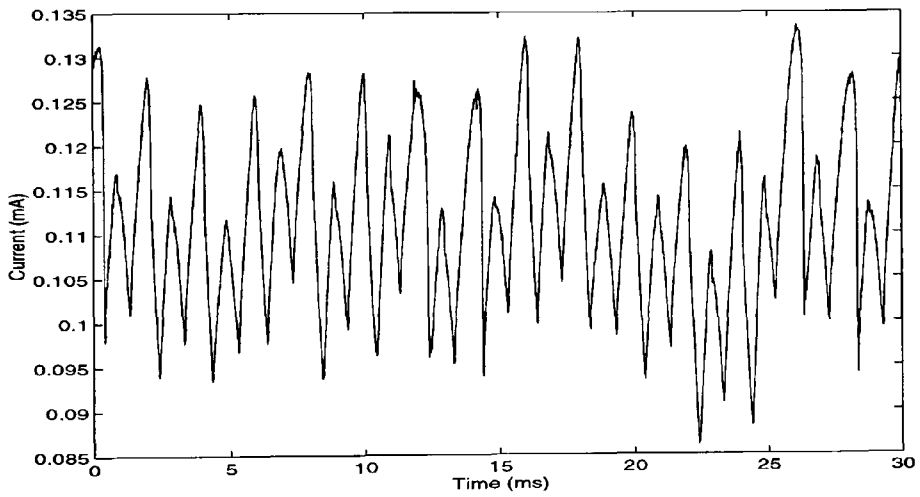

Figure 5.30: Sample segment of the current waveform of a motor that was tested for 150,000 cycles.

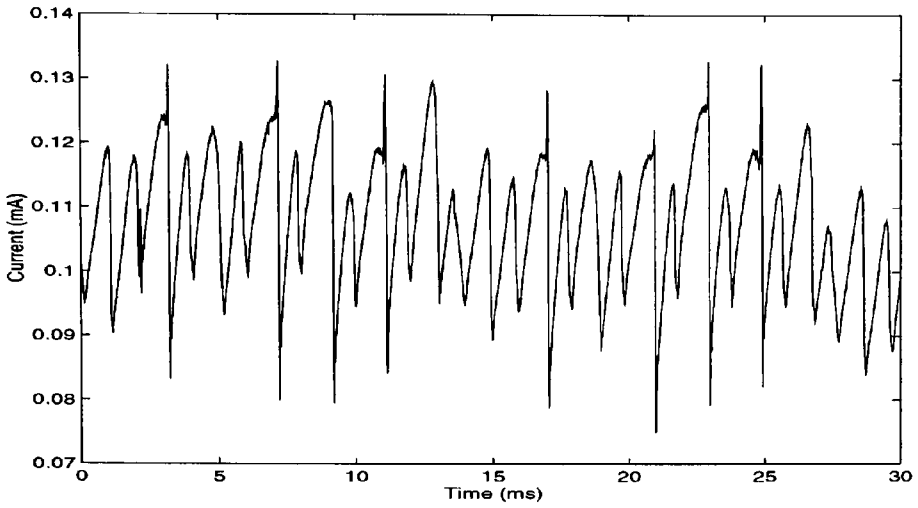

Figure 5.31: Sample segment of the current waveform of a motor that was tested for 450,000 cycles.

Time domain processing

Mean current value The mean value of the current waveforms did not show any significant trend in all operational modes that were used for wear analysis. The range in the mean currents can be seen in table 5.8. The difference between the maximum and minimum mean current value of the eight tested motors in the first 1.5 million cycles was approximately 11% (table 5.8). During the initial 5% of the first 1.5 million cycles of testing a significant current drop was observed which is likely to have been caused by the initial bedding-in of the motor parts such as the carbon brushes. The reverse current and forward current without load showed an increase of over 7% in the first 1.5 million cycles. The mean values of the current waveform for 1.5-4.5 million cycles of testing did not show any significant change or trend and are therefore not included here.

Operation mode	*Mean current (mA)*	*Range (%)*
Forward, without Load	116	+7.55% −3.52%
Forward, with Load	392	+4.48% −3.22%
Reverse	115	+7.61% −3.84%

Table 5.8: Mean currents and their ranges for the first 1.5 million cycles.

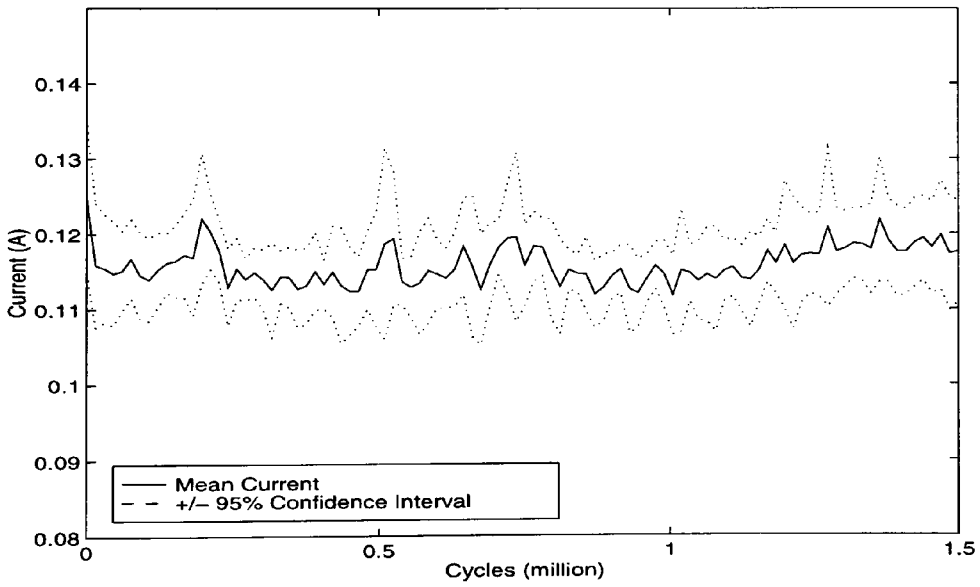

Figure 5.32: Mean value of the current waveform in the forward mode without load during 1.5 million cycles. Results were obtained from 8 tested motors and averaged.

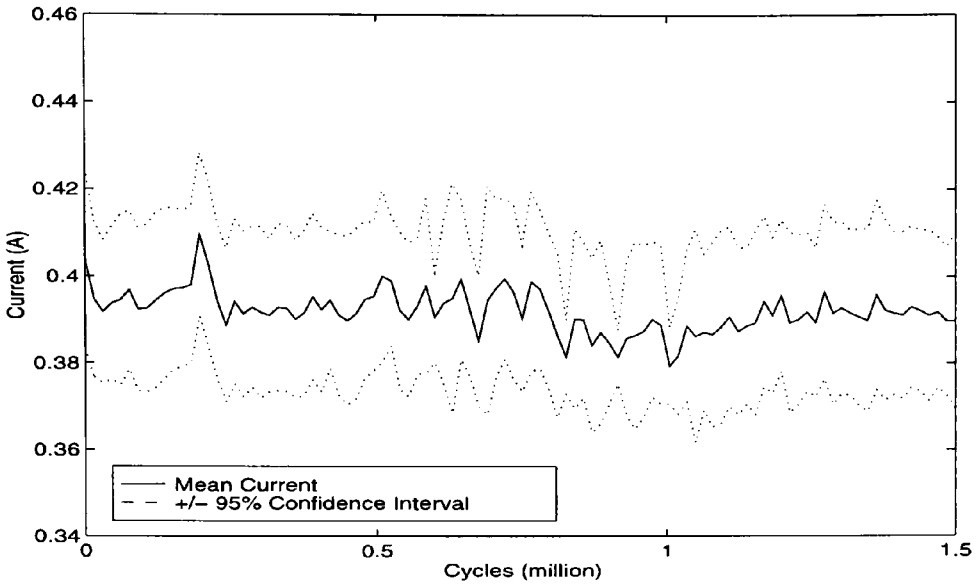

Figure 5.33: Mean value of the current waveform in the forward mode with maximum load during 1.5 million cycles. Results were obtained from 8 tested motors and averaged.

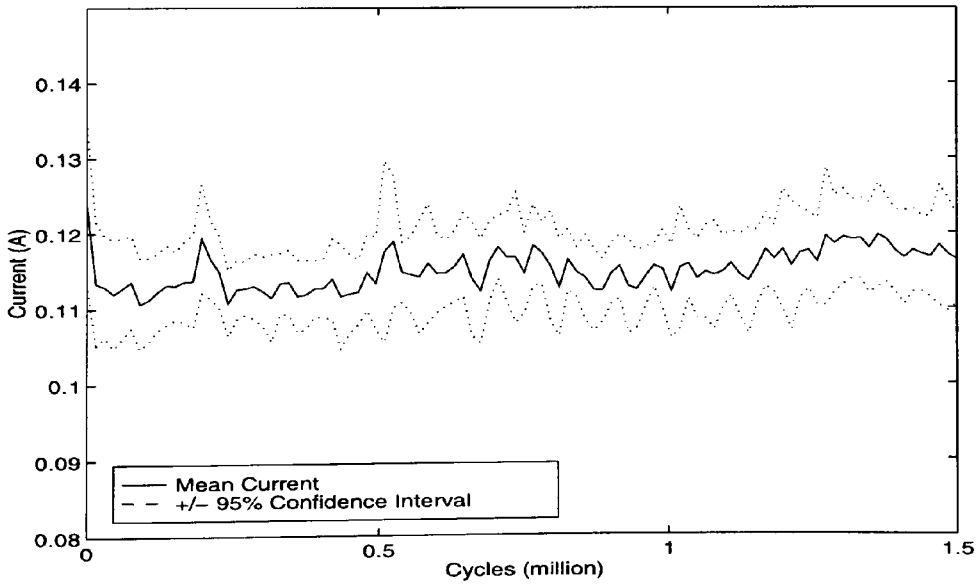

Figure 5.34: Mean value of current waveform in the reverse mode during 1.5 million cycles. Results were obtained from 8 tested motors and averaged.

TFE processing The TFE described in section 5.1.2 was applied to the motor current waveforms. Examples of the feature vector changes in the three operational modes can be seen in figures 5.35 to 5.40. Each plot displays the 19 vectors of the WTFE (equation 5.8) obtained from the recorded current signal of a length of 30,000 sample points. Since 19 vectors were calculated, each vector was plotted against the time interval of the window over which it was calculated. The other two axes are the ruler length, r, and the magnitude of the vectors. The sample results were taken from one motor only (motor 5). The figures show the feature vectors at the beginning of the life test and after 1.5 million cycles. It can be seen that the feature vectors have changed significantly with motor usage.

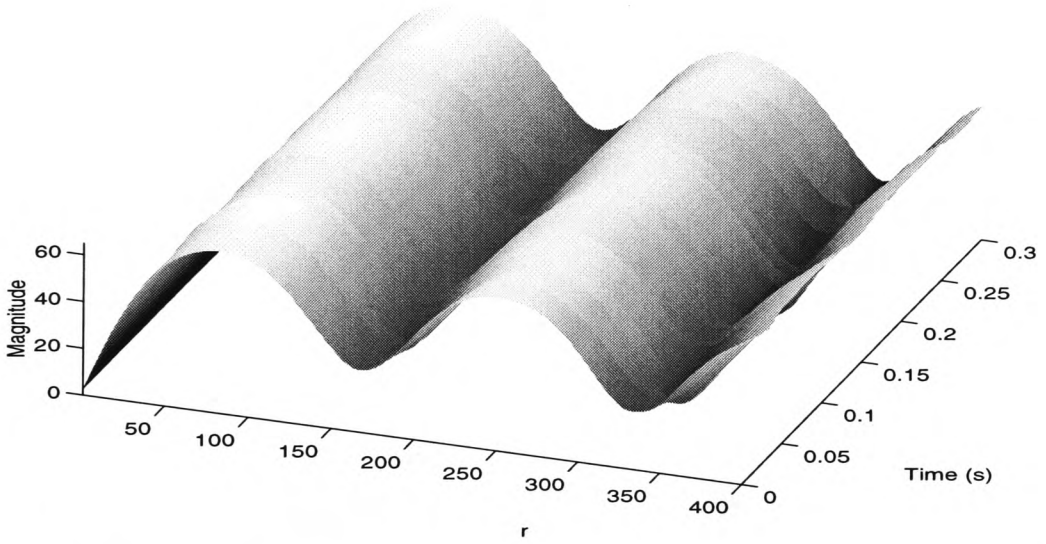

Figure 5.35: WTFE vectors of motor 5 (new) in the forward mode with maximum load.

In order to estimate if the 19 feature vectors of the recorded current signal show any variation a measure of the variation was introduced. A measure of the variations was obtained by calculating the standard deviation of the 19 vectors at each ruler length, r. In order to measure the overall variation the cumulative sums of

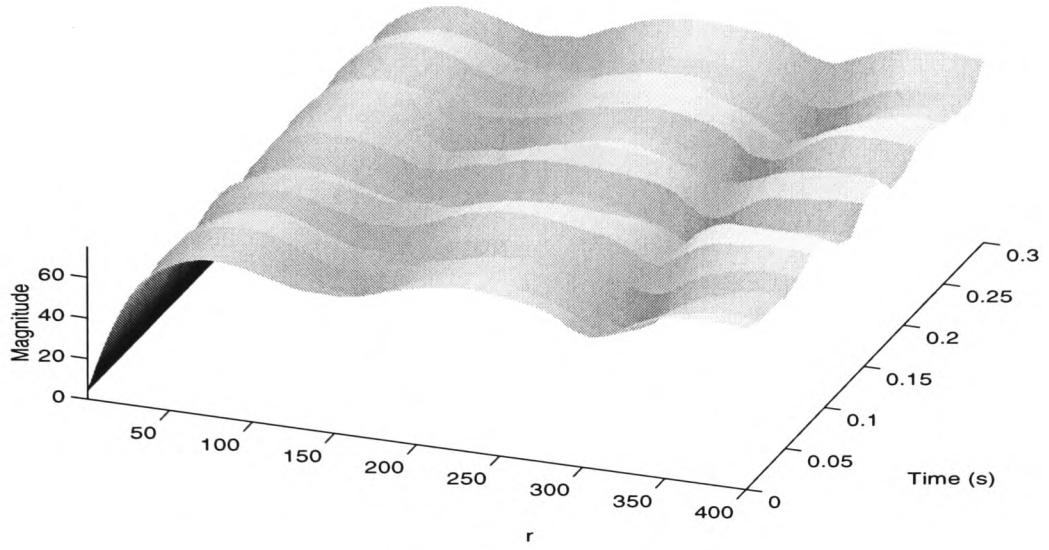

Figure 5.36: WTFE vectors of motor 5 in the forward mode with maximum load after 1.5 million cycles.

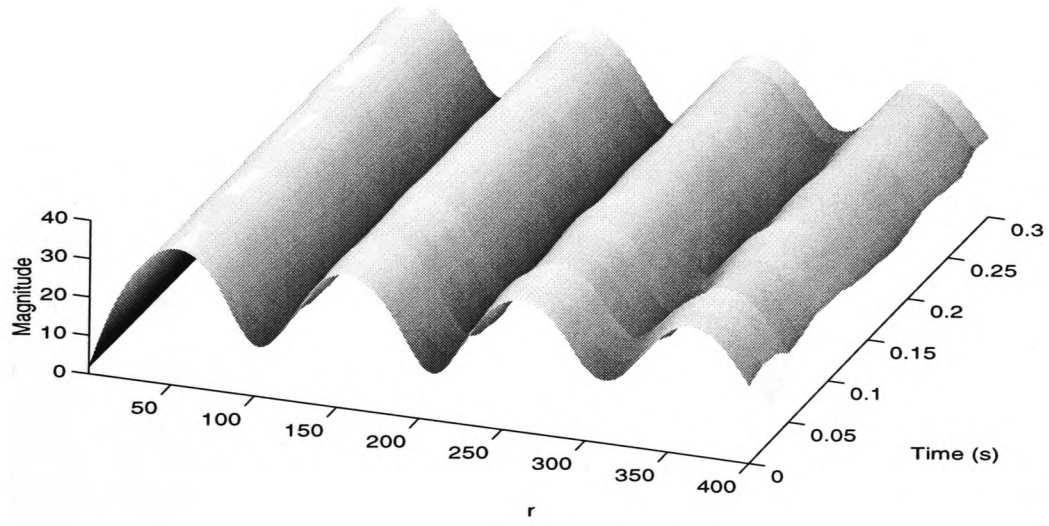

Figure 5.37: WTFE vectors of motor 5 (new) in the forward mode without load.

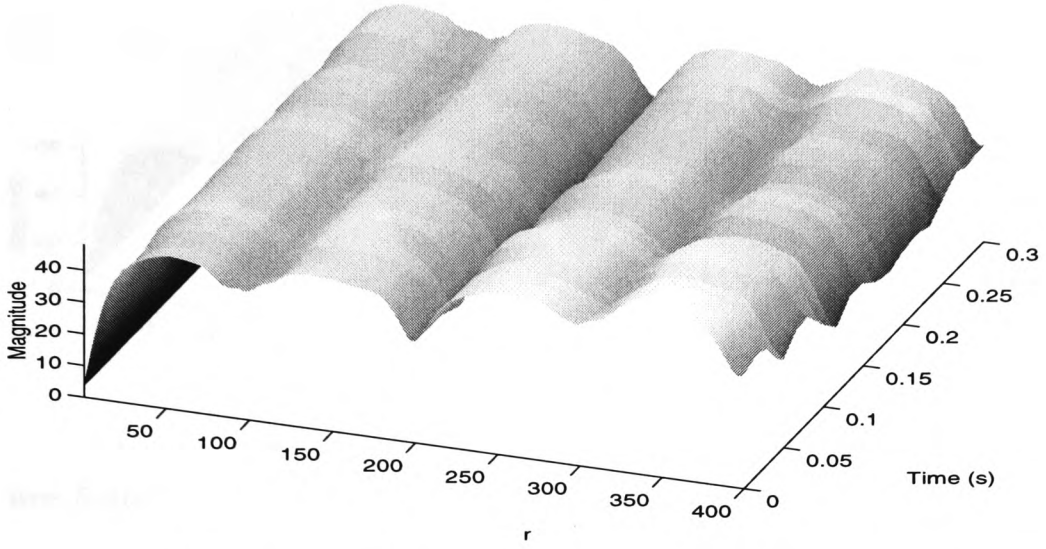

Figure 5.38: WTFE vectors of motor 5 in the forward mode without load after 1.5 million cycles.

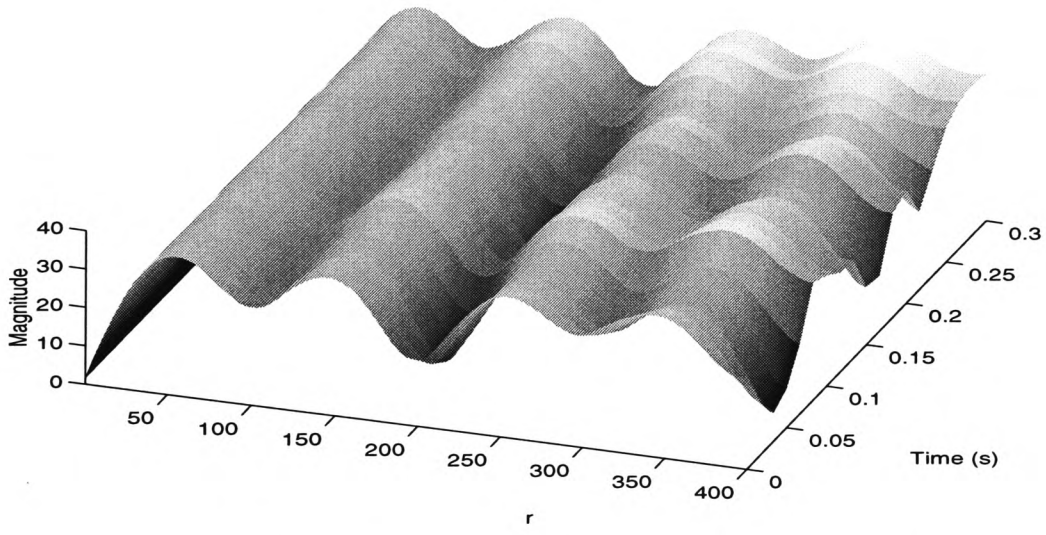

Figure 5.39: WTFE vectors of motor 5 (new) in the reverse mode.

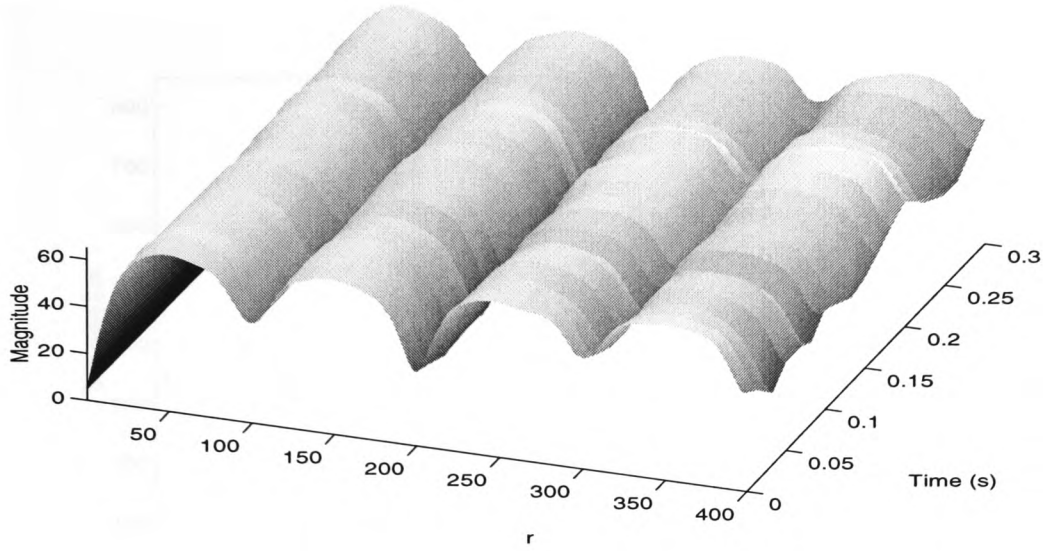

Figure 5.40: WTFE vectors of motor 5 in the reverse mode after 1.5 million cycles.

the obtained standard variations were calculated. The cumulative sums were then plotted against the motor's usage. Figures 5.41 and 5.42 show the changes of the 19 vectors in each sample over usage. The graphs for the two forward modes were not produced here as they are similar to figures 5.41 and 5.42.

It can be seen that the variability of the feature vector increases slightly with motor usage. The variability during the first 300,000 cycles is small. It then increases rapidly and shows only little variation at the end of 1.5 million cycles.

This was investigated further using the coefficient of variation (equation 5.2) calculated from the raw time domain signal. The coefficients of variation of all three operational modes are plotted in figure 5.43 to 5.45.

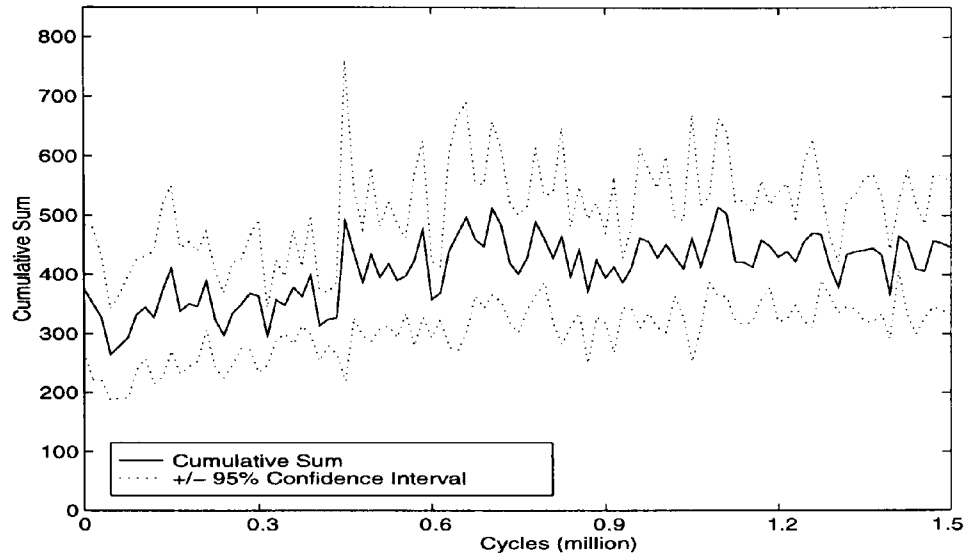

Figure 5.41: Variation of the 19 feature vectors during 1.5 million cycles in the reverse mode. Results were obtained from 8 tested motors and averaged.

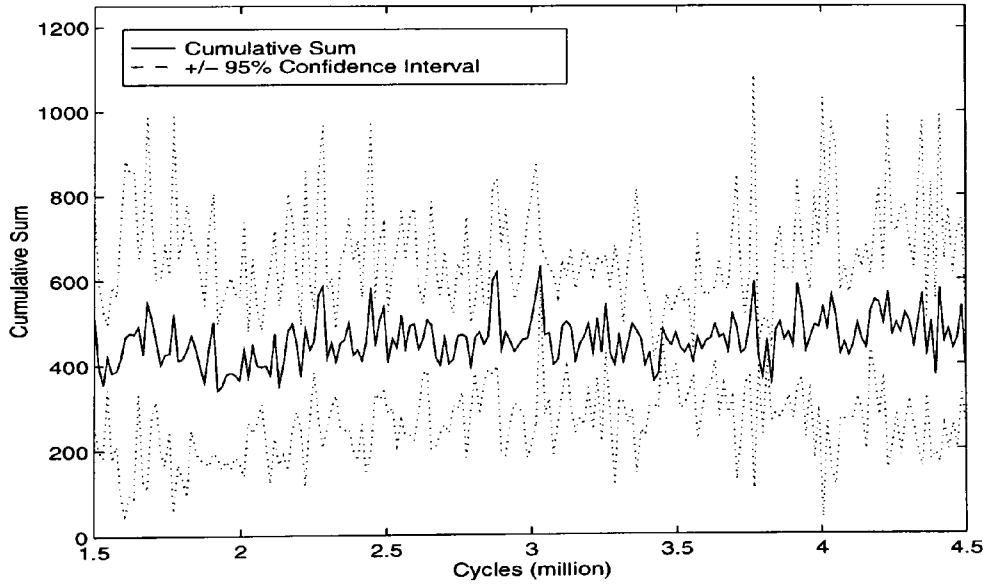

Figure 5.42: Variation of the 19 feature vectors during 1.5-4.5 million cycles in the reverse mode. Results were obtained from 4 tested motors and averaged.

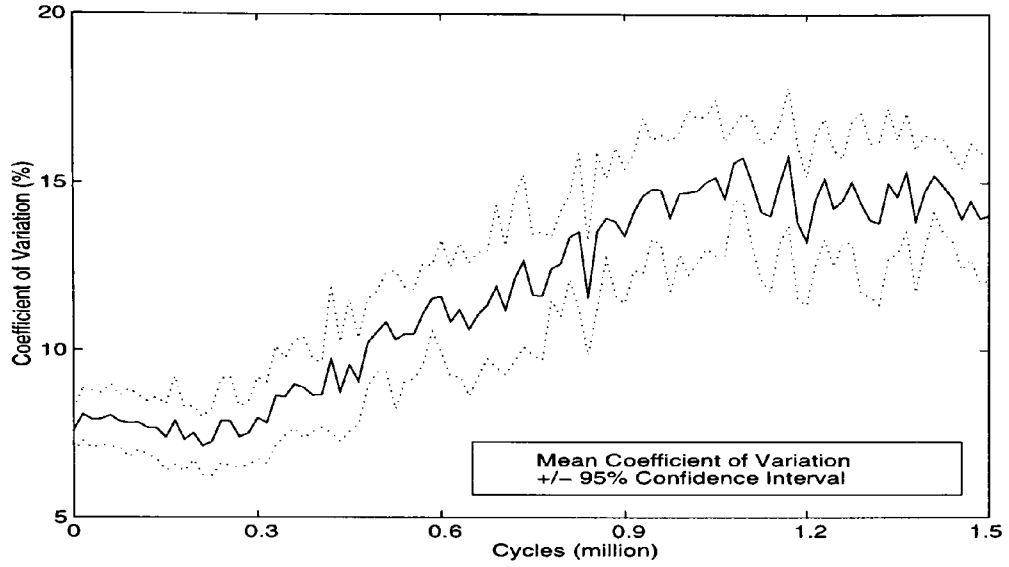

Figure 5.43: Coefficient of variation of the feature vectors during motor usage in the forward mode without load. Results were obtained from 8 tested motors and averaged.

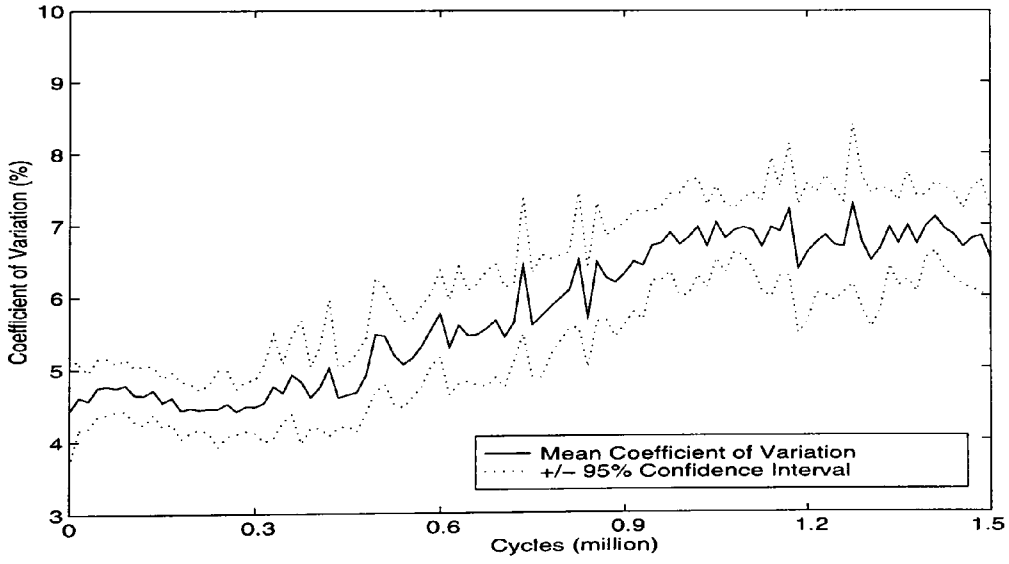

Figure 5.44: Coefficient of variation of the feature vectors during motor usage in the forward mode with load. Results were obtained from 8 tested motors and averaged.

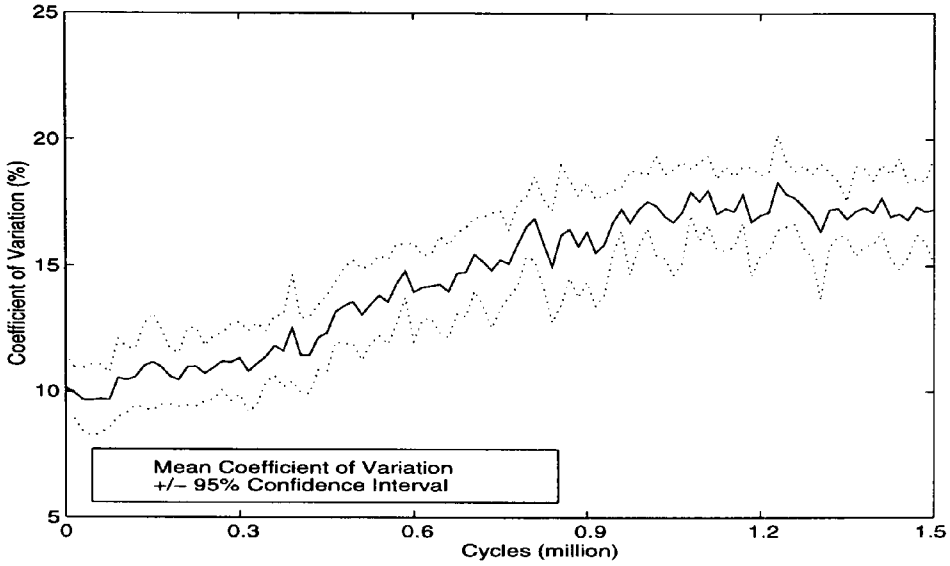

Figure 5.45: Coefficient of variation of the feature vectors during motor usage in the reverse mode. Results were obtained from 8 tested motors and averaged.

It can be seen that the variation of the feature vectors over the motor's usage show an increasing trend as does the coefficient of variation. Figure 5.45 shows that the variation in the reverse mode is noted to be the highest.

Figures 5.46 to 5.48 show the mean of the mean values of all the feature vectors during 4.5 million cycles of testing. In order to visualise the change of the vectors the figures were plotted with a view from the top of the magnitude axis. The different grey levels correspond to different magnitude values. A darker shading represents lower magnitude. It can be seen that the feature vectors show an increase in amplitude with motor usage. This is an indicator that the amplitude differences in the time domain signal are increasing. Due to the summation of the magnitude differences during the calculation of the TFE vector the TFE vectors amplitude is increasing. This correlates well with the coefficient of variation of the current signal. It can also be seen that the shape of the vectors change with motor usage. Specifically, the trough of the feature vectors shows changes in amplitude and shape.

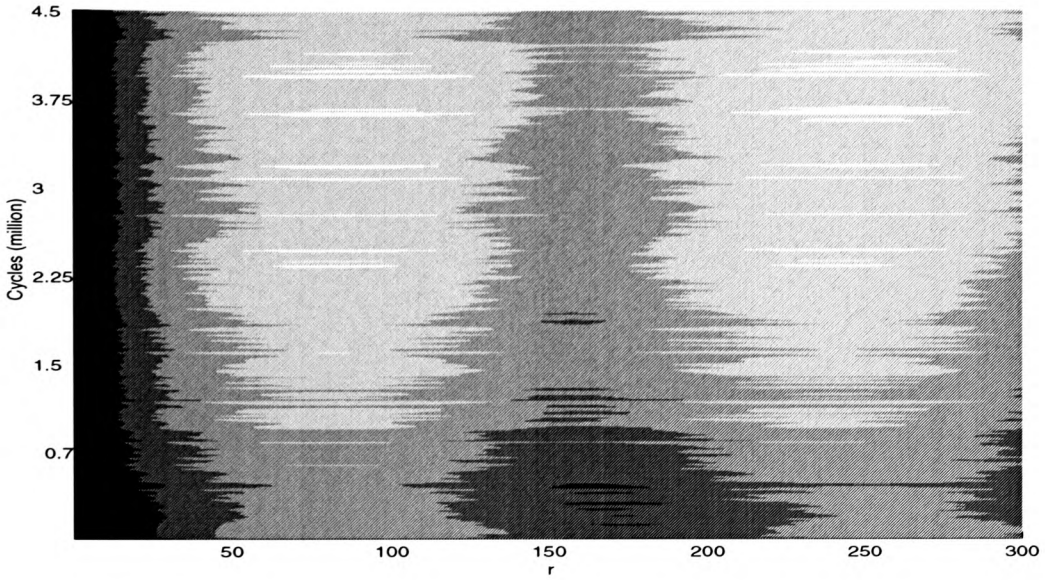

Figure 5.46: Mean feature vector in the forward mode with maximum load during 4.5 million cycles of testing. View from magnitude axis.

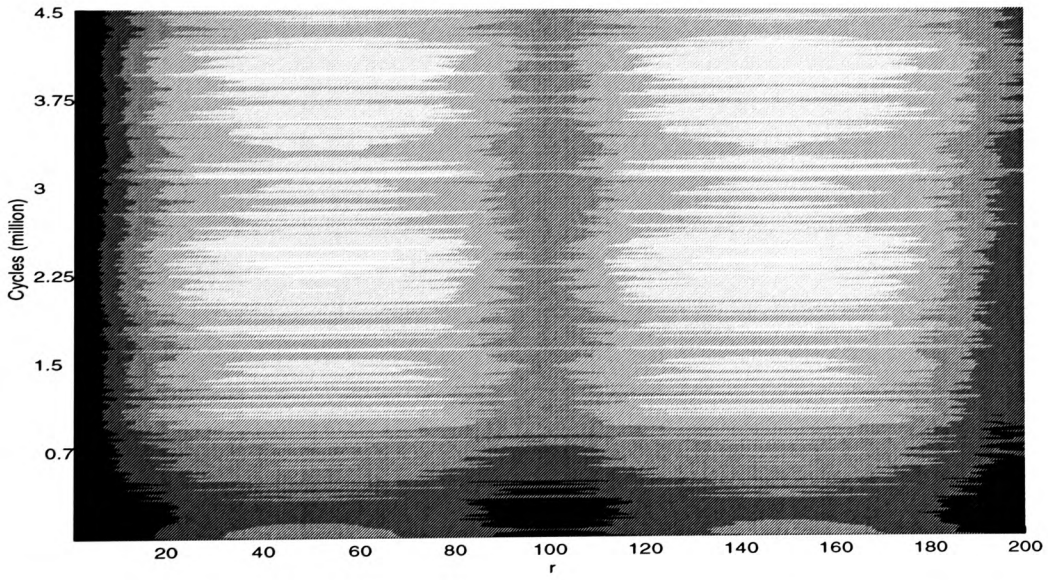

Figure 5.47: Mean feature vector in the forward mode without load during 4.5 million cycles of testing. tor view. View from magnitude axis.

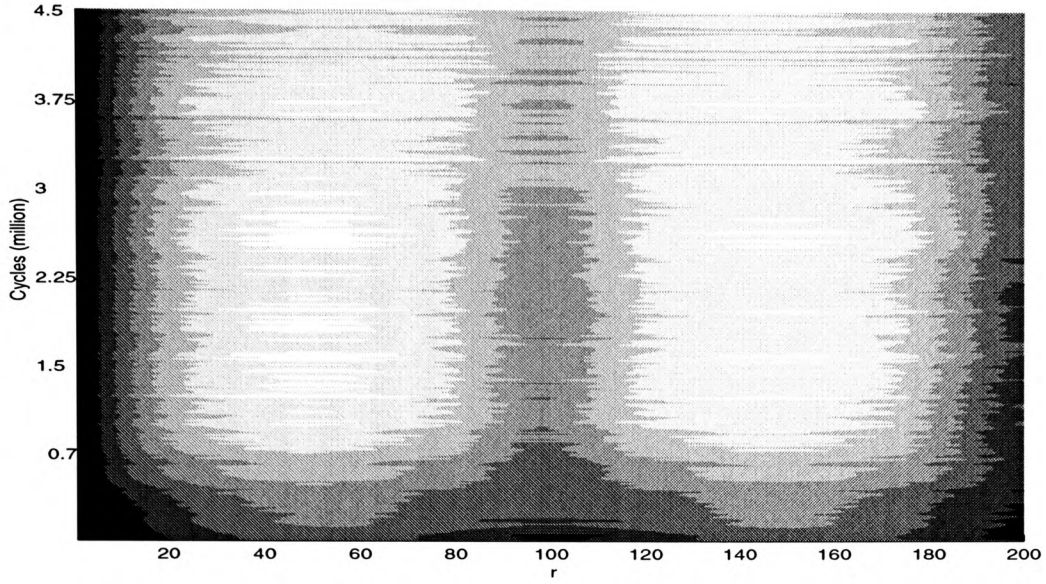

Figure 5.48: Mean feature vector in the reverse mode without load during 4.5 million cycles of testing. View from magnitude axis.

Frequency domain processing

The spectra of the current signals confirmed the TFE vector changes during the test time. As an example consider the spectra of motor 1 which are shown in figure 5.49 to 5.51. The largest change took place after approximately 450,000 cycles of testing. Frequency components above 3 kHz started to appear at this point. However, no major changes took place after 1.5 million cycles. In order to visualise the change of the vectors the figures have been plotted with a view from the top of the magnitude axis. Higher magnitudes correspond to a darker shading.

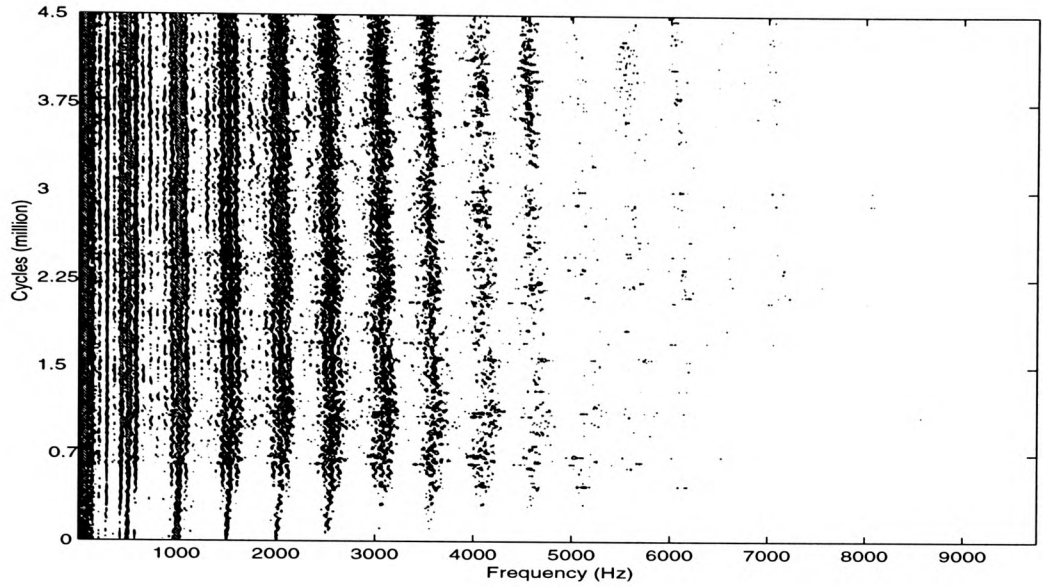

Figure 5.49: Current spectra in the forward mode without load during 4.5 million cycles of testing.

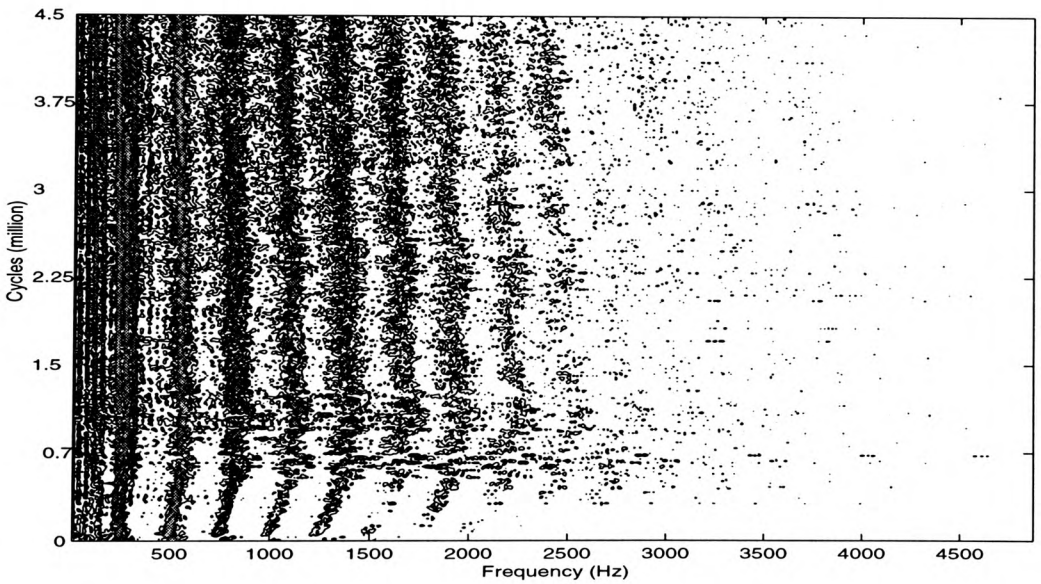

Figure 5.50: Current spectra in the forward mode with maximum load during 4.5 million cycles of testing.

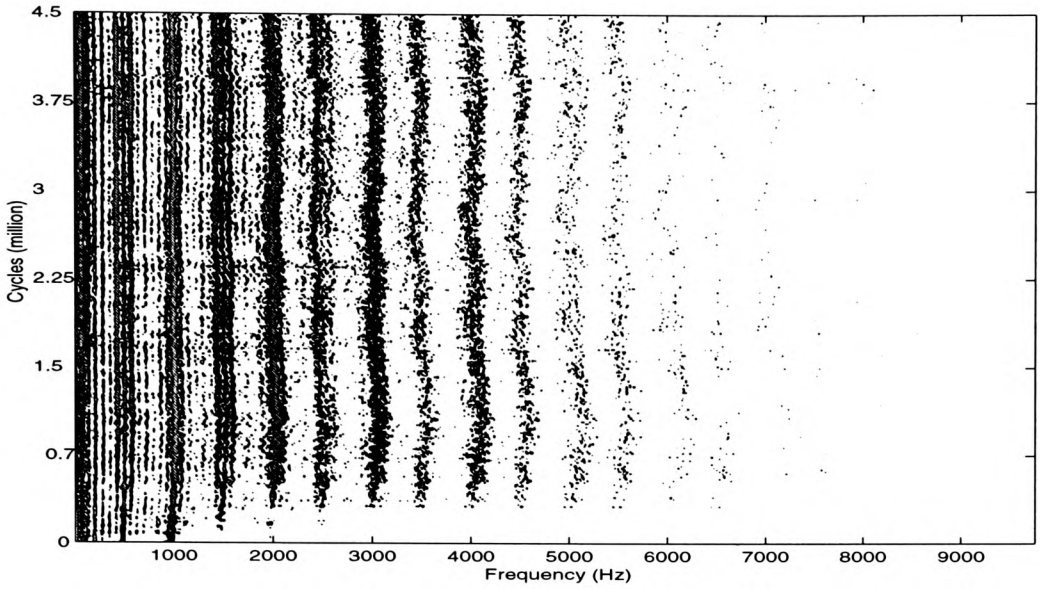

Figure 5.51: Current spectra in the reverse mode during 4.5 million cycles of testing.

5.2.7 Vibration

Vibration signals were recorded using the accelerometer that was attached to the gearbox of one test motor. The purpose of the vibration measurement was to detect if changes in the characteristics of the mechanical components, such as the gearbox of the motor, take place with motor usage. Figure 5.52 shows a sample segment of the vibration waveform of a motor that was tested for 150,000 cycles. Figure 5.53 shows a sample segment vibration waveform of the same motor that was tested for 450,000 cycles. A visual inspection of the two figures indicates that the appearance of the time domain signals are not significantly different.

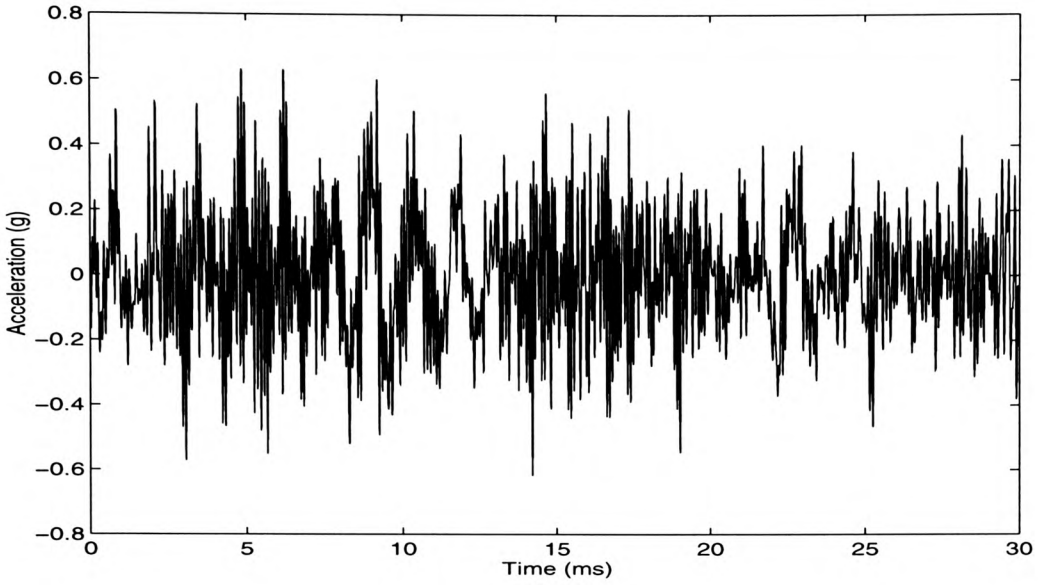

Figure 5.52: Vibration waveform of a motor that was tested for 150,000 cycles.

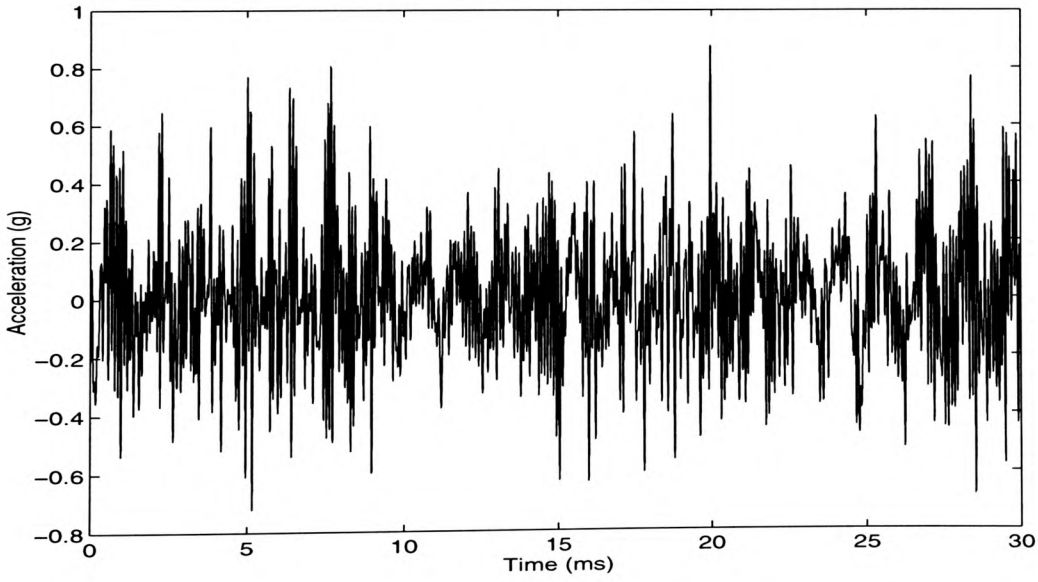

Figure 5.53: Vibration waveform of a motor that was tested for 450,000 cycles.

Time domain processing

All time domain processing methods were conducted on the recorded vibration signals that consisted of 30,000 sample points each.

RMS Various processing methods were applied to the vibration signal to investigate if mechanical wear, especially, gear wear, can be observed during motor usage. Since the vibration processing results showed a similar trend for all operational modes, only the results of one operational mode are presented. No change in trend could be detected during 4.5 million cycles of motor usage. Therefore, graphs for these cycles are not presented here. Figure 5.54 shows the root mean square (RMS) value of the signal, during the first 1.5 million cycles of testing and in the forward mode without load. The results for the same operational mode but with maximum load are presented in figure 5.55. It can be seen that both figures do not show a significant trend but the RMS vibration level was reduced significantly from 0.2 g for the operational mode without load to 0.12 g for the operational mode with maximum load.

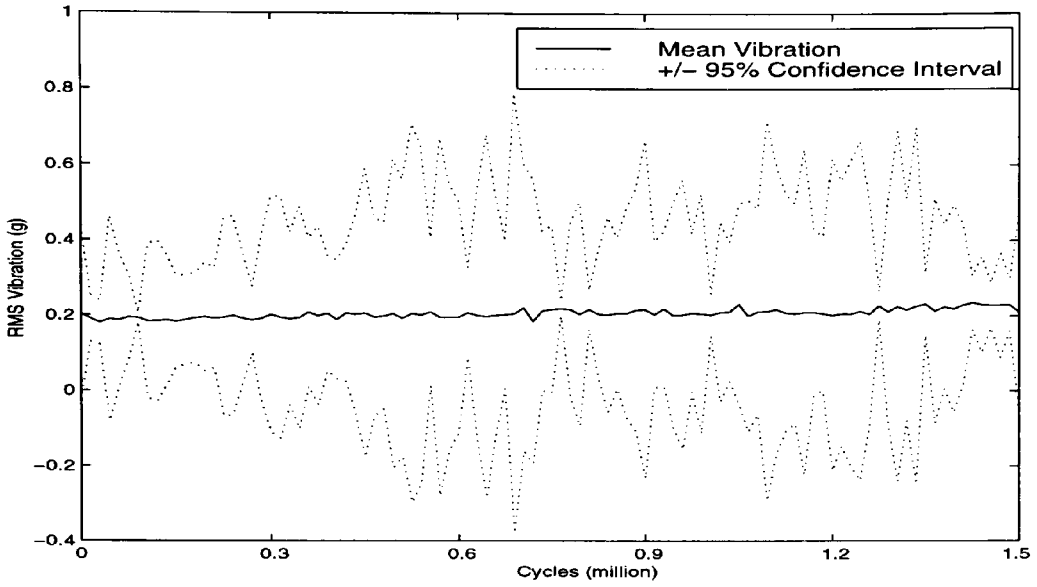

Figure 5.54: RMS values of the vibration signal in the forward mode, without load during the first 1.5 million cycles of testing. Results were obtained from 2 tested motors and averaged.

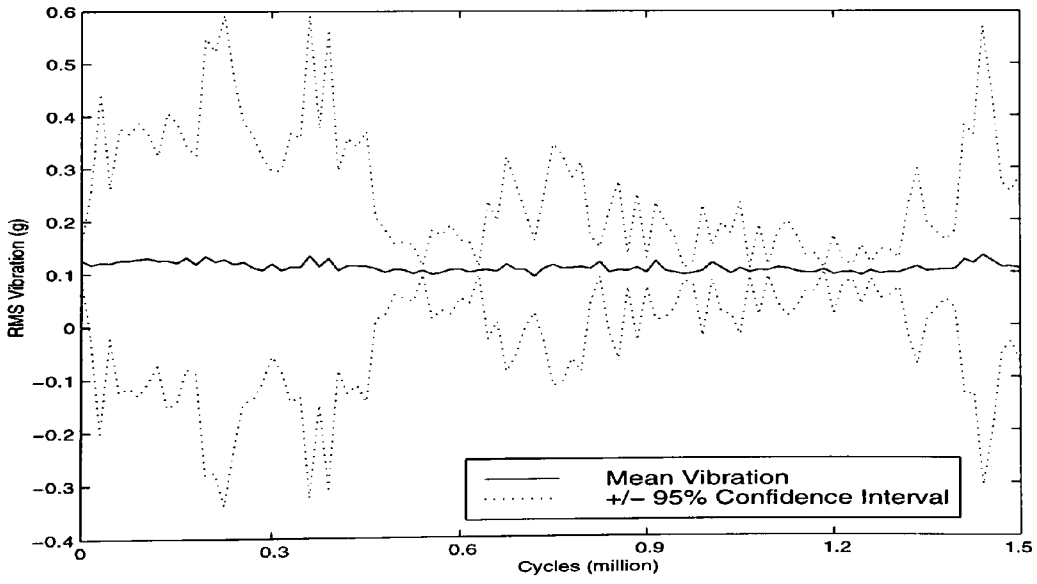

Figure 5.55: RMS values of the vibration signal in the forward mode, with load during the first 1.5 million cycles of testing. Results were obtained from 2 tested motors and averaged.

Skewness and kurtosis Skewness and kurtosis were also used in order to extract features from the vibration signal. The results of the two operational modes are plotted in figures 5.56 and 5.57. The result of the kurtosis can be seen in figure 5.58.

The 95% confidence interval shows a broad appearance, which is likely to be due to the fact that the vibration signal has been monitored for only two motors. However, a significant change cannot be seen in any of the figures 5.56 to 5.58.

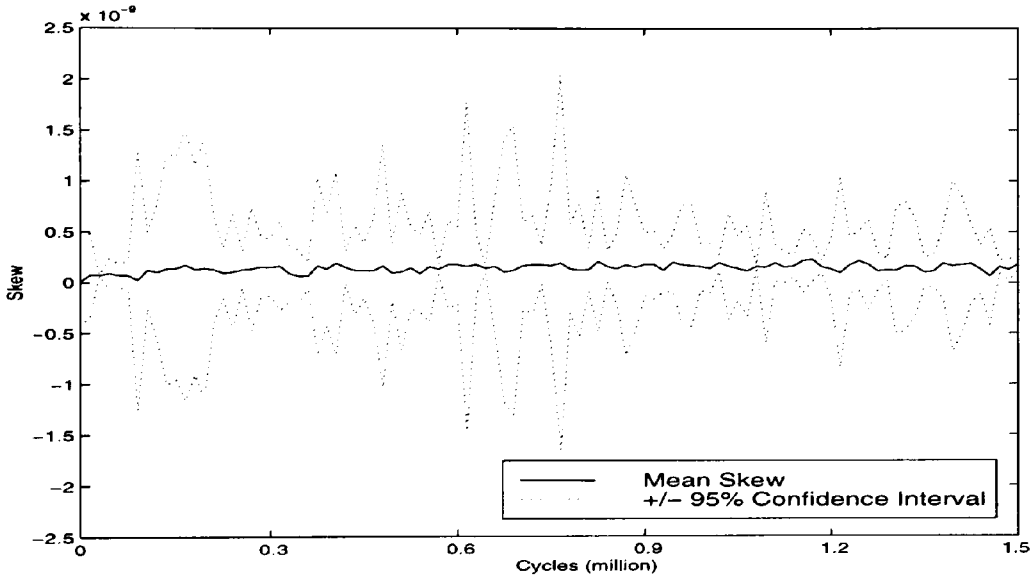

Figure 5.56: Skewness in the forward mode without load during the first 1.5 million cycles of testing. Results were obtained from 2 tested motors and averaged.

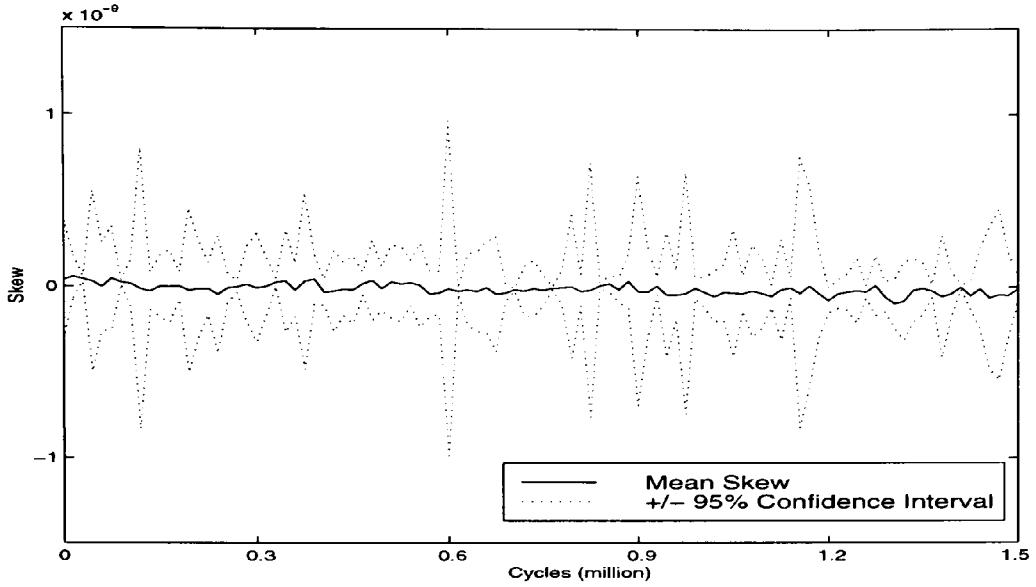

Figure 5.57: Skewness in the forward mode with load during the 1.5 million cycles of testing. Results were obtained from 2 tested motors and averaged.

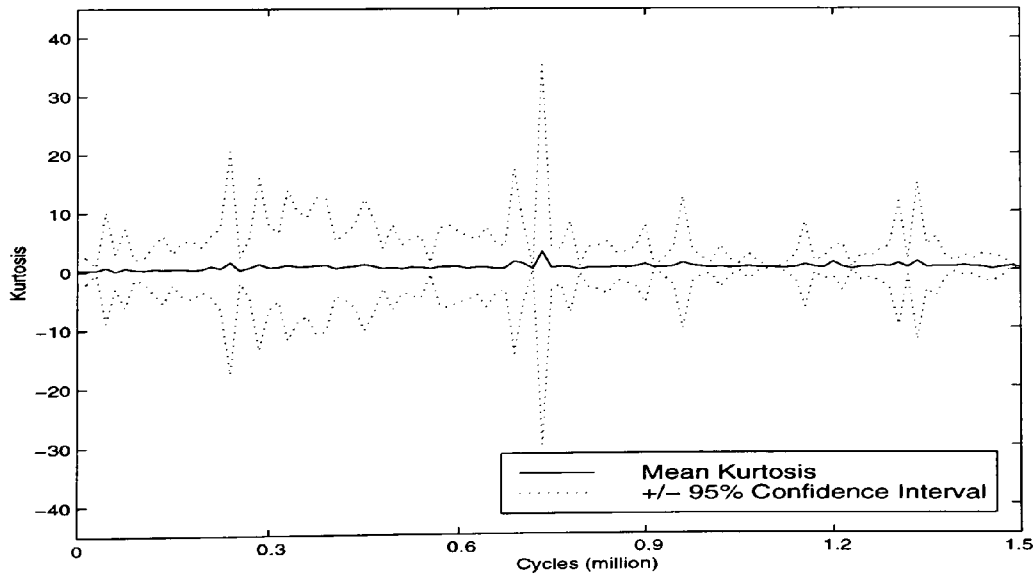

Figure 5.58: Kurtosis in the forward mode, without load during the 1.5 million cycles of testing. Results were obtained from 2 tested motors and averaged.

TFE processing Similar results were obtained by applying the TFE which has been calculated in the same way as described in section 5.2.6 for the TFE processing of the current signals. Figures 5.59 to 5.61 show the results of applying the WTFE to the vibration signals. It can be seen that no significant changes took place in the first 1.5 million cycles of testing. The plots for the 1.5-4.5 million cycles test results were not displayed since they show the same trend as in the first 1.5 million cycles.

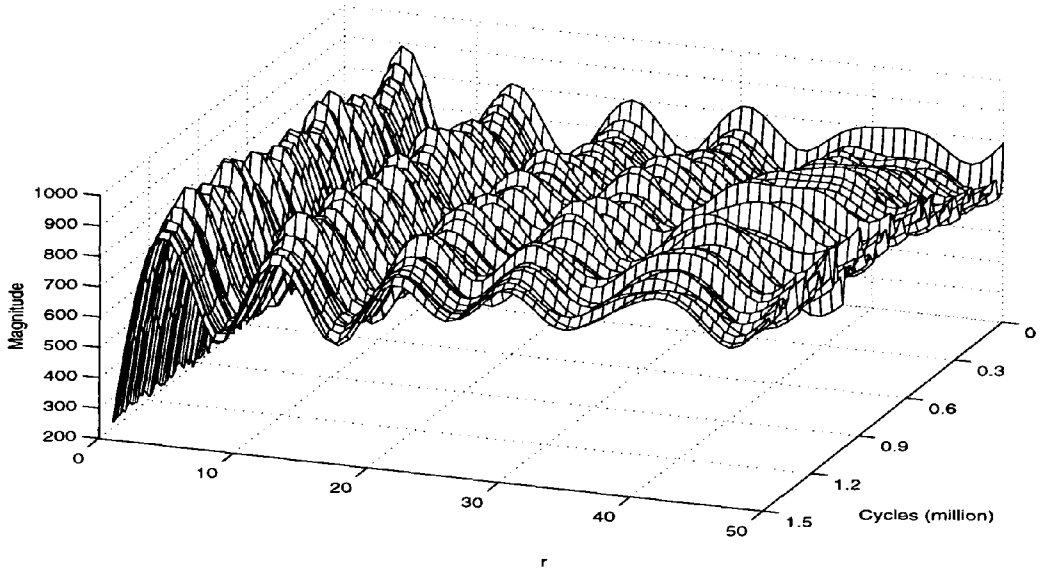

Figure 5.59: Mean feature vectors in the forward mode without load during the first 1.5 million cycles of testing. Results were obtained from 2 tested motors and averaged.

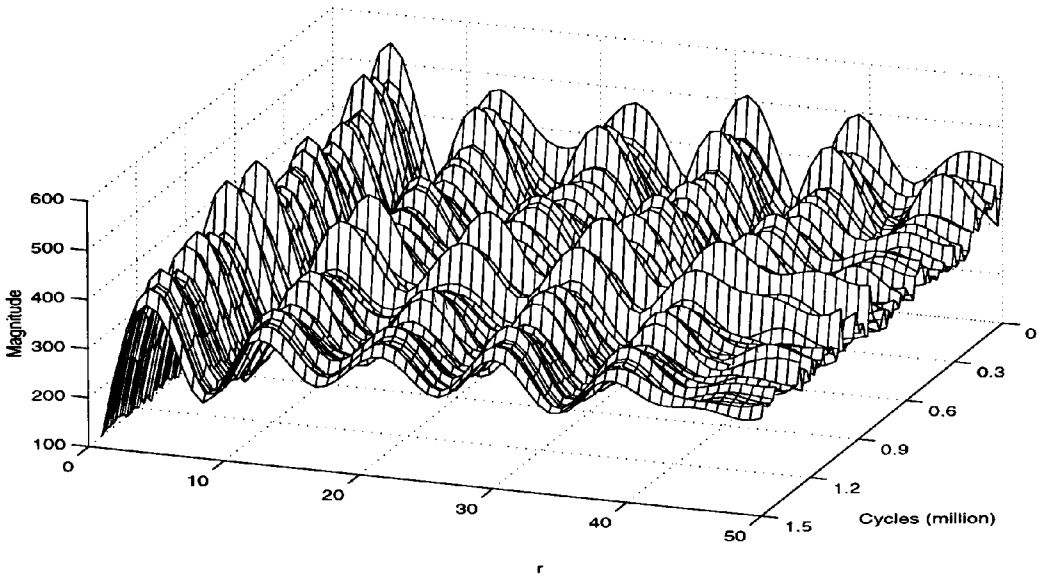

Figure 5.60: Mean feature vectors in the forward mode with maximum load during the first 1.5 million cycles of testing. Results were obtained from 2 tested motors and averaged.

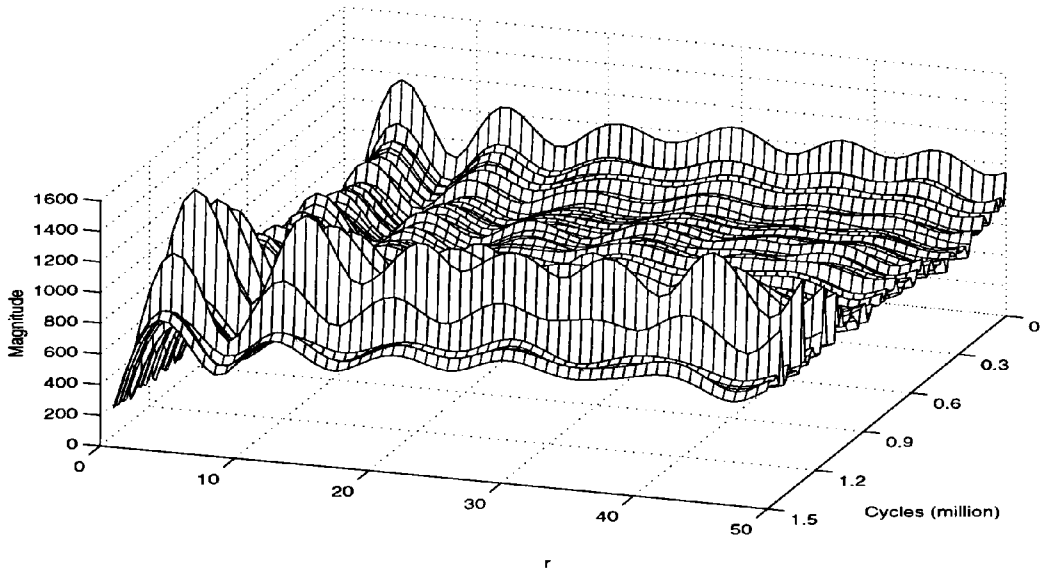

Figure 5.61: Mean feature vectors in the reverse mode during the first 1.5 million cycles of testing. Results were obtained from 2 tested motors and averaged.

Frequency domain processing

The frequency spectra for the vibration signal were plotted and displayed using the same method as for the current results. The two forward modes showed similar frequency spectra and therefore, only one graph is displayed (figure 5.62). It can be seen that the main frequency components fall in the region between 9 kHz and 10 kHz. The reverse vibration signals exhibited a similar behaviour (figure 5.63). No significant changes can be observed during the 4.5 million motor cycles of testing. This correlates with the observation from the previous analyses of the vibration signal.

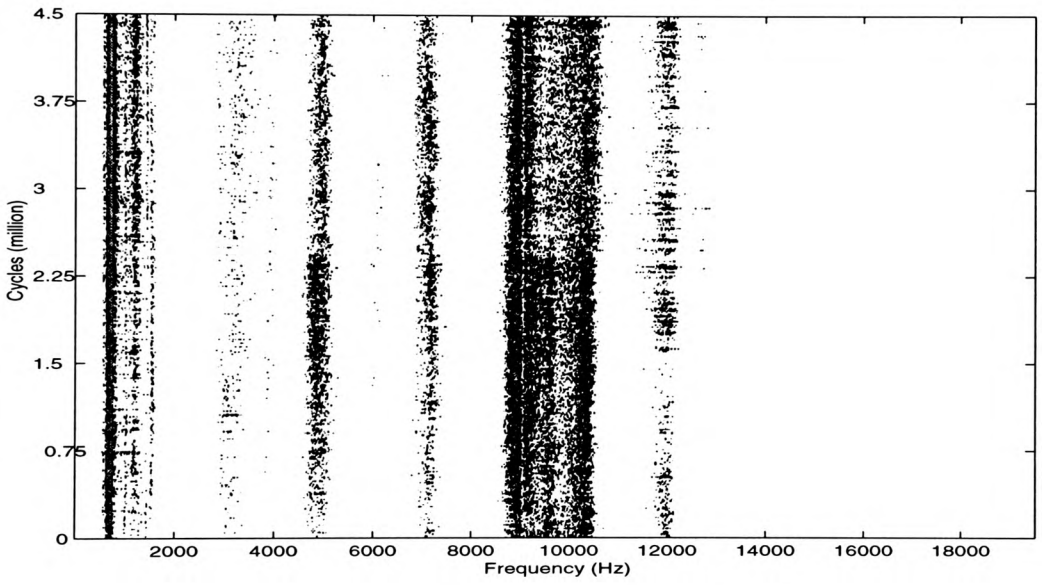

Figure 5.62: Vibration spectrum in the forward mode without load during 4.5 million cycles of testing.

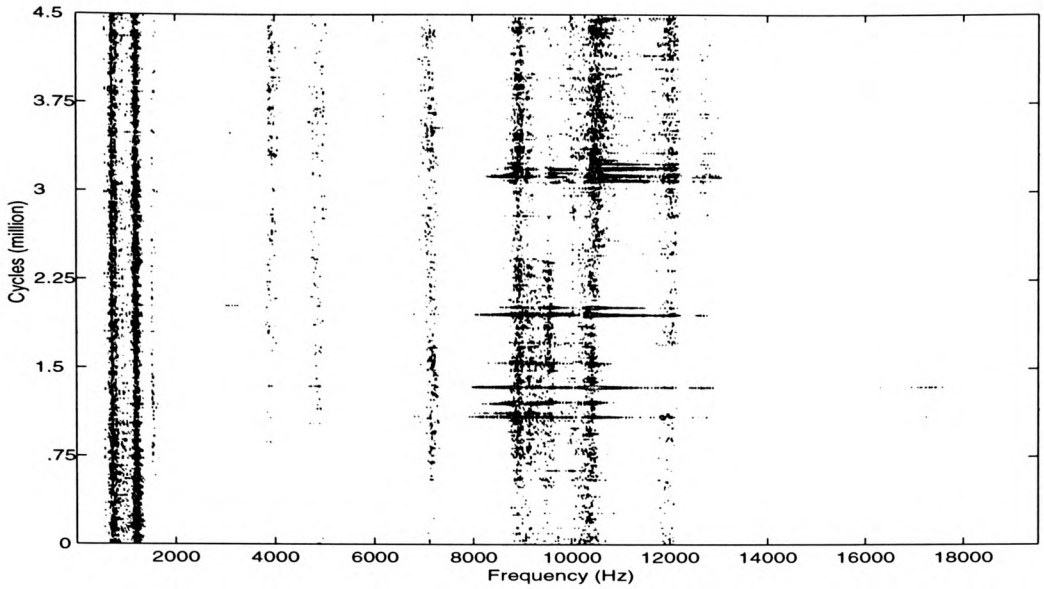

Figure 5.63: Vibration spectrum in the reverse mode during 4.5 million cycles of testing.

5.3 Acoustic Noise of the Motor

The acoustic noise characteristics of the dc motors were investigated using the equipment and methodology described in section 4.4. The investigation covered both, the influence of the motor design and the difference between used and new motors of the same design.

5.3.1 Acoustic noise characteristics of different motor designs

As a result of the initial investigation into the different motor designs it was noted that different gear design may result in different acoustic noise emissions (section 3.4.1). Investigations into the acoustic noise levels of different motor designs and their load dependency were conducted. It has to be noted that all the acoustic measurements were conducted in the forward operational mode since this is the mode in which the motor is used in the paper trays of a 5047 copying machine. Figures 5.64 to 5.67 show the mean sound pressure levels (SPLs) of the different

motor designs. Figures 5.68 to 5.71 show the frequency spectra of the acoustic noise emitted by the investigated motor designs. The spectra were calculated using the DFT averaging method to obtain a representative frequency spectrum for each motor model (section 5.1.3). Each acoustic motor signal is an average of three spectra, which in turn were averaged using the spectra from all motors of the same type. Table 5.9 relates figures 5.64 to 5.71. to the gear design. An illustration of the gear arrangement, including the position of gear G3 and gear G4 in the gearbox was shown in figure 3.3 of section 3.4.1.

Figure no.	*Motor type*	*Motor condition*	*Sample size*	*G3*	*G4*
5.64 / 5.68	61.46.16	used	19	steel, spur	steel, spur
5.65 / 5.69	61.46.20	used	18	nylon, helical	brass, helical
5.66 / 5.70	61.46.020	new	4	nylon, helical	brass, helical
5.67 / 5.71	61.46.020	used	2	nylon, helical	brass, helical

Table 5.9: Gearbox configurations in different designs.

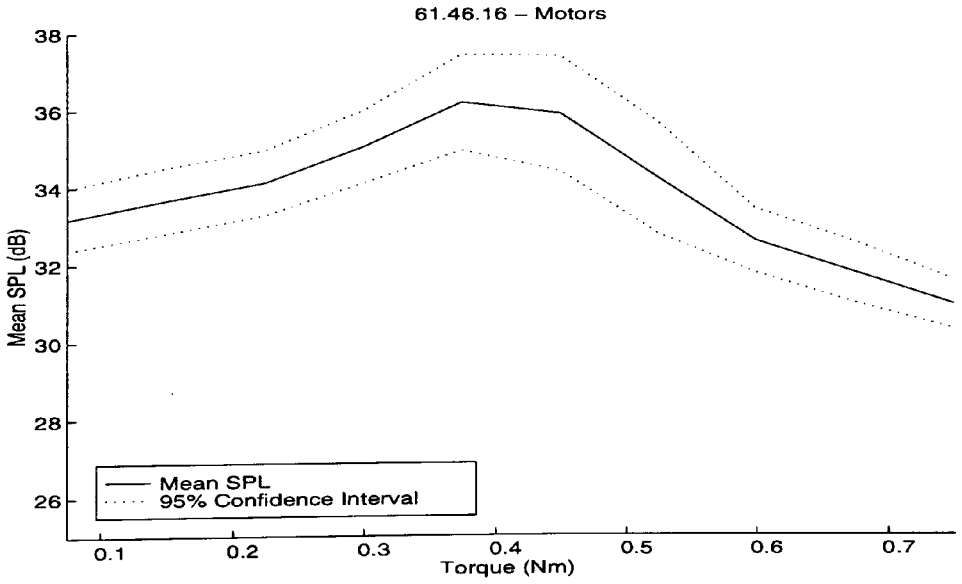

Figure 5.64: Mean SPL for used motors of type 61.46.16. Results were obtained from 19 tested motors and averaged.

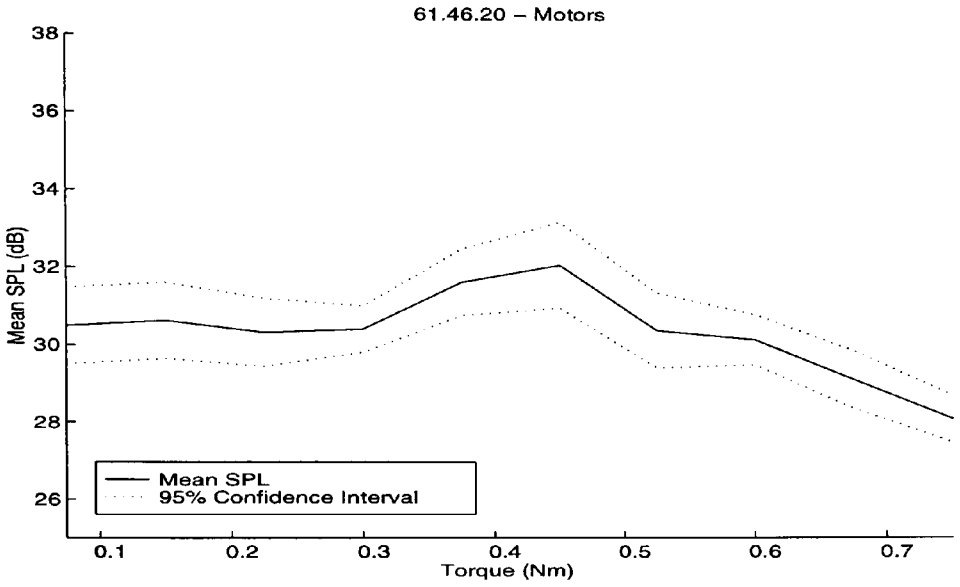

Figure 5.65: Mean SPL for used motors of type 61.46.20. Results were obtained from 18 tested motors and averaged.

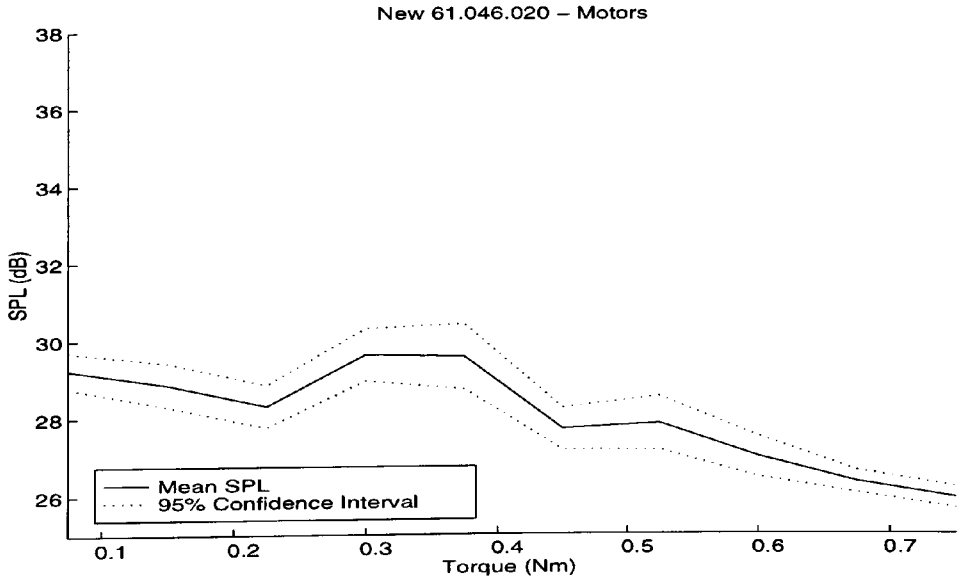

Figure 5.66: Mean SPL for new motors of type 61.046.020. Results were obtained from 4 tested motors and averaged.

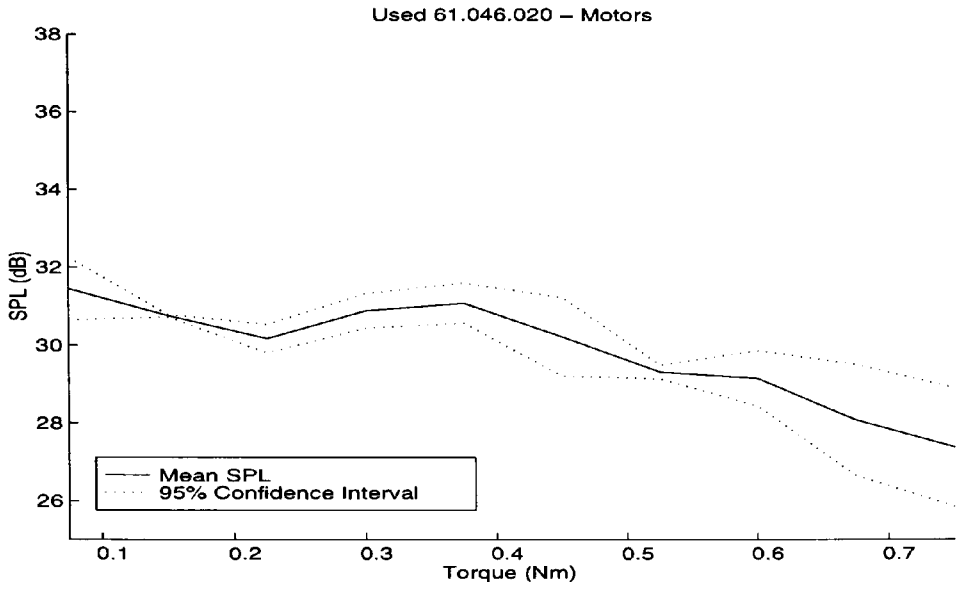

Figure 5.67: Mean SPL for used motors of type 61.046.020. Results were obtained from 2 tested motors and averaged.

The investigations showed that the motor's sound pressure level and therefore, its acoustic noise level is torque dependent. All figures show that the SPLs are lower at maximum torque than with lower loads. The SPLs for the 61.46.16 and 61.46.20 motors show a maximum in the region around 0.4 Nm to 0.5 Nm. Even the 61.046.020 helical gear motors show a maximum, but it is shifted to the region of 0.3 Nm to 0.4 Nm. It can be clearly seen that the change of the gear design and materials have decreased the maximum SPL significantly. The SPL is approximately 4 dB lower for the helical gear design of the 61.46.20 motors compared to the 61.46.16 motors. An increase in the acoustic noise level in the mid torque range of the motor may have a disturbing effect for the user during the usage of a photocopy machine. Table 3.4 has shown that the torque in the heavily used A4 paper tray of the 5047 copying machine is 0.427 Nm. This means that the motor is operated at the peak of its acoustic noise characteristic which indicates a weakness in the product design, since a quiet product is desirable to achieve a high level of customer satisfaction.

A relationship between acoustic noise and motor usage could only be observed in a small number of type 61.046.020 motors, since more samples could not be provided by Xerox. Since it is the latest motor design only few motors of this type have been used in products until now. The characteristics of the two groups are presented in figure 5.66 and 5.67. It can be seen that the average SPL level of the used motors is greater by 1.5 dB than that of the new motors. The figures also show that the noise maximum around 0.4 Nm is not very pronounced for the used motors.

Figures 5.68 to 5.71 show the acoustic spectra in different operational modes and gearbox designs. All spectra were produced without motor load. Figure 5.70 and 5.71 show that the main difference between a used and a new 61.046.020 motor becomes apparent in the frequency region of 3 kHz and 5 kHz.

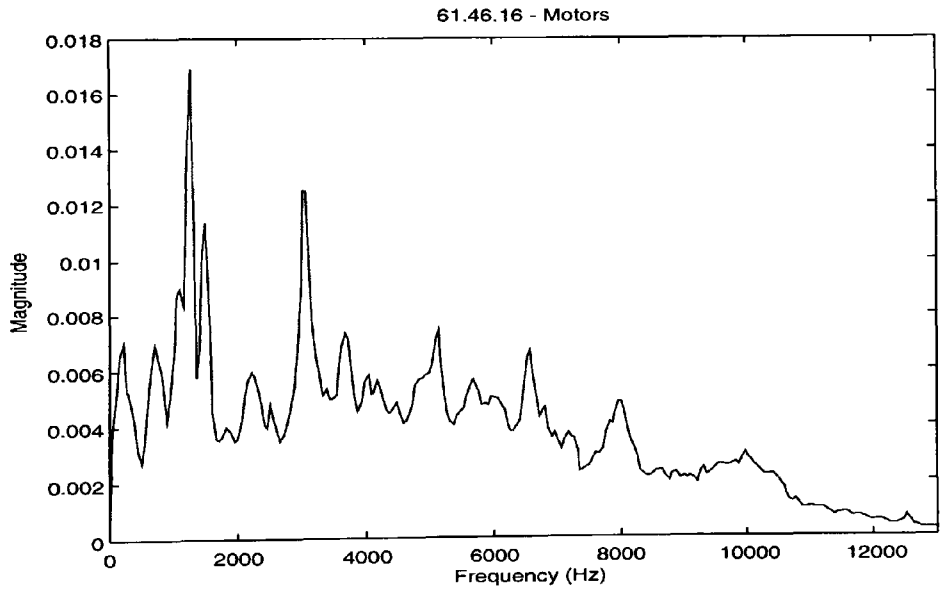

Figure 5.68: Frequency spectrum for used motors of type 61.46.16. Results were obtained from 19 tested motors and averaged.

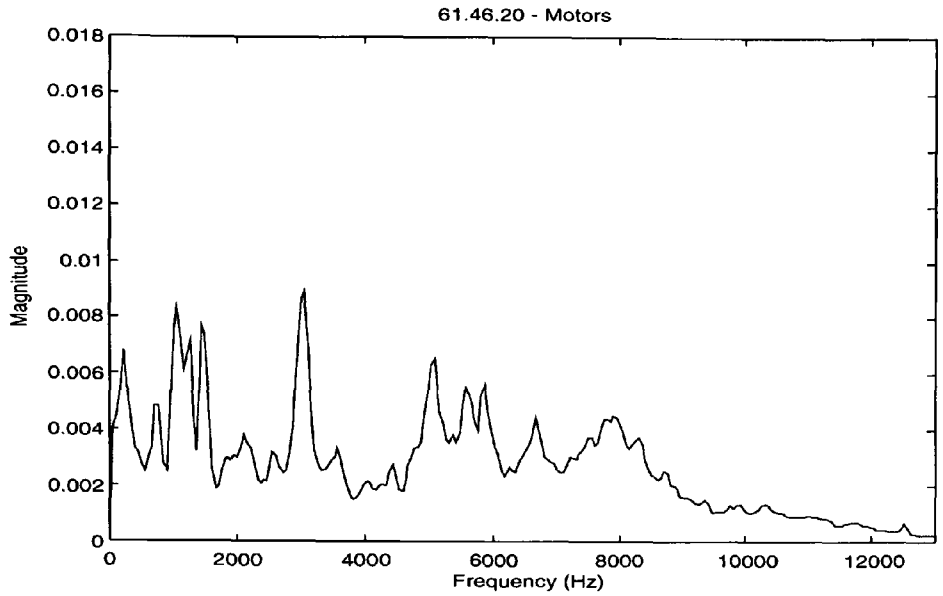

Figure 5.69: Frequency spectrum for used motors of type 61.46.20. Results were obtained from 18 tested motors and averaged.

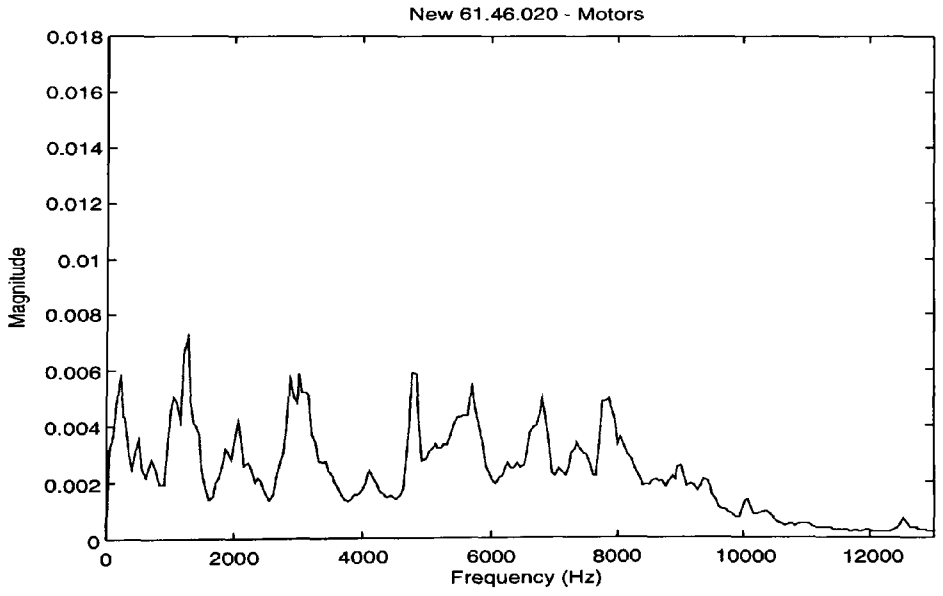

Figure 5.70: Frequency spectrum for new motors of type 61.046.020. Results were obtained from 4 tested motors and averaged.

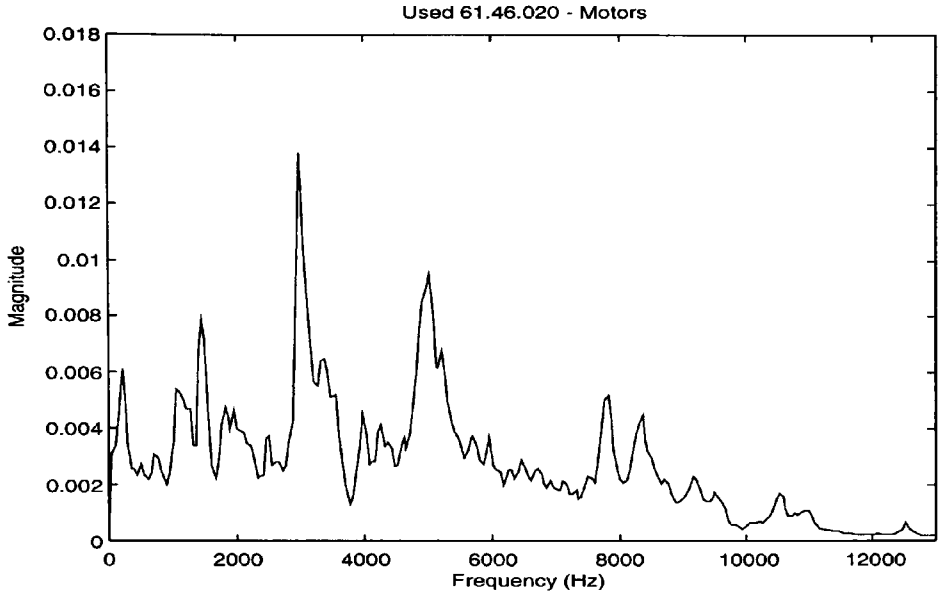

Figure 5.71: Frequency spectrum for used motors of type 61.46.020. Results were obtained from 2 tested motors and averaged.

5.3.2 Influence of lubrication on acoustic noise

In order to determine if gear and bearing lubrication influences the noise level, an experiment was conducted. The noise signals of a motor design with spur gears and helical gears were measured with different degrees of lubrication in changing load steps. The experiments were conducted in the forward mode as follows:

- Measurements of the acoustic motor noise with original lubrication.
- Measurements without lubrication on the output shaft bearing[1].
- Measurements without lubrication on all gears.

The results of the experiments can be seen in figure 5.72 and 5.73. The graphs show that the lubrication of the output shaft bearing did not affect the noise level of the motors significantly. This is due to the brass material used which provides a sliding surface for the stainless steel shaft even without lubrication. A change in

[1]The lubrication was removed by means of methylated spirit.

the noise level occurs when the shaft is exposed to high side loading. On the other hand, the lubrication of the gears had a significant influence on the acoustic noise level of the motor.

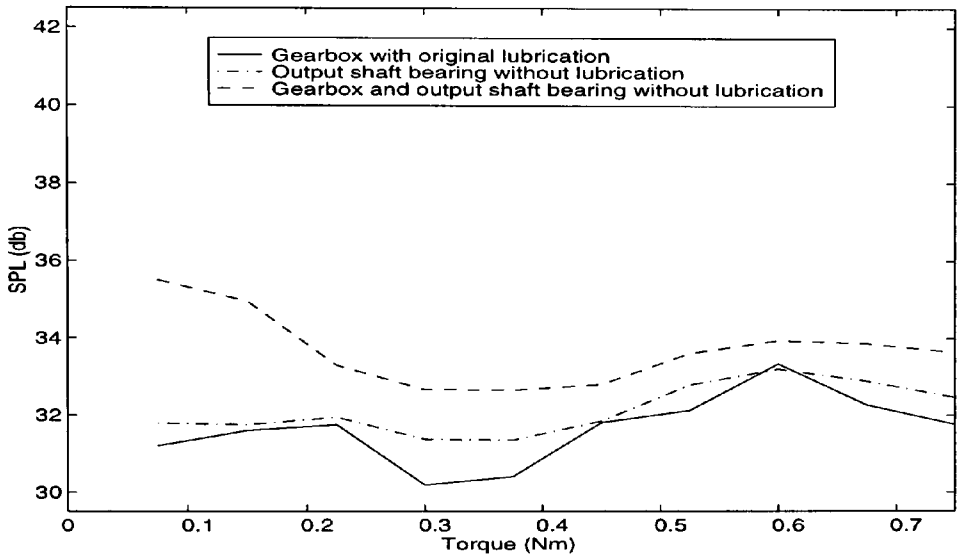

Figure 5.72: Helical gear motor noise with different lubrication levels.

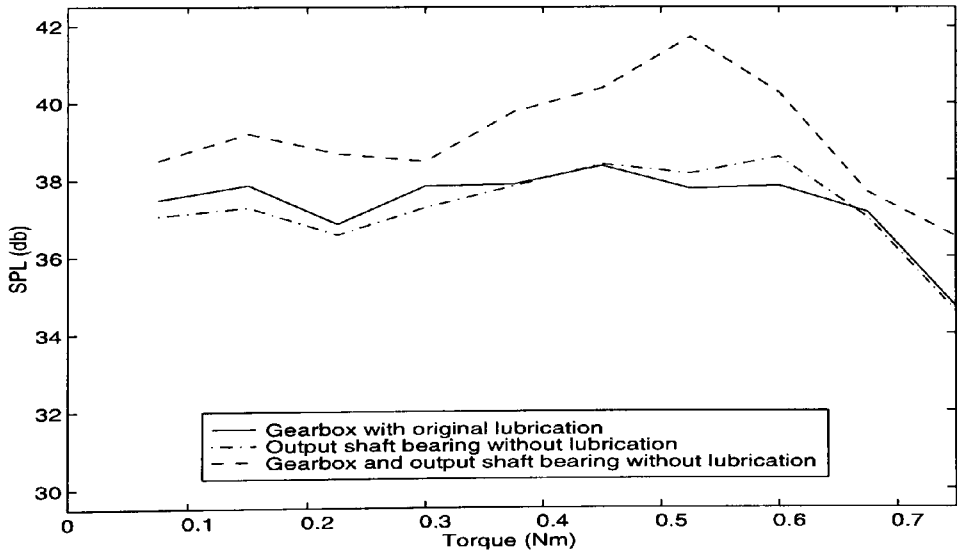

Figure 5.73: Spur gear motor noise with different lubrication levels.

The experiments showed that a change in the lubrication level of the motor due to usage increases the acoustic SPL. It can be seen that the lubrication condition

of the gears influences the SPL parameters more than the output shaft bearings. However, the overall increase of a gearbox and bearing without lubrication, in case of the helical gear design, is less then 2.3 dB (at 0.3 Nm) and may not be noticeable in an application.

5.4 Summary

This chapter has presented the processing methods which were applied to the signals of the motor parameters that were collected during the accelerated life test experiments of this study. The TFE was thoroughly investigated and was shown to have excellent data reduction and feature extraction capabilities in comparison to other processing methods. The WTFE was introduced as an approach for extracting local features in time varying signals. The investigation into the TFE characteristics and performance has not been reported in the literature before.

The results from the eight tested motors have indicated that the vibration, resistance and time-to-speed parameters showed little variation with motor usage during 4.5 million cycles of testing. Different processing methods did not allow the extraction of significant wear related features from these parameters. The current in contrast, showed a significant change in the first 1.5 million cycles of the motor's operation. This change was observed in different operational modes and with different processing methods.
Changes in the current signal in the following 3 million cycles were not very prominent when the results were inspected visually.

It can be assumed that the eight tested motors represented the selected motor

type well. The 95% confidence interval showed a close fit for most of the parameters. Initial variations of parameters were expected in a low cost product such as this motor due to production tolerances. However, they did not cause a significant spread in the analysis of the test data.

The key findings of the accelerated life test can be summarised as follows:

- The parameter changes with life were very similar for all tested motors.
- The motor current waveforms showed a clear trend for the first 1.5 million cycles using different processing methods. This trend did not continue for the following 3 million cycles.

The accelerated life test has demonstrated that certain parameters can be used to identify the wear of the motor under test and its usage level using non-destructive test methods. Motor usage level estimation should use appropriate parameters that can deliver reliable results. This is only possible with parameters that change with motor usage.

The investigation into the acoustic noise of the motor showed that the change from steel spur gears to helical nylon gears has decreased the noise level significantly. A comparison between a set of new and used motors of the same design showed that the noise level increases with usage level even though this may not be noticeable in an application. The observation that the acoustic noise level is higher with no torque than with maximum torque was also confirmed by the RMS vibration level of the accelerated life test. The new gearbox design resulted in less noise than the previous design, but both designs showed noise level maxima at the main operational torque region of the 5047 photo copying machine.

Chapter 6

Motor Usage Level Estimation

Chapter 1 has identified the main problem in the asset recovery process as that of estimating the level of usage of the dc motor under investigation. Chapter 3 has described a number of physical parameters that may be used as indicators of wear and level of usage of the motors. This chapter has also explained that the mathematical relationships between any of these parameters and the degree of wear or level of usage are unknown. In such cases, artificial neural networks (ANNs) present an optimum solution to relate two sets of parameters of unknown mathematical relationships.

Ideally, a solution to the problem of estimating the level of usage of a motor should yield precise figures for the number of run cycles. However, such an estimation system, even when based on ANNs, would require a very large number of samples and lengthy tests to establish the relationships between the wear indicators and the usage level. For ANNs, this will require a high complexity network with a very large number of training and validation vectors. It is not certain that such ANNs would converge into a valid solution.

However, the asset recovery process does not require such high precision in estimating the level of usage of a motor. It is sufficient to estimate the level of usage in discrete classes. The width of each class can be selected depending on the desired accuracy. For example, if the class width is 100,000 motor cycles and the experimental tests have exercised the motors for up to 0.9 million cycles, the available 5 classes are listed in table 6.1.

Using classes will enable the ANN to solve a classification problem instead of emulating a continuous mathematical function. ANNs are very efficient and have been more successful in resolving classification problems.

The complexity of the ANN and its performance is dependent on the number of classes. As a result, there is a compromise between the accuracy of estimating the level of motor usage and the complexity of the ANN.

This chapter describes the process of usage level estimation for the investigated type of dc motor. It shows that classification of motor wear parameters allows the estimation of the motor's usage level. This classification is achieved using recorded and processed signals from the accelerated life tests experiments. Different training sets and ANN paradigms were investigated to allow a usage related classification.

Class	*Number of cycles*
1	0 - 100,000
2	200,000 - 300,000
⋮	⋮
5	800,000 - 900,000

Table 6.1: Example of level of usage classes.

The chapter describes the configuration, training and evaluation methods for ANNs (section 6.1).

It is important for the estimation process to find features that can be utilised to detect usage related changes in the recorded test signals in order to enable an accurate usage level estimation of the motors. Initial results of the ANN training and classification process investigated different operational modes and their effect on the classification process (section 6.2).

The classification results obtained with the TFE vectors of the current signals were compared with those obtained from the current spectra (section 6.3).

The literature review has shown that ANNs have in the past, been successfully used to classify data that combine different parameters. This data fusion capability has been used to optimise the initial classification (section 6.4).

Classification of a sample of used motors with unknown history using trained ANNs was conducted to evaluate the performance of the developed ANNs (section 6.5).

The last section of this chapter summarises the design of the classifiers for motor usage level estimation of a number of used motors (section 6.6).

6.1 ANN Training and Evaluation

The estimation of the motor's usage level is based on the measurements of the accelerated life test experiments. In order to classify these parameters and relate them to the motor usage level, the artificial neural network (ANN) approach is used. Since standard ANN architectures are appropriate for the classification and existing software packages can be used, the focus of this study was on the optimisation of the classification process.

6.1.1 Choice of ANN paradigm

The literature review has shown that back-propagation (BP) ANNs were successfully used in condition monitoring applications (section 2.3.2). Using BP ANNs to solve classification problems may lead to irregular boundaries due to the distributed nature of the network and its transfer function. This is the case if some of the decision regions are bounded. Learning vector quantisation (LVQ) ANNs in contrast allows the network to learn bounded decision regions more readily [92]. In the following section both of these supervised ANN paradigms are investigated and the results of applying them are compared. Supervised ANNs are used because the desired classification outputs, which are related to the motor's usage, are known for both the training and the validation sets from the accelerated life test experiments. Both network types were exposed to all training sets in order to determine the most suitable network paradigm.

6.1.2 NeuralWorks

The ANN software development system NeuralWorks Professional II [1] was used for ANN training and testing in this study. NeuralWorks allows the generation of over two dozen network types such as LVQs, BPs and self organising maps. The performance of the networks generated can be monitored during the learning process. Different optimisation paths and a choice of learning rules offer high flexibility. Another advantage is the automatic generation of a program code for trained ANNs, which in the case of feedforward networks such as LVQ or BP, can be exported as ANSI C program segment. This allows for faster implementation of the fully trained network in a DLL file (section 4.3.4) and enables its integration into the LabView user interface.

Configuration of NeuralWorks for this study

NeuralWorks offers a wide range of possible configurations for ANN design. Experiments with different configurations were conducted, and the most suitable configuration parameter values for this study were found empirically. The configuration parameters for BP and LVQ architecture ANNs, if not mentioned otherwise, were as follows:

- Momentum: a momentum of 0.8 has shown the best test results.
- Learning rule: the most frequently used BP learning rule, the Delta-rule (equation 2.17), has been found to be the most appropriate.
- Transfer function: the standard BP transfer function, the Sigmoid function (equation 2.15), has been chosen.

[1] Neural Ware Inc. Pittsburgh, U.S.A, Version 2.504 for MS-DOS.

- Normalisation: the data presented to the ANNs were scaled between 0 and 1.

In order to avoid over-training of the ANNs, the network weights that gave the best correct classification result were saved automatically. This ensures that the ANN does not loose its generalisation ability due to over exposure to the training set.

6.1.3 ANN accuracy

For every classifier the question of its accuracy is of great importance. Therefore, it is essential to have a measure of how much a classifier is better than random guessing and to compare different classifiers of similar structure. The non-linear structure of an ANN does not allow for statistical evaluation, such as the calculation of confidence intervals, easily.

Validation set

A standard method to evaluate the performance of ANN classifiers is to divide the data into two sets. The first is the training set used for computing the gradient, and updating the network weights and biases. The second is the validation set which is used to compare the classifier output with the expected output [92]. Normally half the data set is used for training and the other half for validation. This method is suitable for supervised ANN structures where the desired ANN results are known.

In this study both, the validation and the test set comprised 50% of the overall data. The classification results in this study were tabulated in a classification matrix as shown in the example of table 6.2. The table has a size of $n \times n$ where, n, is the number of ANN outputs. The columns of the matrix show the actual outputs

of the ANN. The rows show the desired outputs of the ANN. The entries in the 3x3 matrix list the percentage of vectors classified. It can be seen that in the class 0-0.495 million cycles and 1.005-1.5 million cycles, the ANN output is equivalent to the desired output and 100% of the test vectors were classified correctly. In the class 0.51-0.99 million cycles only 80% of the input vectors were classified correctly. The remaining 20% of the input vectors were wrongly classified as belonging to the classes 0-0.495 million cycles (5%) and 1.005-1.5 million cycles (15%). The overall percentage of correct classifications is therefore, 93.33%. This is calculated by averaging the diagonal entries of the matrix.

	Vector classification (%)		
ANN Classes (10^6 cycles)	0-0.495	0.51-0.99	1.005-1.5
0-0.495	**100**	5	0
0.51-0.99	0	**80**	0
1.005-1.5	0	15	**100**

Table 6.2: Example of classification matrix with an overall 93.99% correct classification of the test vectors.

Receiver operating characteristics

Receiver operating characteristic (ROC) analysis is a procedure, derived from statistical decision theory and can be used to assess the performance of ANNs [123,124].

The standard method of generating a ROC curve is to vary the threshold in the output layer of the ANN. The threshold is varied in discrete steps from 0 to 1. Output nodes which generate values greater than the actual threshold value are classified as 1, otherwise they are classified as 0. The next step is to calculate the

sensitivity and specifity of the classification result. They are defined as follows [125],

$$\text{sensitivity} = \frac{\text{Results which are both real positive and test positive}}{\text{Results which are real positive}} \tag{6.1}$$

$$\text{specificity} = \frac{\text{Results which are both real negative and test negative}}{\text{Results which are real negative}} \tag{6.2}$$

The ROC curve is then generated by plotting the true positive rate (*sensitivity*) against the false positive rate ($1 - $ *specificity*). An example of ROC curves is shown in figure 6.1.

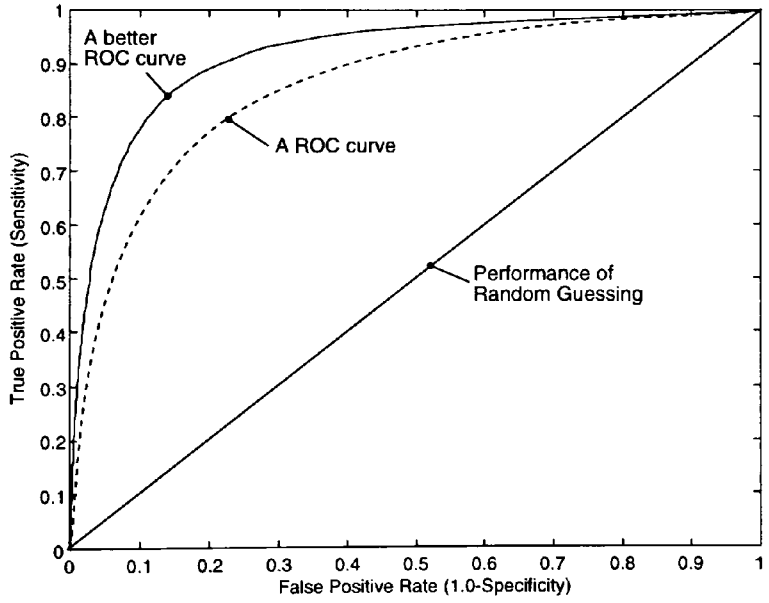

Figure 6.1: Examples of ROC curves.

A different method of generating ROC curves has been suggested by Woods [126]. Instead of varying the threshold value for the output layer he varied the bias of the first hidden layer. This method is more time consuming than the standard method and offers significantly better ROC curves for only 40% to 50% of the cases.

Since the output of LVQ network is either 1 or 0 and not a real number as for BP ANNs, ROC curves cannot be computed for LVQ networks. Therefore, a variation of the threshold value will not change the result. Specificity and sensitivity values, however, can be calculated for the trained LVQ network.

6.2 Initial Classification

The aim is to enable a classification with maximum resolution for the motor usage level. Initial tests using the accelerated life test data were carried out in order to estimate the maximum possible resolution for the motor usage estimation.

To achieve the maximum possible resolution different ANNs were trained. These ANNs had different architectures and parameters. This resulted in the selection of two different ANN architectures which were examined further in order to identify the most appropriate architecture for the motor usage level application.

6.2.1 Initial motor usage estimation

The mean TFE vectors (section 5.1.2) were used to estimate the resolution of the classification process. The initial ANN was trained to discriminate between two classes of motor usage levels.

The TFE vector of the reverse current with a length of 200 points was used to train the initial ANN. The aim is to classify a set of motors that have already been used in one or more products (table 5.9). The classifier was trained to discriminate between the first 1.5 million cycles of usage as one class and 1.515 to 4.5 million cycles of usage as another class. The BP ANN trained extremely well and the test

set was classified with an accuracy of 100%.

The result of this classification is that all of these motors were classified as being in the first class (0-1.5 million cycles). This means that the focus in the motor classification process should be on the first 1.5 million motor cycles.

6.2.2 Classification resolution for the first 1.5 million cycles

The current feature vectors obtained from the TFE were used to investigate the relationship between resolution and accuracy of classification. The first 1.5 million cycles were divided into equally sized classes. The results of this investigation have helped to improve the classifier design. The following constraints had to be met:

- The resolution should be high.
- The classification should be accurate.
- False classifications should not result in classifying the vector in a class of a lesser usage level.

Two classes The initial network was trained to separate the motor usage level into two classes (0-0.75 million and 0.765-1.5 million cycles). The training TFE vector derived from the reverse current had a length of 200 points. The best BP network consisted of one hidden layer with 40 neurons. It achieved an overall correct classification rate of 86.05% with the validation set. The best LVQ network consisted of 40 hidden layer neurons. It achieved an overall classification rate of 84.55% with the validation set.

The classification matrix of the two networks are shown in tables 6.3 and 6.4.

	Classification (%)	
Classes (10^6 cycles)	0-0.75	0.765-1.5
0-0.75	**75.5**	3.4
0.765-1.5	24.3	**96.6**

Table 6.3: BP classification result with two classes.

	Classification (%)	
Classes (10^6 cycles)	0-0.75	0.765-1.5
0-0.75	**73.5**	4.4
0.765-1.5	26.5	**95.6**

Table 6.4: LVQ classification result with two classes.

It is obvious that the BP network performed slightly better than the LVQ network. Both networks achieved a high correct classification rate of over 94% with the training set.

Three classes Using the same feature vector and ANN structures as before, the first 1.5 million cycles were divided into three classes of 500,000 cycles each. The best results were achieved with one hidden layer of 40 neurons. The best performing LVQ network achieved an overall classification rate of the test set of 71.17%. The best BP network achieved an overall correct classification rate of 72.8%. The classification matrix of the two networks can be seen in tables 6.5 and 6.6.

	Classification (%)		
Classes (10^6 cycles)	0-0.495	0.51-0.99	1.005-1.5
0-0.495	**75**	0	0
0.51-0.99	25	**76.5**	33
1.005-1.5	0	23.5	**66.9**

Table 6.5: BP classification result with three classes.

The tables show that the overall accuracy has decreased in comparison with the classification into two classes. Although the BP network shows the best correct

	Classification (%)		
Classes (10^6 *cycles)*	0-0.495	0.51-0.99	1.005-1.5
0-0.495	**81.1**	5.9	0.7
0.51-0.99	17.4	**55.2**	22.1
1.005-1.5	1.5	39	**77.2**

Table 6.6: LVQ classification result with three classes.

classification rate, the LVQ network result is more favourable. It is an important requirement that a motor should not be wrongly classified into a lesser usage class. It can be seen that the average misclassification in the lesser usage class ($\overline{E_{less}}$) is 9.57% for the LVQ network and 11% for the BP network. However, the difference is marginal. Classification into a lesser usage class may result in an unsafe decision being made during the asset recovery screening process.

Four classes Networks that can discriminate between four classes were trained using a feature vectors which are 100 points long. Tests have shown that the length of the feature vector can be reduced without losing classification performance. These vectors were derived from the original 200 points feature vector by selecting every second point. In general, reducing the length of the feature vector, x can be accomplished by sub-sampling it by an integer factor, M, to produce an output vector, x_d, according to equation 6.3.

$$x_d(n) = x(nM) \quad , \; M = 1, 2, 3... \tag{6.3}$$

Figure 6.2 shows the graphical representation of equation 6.3 [59].

The analysis results were compared to decide which operational mode vectors are the most suitable for further optimisation of the classification process. Three different ANNs were trained using TFE vectors derived from the current waveforms

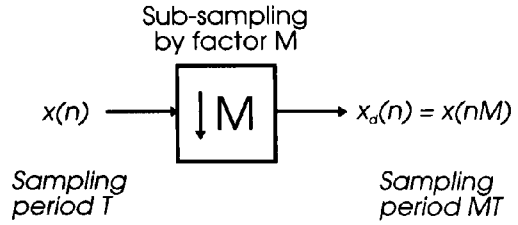

Figure 6.2: Sub-sampling of the feature vector.

of all three operational modes that were used in the accelerated life test experiments. All three ANNs were trained using the same network parameters. The number of hidden neurons were individually optimised for each ANN. Several ANNs were trained and the most favourable was chosen for comparison. In all cases the BP ANNs performed better than the LVQ ANNs. The correct classification rates were in the region of 57-68%. The results are shown in tables 6.7 to 6.9.

	Classification (%)			
Classes (10^6 *cycles)*	0-0.375	0.39-0.75	0.765-1.125	1.14-1.5
0-0.375	**66**	3.8	0	0
0.39-0.75	17	**66.4**	18	13
0.765-1.125	2	20.2	**31**	21
1.14-1.5	15	9.6	51	**66**

Table 6.7: BP classification results of the feature vectors for the fully loaded motors operating in the forward mode with four classes for the motor usage level.

	Classification (%)			
Classes (10^6 *cycles)*	0-0.375	0.39-0.75	0.765-1.125	1.14-1.5
0-0.375	**83**	6.7	0	0
0.39-0.75	7	**28.9**	5	4
0.765-1.125	4	45.2	**75**	40
1.14-1.5	6	19.2	20	**56**

Table 6.8: BP classification results of the feature vectors for the unloaded motors operating in the forward mode with four classes for the motor usage level.

	Classification (%)			
Classes (10^6 *cycles)*	0-0.375	0.39-0.75	0.765-1.125	1.14-1.5
0-0.375	**88**	5.8	0	0
0.39-0.75	9	**51**	3	4
0.765-1.125	1	38.5	**66**	30
1.14-1.5	2	4.8	31	**66**

Table 6.9: BP classification results of the feature vectors for the motors operating in the reverse mode with four classes for the motor usage level.

A summary of the classification resulted is presented in table 6.10. The table shows that the reverse mode feature vector has produced the best result. The correct classification rate is 7.02% better than in forward mode without load and the average misclassifications in a lesser usage class ($\overline{E_{less}}$ errors) were 3.23% less. Significant differences in specificity for the three types of vectors were not apparent. The sensitivity for the reverse current feature vector in contrast was the highest observed in this investigation.

Figure 6.3 shows the ROC curves of the classifiers operating on the vectors from the three motor operational modes. It can be seen that all three operational modes produce curves that are significantly better than random guessing. The area below the ROC curve produced using the reverse current feature is larger than these for the other two curves which indicates that the reverse mode feature vector produced the best classification result.

The initial classification tests have shown that the correct classification rate decreases with an increase in the number of classes. Figure 6.4 shows the ROC curves of the validation data for different number of ANN classes. It can be seen that the area under the curves decreases with an increasing number of classes. With increasing numbers of classes the available number of training vectors per class

Operation mode	*Correct classification rate (%)*	$\overline{E_{less}}$ *(%)*	*Sensitivity (%)*	*Specificity (%)*
Forward with load	57.35	13.95	62.13	91.67
Forward without load	60.73	13.93	74.26	93.32
Reverse without load	67.75	10.7	77.97	93.32

Table 6.10: Summary of the ANN classification result for current feature vectors of different motor operational modes.

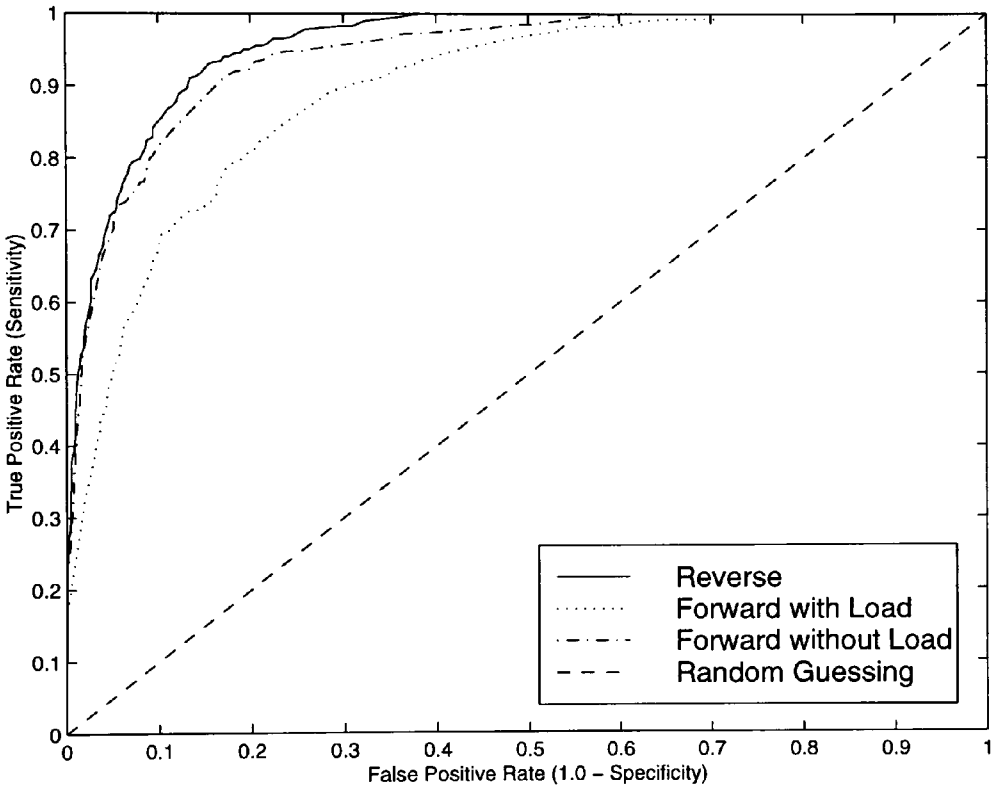

Figure 6.3: Training set ROC curves for the current TFE vectors obtained from the three motor operation modes. These curves are related to the four class ANNs.

decreases. This phenomenon decreases the generalisation ability of the ANN and worsens the classification rate.

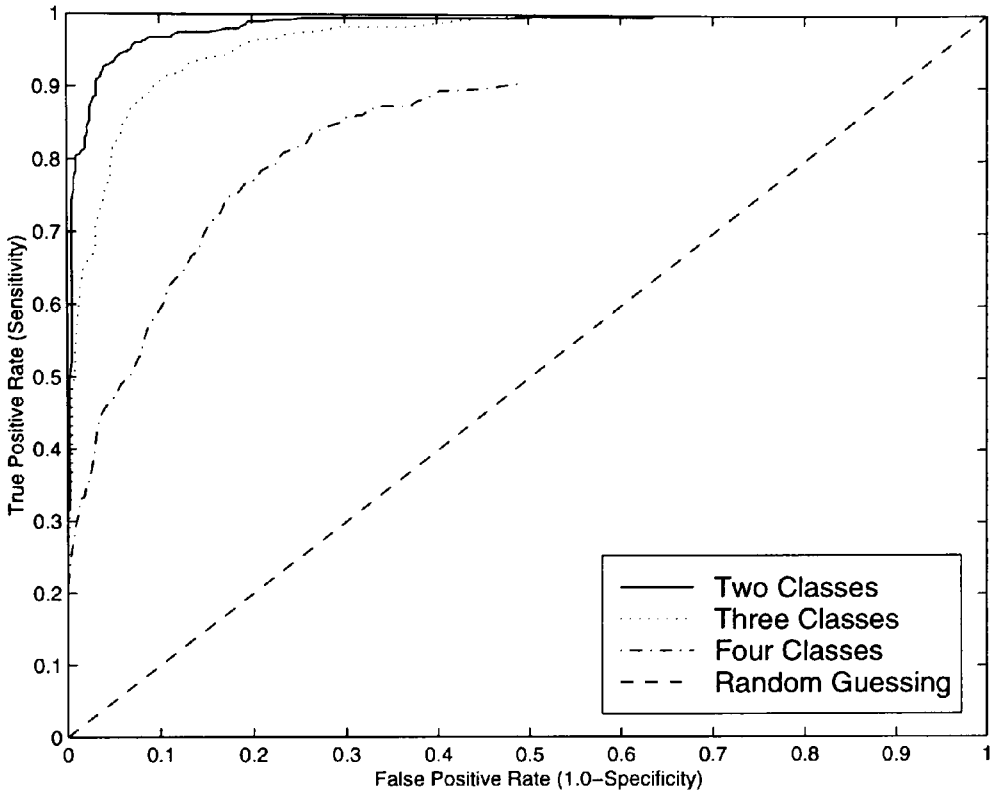

Figure 6.4: ROC curves for different numbers of ANN classes.

The classification results of the sample of used motor test vectors are summarised in table 6.11. These motors were provided by the Asset Recovery Department of Xerox Mitcheldean. They were used in one or more products, but their history is unknown. The 4 class ANN, which was trained on the data of the accelerated life test experiments was used to classify these motors. Table 6.12 shows the distribution of the used motors according to the design version. These results were confirmed by using ANNs trained on feature vectors in the two forward modes.

Cycles (10^6 cycles)	*Classification result (%)*
0-0.375	93.75
0.39-0.75	2.08
0.765-1.125	2.08
1.14-1.5	2.08

Table 6.11: BP classification of the sample of used motors.

	Cycles (10^6 cycles)			
Motor type	0-0.375	0.39-0.75	0.765-1.125	1.14-1.5
61.46.16	94.7	0	5.3	0
61.46.20	94.4	5.6	0	0
1.61.046.020	100	0	0	0
61.46.025	100	0	0	0
Motors from life test	0	0	0	100

Table 6.12: Classification of the used motors sample by different motor designs.

As a result of the initial classification experiments the reverse current TFE vector was selected for further investigations. Additional parameters were also considered to increase the correct classification rate. A maximum separation of the first 1.5 million cycles into four classes appears to be achievable if additional parameters lead to an increase in correct classifications. Tables 6.5 and 6.9 suggest that it is difficult for the ANN to separate between classes after the first 0.99 million cycles. Ideally the ANN should be able to separate classes that overlap. This is due to slight differences in wear patterns and wear speed. Since the signals have been sampled with an accuracy of 15,000 cycles it is likely that the TFE vector of the class 0.39-0.75 million cycles could also be classified within the class 0.765-1.125 million cycles of motor usage. This can easily be caused by a variation of 15,000 cycles of usage in the wear characteristic.

6.3 Comparison of TFE Vector and Frequency Spectrum Training Sets

A number of researchers have used frequency domain parameters as a classifier input, such as Altawil and Rodd [55]. They used the ac motor current harmonics as inputs to a BP ANN for classification with a reported 95% correct classifications.

The use of the current spectrum was also investigated in this study. The ANN training and test sets consisted of the reverse current spectra. These spectra were used as feature vectors and were divided into four classes as in section 6.2.2. The test and training vectors consisted of 270 points covering a frequency range from 0 to 18 kHz with a resolution of 66.6 Hz. The optimal number of neurons in the hidden layer was found to be 15. The results of the investigation into the classification ability of ANNs trained on frequency spectra of the reverse mode current are summarised in table 6.13.

The overall correct classification rate is 55.3%. The $\overline{E_{less}}$ error is 15.25%. In comparison with the results of the reverse current feature vector of table 6.10, the use of the current spectrum reduced the correct classifications by 12.45% and increased

	Classification (%)			
Classes (10^6 cycles)	0-0.375	0.39-0.75	0.765-1.125	1.14-1.5
0-0.375	**77**	1	0	0
0.39-0.75	23	**44.2**	5	0
0.765-1.125	0	46.2	**55**	55
1.14-1.5	0	8.67	40	**45**

Table 6.13: BP classification results using the frequency spectrum.

the misclassifications in a lesser usage class ($\overline{E_{less}}$ error) by 4.55%. It should be noted that with both methods the classification results were obtained with the parameter settings listed in section 6.1.2. The results showed that the TFE vector is suitable as a classification input. The ROC curves of the classifiers of both methods can be seen in figure 6.5. It is obvious that the performance of the spectrum classifier is worse than the TFE vector classifier.

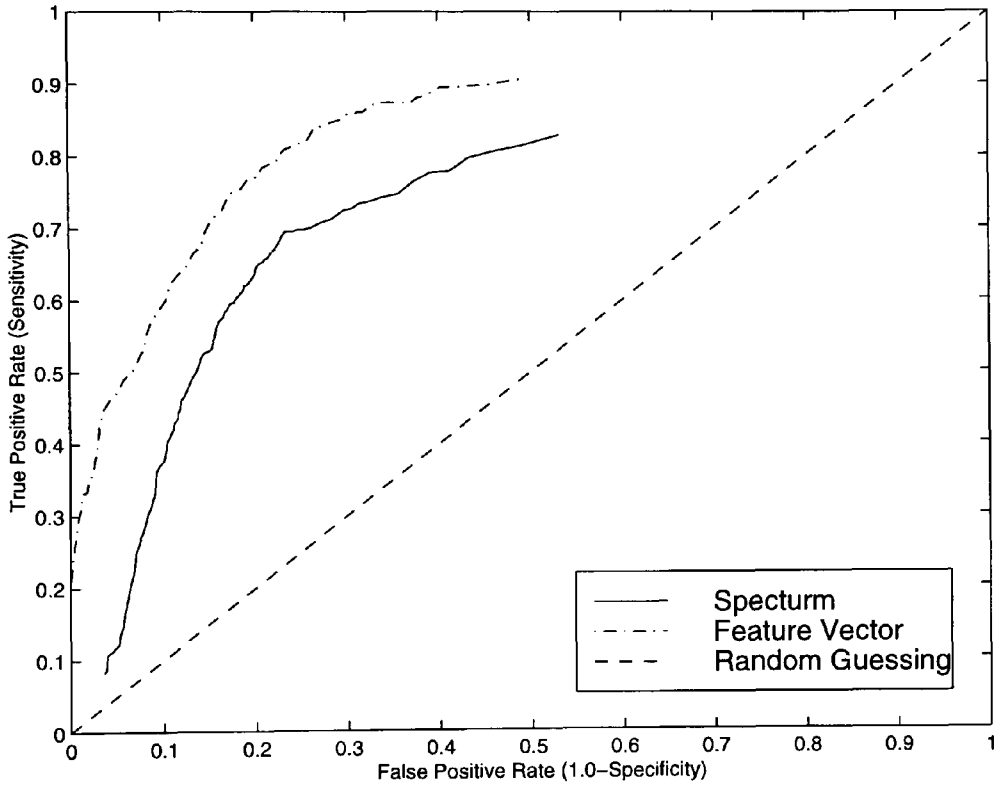

Figure 6.5: ROC curves using the spectrum and the TFE vectors for classification.

The comparison has shown that the current TFE vectors produced significantly better results than the current frequency spectra. Based on these findings the classification method was optimised using the current TFE vector.

6.4 ANN Optimisation

The previous section has established that the TFE vectors of the reverse motor current produced the best classification results. This section describes the investigations that were conducted to improve the results of the reverse current ANNs and optimise their performance. Two areas of investigation were considered. The first was to utilise additional parameters to enhance the performance of the reverse current ANN (section 6.4.1). The second area covered the utilisation of multiple ANNs (section 6.4.2).

6.4.1 Use of additional parameters

The accelerated life test showed that not only the TFE vector changes with motor usage other parameters also change such as the pure variation of the current. These parameters can be used in addition to the existing TFE vector to improve the classification results.

For the optimisation of the classifier, the feature vector can be sub-sampled. Experiments showed that sub-sampling by a factor of 2 for the 100 point original feature vector yields the best results. In addition to the 50 points long feature vector the coefficient of current variation, in the reverse mode, was also used. The first 50 points of the training and test vectors consisted of the TFE vector and the 51st point was the value of the coefficient of variation, both related to the reverse mode current. The ability to fuse data of different parameters is one of the advantages of using ANNs.

Table 6.14 shows the results of this investigation. The motor usage classes of

	Classification (%)			
Classes (10^6 *cycles)*	0-0.375	0.39-0.75	0.765-1.125	1.14-1.5
0-0.375	**93**	0.9	1	0
0.39-0.75	7	**80.8**	7	4
0.765-1.125	0	16.4	**55**	15
1.14-1.5	0	1.9	37	**81**

Table 6.14: BP classification result using a composite reverse current vector consisting of the TFE vector and the coefficient of variation.

the ANN are identical to the ones that were shown in table 6.9. Table 6.14 was produced using a BP network with a single hidden layer consisting of eight neurons. By changing the training vector the correct classification rate was improved by 9.65% from 67.75% to 77.4%. The $\overline{E_{less}}$ error was decreased from 10.7% to 6.2%, which represents an improvement of 4.5%. This clearly demonstrates the benefits of using additional parameters. An additional effect may also be that the reduction of the training and test vector lengths. This has enabled the use of fewer neurons in the hidden layer which resulted in a simpler ANN structure and lesser connections. Due to this simplification the network has improved its generalisation ability and produced better classification results.

6.4.2 Multiple ANNs

Splitting the data into five classes for the first 1.5 million cycles showed an overall correct classification of 66.9%. This result was achieved using the same training set that was used to produce table 6.14. The classes used were 0-0.3, 0.315-0.45, 0.465-0.75, 0.765-1.05 and 1.065-1.5 million cycles. One of the problems in this configuration was that in the class of 0.765-1.05 million cycles, the correct classification rate was only 30%. The overall $\overline{E_{less}}$ error was 15%. This experiment showed that

in this particular application four classes were the limit when using a single ANN. Increasing the number of classes for higher resolution did not produce improved results. A class with a correct classification rate of 30% is useless for test purposes. It was therefore, necessary to investigate an alternative approach to increase the classification resolution.

Multiple ANNs and 8 classes

Improving the classification resolution requires an increase in the number of classes. To increase the number of classes without compromising the performance of the ANN, the use of multiple ANNs was investigated.

These ANNs were used in a hierarchical arrangement. The rationale behind this approach is that each ANN requires to classify the TFE vectors into fewer classes than when a single ANN is used. Therefore, the performance of the individual ANNs would be improved and their complexity reduced. In addition, the overall resolution of the classification system would increase as a result of increasing the number of classes.

In the first investigation, 8 classes were used. The structure of the ANNs is shown in figure 6.6. The training and test vectors used with these ANNs were the same as those used to produce the results of table 6.14.

The first layer of the ANNs hierarchy consisted of a single ANN. This first ANN consisted of a single hidden layer with 21 neurons and 2 output neurons. The ANN classifies the feature vector into two motor usage classes (0-1.5 million cycles and over 1.5 million cycles).

The TFE vectors that were classified by the first ANN as belonging to the first class (0-1.5 million cycles) were then presented to the second ANN. This ANN had a single hidden layer with 14 neurons and 4 output neurons. The second ANN classifies the feature vectors into four classes (0-0.375, 0.390-0.75, 0.765-1.125, 1.14-1.5 million cycles). The vectors in each of these classes were then presented to a separate ANN in the next hierarchy layer. Each ANN in the third layer had a single hidden layer with 8 neurons and two output neurons. These ANNs classified the feature vectors presented to them into two classes as illustrated in figure 6.6. Therefore, the overall result of the classification process using the five ANNs was to classify the feature vectors into eight classes.

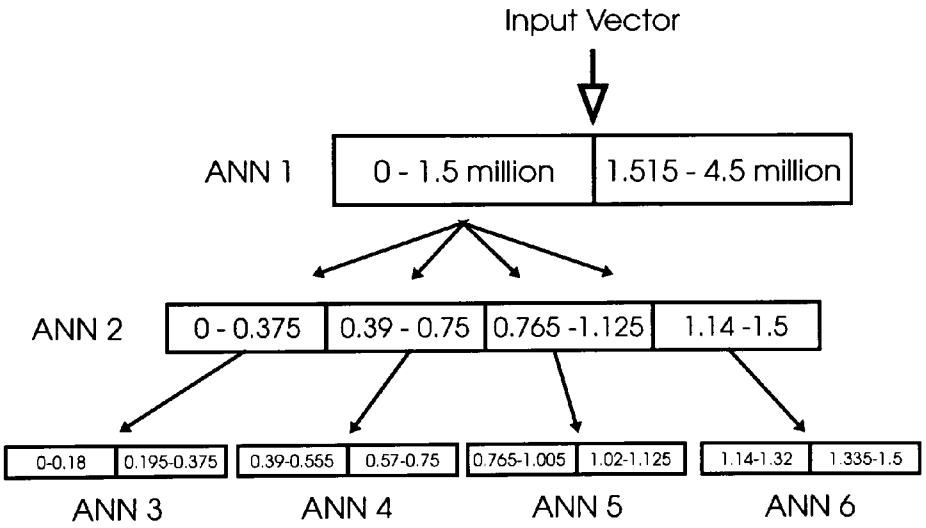

Figure 6.6: Classification using multiple ANNs in a hierarchical arrangement.

The classification results of the ANNs in the third layer of figure 6.6 (ANNs 3 to 6) are listed in tables 6.15 to 6.18.

Table 6.19 summarises the overall classification results of the ANN hierarchy. It can be seen that the use of multiple ANNs has increased the resolution significantly. The class of 1.14-1.5 million cycles showed a poor classification result. This was due to the inherent trends of the input parameters of the feature vector. It was shown

Classes (10^6 cycles)	Classification (%) 0-0.18	0.195-0.375
0-0.18	**96.2**	25
0.195-0.375	3.8	**75**

Table 6.15: Results of ANN 3.

Classes (10^6 cycles)	Classification (%) 0.39-0.555	0.57-0.75
0.39-0.555	**72.9**	30.8
0.57-0.75	27.1	**69.2**

Table 6.16: Results of ANN 4.

Classes (10^6 cycles)	Classification (%) 0.765-1.005	1.02-1.125
0.765-1.005	**85.3**	37.5
1.02-1.125	14.7	**62.5**

Table 6.17: Results of ANN 5.

Classes (10^6 cycles)	Classification (%) 1.14-1.32	1.335-1.5
1.14-1.32	**57.7**	43.7
1.335-1.5	42.3	**56.3**

Table 6.18: Results of ANN 6.

in chapter 5 that the amount of change in most of the parameters diminished after 1.2 million cycles of motor usage.

Classes (10^6 cycles)	Classification rate (%)	$\overline{E_{less}}$ (%)
0-0.375	85.6	12.5
0.39-0.75	71.1	15.4
0.765-1.125	73.9	18.8
1.14-1.5	57.0	21.9
Average	71.9	17.15

Table 6.19: Overall classification results of the ANN hierarchy of figure 6.6.

Multiple ANNs 7 classes

Enhancement of the classification for the first 1.5 million cycles by splitting it into eight sub-classes has shown that a compromise should be found between resolution and classification accuracy. A different division of the sub-classes and ANN structures were investigated to optimise performance. It should be noted that the training and test vectors in both investigations were identical. The new ANNs struc-

ture can be seen in figure 6.7. The classification results of the different ANNs in the hierarchy are shown in tables 6.20 to 6.23. Table 6.24 summarises the overall results.

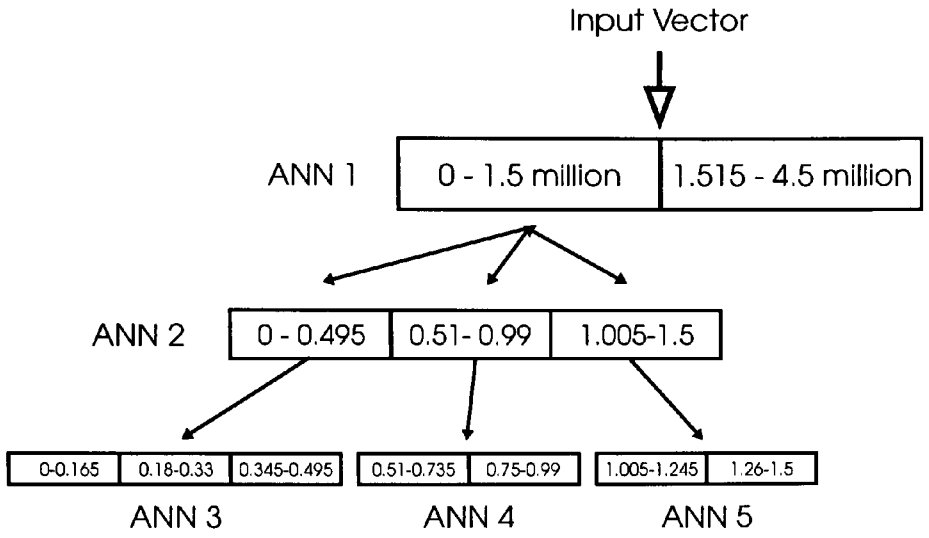

Figure 6.7: Classification using multiple ANNs with 7 output classes.

	Classification (%)		
Classes (10^6 *cycles)*	0-0.495	0.51-0.99	1.005-1.5
0-0.495	**89**	9.1	1.4
0.51-0.99	11	**76.5**	16.2
1.005-1.5	0	14.4	**82.4**

Table 6.20: Results of ANN 2.

Comparing the results of table 6.24 with those in table 6.19 indicates that the average classification rate has increased from 71.9% to 74.3% (+2.4%). The $\overline{E_{less}}$ error has decreased from 17.2% to 13.1% (-4.1%).

After considering the classification rates of the validation set, the third layer ANNs were analysed using the ROC analysis. The ROC curves are shown in figures 6.8 and 6.9. It can be seen from figures 6.8 and 6.9 that the classifier with

	Classification (%)		
Classes (10^6 cycles)	0-0.165	0.18-0.33	0.345-0.495
0-0.165	**85.4**	29.6	0
0.18-0.33	14.6	**63.6**	6.8
0.345-0.495	0	6.8	**93.2**

Table 6.21: Results of ANN 3.

	Classification (%)	
Classes (10^6 cycles)	0.51-0.735	0.75-0.99
0.51-0.735	**80**	17.6
0.75-0.99	20	**82.4**

Table 6.22: Results of ANN 4.

	Classification (%)	
Classes (10^6 cycles)	1.005-1.245	1.26-1.5
1.005-1.245	**58.5**	36.8
1.26-1.5	51.5	**63.2**

Table 6.23: Results of ANN 5.

Classes (10^6 cycles)	*Classification rate (%)*	$\overline{E_{less}}$ *(%)*
0-0.495	80.7	12.1
0.51-0.99	81.2	8.8
1.005-1.5	61.0	18.4
Average	74.3	13.1

Table 6.24: Overall classification results of the ANN hierarchy in figure 6.7.

seven classes (figure 6.7) performed significantly better than the one with eight classes (figure 6.6). Figure 6.8 also shows that ANN 6 is very close to the random guessing curve. As mentioned previously LVQ ANN outputs cannot be displayed in a ROC curve and therefore, a circle shows the operating point for this particular ANN (ANN 5) in figure 6.9. A measure of classifier performance is the area under the ROC curve [124]. Due to the obvious difference in performance this is not necessary since it is possible to compare the classifiers visually using the ROC curves in the two figures.

In a single instance only the LVQ paradigm showed a better classification performance than the BP paradigm. This suggests that the BP paradigm is better suited to deal with the data of this study.

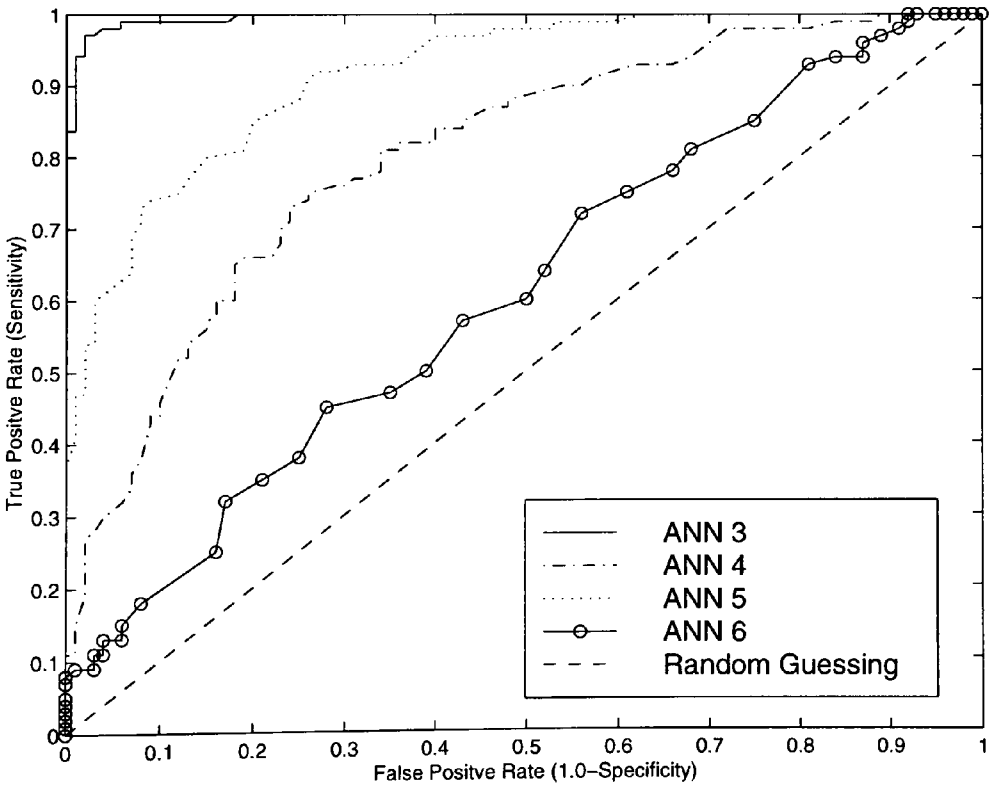

Figure 6.8: ROC curves of the ANNs in the third layer of the ANN classifier with 8 output classes (figure 6.6).

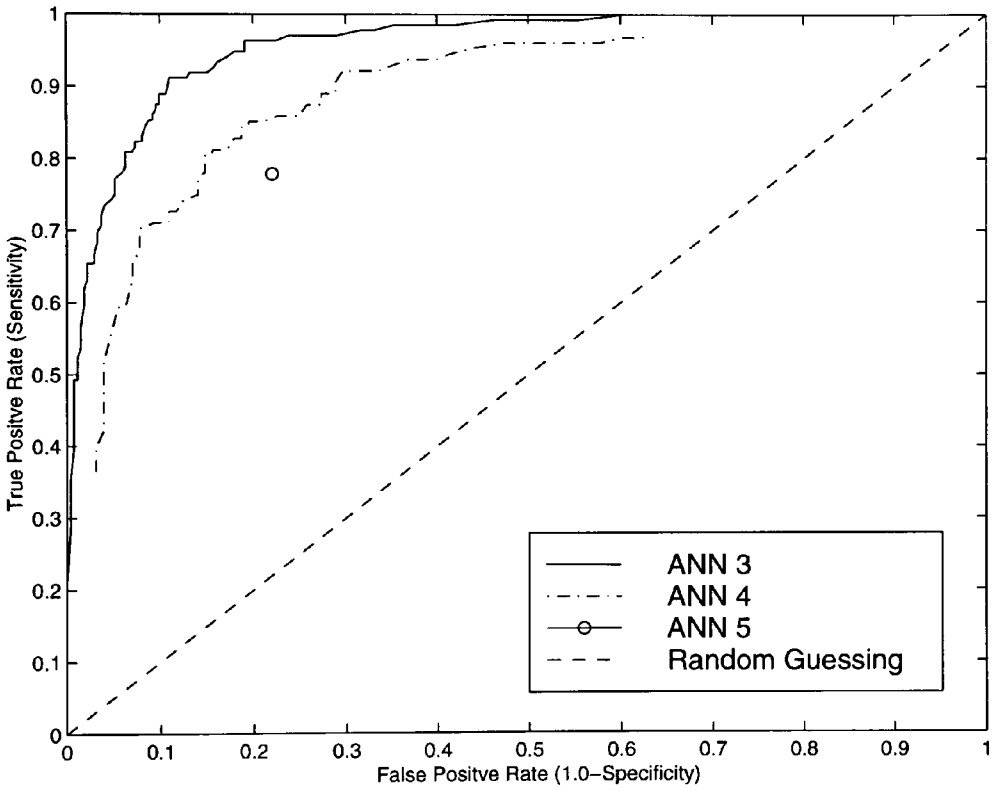

Figure 6.9: ROC curves of the ANNs in the third layer of the ANN classifier with 7 output classes (figure 6.7).

6.5 Classification of Used Motors

A sample of 48 used motors was provided by Xerox. These motors have been used in one or more products. However, their level of usage was unknown. This sample of used motors was used in this study to estimate their level of usage and to evaluate the performance of the trained ANNs.

The initial classification, as outlined in table 6.12 of section 6.2.2 has shown that 93.75% of the used motors were classified with a usage level of less then 0.375 million cycles.

In this part of the study, classification was conducted using the two multiple ANNs classifiers described in section 6.4.2. The tests were conducted with the accelerated life test equipment and the newly developed production test system, in order to guarantee that the tests using the production system were carried out under identical conditions to those of the accelerated life test experiments. All motors were re-attached three times in order to test the repeatability of the results. The results were the same in all cases.

	Motor usage (million cycles)			
Motor type	0-0.18	0.195-0.375	0.57-0.75	1.335-1.5
61.46.16	68.4	21	5.3	5.3
61.46.20	100	0	0	0
1.61.046.020	100	0	0	0
61.46.025	100	0	0	0

Table 6.25: Classification of different motor designs using the ANN classifier with eight outputs (figure 6.6).

The results of these tests can be seen in table 6.25 and 6.26. The majority of used

	Motor usage (million cycles)			
Motor type	0-0.165	0.51-0.735	0.75-0.99	1.26-1.5
61.46.16	89.4	5.3	5.3	0
61.46.20	100	0	0	0
1.61.046.020	100	0	0	0
61.46.025	100	0	0	0

Table 6.26: Classification of different motor designs using the ANN classifier with seven outputs (figure 6.7).

motors were classified as being in the first class (0-0.18 million cycles). Only the 61.46.16 motors were classified differently. Motors of this type were used between the years 1987 to 1990 (table 3.1) and are therefore, the oldest motors in the test sample. The machines using this type of motor were manufactured between 1987 and 1990. Therefore, it is likely that these motors have been used for a longer period of time than those in machines of a later design. This assumption correlates with the classification results.

6.6 Summary

This chapter has presented the ANN paradigms that were used to classify the results of the accelerated life test experiments for motor usage level estimation. The performance of different ANN structures was investigated thoroughly to arrive at an optimum architecture that can be used as part of an asset recovery motor screening system in a production environment.

The accuracy of the ANNs were investigated with the current TFE vectors obtained from the three motor operational modes. The TFE vector results were compared against the spectra of the current waveforms as ANN classifier inputs.

The chapter has also presented the investigation into optimising the ANN classifiers. This included the use of composite input vectors as ANN inputs, different number of classes with single and hierarchical ANN structures.

A sample of used motors with unknown history supplied by Xerox were classified to assess their usage level and to test the robustness of the developed ANNs.

The key findings of this chapter can be summarised as follows:

1. ANN paradigms and structures

   (a) In general, all BP ANNs performed better than its LVQ counterparts. They produced better percentages of correct classification and smaller values of $\overline{E_{less}}$.

   (b) The accuracy of the single ANN classifiers decreased with increasing the number of classes.

   (c) ANN classifiers consisting of a hierarchy of independent single ANNs with small number of outputs produced significantly better results than single ANN classifiers.

2. Classification data

   (a) The TFE vectors calculated from the reverse motor current waveforms produced the best classification results in comparison with those generated from the current waveforms of the two forward motor operational modes. The reverse motor current is therefore, considered the most reliable parameter for estimating the motor usage level.

(b) The motor current TFE vectors produced better classification results than the spectra of the same current waveforms.

(c) Using a composite vector consisting of the TFE vector and the coefficient of variation of the motor current waveform produced significantly better results than using the TFE vector alone.

3. The classification results of the motor parameters above 1.5 million cycles did not produce reliable results. The reason for this is that the characteristics of the current waveforms did not vary significantly and consistently after 1.5 million cycles of motor usage. This is consistent with the findings of chapter 5.

4. Most of the used motors in the sample supplied by Xerox were classified as having been used for less then 375,000 cycles. The remainder of the motors in the sample were classified as having been used for less than 1.5 million cycles. As the motor sample was typical and randomly collected, it is safe to assume that the selected wear indicating parameter and the developed ANN classifiers are more than sufficient for the asset recovery screening of the test motors.

Chapter 7

Discussion

The aim of this study was to investigate wear development and usage level estimation of small dc motors for the purpose of establishing reliable industrial asset recovery processes. To achieve this aim, the operation of selected test motors was investigated thoroughly and a set of wear indicating physical parameters were identified for detailed study. An accelerated life test system was developed and utilised to conduct controlled experiments on a set of motors to investigate the changes in the characteristics of the wear indicating parameters with usage level of the motors. The acquired signals of the wear indicating parameters were processed for feature extraction and data reduction. The resulting data were analysed using ANN classifiers to provide an automated mechanism for motor screening during asset recovery. The processing and analysis methods developed in this study were shown to provide reliable results for the problem of classifying the dc motors according to their usage level.

This chapter discusses the results of the various investigations conducted during this study. It considers the developed methodologies and presents the rationale for

adopting them. Section 7.1 discusses the significance of the accelerated life test and the design of the experimental test system.

The wear parameters investigated in this study are discussed in section 7.2. This discussion includes the physical interpretation of the trends that were shown by these parameters during the accelerated life test experiments.

The signal processing techniques and the data analysis methods that were utilised to interpret and classify the results of the experimental tests are discussed in section 7.3.

7.1 Accelerated Life Test

After considering a variety of possible test approaches (section 4.1), the marginal test procedure was chosen as the preferred accelerated life test method. The test results confirmed that this was the most appropriate test method for this study. If the tests were conducted according to the enhanced stresses or STRIFE procedures, it would have been difficult to relate the test results to the motor's usage in its real application.

It is essential to discuss the purpose of the accelerated life test in the context of the asset recovery process for this type of motor. Motor screening within the asset recovery process is aimed at assessing if the motor can be used in a product without a failure in the field for the life of the product. The concept of life is related to the product and not to the motor. Therefore, if the 5047 copying machine is known to

produce a maximum of 750,000 copies throughout its life, then it is only necessary to assess that the motor can function reliably for the same number of cycles. Since the motor is specified as being capable of functioning for 1.5 million cycles at a maximum load of 0.75 Nm, it is only necessary for the screening process to indicate if the motor will not exceed its specified parameters for the full life of the next product. The accelerated life test experiments of this study were designed using this reasoning. As a result it was decided early in the study that it was not necessary to test the motors to destruction. The experimental investigations produced consistent and reliable results for the motor usage level below 1.5 million cycles at maximum load. This is more than sufficient for the motor under study as it will never be reused in a new product if its usage level exceeds the maximum specified number of cycles.

The design of the test system enabled the monitoring and assessment of the most important parameters which included current, time-to-speed, internal motor resistance, vibration and acoustic noise. The use of a second motor as a brake was advantageous. This made it possible to measure the internal motor resistance by using the brake motor to drive the test motor in generator mode. Torque measurements before the start of the accelerated life tests and after its completion showed that the torque of the brake motor remained constant over the test time. A potential problem was the influence of the inertia of the brake motor on the time-to-speed measurement. This was due to the additional mass that the test motor had to drive. However, measurements in the laboratories of Xerox at Mitcheldean, showed that the time-to-speed measurements of the same motors but using a magnetic brake, which had a much lower inertia then the brake motor, produced the same results as in the accelerated life test experiments of this study. The brake motor appeared not

to cause noticeable changes in the measurements and its inertia effect was therefore, negligible.

Vibration measurements were conducted using an accelerometer attached to the motor gearbox to monitor any vibration changes, caused by motor usage. The vibration signals measured at this position did not show any significant changes over time. It is unlikely that a different mounting position of the accelerometer would have shown a different result.

7.2 Wear Parameters

The analyses of the wear parameters, which were observed during this study, showed that only few of them could characterise wear in small motors, and thus can be used for estimating the usage level of the motor. The time-to-speed parameter and the internal resistance remained almost constant during 4.5 million cycles of testing. This demonstrated how well the motor was designed for this application. None of the motors tested, failed to perform according to specification during 4.5 million cycles.

7.2.1 Motor speed

A parameter that was not expected to change significantly with usage was the speed of the motor. Remarkably, this parameter changed in a similar fashion in all observed motors and in all motor operational modes. The speed change was not due to a change in the motor supply voltage, because the variation in the motor voltage was below $\pm 0.5\%$ during the 4.5 million cycles of testing (table 5.3). It was either due to a decrease in the magnetic flux or bearing and gear friction. A decreasing friction

as a cause of the speed change can be neglected. The gear friction using nylon gears is low even without optimal lubrication. A speed increase due to the bedding-in of the plain brass bearings is also unlikely. Visual inspection of the bearings did not show any marks that could be related to wear. The visual inspection of the bearings from the used motors, confirmed this observation. Therefore, bearing wear can be neglected as a cause for the speed change of this motor type. This observation was also confirmed by Xerox's Asset Recovery Department [127]. Generally, a reduction in mechanical friction should have caused a decrease in the mean motor current, but this effect was not observed.

As suggested in section 5.2.4, the speed increase over time was probably due to a decrease in the magnetic flux of the permanent magnets. The main causes of magnetic instability are temperature changes, exposure to stray magnetic fields, and mechanical shock or vibration. At room temperature, permanent magnets are likely to remain stable for many years [128]. In the case of the investigated dc motor it can be assumed that the operating temperature, as a cause for high demagnetisation, had a minor effect because the motor operated at room temperature. This is lower than the maximum specified temperature for the motor. The motor design assumes that it is used in an indoors office environment with an average temperatures below 35 °C .

The observed average RMS vibration level of 0.2 g and a peak vibration level of less then 0.5 g are unlikely to cause significant demagnetisation. The most likely cause of this effect is the exposure to a magnetic stray field. In general, the greater the coercivity of the magnet, the less serious the loss from stray-field effects. A permanent magnet is usually stabilised against stray-field losses by subjecting it to

an alternating field with a strength slightly greater than any other field it is likely to encounter during its use. The motor in this study was used in a stop/go mode. It is likely that the stray field in this operational mode is higher, due to the high start-up current, than in a mode where it is operated steadily. Therefore, it is reasonable to conclude that this is the cause of the demagnetisation.

Such demagnetisation should be noticeable by measuring the motor current. The relationship between the mean current of the motor, i_a and the magnetic flux, Φ, is given by,

$$i_a = \frac{T}{k\Phi} \tag{7.1}$$

Therefore, the mean current should increase with decreasing magnetic flux. A positive trend in the current waveform was detected in the results of the accelerated life test experiments as shown in table 5.8. If all these effects are taken into account, it can be concluded that the cause of the speed increase is demagnetisation.

7.2.2 Motor current

The motor current waveform was found to be the best indicator for wear during the first 1.5 million cycles of operation. The reverse mode current waveform was the most consistent parameter for all tested motors and showed the best classification results (section 6.2.2).

Many indicators showed that the motor was not loaded in its application to the maximum specified load limit (0.75 Nm). These indicators included the applied torque in the 5047 copying machine (table 3.4), measurements of the brush length

of the used motors (section 3.6.1) and visual inspection of the commutator carbon film (section 3.6.1). These observations were confirmed by the results of classifying the sample of used motors to determine their usage level (section 6.2.2 and 6.5). These results have shown more than 90% of the motors in this sample were classified as having been used for 375,000 cycles. The experience of Xerox suggested that a copying machine of type 5047 would not produce more than 750,000 copies during its full normal life [127]. If it is assumed that the used motors which were tested in this study had been used in at least one product throughout its full life, then there is a discrepancy between the classification results and the minimum usage level indicated by Xerox. This provided further evidence that the used motors were not fully loaded in the application. The ANN classifiers were trained on the data that were obtained from the accelerated life test experiments. In these experiments the motors were loaded at the maximum specified torque level of 0.75 Nm. Therefore, a used motor that has been classified within the 0-375,000 cycles class at maximum load may have done significantly more cycles, but at a lower load level.

Therefore, it is possible to conclude that a motor that has done 750,000 cycles in the application with a maximum load of 0.4 Nm or less, can be considered to have performed less than 375,000 cycles at maximum load. The test system developed in this study with its associated ANNs is therefore, capable of assessing the usage level of a motor based on a reference measure, which is the number of cycles at maximum load. Classifying a motor which has been used in the application at loads below the maximum load specified level does not affect the accuracy of the asset recovery screening process as long as the reference level is clearly defined.

The changes in the current waveform, which were observed both, in the frequency

domain and the TFE vectors, were due to the bedding-in process of the brushes. This effect occurs due to the differences between the commutator and the brushes radii (figure 3.7). This causes a change in the commutation pattern due to the change of the conducting brush contact area during motor usage.

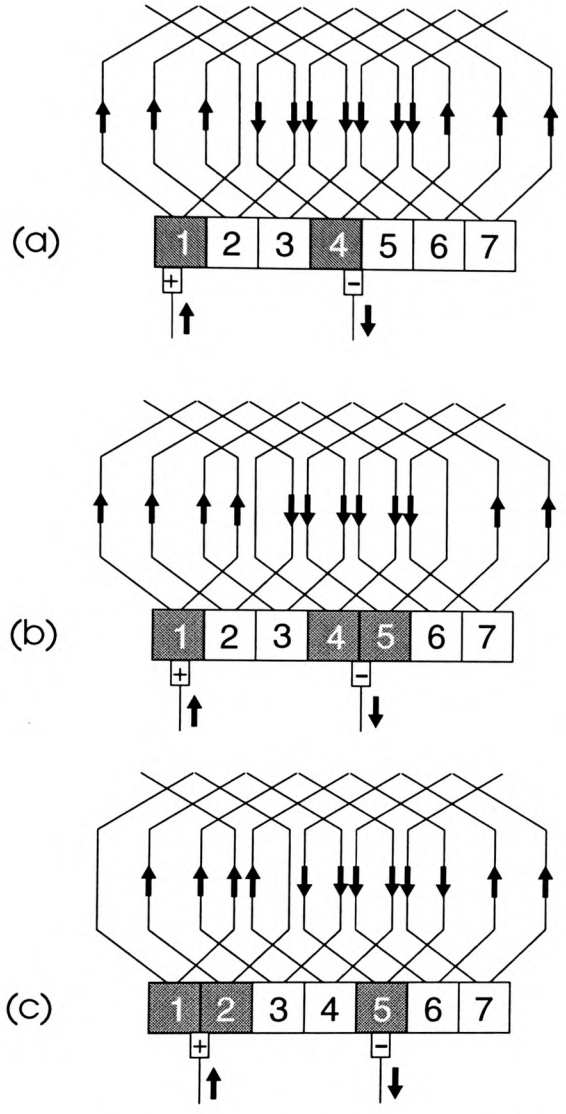

Figure 7.1: Commutation patterns of a motor with a new brush.

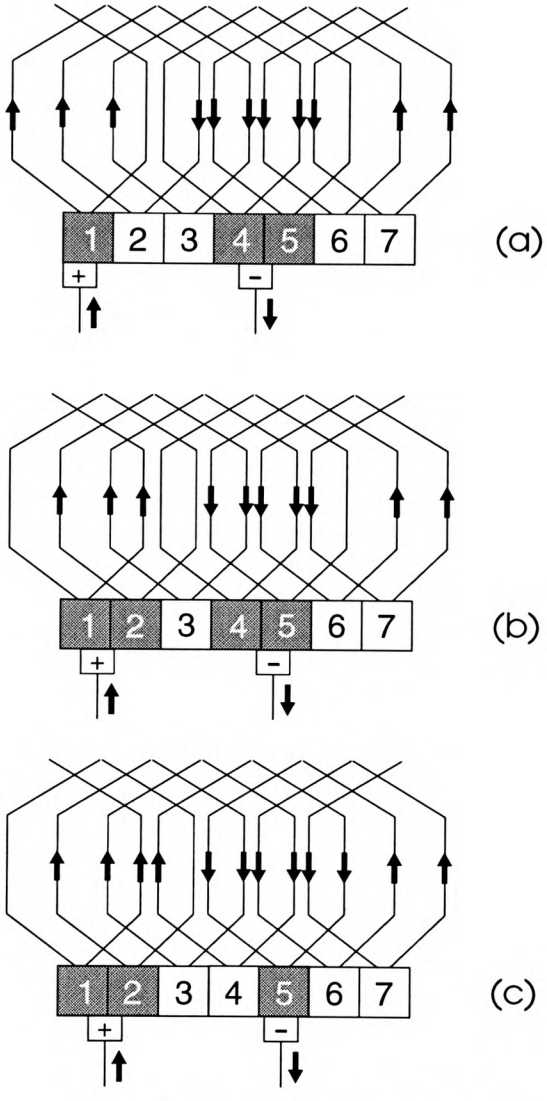

Figure 7.2: Commutation patterns of a motor with a bedded-in brush.

Figures 7.1 and 7.2 illustrate how a bedded-in brush causes a different commutation pattern compared to a new brush. The diagrams are not drawn to scale

but the relative proportions of the seven commutator segments and the widths of the brushes are correct. Due to the differences in the brush and commutator radii, the conducting commutator contact area of a new brush is smaller than that of a bedded-in brush. This results in the commutation patterns shown in figure 7.1. When the brush is fully bedded-in, the conducting brush contact area is at its maximum and the commutation patterns are shown in figure 7.2. When comparing the two commutation patterns it can be seen that one of the two bedded-in brushes will always commutate two adjacent segments (figure 7.2). This is not always the case for new brushes (figure 7.1). Due to this change in the commutation process the current waveform will also change. This effect can also be seen in the frequency spectrum of the reverse current (figure 7.3). Due to the changes in the commutation positions, the noise in the current signal increased from -68 dB to -46 dB. This is indicative of slight commutation sparking (section 3.1.2).

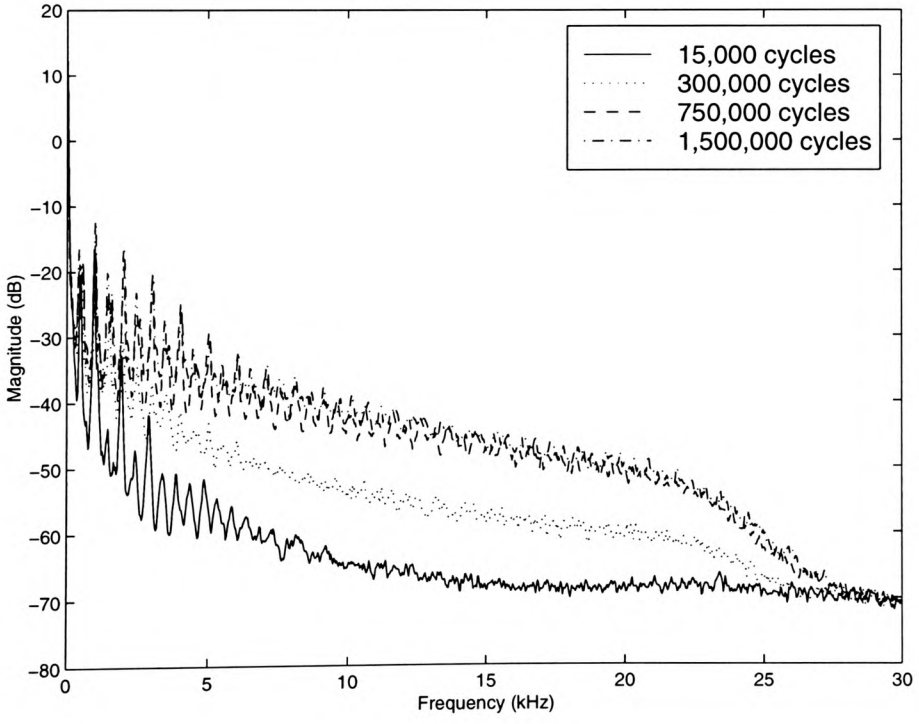

Figure 7.3: Frequency spectrum of the reverse current waveform.

However, this change was not prominent in the mean current value but it had an influence on the internal resistance. The resistance dropped during the first 300,000 cycles of the accelerated life test. This suggests that the conducting contact area of the brushes has increased and as a result, the internal motor resistance has therefore, decreased. Once the brushes are bedded-in, the current waveform did not change significantly. This happened approximately after 1.2 million cycles of motor usage. This is the reason why the classification of the motor current waveforms which were obtained after 1.5 million cycles of testing did not produce accurate results. The extension of the brush bedding-in process to well above one million cycles is a clear indication that the motor was designed for higher torque levels than those specified by the copying machine manufacturer.

The hardness tests on a number of carbon brushes (section 3.4.2, table 3.3) showed that the brush hardness variation was within typical production tolerances. The ±95% confidence intervals of the hardness figures for brushes from different motor designs showed an overlap. This suggests that the brush material did not change between different motor designs. This is important to enable the test system to produce consistent results for motors of different designs.

7.2.3 Gearbox and bearings

Similar to the brushes, the gears bedded-in during the first 1.5 million cycles. This is especially the case if the motor gears have been designed for higher loads considering that the bedding-in process of the gears usually ends in a shorter period of usage. The gearbox and bearings did not wear noticeably. The major design factor for the gears is the load they have to transmit [21]. Since the motor itself has been designed for higher loads than those listed in Xerox's specifications it can be assumed that the gears were also designed to carry higher loads. Otherwise, a significant change

in the vibration signal due to wear would have been observed. The accelerated life test experiments showed that a motor can be used for more then 4.5 million cycles without any loss of performance and significant increase of vibration level.

7.2.4 Acoustic noise and vibration

The investigation into acoustic noise showed that the sound pressure level of the steel spur gear was the highest amongst all tested gear designs. The new gearbox design has two major advantages: helical gear cut and nylon gear material. It was observed that the noise level of a used motor with a helical gear cut was slightly higher than a new one. However, the SPL was not as high as the SPL level of a steel spur gear design.

The acoustic noise tests that were conducted during this study showed that the design of the motors was not optimal for its purpose, considering the noise emission/torque characteristic. The increasing noise level in the main region of operation in a 5047 copying machine ($\approx$0.4 Nm) indicated a design weakness.

Generally, relying on acoustic screening for this motor in a production environment is questionable. The maximum observed SPL of a steel spur gear design was 36 dB and the lowest observed SPL was around 26 dB. For comparison, the noise SPL in a library is 30 dB and the noise SPL in an average living room is around 40 dB [114]. Considering acoustic masking effects, a test environment should provide at least a 3 dB safety margin between the lowest observable motor noise level and the test environment. Therefore, the noise level in the test environment should be 23 dB or lower which can be compared with the noise SPL of a recording room [114]. This means that in order to achieve a meaningful test result the environment should be

acoustically isolated from the shop floor. Currently, screening is conducted at Xerox and other copying machine manufacturers in a production environment. Murphy and Sayegh [8], also observed that the majority of discrimination errors were related to the operator, even when the acoustic tests were carried out in a sound proof chamber. Therefore, operator based acoustic screening of the motors for asset recovery can be considered as an unscientific practice according to the evidence of this study.

In addition, the motor is mounted inside a copying machine, its noise is masked even further in its application. This suggests that the motor does not contribute significantly to the noise level of the application such as the 5047 copying machine.

The vibration signal of the tested motors did not show any significant trend that may be used for wear characterisation. However, a correlation between the vibration signal and the acoustic noise of the tested motors was observed. The average RMS vibration level decreased by 53.4% when the motor was running with a 0.75 Nm load compared to its no load level. This is equivalent to a -5.5 dB decrease in vibration energy. This was also observed in the SPL characteristics of the used 61.046.020 motor design.

7.3 Signal Processing and Analysis

To interpret the information provided by the wear indicating parameters it is essential to arrive at reliable signal processing and data analysis methods. This is also critical for an automated asset recovery process for small motors. The literature review has covered a wide range of signal processing and analysis techniques with special emphasis on those used in condition monitoring and fault diagnosis of elec-

trical machines. As a result of the literature survey a selection of these techniques were chosen for further investigation and application on experimental data of this study.

The transform for feature extraction (TFE) was investigated theoretically to compare its performance against established techniques such as spectral and statistical analyses. This was followed by testing the TFE's performance on the experimental results, especially the reverse motor current. Such investigations of the TFE have not been reported previously in the research literature. A windowed version of the TFE, the WTFE, was introduced in this study to take into account local variations in the signal's shapes. This is similar to the windowing approach of the STFT. All the investigations conducted in this study on the TFE proved that it was superior to spectral and statistical analysis in extracting significant features of the analysed signals. In addition, it provided high data reduction capabilities. The reasons for the improved performance of the TFE over spectral and statistical methods can be attributed to its ability to represent the features of the signal's shape in an effective manner. Unlike other analysis methods which deal with one aspect of the signal, such as the frequency components, number of peaks, maximum amplitude or mean value, the TFE produces a feature vector that represents a fusion of these and other parameters. The feature extraction capability of the TFE was confirmed when its feature vectors were used to train and test the ANNs of this study. In all cases it performed better than the signal spectrum.

ANNs were demonstrated to be very suitable analysis tools for wear characterisation and usage level estimation of the dc motors. This is understandable as the relationships between the usage level and characteristics of the signals of their wear

indicating parameters are not clearly defined and cannot be represented in mathematical terms.

The best performing ANN offered an average resolution of better than 15% for the first 1.5 million cycles with an average correct classification rate of 74.3%. The classification rate was higher for the first 1 million cycles. An average rate of 81% was achieved with an average $\overline{E_{less}}$ error rate for these classes of 10.45%. The achieved classification accuracies are sufficient for the asset recovery process of this motor type.

The comparison of different ANNs showed that the use of the LVQ paradigm did not prove to be advantageous in the classification process because it produced high variability in a single class. The BP algorithm, in contrast, has shown its ability to classify overlapping data correctly.

The combination of the TFE and ANNs produced reasonable results when applied to the reverse current signals of the sample of used motors as discussed in section 7.2. This is demonstrated by the fact that the vast majority of the motors in this sample were identified as having usage levels much lower than the maximum specified motor usage level of 1.5 million cycles.

The processing and classification tools developed in this study were optimised for the test motor used in this study and its wear indicating signals. However, these tools are generic in nature and can be easily customised for use with other types of motors and even sub-assemblies from the copying machine. In fact, the processing and analysis methodologies presented in this thesis may prove to be of

significant value in other fields, such as the analysis of biological and medical signals.

It is possible that the accuracy of the analysis reported in this study could have been improved by expanding the scale of the accelerated life test experiments. This could have been done by using a large number of motors in the experiments and extending the length of the experiments beyond 4.5 million cycles. However, this was not considered to be necessary as the main aim of this study was to investigate the methodologies and enabling technologies for reliable asset recovery of small dc motors. The results of this study were sufficient to demonstrate that this aim has been achieved.

Chapter 8

Conclusions and Future Work

8.1 Conclusions

This study has set out to investigate the wear characteristics of small dc motors and the methods of estimating the usage level of these type of electromechanical assemblies to establish a reliable asset recovery process for photocopying machines. This study was concerned with enabling technologies and methodologies to allow the assessment of the suitability of recovered dc motors for use in a new product. The research work that was presented in this thesis consisted of both, theoretical and experimental investigations into the development and progress of wear in the selected dc motor as it is used in its paper tray application of copying machines.

The study has covered all aspects of the problem defined in section 1.1 of this thesis and achieved all the objectives of the research project which were outlined in section 1.2. The literature survey conducted during this study has clearly shown that wear characterisation and usage level estimation of small dc motors has not been significantly investigated by previous researchers, especially in relation to as-

set recovery for commercial equipment. Therefore, the work that has been presented in this thesis represents a significant contribution to knowledge in the fields of asset recovery and wear understanding for small electromechanical assemblies. The vast majority of previous research was concerned with large electrical machines, especially induction motors.

The literature review, information exchanged with the engineering staff at Xerox, the experimental and analytical investigations during this study lead to the following conclusions:

1. Asset recovery of small electromechanical assemblies has significant economic and environmental benefits. However, current methods of screening these assemblies, especially motors, relies on the subjective assessment of an operator of the suitability for reuse in a new product. This assessment is entirely based on the operator's perception of the acoustic noise emitted by the motor. This study has proven beyond any doubt that acoustic noise does not provide sufficient information on the suitability of a motor for reuse, especially when the screening is conducted subjectively and on the shop floor.

2. The concept of life for a dc motor should be related to the life of the product rather than the life of the motor itself. In asset recovery screening it is only essential to ensure that the motor will not exceed its specified usage level before the end of its product life.

3. A large number of physical parameters can provide information on wear in small dc motors. These parameters include vibration, acoustic noise, time-to-speed value, and the motor current waveform in various operational modes. The experimental investigations conducted during this study have shown that

within the constraints of the maximum specified usage and loading levels of the dc motor, the only parameter that provided consistent and reliable indication of wear was the reverse current waveform. The reason for this is that changes in the motor current are related to changes in the dimensions of the brush and commutation pattern. As the motor is exercised, the length of the brushes and their contact area with the commutator changes. This is part of the brush bedding-in process which continued almost to the maximum specified usage level of the motor (1.5 million cycles). The effect of the gear bedding-in process and the bearing wear were not noticeable in the vibration signals or the acoustic noise measurements. It can be concluded that significant wear in these parts only take place after usage levels several times higher than the maximum specified usage level of the motor.

4. The subtle differences in the shape of the reverse current waveform as they change with usage level of the motor proved to be difficult to identify using spectral analysis and standard statistical methods. On the other hand, the TFE demonstrated its capabilities in extracting the features contained within these waveforms and identifying their differences. This processing technique was investigated thoroughly for the first time during this study and was shown to have a considerable potential of identifying important signal characteristics. In addition, its data reduction capabilities makes it an ideal technique for generating feature vectors for use in conjunction with ANNs.

5. This study has shown that BP ANNs have the capability of estimating the usage level of the dc motor by classifying the TFE vectors of reverse current waveforms into discrete classes. It was shown that the developed ANNs provided sufficient accuracy and resolution for the purposes of asset recovery.

Classifiers consisting of a hierarchy of relatively small ANNs performed consistently better than single ANNs with larger number of outputs. In addition, the performance of the ANNs can be improved by using the TFE vector with the coefficient of variation of the waveform and combine it to a composite input vector.

8.2 Future Work

The results of this study and the conclusions of section 8.1 have shown that screening of small dc motors for asset recovery can be conducted reliably and objectively. This study has investigated the technical issues associated with understanding wear in small dc motors. It has developed the necessary equipment and methodologies to assess the development of wear in dc motors and to estimate their usage level. To take maximum advantage of the results of this study, it is recommended that future research work should include the following areas:

1. Investigation into the applicability of the developed techniques to other types of small electromechanical assemblies, especially dc and ac motors. In addition, it is also important to consider whole sub-assemblies, such as the whole paper tray mechanism. This will enable more than one part to be screened during asset recovery. However, this approach may require careful investigation as the tested assembly is more complex. On the other hand, it enables more realistic tests to be conducted as the interaction of the parts within the assembly are not changed from the real life application.

2. To explore the changes in the wear indication parameters with the usage level for motors which are used close to their specification limits. This may provide

valuable information for designers of copying machines and similar commercial equipment, and enable them to lower the costs of the used parts. The current trend of many machinery manufacturers is to over-specify the motor, as was discovered in this study.

3. To investigate the suitability of the TFE as a signal analysis tool, with or without ANNs, in other fields. The TFE may have significant benefits in applications where signal recognition and signature analysis are required. These application areas may include voice recognition and medical diagnosis.

4. Standard ANNs have shown their classification capabilities in this study. New ANN types have been developed by other researchers in order to combine the neural network approach with other forms of artificial intelligence. An example is the combination of fuzzy logic and genetic algorithms in conjunction with ANN paradigms. Which should be investigated if the use of these network types with the existing set of data will be able to achieve better classification results.

5. A different and probably long term approach to classification using ANNs, is the development of a model that includes the main motor wear factors. This system identification approach may avoid unnecessary and extensive accelerated life testing and may make ANN classification obsolete. If a model exists that includes all factors that contribute to motor wear, it may be possible to extrapolate the results of only a small number of tested motors. This would also be beneficial from a business point of view. It will decrease development time and costs of reliable life prediction tools and therefore, enable asset recovery for more low cost components.

References

[1] R. K. Mobley, *An Introduction to Predictive Maintenance.* Van Nostrand Reinhold, 1990.

[2] J. Spoerre and H.-P. B. Wang, "Machine performance monitoring and fault classification using an exponentially weighted moving average scheme," *International Journal of Production Research*, vol. 33, no. 2, pp. 445–463, 1995.

[3] R. R. Schoen and T. G. Habetler, "Evaluation and implementation of a system to eliminate arbitrary load effects in current-based monitoring of induction machines," in *IAS '96 IEEE Industry Applications Conference*, vol. 1, pp. 671–678, 1996.

[4] J. H. Williams, A. Davies, and P. R. Drake, *Condition-Based Maintenance and Machine Diagnostics.* Chapman & Hall, 1994.

[5] P. J. Tavner and J. Penman, *Condition Monitoring of Electrical Machines.* Research Studies Press Ltd., 1987.

[6] Z. Xiaojun and Y. Shuzi, "Plant condition recognition - a time series model approach," *Computers in Industry*, vol. 11, no. 4, pp. 333–340, 1989.

[7] U.S. - Department of Defense, "Military handbook 217E - reliability prediction of electronic equipment," October 1986.

[8] S. L. Murphy and S. I. Sayegh, "Application of neuronal networks to acoustic screening of small electric motors," in *IEEE/INNS Int. Joint Conf. On Neural Net., Baltimore*, vol. 2, pp. II–472 - II–477, 1992.

[9] R. X. M. P. Turner, Manager of Asset Recovery Operations, "Failures and extensive wear in re-claimed DC motors type 127K01800." Personal Communication, September 1995.

[10] D. L. Story and S. Lloyd, "Environmental & waste management." I.Q.A. Course Book, Department of Mechanical & Manufacturing Engineering, University of Glamorgan, Pontypridd, CF37 1DL, February 1996.

[11] K. Niwa, "Automatic small motor noise measuring equipment," *IEEE Trans. on Industry Applications*, vol. IA-21, pp. 899–905, July/August 1985.

[12] D. Schump, "Reliability testing of electric motors," *IEEE Trans. on Industry Applications*, vol. 25, pp. 386–390, May/June 1989.

[13] P. O'Donnell, "Report of large motor reliability survey of industrial and commercial installations, part I," *IEEE Trans. on Industry Applications*, vol. IA-21, pp. 853–864, July/August 1985.

[14] R. H. Wood and G. A. McGoldrick, "Report of large motor reliability survey of industrial and commercial installations, part II," *IEEE Trans. on Industry Applications*, vol. IA-21, pp. 865–875, July/August 1985.

[15] P. O'Donnell, "Report of large motor reliability survey of industrial and commercial installations: Part III," *IEEE Trans. on Industry Applications*, vol. IA-23, pp. 153–158, January/February 1987.

[16] P. F. Albrecht, J. C. Appiarius, and D. K. Sharma, "Assessment of the reliability of motors in utility applications - updated," *IEEE Trans. on Energy Conversion*, vol. EC-1, pp. 39–46, March 1986.

[17] O. V. Thorsen and M. Dalva, "A survey of faults on induction motors in offshore oil industry, petrochemical industry, gas terminals, and oil refineries," *IEEE Trans. on Industry Applications*, vol. 31, pp. 1186–1196, September/October 1995.

[18] C. Cempel, *Vibroacoustic Condition Monitoring.* Ellis Horwood, 1991.

[19] B. Boashash, *Time-Frequency Signal Analysis*, ch. 18, pp. 406–444. Longman Cheshire Pty Limited, 1992.

[20] M.-Y. Chow, R. N. Sharpe, and J. C. Hung, "On the application and design of artificial neural networks for motor fault detection - part I," *IEEE Trans. Ind. Electron.*, vol. 40, pp. 181–188, April 1993.

[21] J. D. Smith, *Gears and their Vibration.* Marcel Dekker, Inc., 1983.

[22] S. Braun, *Mechanical Signature Analysis - Theory and Applications.* Academic Press, 1986.

[23] G. W. Blankenship and R. Singh, "New rating indices for gear noise based upon vibro-acoustic measurements," *Noise Control Engineering Journal*, vol. 38, pp. 81–92, March-April 1992.

[24] G. J. Trmal and D. E. Johnson, "Reliability of gear fault detection using acoustic noise signature," in *COMADEM'93 Int. VWE Bristol*, pp. 73–78, 1993.

[25] A. Gaylard, A. Meyer, and C. Landy, "Acoustic evaluation of faults in electrical machines," in *7th Int. Conf. On Electrical Machines and Drives*, pp. 147–150, IEE, 11-13 September 1995.

[26] S. L. Ho and K. M. Lau, "Detection of faults in induction motors using artificial neural networks," in *7th Int. Conf. On Electrical Machines and Drives*, pp. 176–181, IEE, 11-13 September 1995.

[27] J. R. Wicking, "Machinery vibration monitoring systems," in *1st Int. Machinery & Diagnostic Conf. & Exhib., Las Vegas*, 11-14 September 1989.

[28] G. Dalpiaz and A. Maggiore, "Monitoring automatic machines," *Mechanical Systems and Signal Processing*, vol. 6, no. 6, pp. 517–534, 1992.

[29] R. A. Collacott, *Mechanical Fault Diagnosis*. Chapman and Hall, 1977.

[30] D. A. Emm, "Motor vibration analysis survey," tech. rep., Rank Xerox Mitcheldean Plant, Asset Recovery Dept., March 1995.

[31] D. E. Knights, "A survey of the causes of vibration and stray-field variation in electric motor drives," tech. rep., ERA Technology Ltd, January 1982.

[32] G. Dalpiaz and A. Rivola, "Condition monitoring and diagnostics in automatic machines: Comparison of vibration analysis techniques," *Mechanical Systems and Signal Processing*, vol. 11, no. 1, pp. 53–73, 1997.

[33] R. R. Schoen, B. K. Lin, T. G. Habetler, H. Schlag, and S. Farag, "An usupervised, on-line system for induction motor fault detection using stator current monitoring," *IEEE Trans. on Industry Applications*, vol. 31, pp. 1280–1286, November/December 1995.

[34] J. E. Timperley, "Incipient fault identification through neutral RF monitoring of large rotating machines," *IEEE Trans. Power App. Syst.*, vol. PAS-102, March 1983.

[35] G. B. Kliman and J. Stein, "Methods of motor current signature analysis," *Electric Machines and Power Systems*, vol. 20, pp. 463–474, 1992.

[36] R. R. Schoen, T. G. Habetler, F. Kamran, and R. G. Bartheld, "Motor bearing damage detection using stator current monitoring," *IEEE Trans. on Industry Applications*, vol. 31, pp. 1274–1279, November/December 1995.

[37] R. Burnett and J. F. Watson, "The current analysis program - a software tool for rotor fault detection in three phase induction motors," in *7th Int. Conf. On Electrical Machines and Drives*, pp. 156–160, IEE, 11-13 September 1995.

[38] W. W. Choi, H. C. Kim, and B. G. Min, "A new automatic cardiac output control algorithm for moving actuator total artificial heart by motor current waveform analysis," *The Int. Journal of Artificial Organs*, vol. 19, no. 3, pp. 189–196, 1996.

[39] P. A. Lynn, *An Introduction to the Analysis and Processing of Signals.* Macmillan, 3rd ed., 1989.

[40] H. Stöcker, *Taschenbuch Mathematischer Formeln und Moderner Verfahren.* Verlag Harri Deutsch, 2nd ed., 1993. [German].

[41] M. N. M. Badi, S. N. Engin, and D. Schonfeld, "Fault classification of a motor drive-line using time domain data," in *Condition Monitoring and Diagnostic Engineering Management* (R. B. K. N. Rao, R. A. Smith, and J. L. Wearing, eds.), pp. 43–50, Proc. of COMADEM '96, Sheffield Academic Press, 1996.

[42] Y. Chen, "Impending failure detection for a discrete process," *Mechanical Systems and Signal Processing*, vol. 7, no. 2, pp. 121–132, 1993.

[43] C. Menéndez, J. B. Ordieres, and F. Ortega, "Importance of infomation preprocessing in the improvement of neural network results," *Expert Systems*, vol. 13, pp. 95–102, May 1996.

[44] J. Netter, W. Wasserman, and G. A. Whitmore, *Applied Statistics*. Allyn and Bacon, 3rd ed., 1988.

[45] J. Cattarius and D. J. Inman, "Time domain analysis for damage detection in smart structures," *Mechanical Systems and Signal Processing*, vol. 11, no. 3, pp. 409–423, 1997.

[46] J. A. Siegler, A. A. Sarkady, and C. Nemarich, "Motor current signal analysis for diagnosis of fault conditions in shipboard equipment," *Naval Engineers Journal*, vol. 107, pp. 77–98, January 1995.

[47] R. B. Randall, "A new method of modelling gear faults," *ASME Journal of Mechanical Design*, vol. 104, pp. 259–262, April 1982.

[48] P. D. McFadden, "Detecting fatigue cracks in gears by amplitude and phase demodulation of the meshing vibration," *Transactions of the ASME Journal of Vibration, Acoustics, Stress, and Reliability in Design*, vol. 108, pp. 165–170, April 1986.

[49] N. A. J. Gough and M. A. Wahab, "SFNET: An artificial neural network for signal recognition," tech. rep., April 1997. UK patent no. GB 2306010A.

[50] J. D. Kueck, J. C. Griscoe, and N. M. Burstein, "Assessment of valve actuator motor rotor degradation," *IEEE Transactions on Energy Conversion*, vol. 7, pp. 460–469, September 1992.

[51] E. O. Brigham, *The Fast Fourier Transform and its Applications.* Prentice-Hall International, 1988.

[52] R. C. Kryter and H. D. Haynes, "How to monitor motor driven machinery by analyzing motor current," *Power Engineering*, vol. 93, pp. 35–39, October 1989.

[53] T. Bortherton, T. Pollard, and D. Jones, "Applications of time-frequency and time-scale representations to fault detection and classification," in *Proc. IEEE Sig. Proc. Symp. On Time Freq. and Time Scale Analysis*, pp. 95–98, October 1992.

[54] G. B. Kliman and R. A. Kögle, "Noninvasive detection of broken rotor bars in operating induction motors," *IEEE-PES Trans. on Energy Conversion*, vol. 3, pp. 873–879, December 1988.

[55] I. A. Altawil and M. G. Rodd, "Non-invasive condition monitoring and diagnosis of power electronic drives using intelligent neural network techniques," in *UPEC '95 30th Universities Power Eng. Conf.*, pp. 5–8, 1995.

[56] I. E. Alguíndigue and R. E. Uhrig, "Vibration monitoring with artificial neural networks," in *Proc. SMORN VI Symp. Nucl. Reactor Surveillance and Diagnostics*, pp. 59.01–59.12, 1991.

[57] "Early warning fault detection in rolling element bearings using MICROLOG enveloping," Tech. Rep. CM3021-US (9-92), SKF Condition Monitoring Inc., September 1992.

[58] M. Chiollaz and B. Favre, "Engine noise characterisation with Wigner-Ville time-frequency analysis," *Mechanical Systems and Signal Processing*, vol. 7, no. 5, pp. 375–400, 1993.

[59] A. V. Oppenheim and R. W. Schafer, *Discrete-Time Signal Processing.* Prentice-Hall, international ed., 1989.

[60] T. Kalayci and Ö. Özdamar, "Wavelet preprocessing for automated neural network detection of EEG spikes," *IEEE Engineering in Medicine and Biology*, pp. 160–166, March/April 1995.

[61] P. Bonato and M. Knaflitz, "Bilinear time-frequency transformations in the analysis of damaged structures," *Mechanical Systems and Signal Processing*, vol. 11, pp. 509–527, July 1997.

[62] T. A. C. M. Claasen and W. F. G. Mecklenbräuker, "The Wigner distribution - a tool for time-frequency signal analysis; part II: Discrete-time signals," *Philips Journal of Research*, vol. 35, no. 4/5, pp. 276–300, 1980.

[63] T. A. C. M. Claasen and W. F. G. Mecklenbräuker, "The Wigner distribution - a tool for time-frequency signal analysis; part I: Continuous-time signals," *Philips Journal of Research*, vol. 35, no. 3, pp. 217–250, 1980.

[64] T. A. C. M. Claasen and W. F. G. Mecklenbräuker, "The Wigner distribution - a tool for time-frequency signal analysis; part III: Relations with other time-frequency signal transformations," *Philips Journal of Research*, vol. 35, no. 6, pp. 372–389, 1980.

[65] Q. Meng and L. Qu, "Rotating machinery fault diagnosis using Wigner distribution," *Mechanical Systems and Signal Processing*, vol. 5, pp. 155–166, 1991.

[66] B. D. Forrester, "Use of Wiger-Ville distribution in helicopter fault detection," in *Proc. ASSPA Conf. On Signal Processing, Theories, Implementation and Applications*, pp. 78–82, 1989.

[67] P. D. McFadden, "Examination of a technique for early detection of failure in gears by signal processing of the time domain average of the meshing vibration.," tech. rep., ARL Aero Propulsion Technical Memorandum 434, 1986.

[68] W. J. Wang and P. D. McFadden, "Early detection of gear failure by vibration analysis - I. Calculation of the time-frequency distribution," *Mechanical Systems and Signal Processing*, vol. 7, no. 3, pp. 193–203, 1993.

[69] O. Rioul and M. Vetterli, "Wavelets & signal processing," *IEEE Signal Processing Magazine*, pp. 14–38, October 1991.

[70] M. Zeller, "Flinkes wellenspiel," *c't*, pp. 258–264, November 1994. in German.

[71] W. J. Staszewski and G. R. Tomlinson, "Application of the wavelet transform to fault detection in a spur gear," *Mechanical Systems and Signal Processing*, vol. 8, no. 3, pp. 289–307, 1994.

[72] S. T. Lin and P. D. McFadden, "Gear vibration analysis by b-spline wavelet-based linear wavelet transform," *Mechanical Systems and Signal Processing*, vol. 11, pp. 603–609, July 1997.

[73] M. A. Tomlinson and K. Shin, "Quality control using acoustic testing," *QW TS*, pp. 38–42, March 1994.

[74] J. P. Woodcock, "Special ultrasonic methods for the assessment and imaging of systemic arterial disease," *British Journal of Anaesth.*, pp. 719–730, 1981.

[75] G. Nakhaeizadeh and C. C. Taylor, *Machine Learning and Statistics - The Interface*. John Wiley & Sons, 1997.

[76] R. J. Erb, "Introduction to backpropagation neural network computation," *Pharmaceutical Research*, vol. 10, no. 2, pp. 165–170, 1993.

[77] L. D. Vena, M. Mastretta, and L. Ricciardiello, "Neural network architectures for industrial applications," *Biosensors & Bioelectronics*, vol. 10, no. 1-2, pp. 231–236, 1995.

[78] M. Kasslin, J. Kangas, and O. Simula, "Process state monitoring using self-organizing maps," in *Proc. I CANN 92: Artificial Neural Networks*, vol. 2, pp. 1531–1534, Elsevier Science Publishers, 1992.

[79] J. J. Forsström and K. J. Dalton, "Artificial neural networks for decision support in clinical medicine," *Annals of Medicine*, vol. 27, no. 5, pp. 509–517, 1995.

[80] E. McDermott and S. Katagiri, "LVQ-based shift-tolerant phoneme recognition," *IEEE Trans. Signal Processing*, vol. 39, pp. 1398–1411, June 1991.

[81] D. S. Kim, Y. S. Shin, and D. K. Carlson, "Machinery diagnostic for rotating machinery using backpropagatin neural networks," in *Proc. Of the 3rd Int. Machinery Monitoring and Diagnostics Conf., Las Vegas*, pp. 309–320, 1991.

[82] S. Zhang, R. Ganesan, and G. D. Xistris, "Self-organising neural networks for automated machinery monitoring systems," *Mechanical Systems and Signal Processing*, vol. 10, no. 5, pp. 517–532, 1996.

[83] T. Brotherton, T. Pollard, and D. Jones, "Applications of time-frequency and time-scale representations to fault detection and classification," in *Proc. IEEE*

Signal Processing Symposium on Time Frequency and Time Scale Analysis, pp. 95–98, October 1992.

[84] D. Rock, D. Malkoff, and R. Steward, "AI and aircraft," *AI Expert*, pp. 28–35, February 1993.

[85] I. A. Altawil, A. M. Koroma, B. J. Roylance, and M. G. Rodd, "Classification of scuffing and scoring wear modes in spur gear using neural network technique," in *Condition Monitoring and Diagnostic Engineering Management* (R. B. K. N. Rao, R. A. Smith, and J. L. Wearing, eds.), pp. 11–20, Proc. of COMADEM '96, Sheffiel Academic Press, 1996.

[86] B. A. Paya, I. I. Esat, and M. N. M. Badi, "Artificial neural network based fault diagnostics of rotating machinery using wavelet transforms as a preprocessor," *Mechanical Systems and Signal Processing*, vol. 11, no. 5, pp. 751–765, 1997.

[87] W. S. McCulloch and W. Pitts, "A logical calculus of the ideas imminent in nervous activity," *Bulletin of Mathematical Biophysics*, vol. 5, pp. 115–133, 1943.

[88] L. Fausett, *Fundamentals of Neural Networks - Architectures, Algorithms, and Applications.* Prentice Hall, 1994.

[89] C. M. Bishop, "Neural networks and their applications," *Review of Scientific Instruments*, vol. 65, pp. 1803–1832, June 1994.

[90] R. L. Harvey, *Neural Network Principles.* Prentice Hall, 1994.

[91] A. Zell, *Simulation Neuronaler Netze.* Addison-Wesley, 1st ed., 1994.

[92] NeuralWare Inc., *Neural Computing - A Technology Handbook for Professional II/PLUS and NeuralWorks Explorer*, 1993.

[93] T. Kohonen, "Things you haven't heard about the self-organizing map," in *IEEE Conf. On Neural Networks ICNN-93*, pp. 1147–1156, 1993.

[94] R. Beale and T. Jackson, *Neural Computing: An Introduction.* IOP Publishing Ltd., 1990.

[95] G. R. Slemon, *Electric Machines and Drives.* Addison-Wesley Publishing Company, 1992.

[96] J. Meisel, *Principles of Electromechanical Energy Conversion.* McGraw-Hill, 1966.

[97] M. E. C. Limited, *Carbon Brushes and Electrical Machines.* Morganite Electrical Carbon Limited, 1978. Reprinted 1988.

[98] R. Robinson and K. Browse, *D.C. Gear Motor.* Xerox, December 1989. DWG. No. 127E00653, Ref. Codes SS.50 /51 /58.

[99] G. Hofmann, *Getriebemotor 127 K 01800.* Gebrüder Bühler Nachfolger GmbH, Nürnberg, July 1995. Ref: EAL/HOF/Ste.

[100] C. L. Mantell, *Carbon and Graphite Handbook*, pp. 23–28. John Wiley and Sons, Inc., 1968.

[101] W. Bolton, *Engineering Materials Technology.* Newnes, 2nd ed., 1994.

[102] R. Miller and M. R. Miller, *Small Electric Motors - Use, Selection, Operation, Repair and Maintenance.* Macmillan, 1992.

[103] D. F. Wilcock and E. R. Booser, *Bearing Design and Application.* McGraw-Hill Book Company, 1st ed., 1957.

[104] T. Gurunatha, "Accelerated component reliability testing and solving problems." June 1995.

[105] J. E. Arsenault and J. A. Roberts, *Reliability & Maintainability of Electronic Systems.* Pitman Publishing, 1980.

[106] P. D. T. O'Connor, *Practical Reliability Engineering.* John Wiley & Sons, 2nd ed., 1986.

[107] D. J. Smith, *Reliability and Maintainability in Perspective.* MacMillian Eductation, 3rd ed., 1988.

[108] E. C. Ifeachor and B. W. Jervis, *Digital Signal Processing - A Practical Approach.* Addison-Wesley Publishing Company Inc., 1993.

[109] G. Held and T. R. Marshall, *Data Compression - Techniques and Applications Hardware and Software Considerations*, pp. 238–248. John Wiley & Sons LTD, 3rd ed., 1991.

[110] National Instruments Corp., *LabView User Manual*, january 1996 ed., January 1996. Part Number 320999A-01.

[111] A. Shrotriya and S. Orth, "An introduction to using Windows dynamic link libraries (DLLs) from LabVIEW," Tech. Rep. Application Note 057, National Instruments Corporation, June 1995.

[112] D. Jernigan, R. Lee, and A. Barton, "Creating dynamic link libraries (DLLs) in Visual C++ or Borland C++ 4.5 for LabWindows/CVI," Tech. Rep. Application Note 071, National Instruments Corporation, June 1995.

[113] A. Shrotriya and S. Orth, "Writing Windows 3.x 16-bit dynamic link libraries (DLLs) and calling them from LabVIEW," Tech. Rep. Application Note 072, National Instruments Corporation, June 1996.

[114] J. D. Turner and A. J. Pretlove, *Acoustics for Engineers.* MacMillian, 1991.

[115] B. J. Smith, R. J. Peters, and S. Owen, *Acoustic and Noise Control.* Longman Group Ltd., 1982.

[116] J. Neter, W. Wasserman, and G. A. Whitmore, *Applied Statistics.* Allyn and Bacon, Inc., 3rd ed., 1988.

[117] M. J. Katz, "Fractals and the analysis of waveforms," *Comput. Biol. Med.*, vol. 18, no. 3, pp. 145–156, 1988.

[118] B. B. Mandelbrot, *The Fractal Geometry of Nature.* W.H.Freeman and Company, 1977.

[119] B. H. Kaye, *A Random Walk Through Fractal Dimensions.* VCH Publishers, 1994.

[120] N. A. J. Gough, "Fractal analysis of fetal heart rate variability," *Physiol. Meas.*, vol. 14, pp. 309–315, 1993.

[121] F. J. Harris, "On the use of windows for harmonic analysis with the discrete fourier transform," *Proc. IEEE*, vol. 66, pp. 51–83, January 1978.

[122] R. Zotl and H.-J. Drewitz, "Mathematische grundlagen der zuverlässigkeitstheorie und sicherheitstechnik (in german)." Colloquium Script of the Fachhochschule BS/WF, 1993.

[123] D. M. Green and J. A. Swets, *Signal Detection Theory and Psychophysics.* John Wiley and Sons, Inc., 1966.

[124] J. A. Hanley, "Receiver operating characteristic (ROC) methodology: The state of the art," *Critical Reviews in Diagnostic Imaging*, vol. 29, no. 3, pp. 307–335, 1989.

[125] M. Bland, *An Introduction to Medical Statistics.* Oxford University Press, 2nd ed., 1996.

[126] K. Woods and K. W. Bowyer, "Generating ROC curves for artificial neural networks," *IEEE Trans. on Medical Imaging*, vol. 16, pp. 329–337, June 1997.

[127] R. X. M. P. Turner, Manager of Asset Recovery Operations, "Bearing wear in re-claimed DC motors type 127K01800." Personal Communication, Mai 1997.

[128] T. J. E. Miller, *Brushless Permanent-Magnet and Reluctance Motor Drives.* Oxford University Press, 1989.

[129] C. A. Kenny, *PC226 High Performance Data Acquisition Board.* Amplicon Liveline Ltd., Centenary Industrial Estate, Hollingdean Road, Brighton, UK BN2 4AW. PC226 Instruction Manual Part No 859243 54 Issue C.

[130] H. L. Krauss, C. W. Bostian, and F. H. Raab, *Solid State Radio Engineering*, ch. 3, pp. 9–36. John Wiley & Sons, 1980.

[131] "4th- and 8th-order continuous -time active filters," Tech. Rep. 19-4191, Maxim Integrated Products, October 1996.

[132] "TL074A, TL074B low-noise JFET-input operational amplifiers," Tech. Rep. SLOS080D, Texas Instruments, August 1996.

Appendix A

Mechanical Drawings

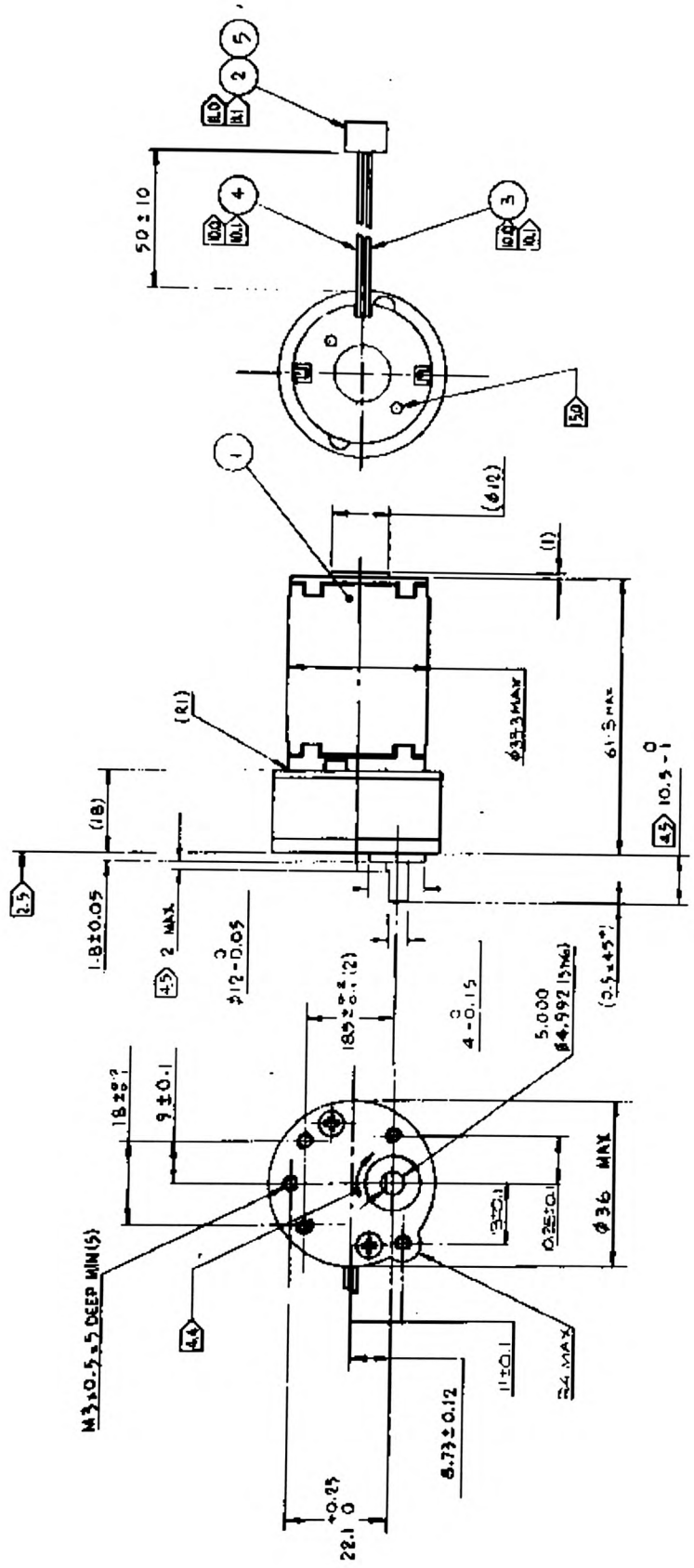

Figure A.1: Measurements of the test motor.

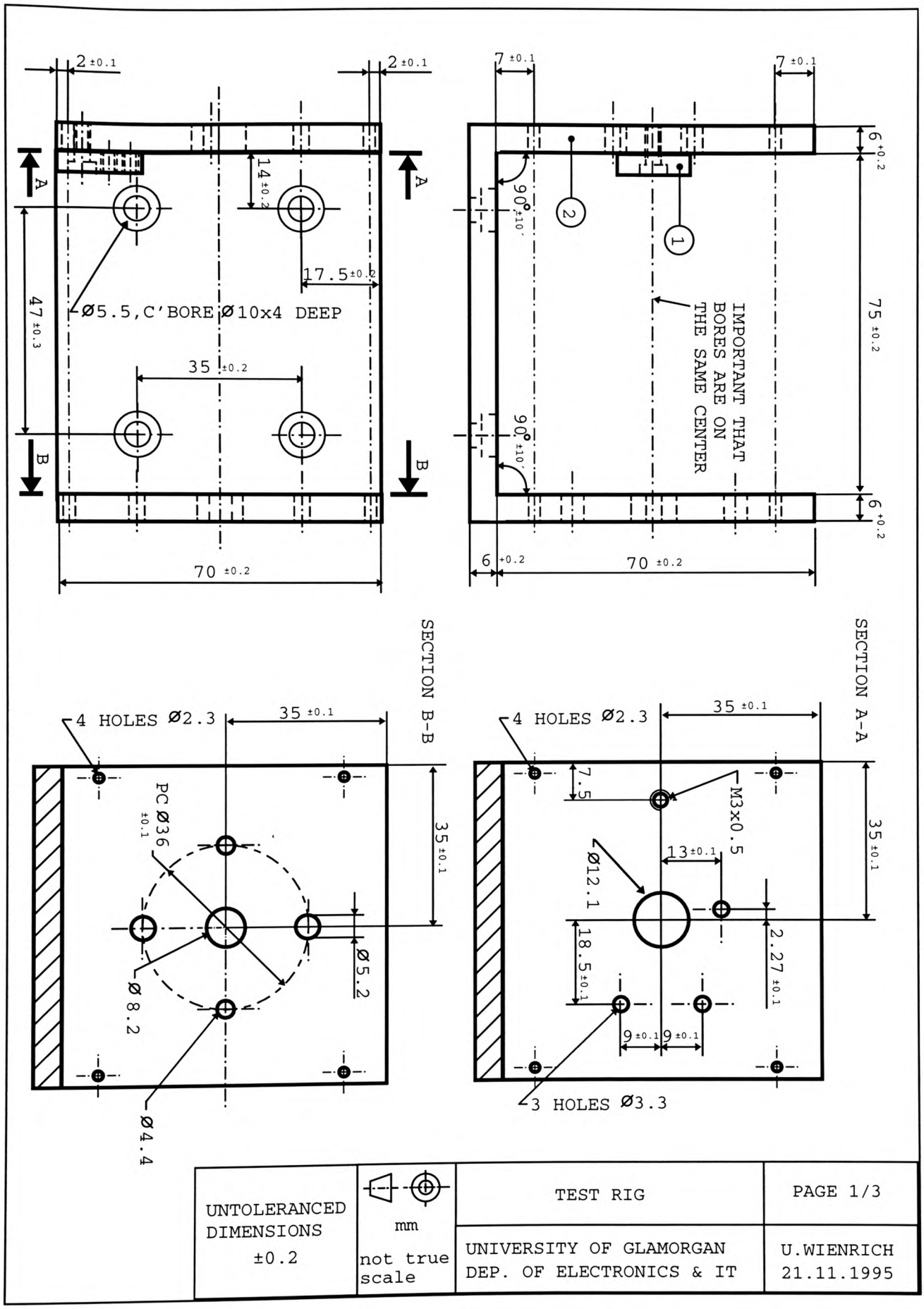

Figure A.2: Fixture for vibration measurements - part I.

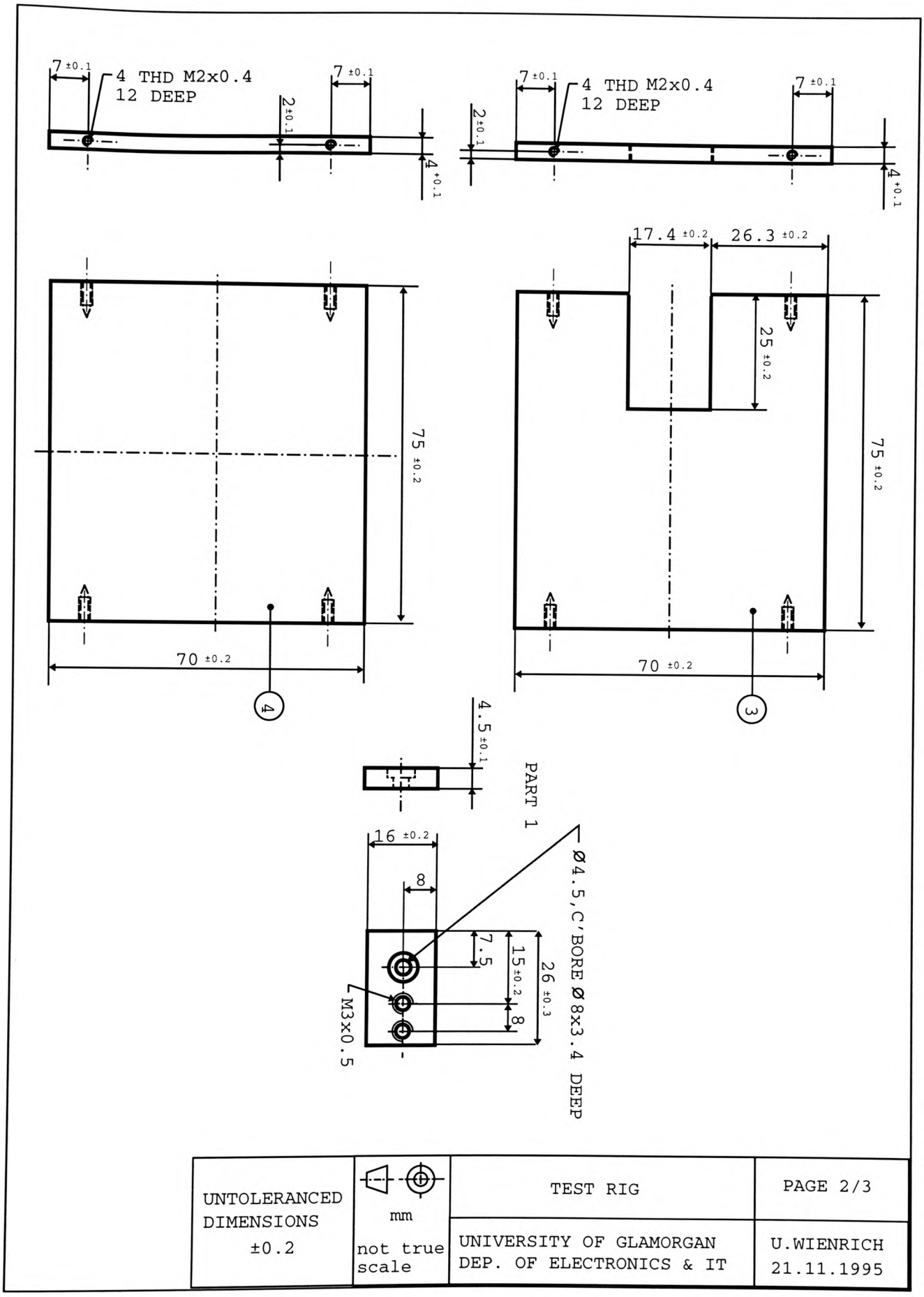

Figure A.3: Fixture for vibration measurements - part II.

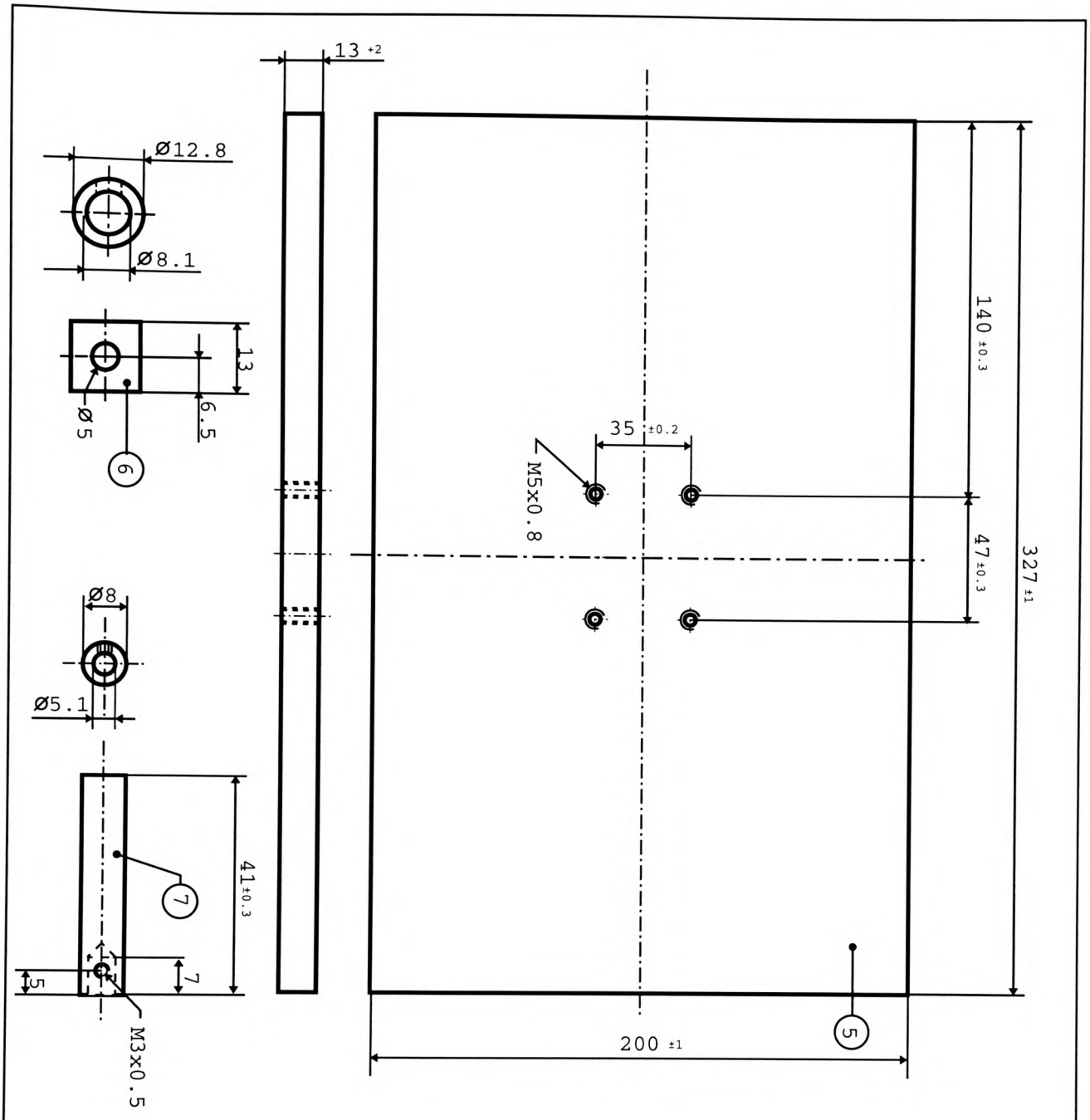

PART	DESCRIPT.	MATERIAL	AMOUNT
7	SHAFT ADAPTER	BRASS	1
6	SHAFT ADAPTER F.CAL.	BRASS	1
5	BASE PLATE	ALUMINIUM	1
4	END PLATE	ALUMINIUM	1
3	END PLATE	ALUMINIUM	1
2	U-PROFILE	ALUMINIUM	1
1	SHAFT ENCODER PLATE	ALUMINIUM	1

UNTOLERANCED DIMENSIONS ±0.2	mm not true scale	TEST RIG	PAGE 3/3
		UNIVERSITY OF GLAMORGAN DEP. OF ELECTRONICS & IT	U.WIENRICH 21.11.1995

Figure A.4: Fixture for vibration measurements - part III.

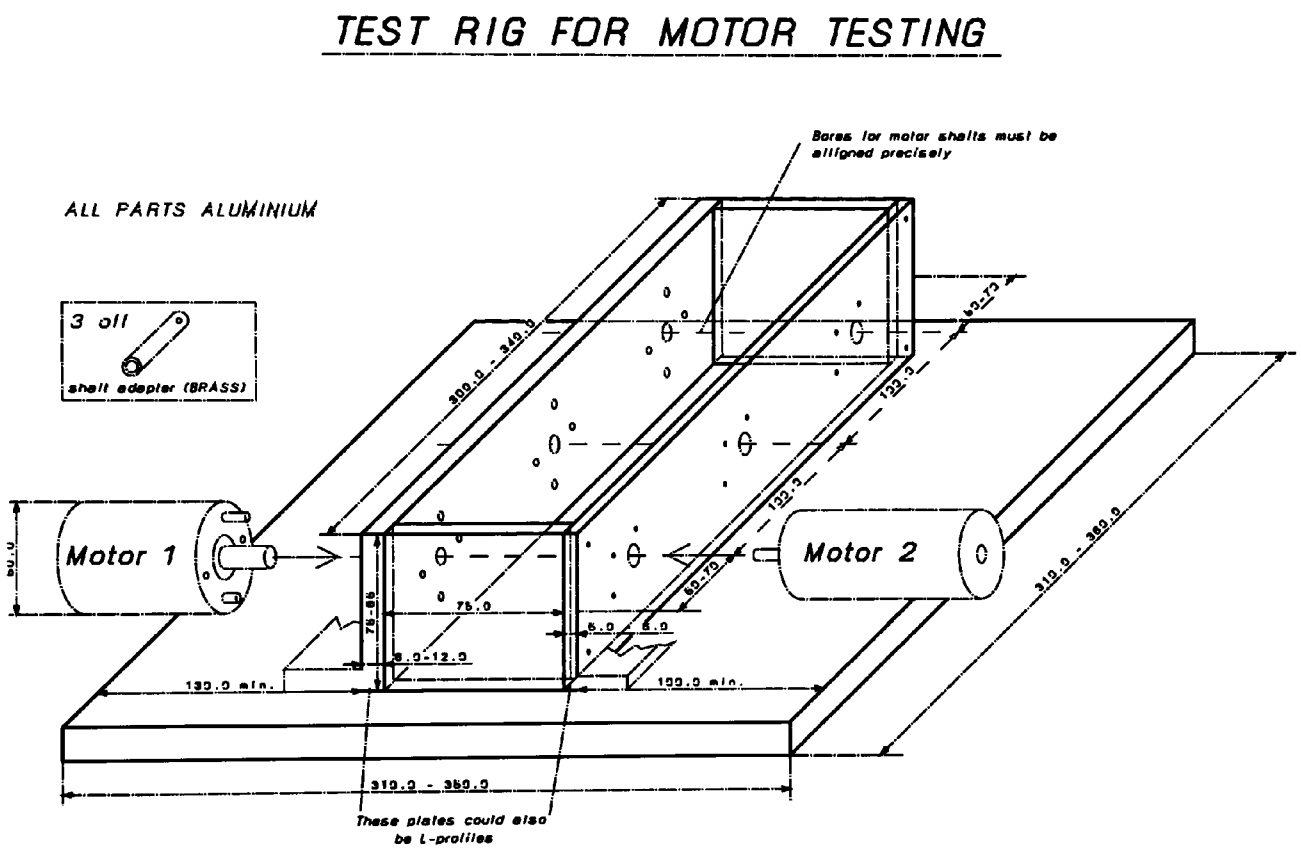

Figure A.5: Fixture for three DC motors.

Appendix B

Schematics

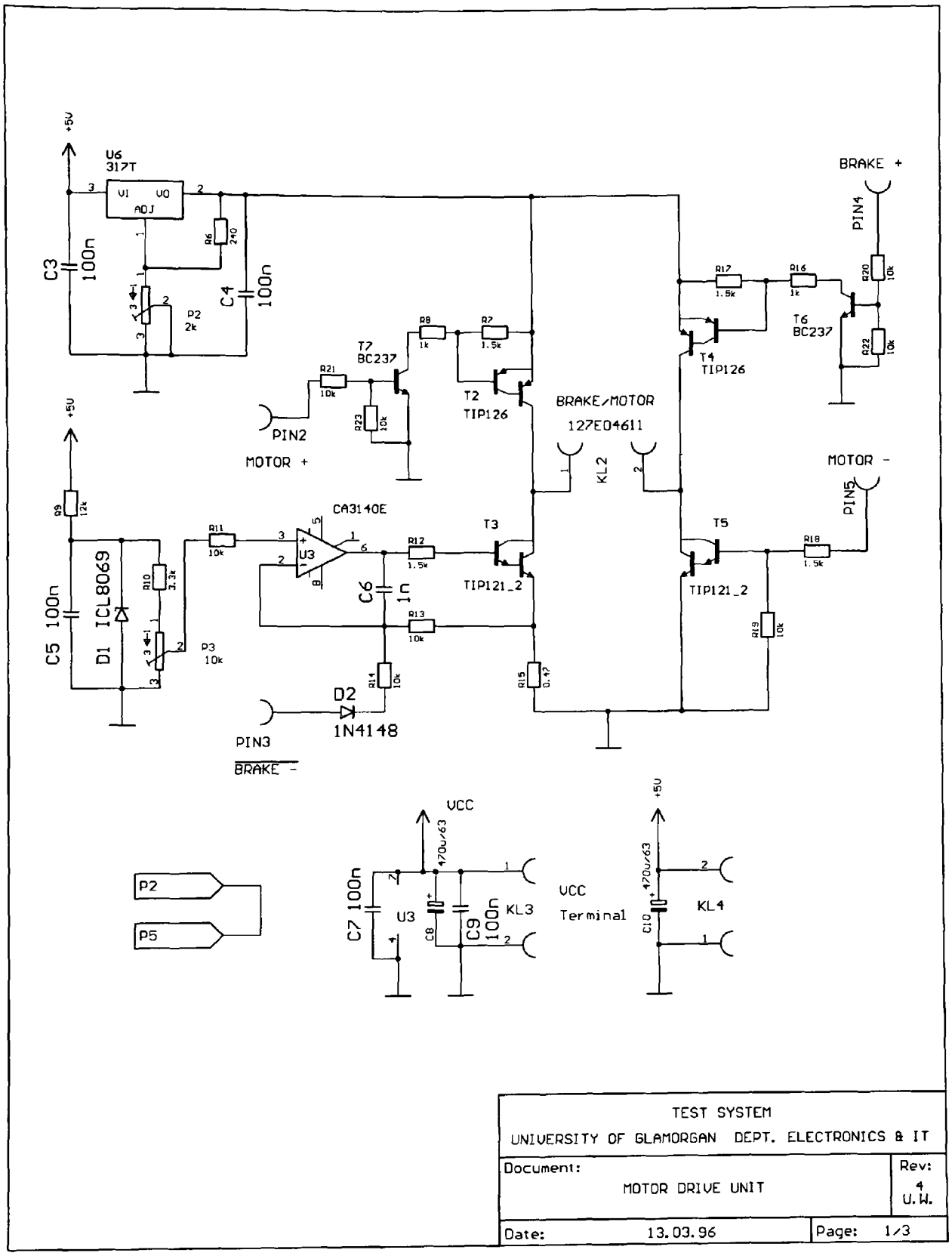

Figure B.1: Accelerated life test system computer/motor interface - part I.

B. 1 Description of the accelerated life test motor circuit function blocks in figure B.1

Stabilised voltage supply

The stabilised voltage supply for the brake motor circuit is designed using the variable voltage regulator U_6 including C_3, C_4, C_{10}, P_2 and R_6. Potentiometer P_2 allows the adjustment of the regulated output voltage. The input voltage for the voltage regulator is connected using KL_4.

Reference voltage of the control circuit

The reference circuit has been design using D_1, C_5, R_{10} and P_3. The reference voltage can be adjusted with P_3.

Brake operation mode circuit

The brake or constant current mode circuit consists of the operational amplifier U_3 and its peripheral components R_{11}, R_{12}, R_{13}, R_{14}, C_6, T_3 and D_2. The current is monitored using shunt resistor R_{15}. The operating voltage is switched to the motor using transistor T_4, R_{16}, R_{17}, T_6, R_{20} and R_{22}. The voltage supply for U_3 is supplied using KL_3 which is buffered by C_7-C_9. Pins P_3 and P_4 are used to enable and disable the brake operation mode. The brake motor is connected using KL_2.

Motor operation mode circuit

The regulated supply voltage is switched to the motor using T_2, R_7, R_8, R_{21}, R_{23}, and T_7 for positive polarity and T_5, R_{18} and R_{19} for the connection to ground. Pins P_2 and P_5 are used to enable and disable the motor operation mode.

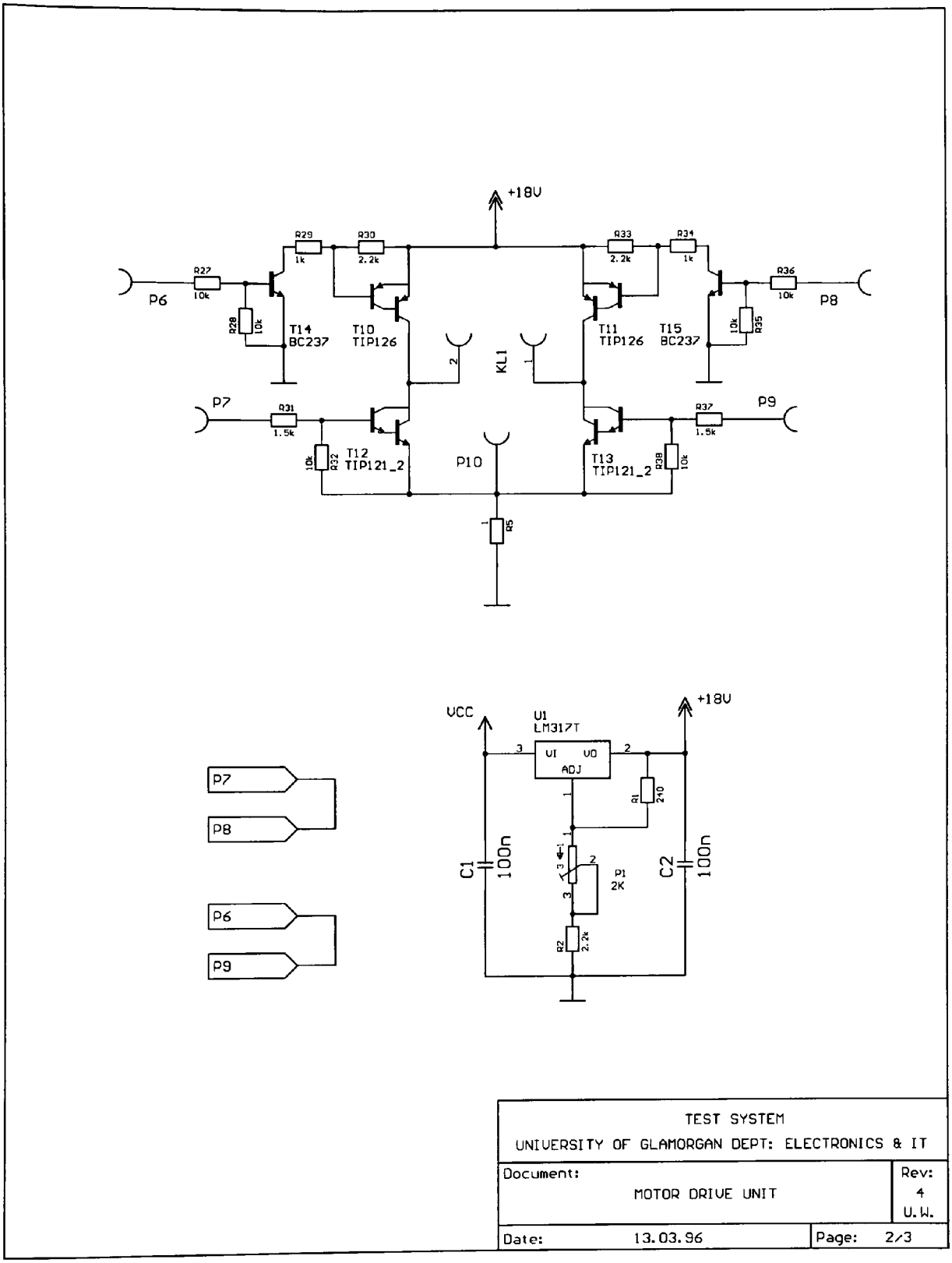

Figure B.2: Accelerated life test system computer/motor interface - part II.

B. 2 Description of the accelerated life test motor circuit function blocks in figure B.2

Stabilised voltage supply +18 V

The stabilised voltage supply for the brake motor circuit is designed using the variable voltage regulator U_1 including C_1, C_2, P_1, R_1 and R_2. Potentiometer P_1 allows the adjustment of the regulated output voltage. The input voltage for the voltage regulator is connected using KL_4.

Forward operation mode

The regulated supply voltage is switched to the motor using T_{11}, R_{33}, R_{34}, T_{15}, R_{35} and R_{36} for positive polarity and T_{12}, R_{31} and R_{32} for the connection to ground. Pins P_7 and P_8 are used to enable and disable the forward operation mode.

Reverse operation mode

The regulated supply voltage is switched to the motor using T_{10}, R_{29}, R_{30}, T_{14}, R_{27} and R_{28} for positive polarity and T_{13}, R_{37} and R_{38} for the connection to ground. The motor current is measured using shunt resistor R_5. Pins P_7 and P_8 are used to enable and disable the forward operation mode.

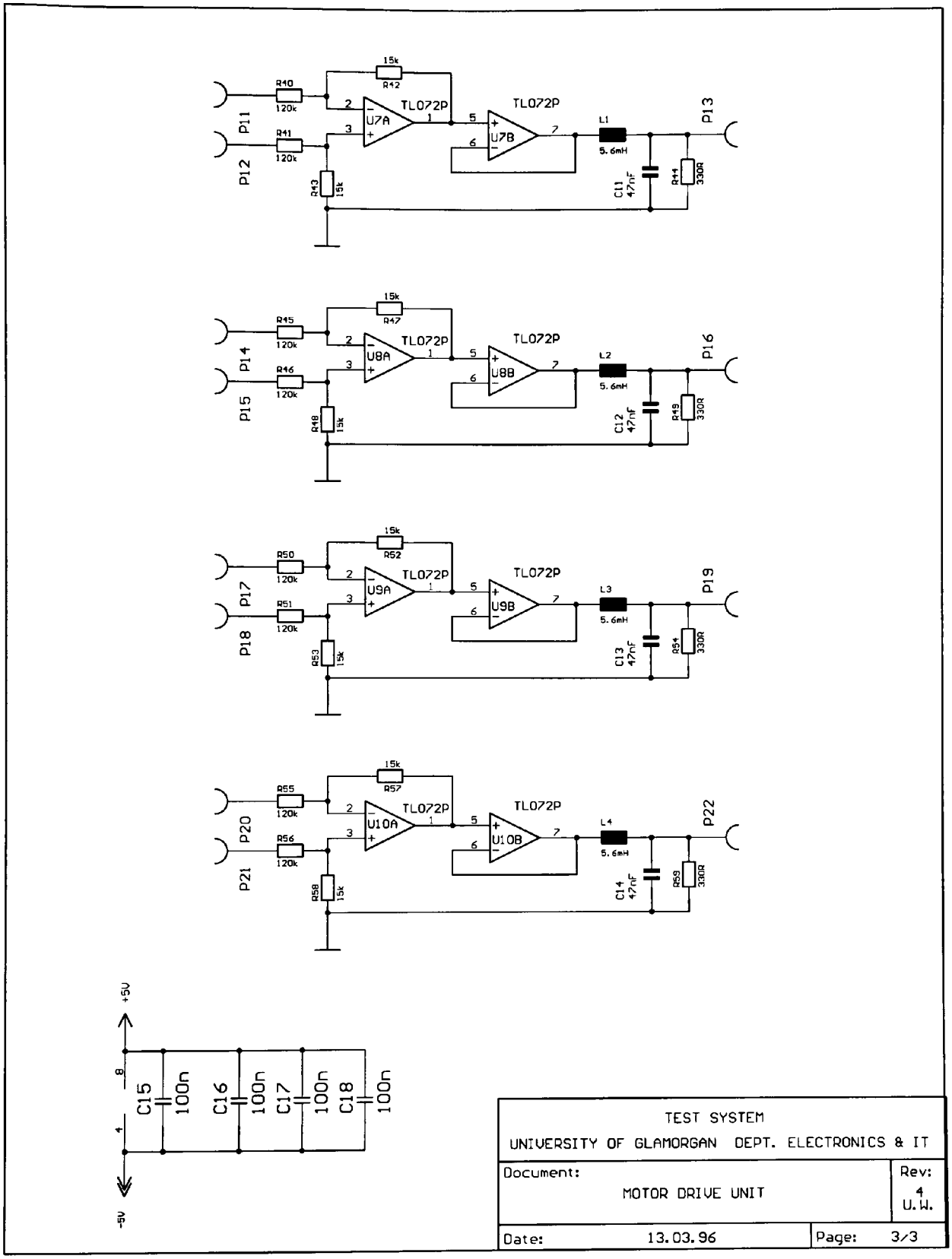

Figure B.3: Accelerated life test system computer/motor interface - part III.

B. 3 Description of the accelerated life test motor circuit function blocks in figure B.3

Motor voltage conditioning circuit

The motor voltage is amplified and filtered for each motor of the four motors using an identical circuit. The motor terminal pin voltage will be connected to pins P_{11}/P_{12} for motor 1, pins P_{14}/P_{15} for motor 2, pins P_{17}/P_{18} for motor 3 and pins P_{20}/P_{21} for motor 4. Described is the function for the motor 1 voltage. The description is explanatory of all four circuits.

The motor terminal voltage is amplified using the operational amplifier U_{7A} and its components R_{40}-R_{43} to amplify the signal by a factor of 0.125 reducing the terminal voltage to the input voltage range of the data acquisition card. The signal is then buffered using U_{7B} followed by a passive low-pass filter consisting of L_1, C_{11} and R_{44}. The voltage supply for IC U_7 is buffered using C_{15}-C_{18}.

The output voltages of the conditioning circuit are present at pins P_{13}, P_{16}, P_{19} and P_{22} for motor 1-4 respectively.

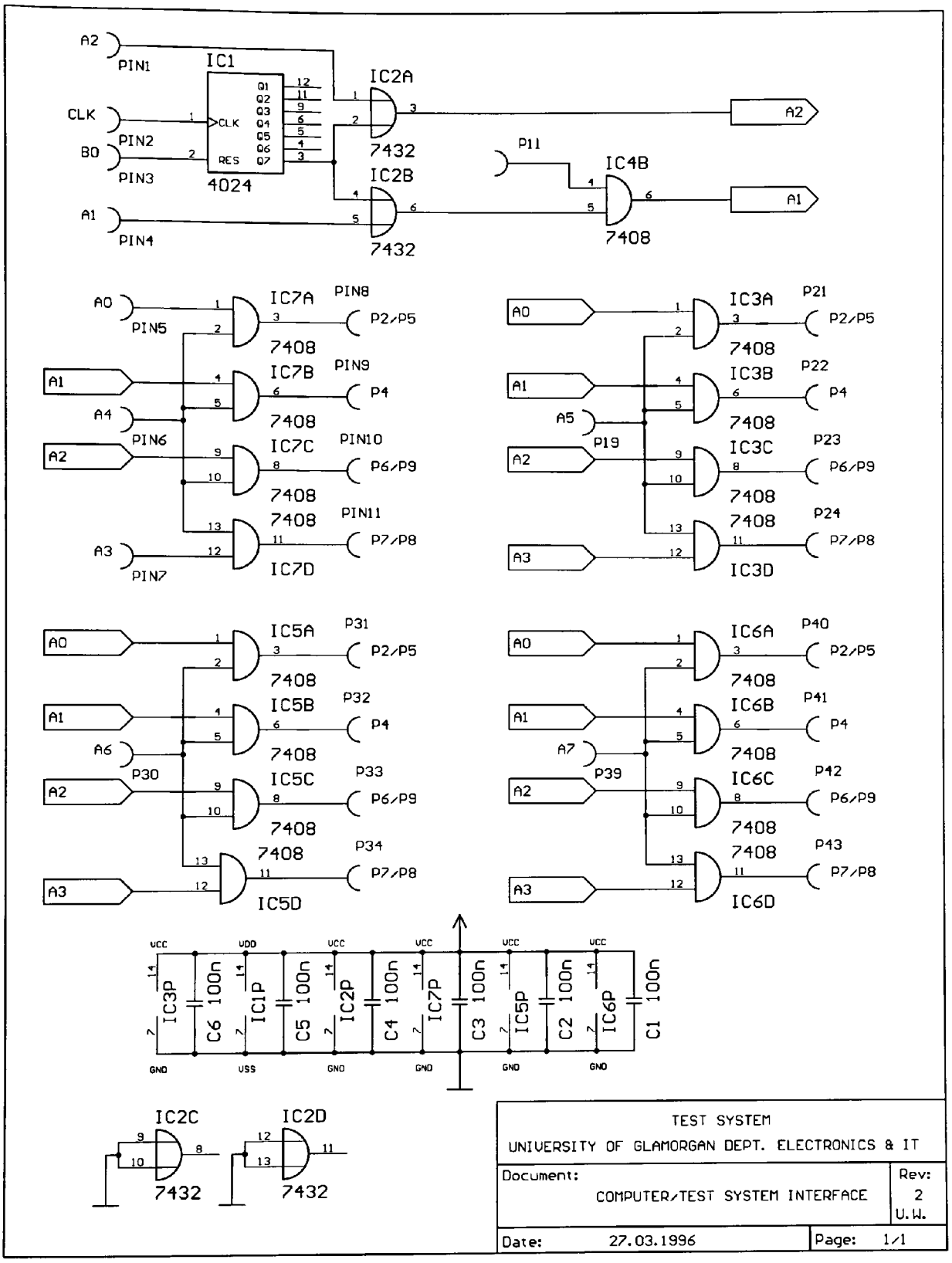

Figure B.4: Accelerated life test system computer/motor interface - part IV.

B. 4 Description of the accelerated life test motor circuit function blocks in figure B.4

Cycle frequency generation circuit

The data acquisition board cannot provide the required 1 Hz clock (0.5 s on 0.5 s off) for the accelerated life test. Therefore a clock frequency of 128 Hz, generated by the data acquisition card was divided by 128 using IC_1. The clock input signal is provided using pin CLK. The IC can be reset with a high signal on pin B_0. The cycle signal can be disabled using pins A_1, A_2 and P_{11} with IC_{2A} and IC_{4B}. The cycle signal is the connected to the four identical circuits to control the brake and test motor circuit. Pins A_0 and A_3 connected to IC_7 are used to control pins P_2/P_5 of the brake circuit and pins P_7/P_8 of the motor circuit. The pins A_4-A_7 are used to disable the brake and motor circuits off in case of a fault. The capacitors C_1-C_6 buffer the 5 V supply voltage.

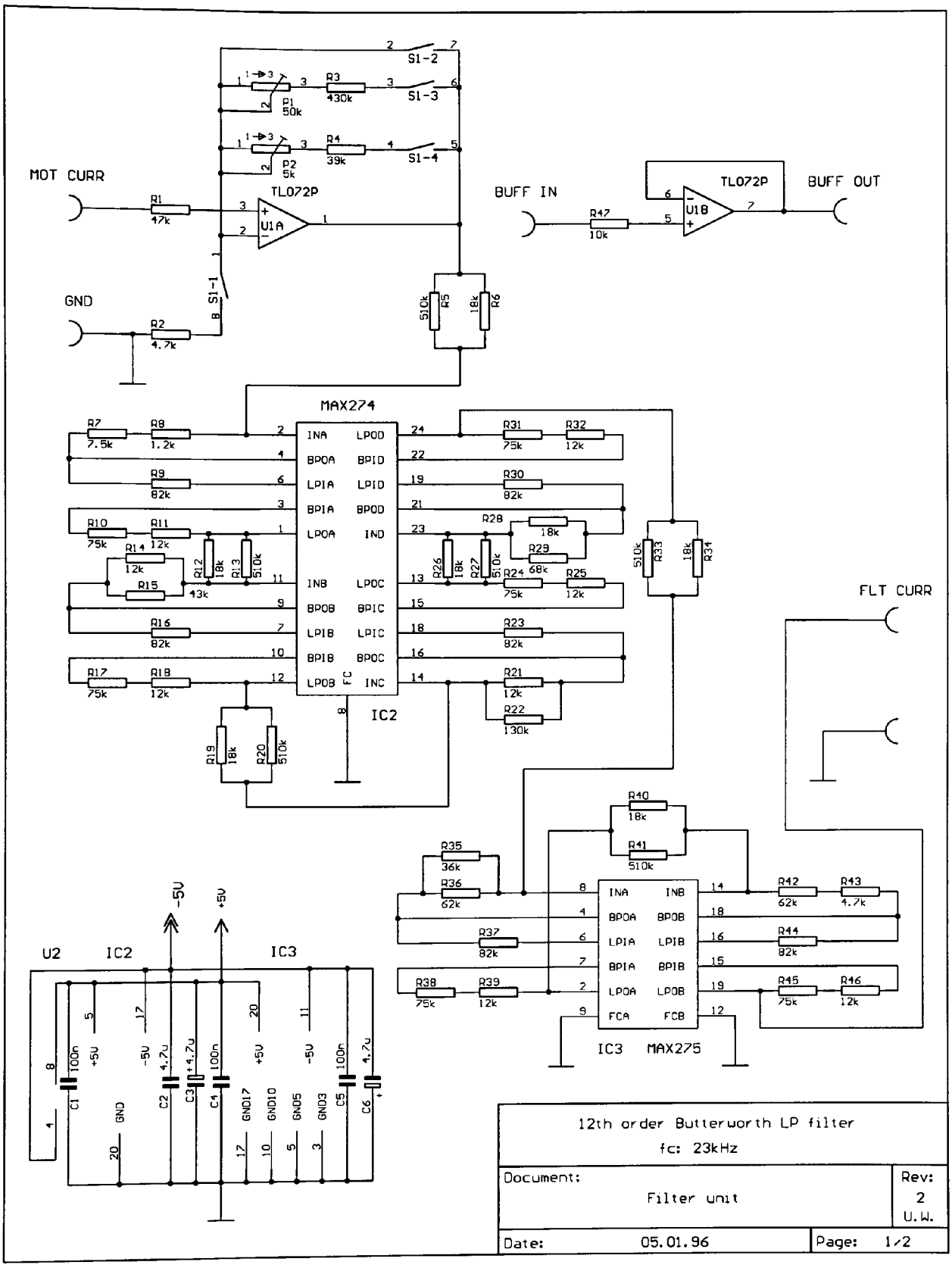

Figure B.5: Accelerated life test system LP-filter - part I.

B. 5 Description of the accelerated life test motor circuit function blocks in figure B.5

Amplification and buffer circuit

This amplification block allows the non-inverting amplification of the input signal using U_{1A} and its comonents R_1-R_4, P_1, P_2 and the DIL switch S_1. The switch allows to select a gain in steps of 1, 10 and 100 by selecting the appropriate switch positions.

IC U_{1B} and R_{47} allow the optional non-inverting buffering of the output signal by connecting this circuit to the output of the anti-aliasing filter.

Anti-aliasing low-pass filter circuit

The active anti-aliasing filter uses the continous filter ICs MAX274 (IC_2) and MAX275 (IC_3) from Maxim. The filter characteristic is determined by the resistors R_5-R_{46}. The capacitors C_1-C_6 buffer the 5 V supply voltage.

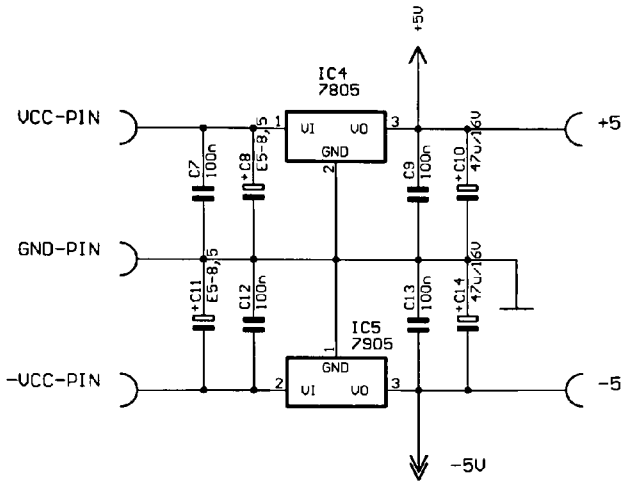

12th order Butterworth LP filter fc: 23kHz		
Document: Power unit		Rev: 2 U.W.
Date: 05.01.1996	Page: 2/2	

Figure B.6: Accelerated life test system LP-filter - part II.

B. 6 Description of the mircophone signal conditioning circuit function blocks in figure B.6

Stabilised voltage supply ±5 V

The stabilised voltage supply for the active filter circuit is designed using the voltage regulator IC_4 and IC_5 including C_7-C_{14}. The dual input voltage is connected to the pins $VCC\text{-}PIN$, $GND\text{-}PIN$ and $-VCC\text{-}PIN$. The voltage regulators provide a regulated output voltage of ±5 V on the output pins.

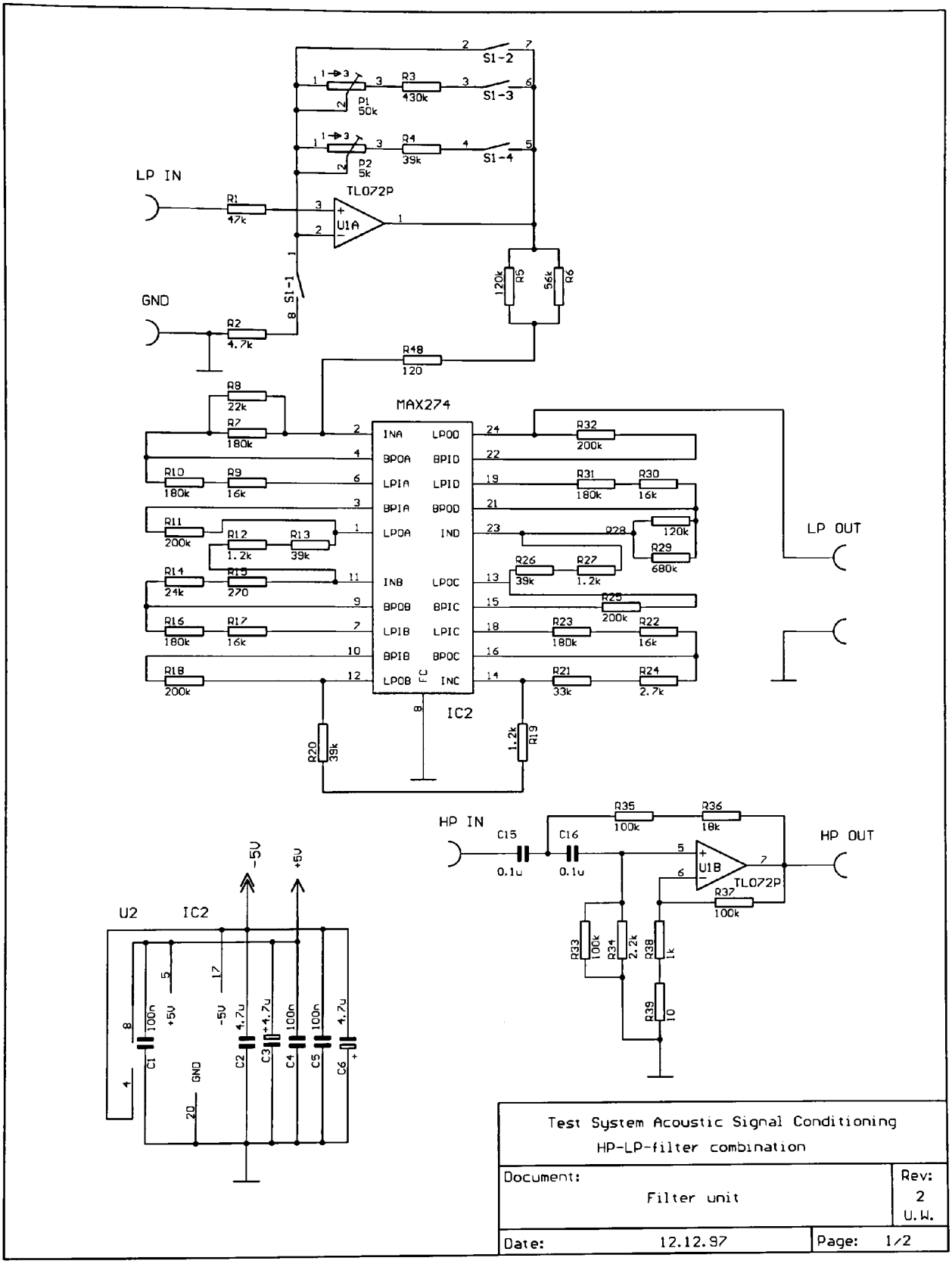

Figure B.7: Microphone signal LP-filter - part I.

B. 7 Description of the mircophone signal conditioning circuit function blocks in figure B.7

Amplification and high-pass filter circuit

This amplification block allows the non-inverting amplification of the input signal using U_{1A} and its components R_1-R_4, P_1, P_2 and the DIL switch S_1. The switch allows to select a gain in steps of 1, 10 and 100 by selecting the appropriate switch position.

IC U_{1B}, R_{33}-R_{39}, C_{15} and C_{16} are connected to an active 2nd order high pass filter. The high-pass filter output can be connected to the low-pass filter input.

Anti-aliasing low-pass filter circuit

The active anti-aliasing filter uses the continuous filter ICs MAX274 (IC_2) and MAX275 (IC_3) from Maxim. The filter characteristic is determined by the resistors R_5-R_{46}. The capacitors C_1-C_6 buffer the 5 V supply voltage.

B. 8 Description of the accelerated life test motor circuit function blocks in figure B.8

Stabilised voltage supply ±5 V

The stabilised voltage supply design is equivialent to the one shown in figure B.6.

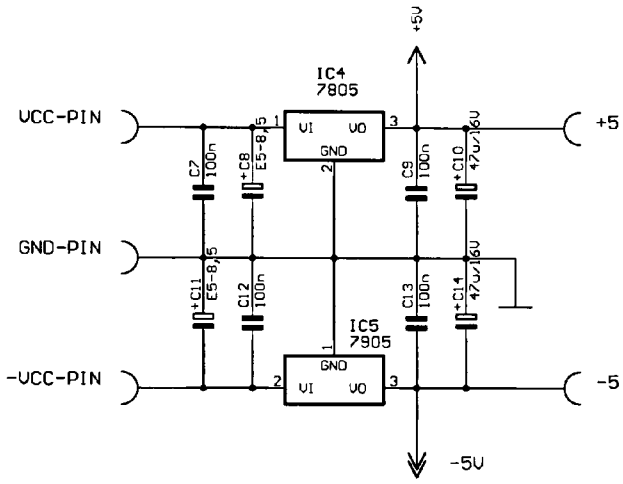

Test System Acoustic Signal Conditioning HP-LP-filter combination		
Document: Power Supply		Rev: 2 U.W.
Date: 12.12.97	Page: 1/2	

Figure B.8: Microphone signal LP-filter - part II.

Appendix C

Measurement Errors

A number of components have been used to condition the signals coming from the transducers to measure the parameters of interest. The calibrations of the overall sytem including the transducers and data aquisition card have been carried out to minimise the errors due to offsets and gain factors. The obtained calibration values have been used to correct the sampled signals to prior data analysis. Therefore, the main source of measurement errors is the noise in the signal conditioning chain that has been estimated.

The errors stated by the manufaturers of the semiconductors and the data aquisition card are as follows:

- Resolution of the data aquisition card: 12 bits
- Overall analog conversion accuracy: 4 LSB [129]

The data aquisition card has been used in an input voltage range of ± 5 V which will result in an equivalent LSB voltage of 2.44 mV. Therefore the overall signal-to-noise error is defined as

$$\left(\frac{S}{N}\right) = 20 \log \frac{V_{Range}}{V_{Noise}} \tag{C.1}$$

which will result in a signal to noise ration of 60.2 dB [130]. The noise of the used low noise operational amplifiers and filter are as follows:

- MAX274 signal-to-noise ratio including distortion: -82 dB
- MAX275 signal-to-noise ratio including distortion: -83 dB [131]
- TL074 Equivalent input noise voltage(10 Hz-10 kHz): 4 μV [132]

The resulting signal-to-noise ratio for the TL074 can be calculated considering that the lowest expected input voltage will be 100 mV (current mode without load). Using equation C.1 the signal-to-noise ratio for the operational amplifier is 88.8 dB. These signal-to-noise ratios of the signal conditioning elements can be seen in figure C.1.

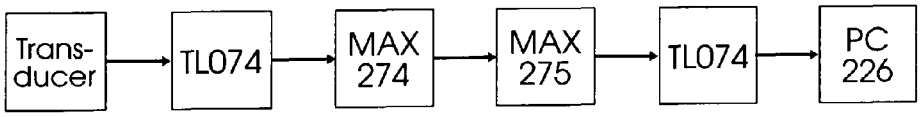

Figure C.1: Signal conditioning elements.

It can be seen that the biggest contributor of noise to the input signal is the data aquisition card. Considering the noise of the card, the noise ratios of the other elements can be neglected due to the $\geq$20 dB difference.

The signal-to-noise ratios of the transducers vary depending on the parameter observed. The noise generated by the shunt resistor for the measurement of the current can be neglected. Similar is the signal-to-noise ratio for the voltage meas-

urement which has been acomplished using resistors as voltage dividers. The accelerometer, however, generates a noise level of 20 μV according to the manufaturer. Considering an average rms vibration level of 0.2 g, the signal-to-noise ratio is 48 dB.

It can be concluded that the overall noise influence to vibration signal is approximately 48 dB. This is high compared to the signal-to-noise ratio of the data aquisition card. For all the other analogue signals the noise ratio will be determined by the data aquisition card resulting in a signal-to-noise ratio of approximately 60.2 dB.

Appendix D

Graphical User Interface

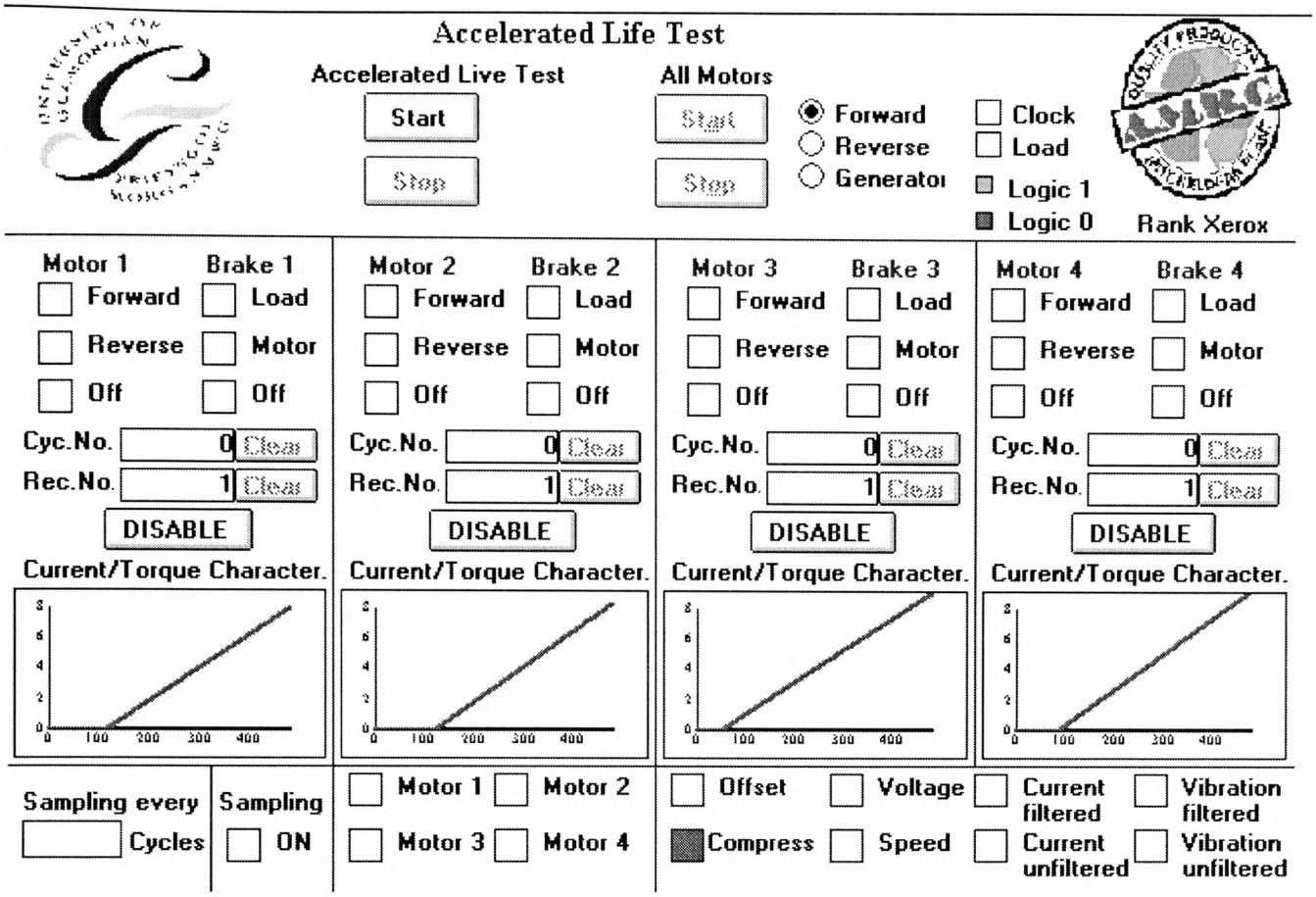

Figure D.1: Graphical user interface of the accelerated life test control software.

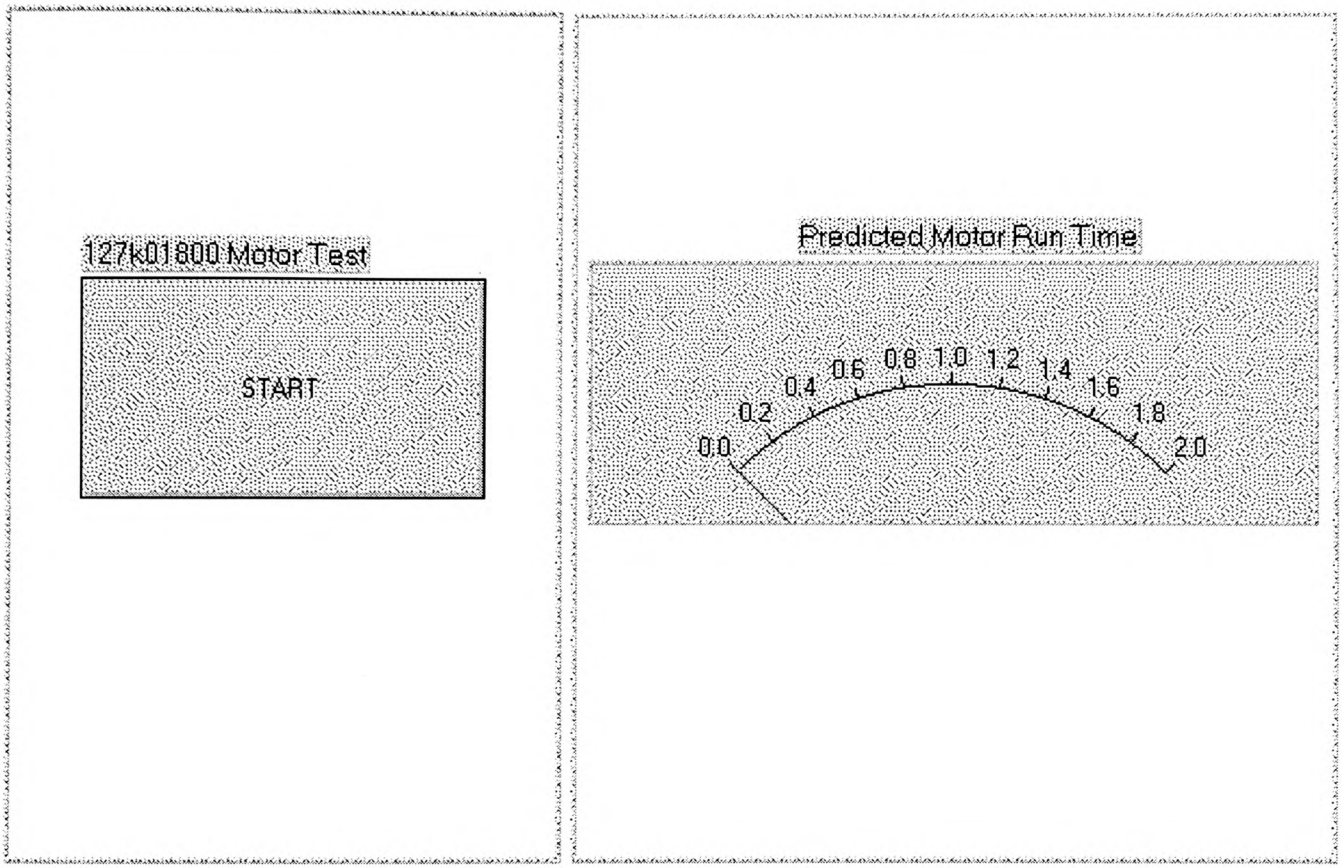

Figure D.2: Graphical user interface of the production prototype test system.